MEMORIAL UNIVERSITY OF NEWFOUNDLAND

Earth's Heat Inventory from Climate Model Simulations and Observations

SUBMITTED BY:
Francisco José Cuesta Valero

to the School of Graduate Studies
in partial fulfillment of the requirements for the degree of

DOCTOR OF PHILOSOPHY

ENVIRONMENTAL SCIENCES PROGRAM

May, 2021

"Eppur si muove"

- Attributed to Galileo Galilei

Abstract

Changes in the Earth system due to anthropogenic activities, such as emissions of greenhouse gases, have altered the response of the climate system to shortwave radiation received from the Sun. This response is mainly determined by several feedbacks that alter the amount of reflected shortwave radiation and emitted longwave radiation into the Space, resulting in a positive radiative imbalance at the top of the atmosphere. Such radiative imbalance causes heat storage within the climate system and modifies the evolution of several physical phenomena, such as permafrost thawing and sea level rise. Therefore, determining the response of the system to anthropogenic activities and the heat distribution among all climate subsystems is crucial to project future climate change.

In this dissertation, I estimate a preindustrial surface temperature climatology over North America and global changes in surface temperature, surface heat flux and continental heat storage from borehole temperature profiles. These observational estimates are used to assess the Earth Heat Inventory (EHI) and the preindustrial climatology over North America represented in an ensemble of transient climate simulations performed by atmosphere-ocean Coupled General Circulation Models (CGCMs) from the fifth phase of the Coupled Model Intercomparison Project (CMIP5).

The retrieved temperature climatology for North America based on borehole profiles is consistent with important features present in meteorological observations over a different period and the same spatial domain. Although the models were not tuned to match these temperatures, part of the analyzed CGCM preindustrial simulations agree with this climatology, while the rest of the models display lower temperatures. Estimates of ground surface temperatures and ground heat content indicates an average increase in land temperatures of 1 °C

since preindustrial times, and higher values of continental heat storage than previously reported. The assessment of the simulated and observed EHI shows that CMIP5 CGCMs constantly underestimate the heat storage in the continental subsurface, while overestimating the observed ocean heat content. These CMIP5 CGCM simulations also achieve values of atmosphere heat content and absorbed heat by sea ice melting similar to observations.

Acknowledgements

First of all, I would like to thank my supervisor Dr. Hugo Beltrami for his immense help and guidance during my stay in Antigonish. He has always had a good idea to discuss as well as a bottle of wine for celebrating the achievements and misfortunes of all these years. Dr. Joel Finnis and Dr. Susan Ziegler have been incredibly patient and supportive although the research included in this thesis is not in their immediate realm of expertise.

This report would be at least half as good without the bright contributions of the co-authors of the assembled manuscripts. I shared ideas and great moments with Dr. Elena Gracía-Bustamante and Dr. J. Fidel González-Rouco at several conferences and during their visits to Antigonish. Dr. Eduardo Zorita was always kind and supportive, and his contributions to Chapter 2 are invaluable. I would like to thank Almudena García-García for her infinite patience and help in crafting all the projects in this thesis. Fernando Jaume-Santero was a colleague of fatigues for a time, and his contribution was essential for Chapter 2.

The School of Graduate Students at Memorial University of Newfoundland and the Research Office at St. Francis Xavier University have funded this work. I am specially grateful to Lisa Sampson, Richard Isnor, Nancy Bishop and Gail Kenny for all their help in this hybrid experiment, halfway between Memorial University and St. Francis Xavier University.

I am grateful to Dmitry Demezhko, an anonymous reviewer and Irina Rogozhina for their constructive comments on the published work of Chapter 2, as well as Dr. Timothy Osborn for his guidance on using the CRU database. I acknowledge the World Climate Research Programme's Working Group on Coupled Modelling, which is responsible for CMIP, and I thank the climate modeling groups responsible for the model simulations used in this thesis for producing and making available their model outputs.

I am also grateful to the community that create and maintain software libre, and freely distribute scripts all over the Internet. I am deeply indebted to the community maintaining bash (and all associated programs), gfortran, the NetCDF libraries for Fortran90[1], CDO, GMT, R, Git and LaTeX. All analyses, figures and tables in this thesis have been performed using the mentioned software, and this document and all manuscripts have been created exclusively using LaTeX.

[1] People at Unidata, you deserve a knighthood.

Contents

List of Tables

List of Figures

List of Abbreviations

AHC Atmosphere heat content

BTP Borehole temperature profile

CE Common era

CGCM Coupled general circulation model

CHC Cryosphere heat content

CMIP5 Fifth phase of the Coupled Model Intercomparison Project

CMIP6 Sixth phase of the Coupled Model Intercomparison Project

CO_2 Carbon dioxide

CRU Climatic Research Unit at the University of East Anglia

ECS Equilibrium climate sensitivity

EHC Earth heat content

EHI Earth heat inventory

ESM Earth system model

GHC Ground heat content

GHFH Ground heat flux history

GIDS Gradient plus Inverse Distance Squared

GSTH Ground surface temperature history

IPCC Intergovernmental Panel on Climate Change

LIA Little ice age

LoST Long-term Surface Temperature database

LSM Land surface model

MIP Model intercomparison project

MWP Medieval warm period

N Net radiative imbalance at top-of-atmosphere

NOAA National Oceanic and Atmospheric Administration

OHC Ocean heat content

piControl Preindustrial control

PM Past millennium

PMIP3 Third phase of the Paleoclimate Modelling Intercomparison Project

PPI Perturbed Parameter Inversion

RMSE Root mean squared error

SAT Surface air temperature

SVD Singular value decomposition

TOA Top-of-atmosphere

1 Introduction

Adequate climate conditions are fundamental to sustain life in any planet. Particularly, the origin of life and its posterior evolution on Earth are directly determined by the specific temperature conditions and liquid water availability at each geological epoch (Pierrehumbert, 2010). All known forms of life require liquid water to exist, from animals to bacteria (Spiegel et al., 2008; Seager, 2013). Therefore, the presence of liquid water has become the principal biomarker in the search for extraterrestrial life, and has led to the definition of the "Goldilocks" zone around stars, which is defined as the range of distances from a star that allows the presence of liquid water in an Earth-like planet. That is, a zone not as close to the star as to evaporate all water and not as far of the star as to freeze all water. Therefore, such definition of "Goldilocks" zone assumes that the planetary climate is determined by the distance of the planet to its star and by the type and amount of radiation emitted by the star, assuming a planet enveloped by an atmosphere (Spiegel et al., 2008). Nevertheless, the total amount of energy and the latitudinal distribution of this energy in a certain planet also depends on a number of orbital parameters beyond the average distance to the star (Spiegel et al., 2010; Dressing et al., 2010; Deitrick et al., 2018a,b). The rotational velocity of the planet affects the heat transport from the region near the equator toward the poles, variations in obliquity changes the annual averaged amount of energy at polar and equatorial regions, precession of the planet's rotational axis and its orbital ellipse alters the position of solstices and equinoxes with respect to apoastron and periastron, and alterations of the shape of the orbit –that is, the orbital eccentricity, changes the total annual radiation received by the planet. The effect of these cyclical alterations of orbital parameters on climate conditions are noticeable in the past evolution of the Earth's climate, as proposed by

Milutin Milanković in the 1920s for the changes in orbital eccentricity, obliquity and the precession of the rotational axis (Milankovitch, 1920). Such factors partially explain the periodic appearance of cold periods in the past, the so-called ice ages, that left a signature in the geological record of the Earth (Meyers et al., 2018).

Applying the criteria discussed above to the Solar system to define an habitability zone reveals that there are missing factors to determine the habitability of a planet, since the Earth, Mars and Venus are located in the "Goldilocks" zone round the Sun, but Venus and Mars do not present signs of life. Furthermore, surface conditions on both planets do not allow the presence of liquid water; on Venus due to extremely high temperatures and pressures caused by a powerful greenhouse effect and a thick atmosphere (Franck et al., 2000; Spiegel et al., 2008; Pierrehumbert, 2010; Seager, 2013), and on Mars due to an excessively thin atmosphere that traps water in the polar caps and as frozen water in the subsurface (Bibring et al., 2004; Pierrehumbert, 2010; Seager, 2013; Kurokawa et al., 2014; Dundas et al., 2018). As seen for the cases of Venus and Mars, it is clear that both the atmosphere composition, particularly the presence of greenhouse gases, and the amount of energy received from the Sun are fundamental for permitting the presence of liquid water in the surface of a planet of the solar system. For example, the mean surface temperature of an Earth-like planet changes abruptly depending on the distance to a Sun-like star, with a surface temperature higher than 100 °C at distances smaller than 0.65 au, and a surface temperature lower than 0 °C if located at a distance of ∼1.03 au (Spiegel et al., 2008). Otherwise, the effect of atmospheric greenhouse gases is quantified to be around 33 °C, as the mean surface temperature of the Earth would be −18 °C without the greenhouse effect. Indeed, variations of the composition of the atmosphere have led to changes in climate conditions during long periods of the Earth's history (Royer, 2006; Sun et al., 2012), with outgassing of Carbon Dioxide (CO_2) due to volcanism related to plate tectonics as the main factor altering the concentration of greenhouse gases in both the ocean and the atmosphere on time scales of tens to hundreds of millions of years (Van Der Meer et al., 2014). Therefore, both the total radiation reaching the Earth from the Sun and the greenhouse effect due to the composition of the atmosphere determine the evolution of global temperature with time, including the appearance of ice ages

or extremely warm periods (Royer, 2006; Sun et al., 2012; Meyers et al., 2018).

1.1 Climate Change as an Energy Problem

Slow changes in eccentricity, obliquity, axis precession and orbital precession, together with changes in solar activity, alter the total amount of shortwave radiation reaching the Earth as well as the latitudinal distribution of shortwave radiation. Meanwhile, changes in the concentration of greenhouse gases in the atmosphere varies the amount of longwave radiation emitted into the Space, modifying the state of the climate system in the process. That is, the absorbed shortwave radiation at the top of the atmosphere must be in equilibrium with the reflected shortwave radiation and the outgoing longwave radiation in order to maintain climate conditions, thus any change in this radiative balance heats (positive imbalance) or cools (negative imbalance) the Earth system (Hansen et al., 2005, 2011; IPCC, 2013; Trenberth et al., 2014; von Schuckmann et al., 2016). Human activities have significantly increased the atmospheric concentration of greenhouse gases since the Industrial Revolution (Hegerl et al., 1996; Barnett et al., 2001), perturbing the radiative imbalance at the top of the atmosphere. Such perturbation of the radiative balance due to anthropogenic activities is denominated radiative forcing, and the difference between this forcing and the induced response of the Earth system, mediated by changes in the emitted longwave radiation and therefore in surface temperature, determines the net radiative imbalance at the top of the atmosphere. The changes in longwave radiation that balance the radiative forcings are driven by climate feedbacks, and are critical to understand and quantify the climate response to anthropogenic emissions of greenhouse gases (Gregory et al., 2002; IPCC, 2013; Knutti et al., 2017). These feedback mechanisms tend to amplify the change in longwave radiation –that is, to enhance the increase in surface temperature as a result of the increase in atmospheric greenhouse gas concentrations. Therefore, quantifying the sensitivity of surface temperature to increases in greenhouse gas concentrations is critical to obtain reliable future projections of climate conditions in order to evaluate their impact on society and ecosystems. The Equilibrium Climate Sensitivity (ECS) is the most popular metric for quantifying the sensitivity to increases in atmospheric concentration of CO_2, which is the main anthropogenic

greenhouse gas. The ECS is a simple metric for determining the change in global mean temperature induced by a doubling of the CO_2 concentrations relative to preindustrial conditions, which can be estimated using different datasets and techniques. Nevertheless, although several methodologies for estimating ECS have been used based on meteorological observations, numerical models and paleoreconstructions, determining the ECS has proven to be complex since different sources yield different results with large uncertainties for most of the available methodologies (Knutti et al., 2017). The main limitation for accurately determining the value of ECS resides in the complexity of the radiative response to external forcings (Goodwin, 2018). That is, the climate sensitivity of the system depends on different climate feedbacks which in turn are governed by a broad range of factors that evolve with time. Thus, this sensitivity has probably changed with time, as relevant factors for the climate state and climate feedbacks such as vegetation patterns and ice sheet extension and volume have also evolved with time. Since future projections of climate change performed by atmosphere-ocean Coupled General Circulation Models (CGCMs) are directly related to the represented climate sensitivity, and these advanced climate models exhibit a wide range of ECS estimates, there is a large spread in future warming projections that hampers the assessment of future climate change impacts (Sherwood et al., 2014; Knutti et al., 2017; Goodwin, 2018).

Monitoring the radiative imbalance at the top of the atmosphere is essential to evaluate the magnitude and evolution of climate change. Satellite instrumentation is the first logic tool for monitoring the imbalance, as it measures the solar incoming and reflected shortwave radiation from Space, as well as the emitted longwave radiation by the Earth system (Loeb et al., 2009; Johnson et al., 2016). Indeed, satellites provide high-quality measurements of incoming shortwave flux, reflected shortwave flux and outgoing longwave flux, but the estimates of the net radiative imbalance present large uncertainties. The net radiative imbalance from satellite data is obtained as the difference between solar incoming radiation and total outgoing radiation (solar reflected and thermal emitted radiation), quantities that are well over two orders of magnitude larger than the magnitude of the final imbalance (Loeb et al., 2012). Hence, satellite data have been combined with measurements of variations in ocean heat content, several reanalysis products and numerical simulations performed with

CGCMs to improve the net radiative imbalance from satellite instrumentation (Loeb et al., 2012; Allan et al., 2014; Smith et al., 2015). There is, nevertheless, another observational source of information about the magnitude and evolution of the radiative imbalance at the top of the atmosphere: the Earth Heat Inventory (EHI). The current radiative imbalance is causing an increase in the heat stored within the ocean, the continental subsurface, the atmosphere and the cryosphere (Beltrami, 2002; Hansen et al., 2005, 2011; Levitus et al., 2012; IPCC, 2013; von Schuckmann et al., 2016, 2020). The ocean accounts for the largest part of the added energy (89 %), with the continental subsurface the second largest term (6 %), followed by the absorbed heat in ice melting (4 %) and in heating the atmosphere (1 %). This additional energy provides an indirect, alternative method for monitoring the radiative imbalance at the top of the atmosphere, presenting smaller uncertainties than satellite measurements. Additionally, the heat gained by the terms of the EHI during the second half of the 20^{th} century and the first decade of the 21^{st} century has modified several physical phenomena affecting near-surface climate conditions, with potential consequences for society. For example, the heat absorbed by the cryosphere due to melting of glaciers and ice sheets has greatly contributed to sea level rise, while the heat used to thaw permafrost has accelerated the permafrost carbon feedback, strengthening the greenhouse effect (Koven et al., 2011; Jacob et al., 2012; Levitus et al., 2012; MacDougall et al., 2012; Dutton et al., 2015).

1.2 Numerical Climate Models to Understand Climate Change

Determining the value of ECS has been a concern since the early days of climate research in the 1970s, as well as one of the first application of numerical climate models (Charney et al., 1979; Santer et al., 2019). Nevertheless, the development of advanced climate models representing the whole planet, including the recently developed Earth System Models (ESMs) that are able to simulate the movement of carbon through the Earth system, first required increased computational resources and infrastructure. Hence, one of the first missions of the early digital computers was to perform weather forecasts, as forecast are focused on a limited temporal and spatial domain, requiring a markedly lower amount of computational power in comparison with global climate simulations. For those

forecasts, the first weather models were coded to solve a simplified set of equations for a limited atmosphere. Subsequently, the first atmospheric global circulation model was developed to simulate a simplistic global atmosphere (Phillips, 1956) and the first three-dimensional ocean model was developed to represent the ocean circulation (Bryan et al., 1967). At the same time, the scientific community started using these models to study the role of CO_2 on atmospheric radiative transfer (Manabe et al., 1967), as well as questions such as the effect of removing the polar caps or altering the solar constant on the global atmosphere (Sellers, 1969). Those early experiments culminated in the development of the first coupled atmosphere-ocean general circulation model (Manabe et al., 1975; Bryan et al., 1975), which included a representation of feedback mechanisms between the atmosphere and ocean, allowing the study of climate evolution at centennial timescales. After this first climate model, a new generation of coupled general circulation models (Washington et al., 1989; Stouffer et al., 1989) was developed and dedicated to assess the influence of anthropogenic activities on the climate system (Santer et al., 1996). More recent steps in climate model development include the addition of the global carbon cycle (Cox et al., 2000) and the atmospheric chemistry (IPCC, 2007). The representation of biogeochemical processes is now standard in the new generation of ESMs, providing the most comprehensive tools available for simulating past and future responses of the climate system to external forcings (Flato et al., 2013).

Currently, numerous global climate models are being developed and maintained by several modeling centers around the world, and their ability to simulate different aspects of the climate system is assessed using standard methods and experiments under the guidelines of several Model Intercomparison Projects (MIPs), such as the fifth phase of the Coupled Model Intercomparison Project (CMIP5) (Taylor et al., 2011) that informed the fifth Assessment Report of the Intergovernmental Panel on Climate Change (IPCC-AR5) (IPCC, 2013), or the sixth phase of the Coupled Model Intercomparison Project (CMIP6) (Eyring et al., 2016) that will inform the sixth Assessment Report of the Intergovernmental Panel on Climate Change (IPCC-AR6). In these MIPs, different climate models perform experiments employing the same boundary conditions (e.g., atmospheric concentration of greenhouse gases, solar irradiance) and protocols in a coordinated manner. Using different models to perform experiments with

the same boundary conditions allows for testing numerous hypotheses about the climate system, while sampling the range of plausible climate realizations that are consistent with current knowledge about the Earth system. For example, experiments performed with ensembles of ESMs have let to improved understanding of feedbacks between the carbon cycle and the physical climate (Friedlingstein et al., 2006; Arora et al., 2013). Nevertheless, the most relevant of all these coordinated modeling experiments are projections of future climate change, which inform about the consequences of anthropogenic activities for the future evolution of climate variables critical to the wellbeing and development of society, including temperature, precipitation and the associated extreme events (e.g., drougths, floods and heat waves, Stainforth et al., 2007; IPCC, 2013).

Despite the usefulness of numerical climate simulations, models are limited representations of the physical climate system with several important sources of uncertainty (Flato et al., 2013). Therefore, inconsistencies within these models tend to induce unrealistic features in climate simulations. Climate drifts are one of the most important inconsistencies that appear in climate simulations, consisting of spurious trends in state variables, such as sea surface temperature, that persist during the entire period of the simulation. The incomplete initialization of CGCMs is the most typical source of drifts in simulations (Sen Gupta et al., 2013; Séférian et al., 2016). The initialization procedure of a CGCM consists in a long-term spin-up simulation to achieve an equilibrium state, followed by a control simulation from which to start climate change experiments. Reaching an equilibrium state, nevertheless, may require millennia-long periods of simulated time due to the slow evolution of ocean currents (Peacock et al., 2006; Wunsch et al., 2008; Schmidt et al., 2017), and most modeling groups cannot afford the required computational resources, thus replacing them with centennial simulations. Such replacement may induce some level of drift in the system due to the incomplete spin-up procedure, which is transmitted to the control simulation and to the transient climate change simulations (Sen Gupta et al., 2012, 2013). A control simulation consists of an extension of the spin-up simulation under constant radiative forcing after the CGCM reaches the equilibrium state. Preindustrial control simulations are usually employed as a baseline from which to initialize climate simulations, thus potentially transmitting any artificial climate drift from the spin-up simulation to the transient climate change

experiments. Even if the initialization procedure provides a stable control simulation, ocean model components can reach multiple equilibrium states under a realistic surface forcing (Rahmstorf, 1995), and thus a CGCM equilibrium state may deviate from the observed climatology (e.g., Tang et al., 2016). Furthermore, some parameters of CGCMs are typically tuned (adjusted) to bring the simulations closer to observations (Voosen, 2016; Mauritsen et al., 2012; Hourdin et al., 2017; Schmidt et al., 2017), primarily matching the surface temperature evolution since the Industrial Revolution. Nevertheless, control simulations attempt to reproduce the preindustrial long-term equilibrium state of the climate system, and thus this tuning may bias the represented equilibrium state in control simulations towards observations collected after the Industrial Revolution. Therefore, it may happen that a climate simulation starts from an unrealistic equilibrium state, representing a biased climate trajectory during the entire climate experiment.

Another inconsistency that affects all CGCMs is the use of parameterizations. The term parameterization refers to the representation of unsolvable processes within climate models. Parameterizations assume the existence of certain relationships between resolved and unresolved processes that allow the effect of these unresolved processes to be incorporated into climate simulations (McFarlane, 2011). The sophistication of parameterizations varies greatly depending on the available knowledge about the phenomenon of interest and the computational resources devoted to understand and simulate the process. Simple and complex parameterizations incorporate some degree of error and uncertainty in climate simulations that needs to be carefully managed to avoid the generation of spurious drifts (Sen Gupta et al., 2013). Even aspects of parameterizations that may seem trivial or negligible, such as the order in which parameterizations are applied, should be monitored and their impact assessed during the development of parameterization schemes and their implementation in climate models to minimize artificial inconsistencies in simulations (Donahue et al., 2018). Constant efforts are devoted to enhance the representation and implementation of unresolved phenomena in climate model simulations, although the partition of available computational resources employed to represent the different parts of the climate system still does not allow for the full resolution of all the parameterized processes. Thus, ongoing efforts are focused on gener-

ating new mathematical techniques to incorporate more detailed descriptions of unresolved processes in global climate models while balancing the required computational power for these new parameterizations (McFarlane, 2011).

Implementing simplified or idealized parameterizations to account for unresolved processes on climate models results in several quantities that are not determined by theory or observations, whose values need to be adjusted empirically by model tuning. Once the physical laws of the climate system are implemented in a climate model and the processes that cannot be resolved are parameterized, a small subset of parameters remains undetermined. These parameters are then tuned or adjusted with the aim of improving the match between mode output and observed values of relevant climate variables (Mauritsen et al., 2012; Hourdin et al., 2017; Schmidt et al., 2017). Tuning is typically applied to parameters belonging to processes that are poorly constrained by observations and theory, always attempting to be consistent with physical laws. The methodology employed by most modeling groups consists in controlling the simulated surface temperature by modifying the simulated net radiative imbalance at the top of the atmosphere, which is achieved by adjusting several cloud parameters. This practice alters the representation of important physical processes, such as rainfall and cloud cover, and thus a balance between tuning necessities and the realism of simulations should be reached. Other factors may affect the tuning process, such as the uncertainty in the prescribed forcings, artificial energy leakages (Mauritsen et al., 2012; Hobbs et al., 2016) or local biases in sea surface temperatures within control simulations (Sen Gupta et al., 2013; Séférian et al., 2016). The fundamental problem of model tuning is that the tuning process does not ensure an improvement in the model physics. Unrealistic parameter values may improve the realism of the simulated climate in comparison with observations (Schmidt et al., 2017), but at the cost of introducing compensating errors that do not enhance the representation of physical phenomena within the model (Dommenget et al., 2017). Even more, parameter adjustments make all model components interdependent. That is, a tuned atmosphere component simulating climate fields in agreement with observations cannot be coupled with a tuned ocean component without further adjustments. And these additional adjustments are the most likely source of compensating errors. For instance, selecting parameter values that improve the simulation of the ocean mixing in

order to reduce a bias in the sea surface temperature may compensate for a flaw in the employed cloud scheme. Thereby, the coupled atmosphere and ocean components of the model become dependent on each other, and will not work well if coupled to different model components. Despite all these deficiencies, tuning is still considered preferable to not tuning at all (Schmidt et al., 2017) or the unphysical correction of heat flux in the ocean (Taylor et al., 2011; Flato et al., 2013). Although model tuning is a crucial part of climate model development (Flato et al., 2013), the tuning techniques and strategies used by each model group are not as well documented as model components and their configurations (Mauritsen et al., 2012).

1.3 Evaluating Climate Models

Although the inconsistencies in numerical climate models described in the previous section are generally unavoidable, the performance of CGCM simulations needs to be evaluated against observational references in order to gain confidence in the ability of models to represent the physical climate system and to perform realistic projections of future climate change. Global climate models are designed to reproduce the observed temperature change during the 20^{th} century. This is the first and foremost test that a climate model has to undergo in order to be trusted by the scientific community. That is, if a model does not reproduce the observed trend in temperature during the last century, the model cannot be considered reliable (Baumberger et al., 2017). Assessing the reliability of a complex global climate model composed of many components just by comparing its 20^{th} century simulations with the evolution of a single climate variable may seem a limited test, but surface air temperature is the best-measured climate variable across many spatial and temporal scales (Knutti et al., 2010), and temperature is also one of the most important indicators to quantify the impact of climate change on society. The comparison between model simulations of the 20^{th} century and observed surface temperature is, therefore, the last and crucial phase of model development.

Nevertheless, tuning practices reduce the available observations for climate model evaluation. That is, modeling groups employ all available observations to calibrate their models, rendering the data useless for model evaluation (Baum-

berger et al., 2017). Independent data is needed for testing the models, but waiting for new observations is an inefficient approach due to the time required to generate datasets suitable for climate studies. Furthermore, the temporal extent of the instrumental period is not long enough to correctly characterize the natural variability of the climate system, requiring additional information about the past evolution of climate. Paleoreconstructions –that is, estimates of the past evolution of the climate system from proxy and geothermal data, provide an unique opportunity to evaluate climate models outside the range of observations. Since paleoreconstructions are not considered during the tuning phase of model development, agreement between reconstructed and simulated past climate changes reinforces our confidence in model outputs as physically coherent representations of the climate system (Knutti et al., 2010; Braconnot et al., 2012; Schmidt et al., 2014; Harrison et al., 2015). Simulations of the last millennium (i.e., from 850 CE to present) allow to test the ability of models in representing the effects of volcanic eruptions on global climate, some regional climate changes such as the Little Ice Age and the Medieval Warm Anomaly, or the natural climate variability in both temperature and hydrology (PAGES 2k-PMIP3 Group, 2015; PAGES Hydro2k Consortium, 2017). The natural climate variability during the last millennium is of especial importance for studying the dynamics of the climate system at long temporal scales, since the temporal range sampled by meteorological observations may not be long enough to fully characterize the natural variability of the system. An illustrative example can be the reconstructed multidecadal megadroughts in the southwest of the US that have not been captured by observations and provides information to understand the risk of megadroughts in the future (Cook et al., 2015). Despite the potential usefulness of the comparison between paleoreconstructions and paleosimulations, their associated uncertainties are large and need to be considered for evaluating the ability of CGCMs to reproduce the evolution of the climate system (Braconnot et al., 2012; Schmidt et al., 2014; Harrison et al., 2015).

Numerous reconstructions of past changes in temperature, water availability and other variables relevant for model evaluation have been obtained from proxy data (PAGES 2k-PMIP3 Group, 2015; PAGES Hydro2k Consortium, 2017). The development rate of physical characteristics in some biological (e.g., trees, corals) and geological (e.g., speleotherms, sediments) systems is affected by changes in

climate conditions. The recorded development rate in proxies is measured and then calibrated against observations to obtain information about the past evolution of the associated climate variables. However, the relationship between proxies and observations is not straightforward due to difficulties retrieving the climate signals from proxies. The development of each proxy is affected by several factors that may hide the climate signal, adding uncertainty into the reconstruction. For instance, tree-ring proxy measurements reflect a combination of influences on tree growth beyond the climate signal, such as the age of the tree, its geometry or the impact of tree-level and site-level disturbances (PAGES Hydro2k Consortium, 2017). Another issue with paleoreconstructions is the scarcity of data and its inhomogeneous distribution, with higher proxy densities at mid-latitudes of the northern hemisphere. Thus, climate field reconstructions aimed at estimating the past spatiotemporal evolution of climate variables often require advanced statistical techniques to obtain high-quality reconstructions from a sparse network of proxies (Smerdon, 2012; Hakim et al., 2016; Gómez-Navarro et al., 2017). Other reconstruction approaches that do not rely on proxy systems are possible, such as those based on borehole temperature profiles. Measurements of borehole temperature profiles –that is, measurements of the ground temperature with depth, allow for the estimation of past changes in surface temperature and surface heat flux at multi-decadal scales (Harris et al., 2001; Beltrami, 2002; Jaume-Santero et al., 2016). Variations in the surface energy balance are propagated through the ground following the heat diffusion equation, altering the subsurface quasi-equilibrium profile. The recorded deviations from the quasi-equilibrium state can be inverted to retrieve past changes in ground surface temperature for a specific temporal period determined by the depth of the profile. Proxy-independent reconstructions of past temperature changes also provide context to interpret proxy-based reconstructions, and the comparison of results obtained by each technique aids in detecting and understanding their respective limitations and biases (Masson-Delmotte et al., 2013). Furthermore, reconstructions from borehole temperature profiles are critical to determine the land component of the EHI, as geothermal measurements are the only source to estimate long-term changes in surface heat flux and continental heat storage (Levitus et al., 2005; Church et al., 2011; Hansen et al., 2011; Rhein et al., 2013; von Schuckmann et al., 2020).

1.4 Research Focus

The objective of this thesis is to improve our understanding of the EHI within advanced CGCM simulations and to provide observational references to evaluate transient climate simulations. Particularly, this thesis provides: i) a new method to estimate the preindustrial long-term temperature climatology of North America, ii) a new global estimate of continental heat storage from the 1600s to the present, iii) an assessment of the ability of state-of-the-art CGCMs to reproduce the estimated temperature climatology over North America, and iv) a comparison between the EHI retrieved from observations and from CGCM simulations.

The simulated partition of energy within the different climate subsystems depends on several factors, such as the sensitivity of the system to changes in atmospheric CO_2 concentrations and the representation of the different subsystems in the models. Additionally, the represented temperature climatology in preindustrial control simulations determines the evolution of several important physical processes that affect the total heat content of the Earth system as well as the distribution of heat among the different subsystems in climate simulations. Particularly, the temperature climatology in control simulations partially determines the evolution of the ECS, the permafrost extension, the amount of water vapor in the atmosphere, and the volume of sea ice within transient climate simulations. Nevertheless, there are no climatological references for absolute temperatures before the Industrial Revolution, which hampers the evaluation of climate simulations. A new database containing preindustrial, long-term, absolute surface temperatures over North America from measurements of borehole temperature profiles is developed in this thesis. Although this database only covers a small part of the land surface, a generalization using the global borehole network should be easy to implement. All the details about the development and implications of this database are explained in Chapter 2.

The temperature database described in Chapter 2 is based on a combination of old and new Borehole Temperature Profile (BTP) measurements assembled by Jaume-Santero et al. (2016). Since the majority of BTPs are acquired from holes of opportunity, i.e from mining explorations, the available data is scarce and rather inhomogeneous, with several decades being necessary for collecting a sufficient number of new profiles in order to update global studies. This is the

case for the database compiled for North America in Jaume-Santero et al. (2016), which included a high number of new BTP measurements now available for analysis. Using all these new BTP measurements, this thesis provides with an update of the global estimates of ground surface temperature, ground heat flux and ground heat content performed in Beltrami et al. (2002) and Beltrami (2002). Additionally, a new technique to characterize uncertainties in reconstructions of past surface temperatures and fluxes from subsurface temperature profiles is developed in this thesis (Chapter 3), including a full explanation of the assembled new global database, and the obtained estimates of surface temperature, surface flux and continental heat storage from geothermal data.

The new estimates of continental heat storage presented in Chapter 3 were compiled in a new database of EHI observations, together with estimates of heat storage in the ocean (at several depths), the atmosphere, the ice sheets in Greenland and Antarctica, sea ice and global glaciers performed by other research groups (von Schuckmann et al., 2020). The simulated EHI by an ensemble of thirty CGCMs from the CMIP5 archive is evaluated against that observational database and previous observational estimates in Chapter 4. The results displayed in Chapter 4 constitute the first comprehensive assessment of the total heat storage and the proportion of heat within the climate subsystems in advanced CGCM simulations.

1.5 Co-Authorship Statement

The three research projects included in this thesis are the result of several discussions with my co-supervisor Dr. Hugo Beltrami (St. Francis Xavier University), who has been my main supervisor. My other co-supervisor, Dr. Joel Finnis (Memorial University), and the third member of my supervisory committee, Dr. Susan Ziegler (Memorial University), approved the proposal for this line of research. I performed all analyses and created all figures contained in this report. I gathered all model outputs from the CMIP5 archive in collaboration with my colleague Almudena García-García, as we both used the same model experiments for different pourposes in our theses. The borehole measurements were retrieved from different databases freely available for research. The different contributions for each project conforming this thesis are detailed below:

Chapter 2 I designed the study with the help of Dr. Hugo Beltrami, Almudena García-García, and Dr. Eduardo Zorita (Hemlholtz-Zentrum Geesthacht, Geesthacht, Germany), who provided insightful comments and suggestions. I wrote all versions of the text and performed all analyses and figures displayed in this chapter. The long-term surface temperatures (T_0 temperatures) in which this project is based were provided by Fernando Jaume-Santero from the database described in Jaume-Santero et al. (2016). All co-authors reviewed the results and text, and contributed edits to the manuscript before submitting it to *Climate of the Past*. I answered all comments by the referees and made the corresponding modifications in the original manuscript.

Chapter 3 As in Chapter 2, I designed the study with the guidance of Dr. Hugo Beltrami and the help of my colleague Almudena García-García. Fruitful discussions with Dr. Elena García-Bustamante (Centro de Investigaciones Energéticas, Medioambientales y Tecnológicas, CIEMAT, Spain) and Dr. J. Fidel González-Rouco (Universidad Complutense de Madrid, Spain) led to several improvements to the project. I wrote all versions of the manuscript and performed the analysis and figures displayed in this chapter. I also developed the new technique to characterize the uncertainty in borehole reconstructions detailed in the chapter. I was responsible for collecting the borehole data from three freely available datasets: the National Oceanic and Atmospheric Administration (NOAA) database, that is based on previous efforts to create a global borehole database by the International Heat Flow Commission (NOAA, 2019), and the databases published in Suman et al. (2017) (Australia), Jaume-Santero et al. (2016) (North America), and Pickler et al. (2018) (Chile). All co-authors reviewed the results and text, and contributed to improve the manuscript before submitting it to *Climate of the Past*.

Chapter 4 Dr. Hugo Beltrami and Almudena García-García provided useful comments during the different phases of this project. Dr. Joel Finnis also contributed to the enhancement of the study since the beginning of my PhD. I wrote all versions of the text and performed all analyses and figures displayed in this chapter. I was responsible for collecting the data from the

CMIP5 archive in collaboration with Almudena García-García, while observational data was obtained from Church et al. (2011), von Schuckmann et al. (2020) and Chapter 3. All co-authors reviewed the results and text, and contributed to improve the manuscript.

1.6 References

Allan, R. P., Liu, C., Loeb, N. G., Palmer, M. D., Roberts, M., Smith, D., and Vidale, P.-L. (2014). Changes in global net radiative imbalance 1985–2012. *Geophysical Research Letters*, **41**(15), 5588–5597. DOI: 10.1002/2014GL060962.

Arora, V. K., Boer, G. J., Friedlingstein, P., Eby, M., Jones, C. D., Christian, J. R., Bonan, G., Bopp, L., Brovkin, V., Cadule, P., Hajima, T., Ilyina, T., Lindsay, K., Tjiputra, J. F., and Wu, T. (2013). Carbon–Concentration and Carbon–Climate Feedbacks in CMIP5 Earth System Models. *Journal of Climate*, **26**(15), 5289–5314. DOI: 10.1175/JCLI-D-12-00494.1.

Barnett, T. P., Pierce, D. W., and Schnur, R. (2001). Detection of Anthropogenic Climate Change in the World's Oceans. *Science*, **292**(5515), 270–274. DOI: 10.1126/science.1058304.

Baumberger, C., Knutti, R., and Hirsch Hadorn, G. (2017). Building confidence in climate model projections: an analysis of inferences from fit. *Wiley Interdisciplinary Reviews: Climate Change*, **8**(3). e454–n/a. DOI: 10.1002/wcc.454.

Beltrami, H. (2002). Climate from borehole data: Energy fluxes and temperatures since 1500. *Geophysical Research Letters*, **29**(23). 26–1–26–4. DOI: 10.1029/2002GL015702.

Beltrami, H., Smerdon, J. E., Pollack, H. N., and Huang, S. (2002). Continental heat gain in the global climate system. *Geophysical Research Letters*, **29**(8), 8–1–8–3. DOI: 10.1029/2001GL014310.

Bibring, J.-P., Langevin, Y., Poulet, F., Gendrin, A., Gondet, B., Berthé, M., Soufflot, A., Drossart, P., Combes, M., Bellucci, G., Moroz, V., Mangold, N., Schmitt, B., and OMEGA team, t. (2004). Perennial water ice identified in the south polar cap of Mars. *Nature*, **428**(6983), 627–630. DOI: 10.1038/nature02461.

Braconnot, P., Harrison, S. P., Kageyama, M., Bartlein, P. J., Masson-Delmotte, V., Abe-Ouchi, A., Otto-Bliesner, B., and Zhao, Y. (2012). Evaluation of climate models using palaeoclimatic data. *Nature Clim. Change*, **2**(6), 417–424. DOI: 10.1038/nclimate1456.

Bryan, K. and Cox, M. D. (1967). A numerical investigation of the oceanic general circulation. *Tellus*, **19**(1), 54–80. DOI: 10.3402/tellusa.v19i1.9761.

Bryan, K., Manabe, S., and Pacanowski, R. C. (1975). A Global Ocean-Atmosphere Climate Model. Part II. The Oceanic Circulation. *Journal of Physical Oceanography*, **5**(1), 30–46. DOI: 10.1175/1520-0485(1975)005<0030:AGOACM>2.0.CO;2.

Charney, J. G., Arakawa, A., Baker, D. J., Bolin, B., Dickinson, R. E., Goody, R. M., Leith, C. E., Stommel, H. M., and Wunsch, C. I. (1979). *Carbon dioxide and climate: a scientific assessment*. National Academy of Sciences, Washington, DC.

Church, J. A., White, N. J., Konikow, L. F., Domingues, C. M., Cogley, J. G., Rignot, E., Gregory, J. M., van den Broeke, M. R., Monaghan, A. J., and Velicogna, I. (2011). Revisiting the Earth's sea-level and energy budgets from 1961 to 2008. *Geophysical Research Letters*, **38**(18). n/a–n/a. DOI: 10.1029/2011GL048794.

Cook, B. I., Ault, T. R., and Smerdon, J. E. (2015). Unprecedented 21st century drought risk in the American Southwest and Central Plains. *Science Advances*, **1**(1). DOI: 10.1126/sciadv.1400082.

Cox, P. M., Betts, R. A., Jones, C. D., Spall, S. A., and Totterdell, I. J. (2000). Acceleration of global warming due to carbon-cycle feedbacks in a coupled climate model. *Nature*, **408**, 184 EP –.

Deitrick, R., Barnes, R., Quinn, T. R., Armstrong, J., Charnay, B., and Wilhelm, C. (2018a). Exo-Milankovitch Cycles. I. Orbits and Rotation States. *The Astronomical Journal*, **155**(2), 60. DOI: 10.3847/1538-3881/aaa301.

Deitrick, R., Barnes, R., Bitz, C., Fleming, D., Charnay, B., Meadows, V., Wilhelm, C., Armstrong, J., and Quinn, T. R. (2018b). Exo-Milankovitch Cycles. II.

Climates of G-dwarf Planets in Dynamically Hot Systems. *The Astronomical Journal*, **155**(6), 266. DOI: 10.3847/1538-3881/aac214.

Dommenget, D. and Rezny, M. (2017). A Caveat Note on Tuning in the Development of Coupled Climate Models. *Journal of Advances in Modeling Earth Systems*, n/a–n/a. DOI: 10.1002/2017MS000947.

Donahue, A. S. and Caldwell, P. M. (2018). Impact of Physics Parameterization Ordering in a Global Atmosphere Model. *Journal of Advances in Modeling Earth Systems*, n/a–n/a. DOI: 10.1002/2017MS001067.

Dressing, C. D., Spiegel, D. S., Scharf, C. A., Menou, K., and Raymond, S. N. (2010). Habitable Climates: The Influence Of Eccentricity. *The Astrophysical Journal*, **721**(2), 1295–1307. DOI: 10.1088/0004-637x/721/2/1295.

Dundas, C. M., Bramson, A. M., Ojha, L., Wray, J. J., Mellon, M. T., Byrne, S., McEwen, A. S., Putzig, N. E., Viola, D., Sutton, S., Clark, E., and Holt, J. W. (2018). Exposed subsurface ice sheets in the Martian mid-latitudes. *Science*, **359**(6372), 199–201. DOI: 10.1126/science.aao1619.

Dutton, A., Carlson, A. E., Long, A. J., Milne, G. A., Clark, P. U., DeConto, R., Horton, B. P., Rahmstorf, S., and Raymo, M. E. (2015). Sea-level rise due to polar ice-sheet mass loss during past warm periods. *Science*, **349**(6244). DOI: 10.1126/science.aaa4019.

Eyring, V., Bony, S., Meehl, G. A., Senior, C. A., Stevens, B., Stouffer, R. J., and Taylor, K. E. (2016). Overview of the Coupled Model Intercomparison Project Phase 6 (CMIP6) experimental design and organization. *Geoscientific Model Development*, **9**(5), 1937–1958. DOI: 10.5194/gmd-9-1937-2016.

Flato, G., Marotzke, J., Abiodun, B., Braconnot, P., Chou, S., Collins, W., Cox, P., Driouech, F., Emori, S., Eyring, V., Forest, C., Gleckler, P., Guilyardi, E., Jakob, C., Kattsov, V., Reason, C., and Rummukainen, M. (2013). "Evaluation of Climate Models". In: *Climate Change 2013: The Physical Science Basis. Contribution of Working Group I to the Fifth Assessment Report of the Intergovernmental Panel on Climate Change*. Ed. by T. Stocker, D. Qin, G.-K. Plattner, M. Tignor, S. Allen, J. Boschung, A. Nauels, Y. Xia, V. Bex, and P. Midgley.

Cambridge, United Kingdom and New York, NY, USA: Cambridge University Press. Chap. 9, pp. 741–866. DOI: 10.1017/CBO9781107415324.020.

Franck, S, Block, A, von Bloh, W, Bounama, C, Schellnhuber, H.-J, and Svirezhev, Y (2000). Habitable zone for Earth-like planets in the solar system. *Planetary and Space Science*, **48**(11). 1099 –1105. DOI: https://doi.org/10.1016/S0032-0633(00)00084-2.

Friedlingstein, P., Cox, P., Betts, R., Bopp, L., von Bloh, W., Brovkin, V., Cadule, P., Doney, S., Eby, M., Fung, I., Bala, G., John, J., Jones, C., Joos, F., Kato, T., Kawamiya, M., Knorr, W., Lindsay, K., Matthews, H. D., Raddatz, T., Rayner, P., Reick, C., Roeckner, E., Schnitzler, K. G., Schnur, R., Strassmann, K., Weaver, A. J., Yoshikawa, C., and Zeng, N. (2006). Climate–Carbon Cycle Feedback Analysis: Results from the C4MIP Model Intercomparison. *Journal of Climate*, **19**(14), 3337–3353. DOI: 10.1175/JCLI3800.1.

Gómez-Navarro, J. J., Zorita, E., Raible, C. C., and Neukom, R. (2017). Pseudo-proxy tests of the analogue method to reconstruct spatially resolved global temperature during the Common Era. *Climate of the Past*, **13**(6), 629–648. DOI: 10.5194/cp-13-629-2017.

Goodwin, P. (2018). On the Time Evolution of Climate Sensitivity and Future Warming. *Earth's Future*, **6**(9), 1336–1348. DOI: 10.1029/2018EF000889.

Gregory, J. M., Stouffer, R. J., Raper, S. C. B., Stott, P. A., and Rayner, N. A. (2002). An Observationally Based Estimate of the Climate Sensitivity. *Journal of Climate*, **15**(22), 3117–3121. DOI: 10.1175/1520-0442(2002)015<3117:AOBEOT>2.0.CO;2.

Hakim, G. J., Emile-Geay, J., Steig, E. J., Noone, D., Anderson, D. M., Tardif, R., Steiger, N., and Perkins, W. A. (2016). The last millennium climate reanalysis project: Framework and first results. *Journal of Geophysical Research: Atmospheres*, **121**(12). 6745–6764. DOI: 10.1002/2016JD024751.

Hansen, J., Nazarenko, L., Ruedy, R., Sato, M., Willis, J., Del Genio, A., Koch, D., Lacis, A., Lo, K., Menon, S., et al. (2005). Earth's energy imbalance: Confirmation and implications. *Science*, **308**(5727), 1431–1435.

Hansen, J., Sato, M., Kharecha, P., and Schuckmann, K. v. (2011). Earth's energy imbalance and implications. *Atmospheric Chemistry and Physics*, **11**(24), 13421–13449.

Harris, R. N. and Chapman, D. S. (2001). Mid-latitude (30 °–60 ° N) climatic warming inferred by combining borehole temperatures with surface air temperatures. *Geophysical Research Letters*, **28**(5), 747–750. DOI: 10.1029/2000GL012348.

Harrison, S. P., Bartlein, P. J., Izumi, K., Li, G., Annan, J., Hargreaves, J., Braconnot, P., and Kageyama, M. (2015). Evaluation of CMIP5 palaeo-simulations to improve climate projections. *Nature Clim. Change*, **5**(8), 735–743.

Hegerl, G. C., von Storch, H., Hasselmann, K., Santer, B. D., Cubasch, U., and Jones, P. D. (1996). Detecting Greenhouse-Gas-Induced Climate Change with an Optimal Fingerprint Method. *Journal of Climate*, **9**(10), 2281–2306. DOI: 10.1175/1520-0442(1996)009<2281:DGGICC>2.0.CO;2.

Hobbs, W., Palmer, M. D., and Monselesan, D. (2016). An Energy Conservation Analysis of Ocean Drift in the CMIP5 Global Coupled Models. *Journal of Climate*, **29**(5), 1639–1653. DOI: 10.1175/JCLI-D-15-0477.1.

Hourdin, F., Mauritsen, T., Gettelman, A., Golaz, J.-C., Balaji, V., Duan, Q., Folini, D., Ji, D., Klocke, D., Qian, Y., Rauser, F., Rio, C., Tomassini, L., Watanabe, M., and Williamson, D. (2017). The Art and Science of Climate Model Tuning. *Bulletin of the American Meteorological Society*, **98**(3), 589–602. DOI: 10.1175/BAMS-D-15-00135.1.

IPCC (2007). *Climate Change 2007: The Physical Science Basis. Contribution of Working Group I to the Fourth Assessment Report of the Intergovernmental Panel on Climate Change*. Ed. by S. Solomon, D. Qin, M. Manning, Z. Chen, M. Marquis, K. Averyt, M. Tignor, and H. Miller. Cambridge, United Kingdom and New York, NY, USA: Cambridge University Press, p. 996.

— (2013). *Climate Change 2013: The Physical Science Basis. Contribution of Working Group I to the Fifth Assessment Report of the Intergovernmental Panel on Climate Change*. Cambridge, United Kingdom and New York, NY, USA: Cambridge University Press, p. 1535. DOI: 10.1017/CBO9781107415324.

Jacob, T., Wahr, J., Pfeffer, W. T., and Swenson, S. (2012). Recent contributions of glaciers and ice caps to sea level rise. *Nature*, **482**(7386), 514–518.

Jaume-Santero, F., Pickler, C., Beltrami, H., and Mareschal, J.-C. (2016). North American regional climate reconstruction from ground surface temperature histories. *Climate of the Past*, **12**(12), 2181–2194. DOI: 10.5194/cp-12-2181-2016.

Johnson, G. C., Lyman, J. M., and Loeb, N. G. (2016). Improving estimates of Earth's energy imbalance. *Nature Climate Change*, **6**, 639 EP –.

Knutti, R., Furrer, R., Tebaldi, C., Cermak, J., and Meehl, G. A. (2010). Challenges in Combining Projections from Multiple Climate Models. *Journal of Climate*, **23**(10), 2739–2758. DOI: 10.1175/2009JCLI3361.1.

Knutti, R., Rugenstein, M. A. A., and Hegerl, G. C. (2017). Beyond equilibrium climate sensitivity. *Nature Geoscience*, **10**, 727–736. DOI: 10.1038/ngeo3017.

Koven, C. D., Ringeval, B., Friedlingstein, P., Ciais, P., Cadule, P., Khvorostyanov, D., Krinner, G., and Tarnocai, C. (2011). Permafrost carbon-climate feedbacks accelerate global warming. *Proceedings of the National Academy of Sciences*, **108**(36), 14769–14774. DOI: 10.1073/pnas.1103910108.

Kurokawa, H., Sato, M., Ushioda, M., Matsuyama, T., Moriwaki, R., Dohm, J., and Usui, T. (2014). Evolution of water reservoirs on Mars: Constraints from hydrogen isotopes in martian meteorites. *Earth and Planetary Science Letters*, **394**, 179 –185. DOI: https://doi.org/10.1016/j.epsl.2014.03.027.

Levitus, S., Antonov, J., and Boyer, T. (2005). Warming of the world ocean, 1955–2003. *Geophysical Research Letters*, **32**(2). n/a–n/a. DOI: 10.1029/2004GL021592.

Levitus, S., Antonov, J. I., Boyer, T. P., Baranova, O. K., Garcia, H. E., Locarnini, R. A., Mishonov, A. V., Reagan, J. R., Seidov, D., Yarosh, E. S., and Zweng, M. M. (2012). World ocean heat content and thermosteric sea level change (0–2000 m), 1955–2010. *Geophysical Research Letters*, **39**(10). n/a–n/a. DOI: 10.1029/2012GL051106.

Loeb, N. G., Wielicki, B. A., Doelling, D. R., Smith, G. L., Keyes, D. F., Kato, S., Manalo-Smith, N., and Wong, T. (2009). Toward Optimal Closure of the Earth's Top-of-Atmosphere Radiation Budget. *Journal of Climate*, **22**(3), 748–766. DOI: 10.1175/2008JCLI2637.1.

Loeb, N. G., Lyman, J. M., Johnson, G. C., Allan, R. P., Doelling, D. R., Wong, T., Soden, B. J., and Stephens, G. L. (2012). Observed changes in top-of-the-atmosphere radiation and upper-ocean heating consistent within uncertainty. *Nature Geosci*, **5**(2), 110–113.

MacDougall, A. H., Avis, C. A., and Weaver, A. J. (2012). Significant contribution to climate warming from the permafrost carbon feedback. *Nature Geosci*, **5**(10), 719–721. DOI: 10.1038/ngeo1573.

Manabe, S. and Wetherald, R. T. (1967). Thermal Equilibrium of the Atmosphere with a Given Distribution of Relative Humidity. *Journal of the Atmospheric Sciences*, **24**(3), 241–259. DOI: 10.1175/1520-0469(1967)024<0241:TEOTAW>2.0.CO;2.

Manabe, S., Bryan, K., and Spelman, M. J. (1975). A Global Ocean-Atmosphere Climate Model. Part I. The Atmospheric Circulation. *Journal of Physical Oceanography*, **5**(1), 3–29. DOI: 10.1175/1520-0485(1975)005<0003:AGOACM>2.0.CO;2.

Masson-Delmotte, V., Schulz, M., Abe-Ouchi, A., Beer, J., Ganopolski, A., González Rouco, J., Jansen, E., Lambeck, K., Luterbacher, J., Naish, T., Osborn, T., Otto-Bliesner, B., Quinn, T., Ramesh, R., Rojas, M., Shao, X., and Timmermann, A. (2013). "Information from Paleoclimate Archives". In: *Climate Change 2013: The Physical Science Basis. Contribution of Working Group I to the Fifth Assessment Report of the Intergovernmental Panel on Climate Change*. Ed. by T. Stocker, D. Qin, G.-K. Plattner, M. Tignor, S. Allen, J. Boschung, A. Nauels, Y. Xia, V. Bex, and P. Midgley. Cambridge, United Kingdom and New York, NY, USA: Cambridge University Press. Chap. 5, pp. 383–464. DOI: 10.1017/CBO9781107415324.013.

Mauritsen, T., Stevens, B., Roeckner, E., Crueger, T., Esch, M., Giorgetta, M., Haak, H., Jungclaus, J., Klocke, D., Matei, D., Mikolajewicz, U., Notz, D.,

Pincus, R., Schmidt, H., and Tomassini, L. (2012). Tuning the climate of a global model. *Journal of Advances in Modeling Earth Systems*, **4**(3). n/a–n/a. DOI: 10.1029/2012MS000154.

McFarlane, N. (2011). Parameterizations: representing key processes in climate models without resolving them. *Wiley Interdisciplinary Reviews: Climate Change*, **2**(4), 482–497. DOI: 10.1002/wcc.122.

Meyers, S. R. and Malinverno, A. (2018). Proterozoic Milankovitch cycles and the history of the solar system. *Proceedings of the National Academy of Sciences*, **115**(25), 6363–6368. DOI: 10.1073/pnas.1717689115.

Milankovitch, M. (1920). *Théorie Mathématique des Phénomènes Thermiques Produits par la Radiation Solaire*. Paris Gauthier-Villars.

NOAA (2019). *Borehole Database at National Oceanic and Atmospheric Administration's Server*. https://www.ncdc.noaa.gov/data-access/paleoclimatology-data/datasets/borehole [Last acessed September 2019].

PAGES 2k-PMIP3 Group (2015). Continental-scale temperature variability in PMIP3 simulations and PAGES 2k regional temperature reconstructions over the past millennium. *Climate of the Past*, **11**(12), 1673–1699. DOI: 10.5194/cp-11-1673-2015.

PAGES Hydro2k Consortium (2017). Comparing proxy and model estimates of hydroclimate variability and change over the Common Era. *Climate of the Past*, **13**(12), 1851–1900. DOI: 10.5194/cp-13-1851-2017.

Peacock, S. and Maltrud, M. (2006). Transit-Time Distributions in a Global Ocean Model. *Journal of Physical Oceanography*, **36**(3), 474–495. DOI: 10.1175/JPO2860.1.

Phillips, N. A. (1956). The general circulation of the atmosphere: A numerical experiment. *Quarterly Journal of the Royal Meteorological Society*, **82**(352), 123–164. DOI: 10.1002/qj.49708235202.

Pickler, C., Gurza Fausto, E., Beltrami, H., Mareschal, J.-C., Suárez, F., Chacon-Oecklers, A., Blin, N., Cortés Calderón, M. T., Montenegro, A., Harris, R., and Tassara, A. (2018). Recent climate variations in Chile: constraints from

borehole temperature profiles. *Climate of the Past*, **14**(4), 559–575. DOI: 10.5194/cp-14-559-2018.

Pierrehumbert, R. T. (2010). *Principles of planetary climate*. Cambridge University Press.

Rahmstorf, S. (1995). Climate drift in an ocean model coupled to a simple, perfectly matched atmosphere. *Climate Dynamics*, **11**(8), 447–458. DOI: 10.1007/BF00207194.

Rhein, M., Rintoul, S., Aoki, S., Campos, E., Chambers, D., Feely, R., Gulev, S., Johnson, G., Josey, S., Kostianoy, A., Mauritzen, C., Roemmich, D., Talley, L., and Wang, F. (2013). "Observations: Ocean". In: *Climate Change 2013: The Physical Science Basis. Contribution of Working Group I to the Fifth Assessment Report of the Intergovernmental Panel on Climate Change*. Ed. by T. Stocker, D. Qin, G.-K. Plattner, M. Tignor, S. Allen, J. Boschung, A. Nauels, Y. Xia, V. Bex, and P. Midgley. Cambridge, United Kingdom and New York, NY, USA: Cambridge University Press. Chap. 3, pp. 255–316. DOI: 10.1017/CBO9781107415324.010.

Royer, D. L. (2006). CO2-forced climate thresholds during the Phanerozoic. *Geochimica et Cosmochimica Acta*, **70**(23). 5665 –5675. DOI: https://doi.org/10.1016/j.gca.2005.11.031.

Santer, B. D., Taylor, K. E., Wigley, T. M. L., Johns, T. C., Jones, P. D., Karoly, D. J., Mitchell, J. F. B., Oort, A. H., Penner, J. E., Ramaswamy, V., Schwarzkopf, M. D., Stouffer, R. J., and Tett, S. (1996). A search for human influences on the thermal structure of the atmosphere. *Nature*, **382**, 39 EP –. DOI: 10.1038/382039a0.

Santer, B. D., Bonfils, C. J. W., Fu, Q., Fyfe, J. C., Hegerl, G. C., Mears, C., Painter, J. F., Po-Chedley, S., Wentz, F. J., Zelinka, M. D., and Zou, C.-Z. (2019). Celebrating the anniversary of three key events in climate change science. *Nature Climate Change*, **9**(3), 180–182. DOI: 10.1038/s41558-019-0424-x.

Schmidt, G. A., Annan, J. D., Bartlein, P. J., Cook, B. I., Guilyardi, E., Hargreaves, J. C., Harrison, S. P., Kageyama, M., LeGrande, A. N., Konecky, B., Lovejoy,

S., Mann, M. E., Masson-Delmotte, V., Risi, C., Thompson, D., Timmermann, A., Tremblay, L.-B., and Yiou, P. (2014). Using palaeo-climate comparisons to constrain future projections in CMIP5. *Climate of the Past*, **10**(1), 221–250. DOI: 10.5194/cp-10-221-2014.

Schmidt, G. A., Bader, D., Donner, L. J., Elsaesser, G. S., Golaz, J.-C., Hannay, C., Molod, A., Neale, R. B., and Saha, S. (2017). Practice and philosophy of climate model tuning across six US modeling centers. *Geoscientific Model Development*, **10**(9), 3207–3223. DOI: 10.5194/gmd-10-3207-2017.

Seager, S. (2013). Exoplanet Habitability. *Science*, **340**(6132), 577–581. DOI: 10.1126/science.1232226.

Séférian, R., Gehlen, M., Bopp, L., Resplandy, L., Orr, J. C., Marti, O., Dunne, J. P., Christian, J. R., Doney, S. C., Ilyina, T., Lindsay, K., Halloran, P. R., Heinze, C., Segschneider, J., Tjiputra, J., Aumont, O., and Romanou, A. (2016). Inconsistent strategies to spin up models in CMIP5: implications for ocean biogeochemical model performance assessment. *Geoscientific Model Development*, **9**(5), 1827–1851. DOI: 10.5194/gmd-9-1827-2016.

Sellers, W. D. (1969). A Global Climatic Model Based on the Energy Balance of the Earth-Atmosphere System. *Journal of Applied Meteorology*, **8**(3), 392–400. DOI: 10.1175/1520-0450(1969)008<0392:AGCMBO>2.0.CO;2.

Sen Gupta, A., Muir, L. C., Brown, J. N., Phipps, S. J., Durack, P. J., Monselesan, D., and Wijffels, S. E. (2012). Climate Drift in the CMIP3 Models. *Journal of Climate*, **25**(13), 4621–4640. DOI: 10.1175/JCLI-D-11-00312.1.

Sen Gupta, A., Jourdain, N. C., Brown, J. N., and Monselesan, D. (2013). Climate Drift in the CMIP5 Models. *Journal of Climate*, **26**(21), 8597–8615. DOI: 10.1175/JCLI-D-12-00521.1.

Sherwood, S. C., Bony, S., and Dufresne, J.-L. (2014). Spread in model climate sensitivity traced to atmospheric convective mixing. *Nature*, **505**(7481), 37–42. DOI: 10.1038/nature12829.

Smerdon, J. E. (2012). Climate models as a test bed for climate reconstruction methods: pseudoproxy experiments. *Wiley Interdisciplinary Reviews: Climate Change*, **3**(1), 63–77. DOI: 10.1002/wcc.149.

Smith, D. M., Allan, R. P., Coward, A. C., Eade, R., Hyder, P., Liu, C., Loeb, N. G., Palmer, M. D., Roberts, C. D., and Scaife, A. A. (2015). Earth's energy imbalance since 1960 in observations and CMIP5 models. *Geophysical Research Letters*, **42**(4), 1205–1213. DOI: 10.1002/2014GL062669.

Spiegel, D. S., Menou, K., and Scharf, C. A. (2008). Habitable Climates. *The Astrophysical Journal*, **681**(2), 1609–1623. DOI: 10.1086/588089.

Spiegel, D. S., Raymond, S. N., Dressing, C. D., Scharf, C. A., and Mitchell, J. L. (2010). Generalized Milankovitch Cycles Aand Long-Term Climatic Habitability. *The Astrophysical Journal*, **721**(2), 1308–1318. DOI: 10.1088/0004-637x/721/2/1308.

Stainforth, D. A., Downing, T. E., Washington, R., Lopez, A., and New, M. (2007). Issues in the interpretation of climate model ensembles to inform decisions. *Philosophical Transactions of the Royal Society of London A: Mathematical, Physical and Engineering Sciences*, **365**(1857), 2163–2177. DOI: 10.1098/rsta.2007.2073.

Stouffer, R. J., Manabe, S., and Bryan, K. (1989). Interhemispheric asymmetry in climate response to a gradual increase of atmospheric CO2. *Nature*, **342**, 660 –662. DOI: 10.1038/342660a0.

Suman, A., Dyer, F., and White, D. (2017). Late Holocene temperature variability in Tasmania inferred from borehole temperature data. *Climate of the Past*, **13**(6), 559–572. DOI: 10.5194/cp-13-559-2017.

Sun, Y., Joachimski, M. M., Wignall, P. B., Yan, C., Chen, Y., Jiang, H., Wang, L., and Lai, X. (2012). Lethally Hot Temperatures During the Early Triassic Greenhouse. *Science*, **338**(6105), 366–370. DOI: 10.1126/science.1224126.

Tang, Y., Li, L., Dong, W., and Wang, B. (2016). Reducing the climate shift in a new coupled model. *Science Bulletin*, **61**(6), 488–494. DOI: 10.1007/s11434-016-1033-y.

Taylor, K. E., Stouffer, R. J., and Meehl, G. A. (2011). An Overview of CMIP5 and the Experiment Design. *Bulletin of the American Meteorological Society*, **93**(4), 485–498. DOI: 10.1175/BAMS-D-11-00094.1.

Trenberth, K. E., Fasullo, J. T., and Balmaseda, M. A. (2014). Earth's Energy Imbalance. *Journal of Climate*, **27**(9), 3129–3144. DOI: 10.1175/JCLI-D-13-00294.1.

Van Der Meer, D. G., Zeebe, R. E., van Hinsbergen, D. J. J., Sluijs, A., Spakman, W., and Torsvik, T. H. (2014). Plate tectonic controls on atmospheric CO2 levels since the Triassic. *Proceedings of the National Academy of Sciences*, **111**(12), 4380–4385. DOI: 10.1073/pnas.1315657111.

Von Schuckmann, K., Palmer, M. D., Trenberth, K. E., Cazenave, A., Chambers, D., Champollion, N., Hansen, J., Josey, S. A., Loeb, N., Mathieu, P. P., Meyssignac, B., and Wild, M. (2016). An imperative to monitor Earth's energy imbalance. *Nature Climate Change*, **6**, 138 EP –.

Von Schuckmann, K., Cheng, L., Palmer, M. D., Hansen, J., Tassone, C., Aich, V., Adusumilli, S., Beltrami, H., Boyer, T., Cuesta-Valero, F. J., Desbruyères, D., Domingues, C., García-García, A., Gentine, P., Gilson, J., Gorfer, M., Haimberger, L., Ishii, M., Johnson, G. C., Killick, R., King, B. A., Kirchengast, G., Kolodziejczyk, N., Lyman, J., Marzeion, B., Mayer, M., Monier, M., Monselesan, D. P., Purkey, S., Roemmich, D., Schweiger, A., Seneviratne, S. I., Shepherd, A., Slater, D. A., Steiner, A. K., Straneo, F., Timmermans, M.-L., and Wijffels, S. E. (2020). Heat stored in the Earth system: where does the energy go? *Earth System Science Data*, **12**(3), 2013–2041. DOI: 10.5194/essd-12-2013-2020.

Voosen, P. (2016). Climate scientists open up their black boxes to scrutiny. *Science*, **354**(6311), 401–402. DOI: 10.1126/science.354.6311.401.

Washington, W. M. and Meehl, G. A. (1989). Climate sensitivity due to increased CO2: experiments with a coupled atmosphere and ocean general circulation model. *Climate Dynamics*, **4**(1), 1–38. DOI: 10.1007/BF00207397.

Wunsch, C. and Heimbach, P. (2008). How long to oceanic tracer and proxy equilibrium? *Quaternary Science Reviews*, **27**(7–8), 637 –651. DOI: http://dx.doi.org/10.1016/j.quascirev.2008.01.006.

2 Long-Term Surface Temperature (LoST) Database as a Complement for GCM Preindustrial Simulations

Reference This chapter is based on the publication: Cuesta-Valero, F. J. et al. (2019). Long-term Surface Temperature (LoST) database as a complement for GCM preindustrial simulations. *Climate of the Past*, **15**(3), 1099–1111. DOI: 10.5194/cp-15-1099-2019.

Abstract Estimates of climate sensitivity from atmosphere-ocean Coupled General Circulation Model (CGCM) simulations still present a large spread despite the continued improvements in climate modeling since the 1970s. This variability is partially caused by the dependence of several long-term feedback mechanisms on the reference climate state. Indeed, state-of-the-art CGCMs present a large spread of control climate states, partially due to the lack of a suitable reference for constraining the climatology of preindustrial simulations. We assemble a new gridded database of long-term ground surface temperatures (LoST database) obtained from geothermal data over North America, and we explore its use as a potential reference for the evaluation of CGCM preindustrial simulations. We compare the LoST database with meteorological observations, as well as with five past millennium transient climate simulations and five preindustrial control simulations from the third phase of the Paleoclimate Modelling

Intercomparison Project (PMIP3) and the fifth phase of the Coupled Model Intercomparison Project (CMIP5). The database is consistent with meteorological observations as well as with both types of preindustrial simulations, which suggests that LoST temperatures can be employed as a reference to narrow the spread of surface temperature climatologies on CGCM preindustrial control and past millennium simulations.

2.1 Introduction

Atmosphere-ocean Coupled General Circulation Model (CGCM) simulations of the Earth's climate are sophisticated tools that reproduce the dominant physical processes of the climate system, helping to understand and characterize the dynamics of the climate system at both global and regional scales, as well as from decadal to millennial timescales (Flato et al., 2013). Despite the large number of different CGCMs developed and maintained by modeling groups around the world, future projections of climate change still present a large degree of uncertainty (Knutti et al., 2012), mainly due to the different climate sensitivity achieved by each model. The Equilibrium Climate Sensitivity (ECS) is typically defined as the change in equilibrium temperature given a doubling of atmospheric CO_2 concentration (Gregory et al., 2002), and it is considered one of the most important metrics for understanding the long-term evolution of the climate system. Numerous studies, nonetheless, have unsuccessfully tried to narrow the uncertainty range of ECS using observations, simulations and paleoreconstructions; the best estimates of ECS have remained between 1.5 °C and 4.5 °C since the 1970s (Knutti et al., 2017).

The large uncertainty in ECS estimates is also present in state-of-the-art CGCMs (Andrews et al., 2012; Flato et al., 2013; Forster et al., 2013; Knutti et al., 2017), mainly as a result of approximating the description of several climate phenomena, tuning practices, and the spread in control climate states. Each CGCM approximates and resolves the differential equations governing the evolution of the climate system using different numerical methods and algorithms, leading to a diverse representation of the climate evolution within the array of models (Dommenget, 2016). Additionally, CGCMs may employ different parameterizations for approximating processes that cannot be resolved due to the

lack of spatial resolution or computational resources, such as radiative transfer, convection or clouds (McFarlane, 2011; Sen Gupta et al., 2013). All these necessary approximations add inconsistencies to simulations, affecting the simulated climate state and trajectory. Parameterizations of radiative forcing by CO_2 in climate models are of special importance, being responsible for nearly 50% of the uncertainties in the estimated values of ECS (Soden et al., 2018). Another practice related to parameterizations that affects the simulated ECS is model tuning (Mauritsen et al., 2012; Hourdin et al., 2017; Schmidt et al., 2017). Tuning practices involve varying model parameters, whose values are poorly constrained by theory or observations or not constrained at all, to obtain a simulated climate evolution compatible with observations. Thereby, this parameter adjustment affects the representation of feedback mechanisms and other physical processes within the model, altering the response to external forcings (Mauritsen et al., 2012; Schmidt et al., 2017).

Furthermore, the magnitude of some important long-term feedback mechanisms depends on the mean climate state – i.e., the model response to external forcings is itself mean state dependent (Dommenget, 2016; Hu et al., 2017, and references therein). Ice-albedo and water vapor feedbacks are two important processes affected by the control climate state (Hu et al., 2017). The strength of both feedbacks is associated with simulated absolute values of surface temperature, since absolute temperature is the main factor governing water phase changes on the Earth. Permafrost stability, and thus permafrost carbon feedback, also depends on the reference climatology and the simulated climate trajectory (Slater et al., 2013). Although many CGCMs are still in the process of implementing permafrost modules in their code, several studies have suggested that the impact of the permafrost carbon feedback on climate evolution would be important (e.g., Koven et al., 2011; MacDougall et al., 2012). Therefore, a constrained preindustrial control simulation may improve the representation of those feedbacks in transient climate experiments, reducing the uncertainty of ECS estimates from model simulations, as well as reducing the spread in projections of future climate change (Dommenget, 2016; Hu et al., 2017). At this point, estimates of preindustrial long-term surface temperatures from geothermal data may be a useful reference for assessing wether the simulated surface temperature climatology is realistic enough in preindustrial climate simulations. Additionally,

such preindustrial long-term absolute temperatures may be employed to define a preindustrial baseline from which to evaluate the temperature change due to the anthropogenic influence on climate (Hawkins et al., 2017).

Borehole Temperature Profile (BTP) measurements have been employed to estimate past trends of both global and regional surface temperature (e.g., Vasseur et al., 1983; Huang et al., 2000; Harris et al., 2001; Beltrami, 2002; Beltrami et al., 2004) and surface flux histories over the last few centuries (e.g., Wang et al., 1999; Beltrami, 2002; Beltrami et al., 2002, 2006; Demezhko et al., 2015a; Demezhko et al., 2015b). Several studies have validated the borehole methodology using past millennium simulations from the ECHO-G CGCM (González-Rouco et al., 2006; González-Rouco et al., 2009) and the PMIP3/CMIP5 CGCMs (García-García et al., 2016), reinforcing results retrieved from subsurface temperatures. Reconstructions of surface temperature and surface flux from borehole measurements have been compared with ECHO-G millennial simulations (Stevens et al., 2008; MacDougall et al., 2010), as well as with estimates of continental heat storage from CMIP5 CGCM simulations (Cuesta-Valero et al., 2016). All these direct comparisons between BTP estimates and CGCM simulations have revealed several strengths and weaknesses of CGCM simulations, and have contributed to the improvement of the represented physical processes relevant for the climate evolution within land surface model components (e.g., Alexeev et al., 2007; MacDougall et al., 2017).

Here, we propose the use of long-term surface temperatures estimated from BTP measurements as an additional tool to better evaluate the accuracy of surface temperature climatology within CGCM preindustrial simulations, and thereby help to improve the representation of mean state dependent feedbacks. These long-term surface temperatures are retrieved from the quasi-equilibrium state of the subsurface thermal regime at the location of each BTP measurement. This is estimated from the deepest section of the temperature profile, which is the part least affected by the recent changes in the surface energy balance. The subsurface temperature at the bottom part of each temperature profile depends linearly on depth, and the extrapolation of this linear behavior to the surface is interpreted as the long-term mean surface temperature at each borehole site (e.g. Huang et al., 2000; Harris et al., 2001; Beltrami, 2002). We present here a gridded Long-term Surface Temperature database (LoST) for most of

continental North America and three Caribbean islands (Cuba, Hispaniola and Puerto Rico) using 514 BTP measurements. This database is freely available for the scientific community at `https://figshare.com/s/f20d6002a57cf3279a1c`. The database is compared with five past millennium and five preindustrial control simulations from the PMIP3/CMIP5 archive to assess the realism of the simulated preindustrial equilibrium state by the current generation of global climate models.

2.2 Data

2.2.1 Meteorological data: Climate Research Unit (CRU) Data

We employ surface air temperatures from the Climatic Research Unit at the University of East Anglia (CRU) TS4.01 gridded dataset (Harris et al., 2014) for evaluation purposes. This dataset consists of a gridded set of climate variables derived from meteorological observations worldwide. Sources of meteorological data include several national meteorological services, CRU archives, the World Meteorological Organization (WMO) and the National Oceanic and Atmospheric Administration (NOAA). Surface air temperatures are supplied at monthly resolution for continental areas except for Antarctica from 1901 to 2016 of the Common Era (CE).

2.2.2 CGCM Data

We use five Past Millennium (PM) and five Preindustrial Control (piControl) CGCM simulations (see Table 2.1 for references) from the third phase of the Paleoclimate Modelling Intercomparison Project (PMIP3) and the fifth phase of the Coupled Model Intercomparison Project (CMIP5) (Braconnot et al., 2012; Taylor et al., 2011) to test the LoST database. PM simulations (Past1000 experiment in the PMIP3/CMIP5 database) simulate the climate response to prescribed external forcings from Schmidt et al. (2011) for the period 850-1850 CE, including orbital variations, changes in solar activity, greenhouse gas concentrations, volcanic aerosols and changes in land use and land cover. Each PMIP3/CMIP5 CGCM also performs a piControl simulation forced with common preindustrial forcings to provide a baseline from which to start transient climate experiments.

For more details about the PMIP3/CMIP5 control simulations and initialization procedures see Sen Gupta et al. (2013) and Séférian et al. (2016).

2.2.3 Borehole Data

Here, we use estimates of long-term surface temperatures from the database described in Jaume-Santero et al. (2016). The BTP measurements of this database have been previously filtered to exclude profiles with non-climatic signals and artifacts, thus providing 514 BTPs suitable for climate studies over North America. The standard methodology to retrieve past temperature and flux histories from geothermal data assumes that each borehole temperature profile results from the superposition of a transient perturbation due to the changes in the surface energy balance with time and the quasi steady-state of the subsurface thermal regime (e.g. Huang et al., 2000; Harris et al., 2001; Beltrami, 2002). Therefore, considering the subsurface as a half space without heat production from radioactive decay or advection, the solution of the heat diffusion equation for a temperature profile can be approximated as (e.g., Jaume-Santero et al., 2016):

$$T(z) = T_0 + q_0 \cdot R(z) + T_t(t), \tag{2.1}$$

where T_t is the surface transient perturbation, T_0 is the long-term surface temperature (T_0 temperature hereafter), q_0 is the subsurface flux at equilibrium and $R(z)$ is the thermal resistance (Bullard et al., 1939). Estimates of thermal resistance require measurements of thermal conductivity through the subsurface profile, but the majority of available BTPs do not provide such conductivity data. Thus, the thermal conductivity is assumed to be constant and Eq. (2.1) is rewritten as

$$T(z) = T_0 + \Gamma \cdot z + T_t(t), \tag{2.2}$$

where Γ is the subsurface thermal gradient at equilibrium. The recorded surface transient perturbation (T_t) can be retrieved from each temperature profile, once the subsurface thermal equilibrium is estimated (for more details about the borehole methodology, see Mareschal et al., 1992; Bodri et al., 2007; Jaume-Santero et al., 2016). As the heat flux from the Earth's interior remains stable at time scales of millions of years and the deepest part of a BTP is the least affected by the recent changes in the surface energy balance, the quasi-equilibrium state of

the subsurface thermal regime can be estimated from the deepest temperatures of each borehole profile (see scheme in Figure 2.1). Once vertical variations in thermal properties of the subsurface rocks are taken into account, temperature depends linearly on depth at the bottom part of the temperature profile, allowing the subsurface thermal equilibrium to be approximated by a linear least-squares regression. The extrapolation of this linear behavior to the surface can be interpreted as the long-term mean surface temperature at each borehole location (T_0 temperature in Eq. 3.1 and Figure 2.1, see Pickler et al., 2016 for further details). Depending on the profile's depth, the T_0 temperatures represent the long-term ground surface temperature for a determined period of time. Due to the nature of heat diffusion through the ground, the required time (t) for a change in the surface energy balance to reach a certain depth (z) is given by (Carslaw et al., 1959; Pickler et al., 2016):

$$t \approx \frac{z^2}{4\kappa}, \tag{2.3}$$

where κ is the thermal diffusivity of the subsurface. We consider κ=$1 \times 10^{-6}\,m^2\,s^{-1}$ for all BTP measurements (Cermak et al., 1982). In this study, all BTPs are truncated at the same depth (300 m) to ensure that all T_0 temperatures are estimated for the same temporal period. We use the last hundred meters of each BTP to estimate the subsurface thermal equilibrium, obtaining an estimated temporal period that approximately ranges from ~ 1300 CE (z=300 m) to ~ 1700 CE (z=200 m). Thereby, this period of time provides a baseline to compare with long-term temperatures from the PMIP3/CMIP5 PM simulations. However, the estimated temporal period is not homogeneous as a result of the non-linear relationship between time and depth (Beltrami et al., 1995b), and thus estimates of relatively recent years (i.e., 1700 CE) are better determined than estimates of past years (1300 CE). Influences of long-term perturbations of the past surface energy budget outside of that temporal window may also affect the temperature within the depth range used here, see Section 2.5 for more details.

2.3 The LoST Database

In order to provide a gridded dataset over continental North America, T_0 temperatures from BTP measurements are spatially interpolated to a 0.5°×0.5° grid

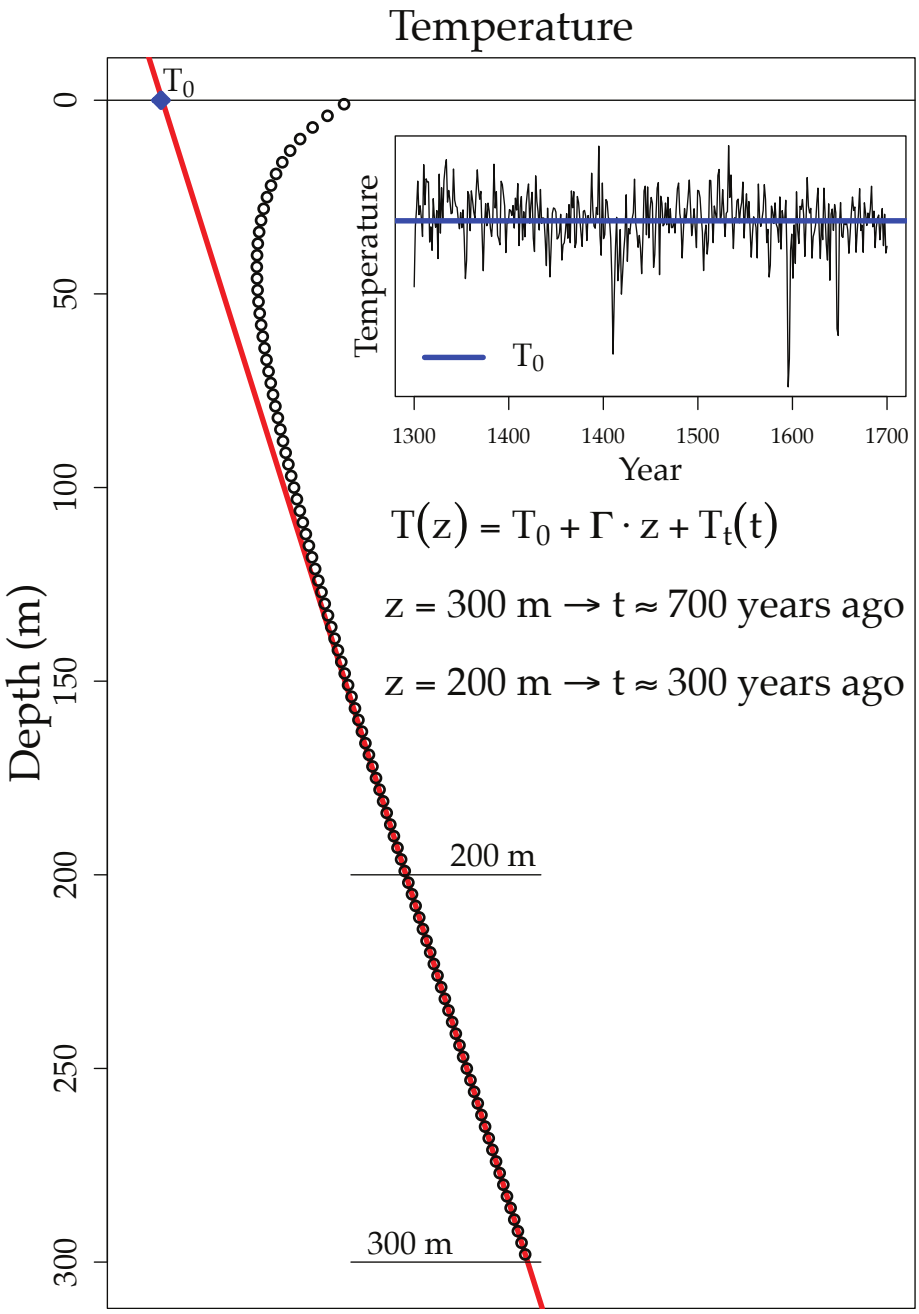

Figure 2.1: Synthetic borehole temperature profile (black dots) using data from the CCSM4 PM simulation (inset) and linear fit of temperatures between 200 m and 300 m (red line). The synthetic temperature profile is generated using the simulated global ground temperature anomaly at 1.0 m depth for the period 1300-1700 CE as transient perturbation (T_t), mean ground temperature as long-term surface temperature (T_0) and a typical thermal gradient (Γ) of 0.01 K m^{-1} (Jaume-Santero et al., 2016). The equivalence between depth (z) and time (t) is given by Eq. 2.3. Thermal diffusivity is considered as κ=1 $\times$ 10^{-6} m^2 s^{-1} (Cermak et al., 1982).

using the Gradient plus Inverse Distance Squared (GIDS) technique. The GIDS method (Nalder et al., 1998) relies on multiple linear regression of observed climate variables to retrieve longitudinal, latitudinal and altitudinal gradients that are employed to estimate values for gridded nodes. The contribution of each measurement is inverse-weighted by their squared distance to the target node, while the coefficients from the regression analysis allow to correct for the location of each measurement:

$$V_0 = \frac{\sum_{i=1}^{N} \left[V_i + (lat_0 - lat_i)C_{lat} + (lon_0 - lon_i)C_{lon} + (z_0 - z_i)C_z\right] d_i^{-2}}{\sum_{i=1}^{N} d_i^{-2}}, \qquad (2.4)$$

where V_0 is the predicted variable at the target node, V_i, lat_i, lon_i and z_i represent the variable, latitude, longitude and altitude of the i^{th} measurement respectively, lat_0, lon_0 and z_0 represent the latitude, longitude and altitude of the target node respectively, C_{lat}, C_{lon} and C_z are the coefficients from the regression analysis, and d_i is the distance from the i^{th} measurement to the target node. The propagation of known errors in the GIDS algorithm is described in Section 2.3.1. The GIDS technique has been used to interpolate surface temperature, precipitation, evapotranspiration and other climate variables in several zones of the world including North America (e.g., Price et al., 2000; Mardikis et al., 2005). Furthermore, the GIDS method performs well in comparison with other broadly used interpolation techniques like co-kriging or smoothing splines (ANUSPLIN suite) (Nalder et al., 1998; Price et al., 2000; Li et al., 2011), and it has been previously employed to downscale CMIP5 simulations (McCullough et al., 2016).

Since the T_0 dataset employed here provides latitudes and longitudes for each temperature profile, we expand the database estimating the altitude above sea level for each BTP measurement from the second version of the 2-minute Gridded Global Relief Data (ETOPO2) of the National Oceanic and Atmospheric Administration (National Geophysical Data Center, 2006). For this study, the regression analysis of T_0 temperatures considering latitude, longitude and altitude yields robust results, with a R^2 value of 0.865 and a p-Value $\ll 0.05$. The distance from the measurements to the nodes is computed using the Vincenty's formula for an ellipsoid with different major and minor axes (Vincenty, 1975), and therefore the altitude of both measurements and grid nodes are not considered in our distance calculations.

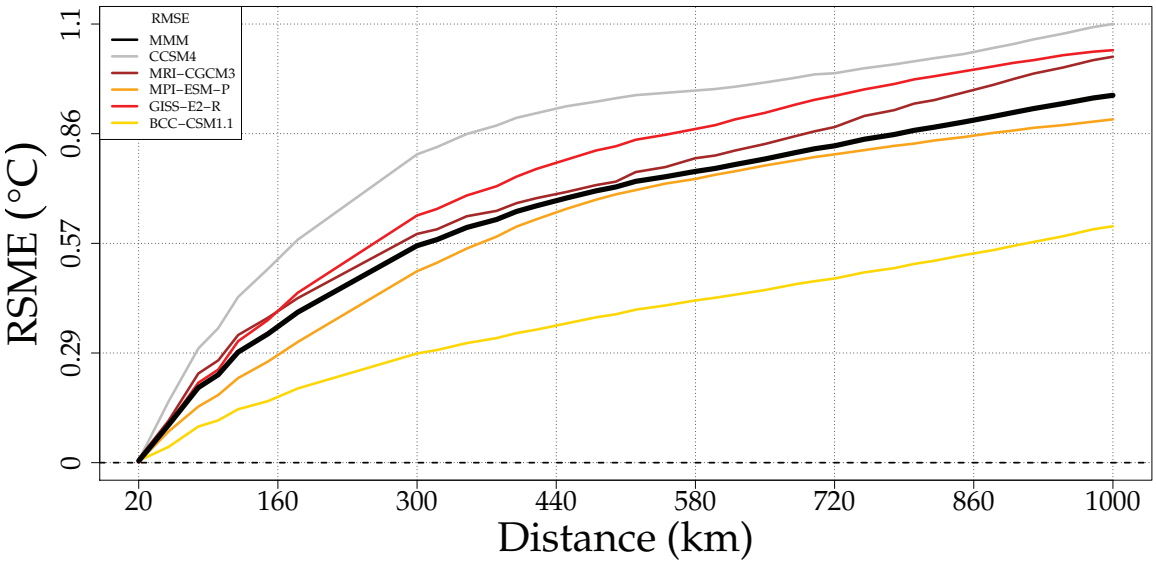

Figure 2.2: Root-Mean Squared Errors of the GIDS interpolation using ground surface temperatures at 1.0 m depth for the period 1300-1700 CE from the PMIP3/CMIP5 PM simulations to obtain a maximum distance criterion to interpolate each BTP measurement. The black line represents the multimodel mean (MMM).

We performed a pseudo-proxy experiment (e.g., Smerdon, 2012) to determine a maximum appropriate distance from a grid node to a BTP measurement to interpolate the T_0 temperatures. That is, we use the long-term mean ground surface temperatures for the period 1300-1700 CE from the five PMIP3/CMIP5 PM simulations as surrogate realities, and apply the interpolation methodology employed to create the LoST database. Thereby, these CGCM simulations were regridded to a $0.5°\times0.5°$ grid, considering grid cells containing BTP measurements as reference for applying Eq. 2.4 to the remaining grid cells. Then, Root Mean Squared Errors (RMSEs) between the interpolated data and the remapped simulations were computed (Figure 2.2). We set 650 km as the maximum distance criterion since this is the maximum distance at which the RMSE is lower than 1.0 °C for the five simulations. This distance criterion, nevertheless, produces results for three grid cells in the Yucatan peninsula (Mexico), which we consider unjustifiable as there are no BTP measurements in or near that part of Mexico. Those grid cells are therefore masked out from our analysis.

2.3.1 Error Propagation for LoST Database

The GIDS algorithm (Eq. 2.4) incorporates errors from the determination of the latitudinal, longitudinal and altitudinal gradients as well as errors from the T_0 estimates. Errors in T_0 temperatures are specified by the linear regression analysis employed to determine the T_0 values from each BTP measurement, while the linear regression analysis of the geographical distribution of T_0 temperatures provides the latitudinal, longitudinal and altitudinal gradients and their errors. Therefore, an estimate of the error in LoST temperatures at each grid cell of the database can by computed just by applying basic error propagation theory to Eq. 2.4, which results in:

$$\Delta V_0 = \frac{1}{\left|\sum_{i=1}^{N} d_i^{-1}\right|}\left[\sum_{i=1}^{N}\left\{\left(\Delta V_i^2 + (|lat_0 - lat_i|\,\Delta C_{lat})^2 + (|lon_0 - lon_i|\,\Delta C_{lon})^2 + (|z_0 - z_i|\,\Delta C_z)^2\right)^{1/2}\left|d_i^{-2}\right|\right\}^2\right]^{1/2}, \tag{2.5}$$

where ΔV_0 is the error of the predicted temperature at the target node, ΔV_i represents the T_0 error from the i^{th} BTP measurement, ΔC_{lat}, ΔC_{lon} and ΔC_z are the errors in the gradients from the regression analysis of the geographical distribution of T_0 data, lat_i, lon_i and z_i represent latitude, longitude and altitude of the i^{th} measurement respectively, lat_0, lon_0 and z_0 represent the latitude, longitude and altitude of the target node respectively, d_i is the distance from the i^{th} measurement to the target node, and N are the number of BTP measurements within a distance of 650 km to the target node. Errors in latitude, longitude and altitude are considered negligible, as well as the error in the distance between measurements and target nodes. Figure 2.3 shows the errors as 2σ values (i.e., $2 \times \Delta V_0$) for each grid cell, with a spatial average of 0.2 °C.

Beyond the propagation of known errors, other sources of uncertainty are possible but difficult to characterize given the limited temporal resolution of the LoST database. The most probable additional source of error is the distance criterion for the interpolation. This criterion was determined using a pseudo-proxy experiment and five PMIP3/CMIP5 PM simulations, obtaining different results

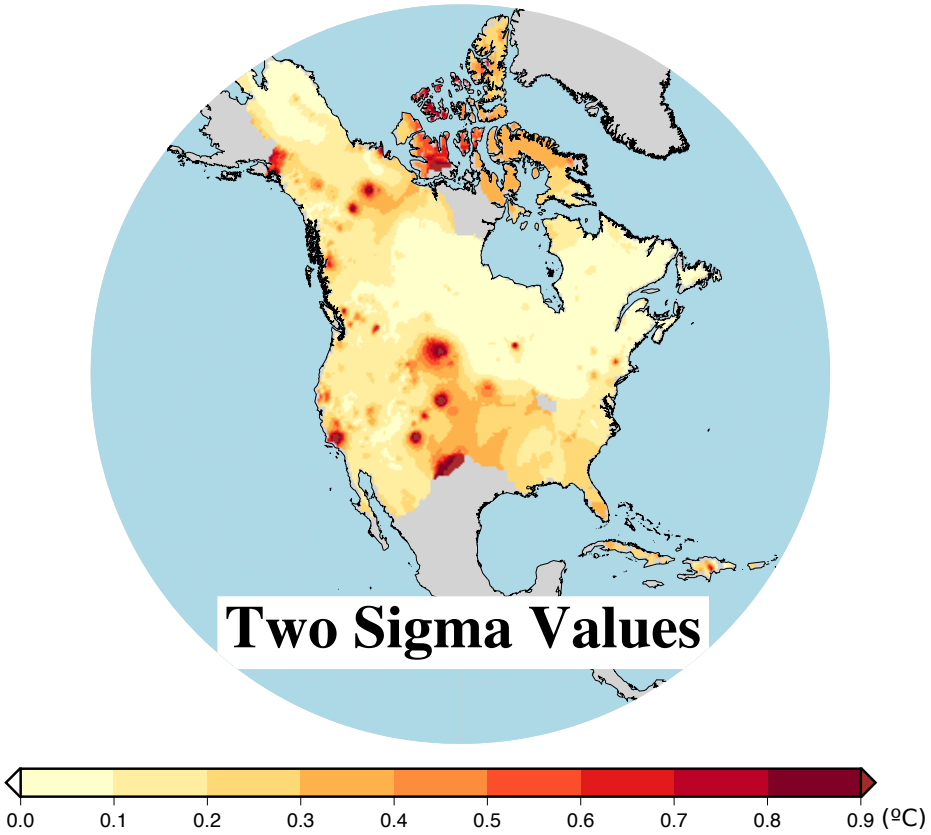

Figure 2.3: Errors (2σ values) of LoST temperatures estimated as described in Section 2.3.1. The spatial average is 0.2 °C.

for each model (Figure 2.2). However, we did not find any adequate method to characterize such error in the LoST database, and further sources of error are possible. Section 2.5 also discusses additional sources of uncertainty in LoST temperatures, but data limitations prevent us to characterize the error caused by those factors.

2.4 Results

The distribution of LoST temperatures at grid cells containing BTP measurements reproduces the shape of the distribution of raw T_0 temperatures (Figure 2.4a), indicating that the GIDS interpolation does not substantially modify the shape of the original distribution of temperatures retrieved from BTP measurements. However, the distribution of the entire LoST database resembles the distribution of CRU temperatures, differing from the distribution of the raw T_0 temperatures. This change in the temperature distribution after the spatial interpolation may be related to the inclusion of interpolated temperatures at higher and lower latitudes than the raw T_0 temperatures, as the majority of BTP measurements cover 35° N to 60° N. Nonetheless, the latitudinal mean temperatures from the LoST database are consistent with T_0 temperatures from BTP measurements, either considering only grid cells with BTP measurements or the entire LoST database (Figure 2.4b). The latitudinal mean temperatures from the LoST database reach higher values than the CRU database at latitudes higher than ~50° N, while both datasets achieve similar mean temperatures at lower latitudes (Figure 2.4b). Previous studies have found warmer ground temperatures than air temperatures in meteorological observations over North America, probably due to the insulating effect of snow cover during winter (e.g., Beltrami et al., 2003; Smerdon et al., 2003). That is, warmer temperatures should be expected for the LoST database than for the CRU database in cold regions, as our results confirm (Figure 2.4a and 2.4b). It should be noted, nevertheless, that the CRU database covers a period with a marked global temperature increase (Hartmann et al., 2013). Therefore, estimates of long-term surface temperatures from CRU data reflect this temperature increase, hindering the direct comparison of these datasets. Despite this difference in the climatology, the long-term surface temperature from the LoST dataset reproduces the expected spatial pattern

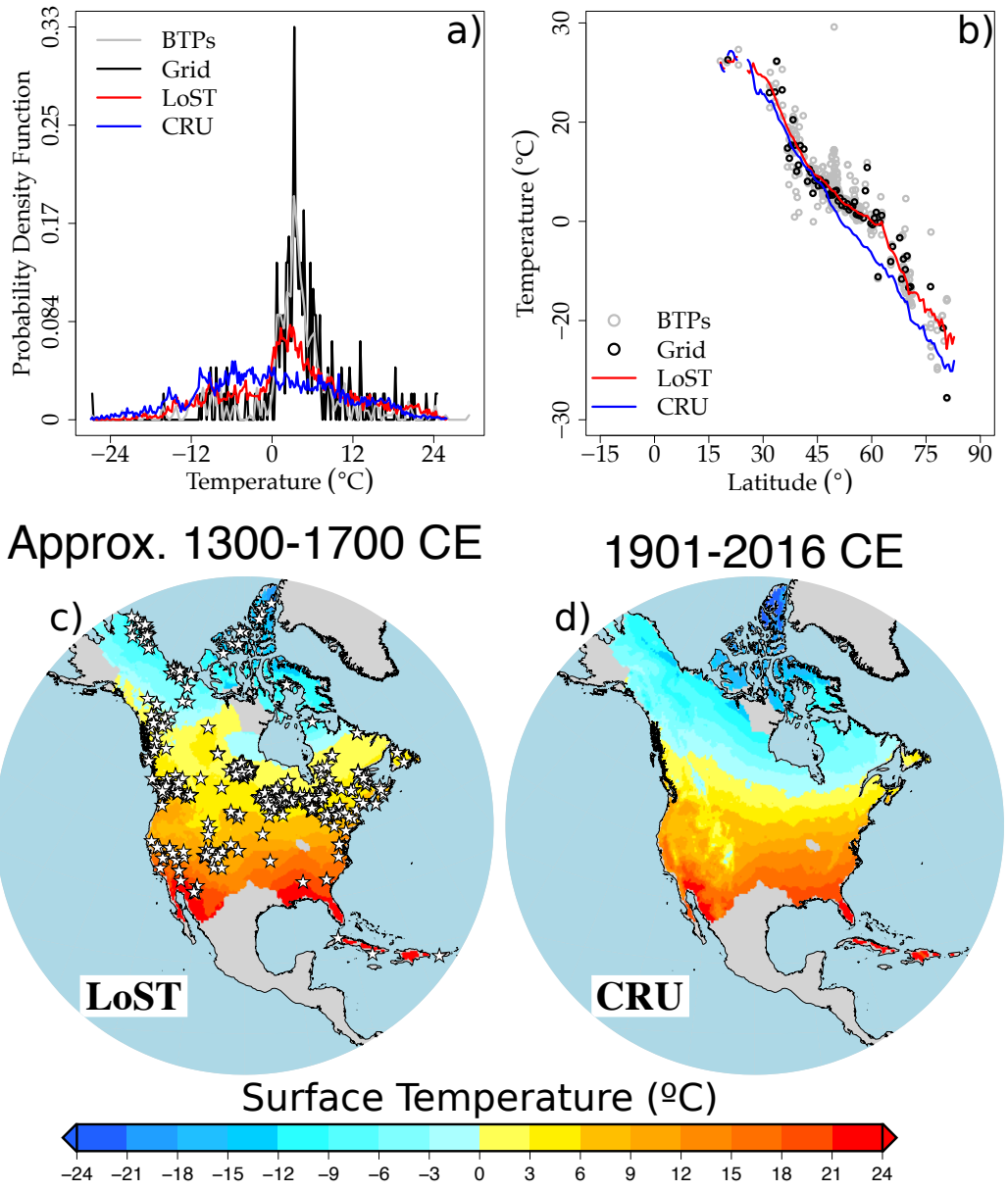

Figure 2.4: Histogram (a) and latitudinal mean temperatures (b) from BTP measurements (gray), LoST temperatures at grid cells containing BTP measurements (black), LoST temperatures (red) and mean surface air temperature from the CRU database (blue). LoST temperatures (~1300-1700 CE) (c) in comparison with mean surface air temperature from CRU data (1901-2015 CE) (d). White stars in (c) indicate the location of the 514 BTP measurements.

Table 2.1: Model name, SAT_0 estimates, GST_0 estimates, SAT_0 and GST_0 differences with the mean LoST temperatures, and references for each PMIP3/CMIP5 CGCM simulation. All results in °C. Ground temperatures for MRI-CGCM3 piControl simulation could not be retrieved from the PMIP3/CMIP5 data servers. Temperature average of the LoST database is 5.2 °C, with a 95% confidence interval between 5.0 °C and 5.4 °C.

			Past Millennium		
Model	SAT_0	GST_0	SAT_0-LoST	GST_0-LoST	Reference
CCSM4	1.53	5.60	-3.65	0.37	Landrum et al. (2013)
MRI-CGCM3	1.38	4.84	-3.81	-0.31	Yukimoto et al. (2012)
MPI-ESM-P	1.63	2.75	-3.56	-2.91	Jungclaus et al. (2014)
GISS-E2-R	1.96	3.10	-3.23	-2.42	Schmidt et al. (2014)
BCC-CSM1.1	0.75	5.39	-4.44	0.22	Xiao-Ge et al. (2013)

			Preindustrial Control		
Model	SAT_0	GST_0	SAT_0-LoST	GST_0-LoST	Reference
CCSM4	2.12	6.03	-3.07	0.80	Gent et al. (2011)
MRI-CGCM3	1.39	-	-3.80	-	Yukimoto et al. (2012)
MPI-ESM-P	2.00	3.10	-3.19	-2.56	Jungclaus et al. (2013)
GISS-E2-R	2.02	3.14	-3.16	-2.35	Miller et al. (2014)
BCC-CSM1.1	1.03	5.58	-4.15	0.42	Wu et al. (2013)

of temperatures for North America (Figures 2.4c and 2.4d), in agreement with long-term surface temperatures estimated from BTP measurements and with long-term surface temperatures from CRU data.

The LoST temperatures were also compared with long-term surface temperature estimates from five Past Millennium (PM) and five piControl simulations (Table 2.1) included in the PMIP3/CMIP5 archive to test the accuracy of forced and control CGCM long-term surface temperatures. Long-term surface temperatures from the PM simulations are estimated as the mean surface air temperature for the period 1300-1700 CE (SAT_0) and the mean ground surface temperature linearly interpolated to 1.0 m depth for the same period (GST_0), in order to be consistent with the estimated temporal range for T_0 temperatures in Section 2.2.3. The PMIP3/CMIP5 simulations are interpolated onto the grid of the LoST database; SAT_0 and GST_0 values are estimated only at grid cells containing LoST temperatures. SAT_0 and GST_0 values are also estimated for piControl simulations following the same method, but averaging over each entire control simulation.

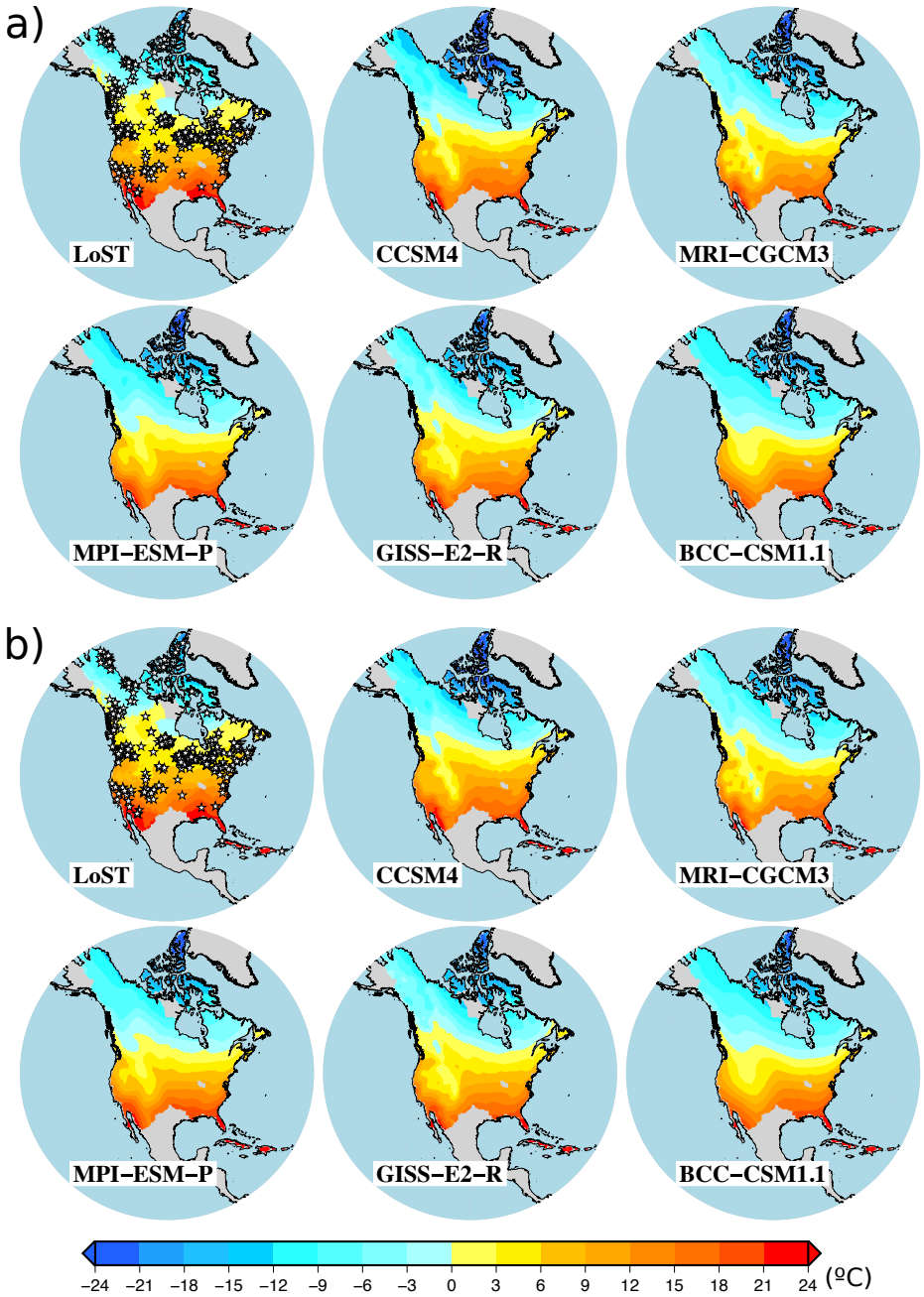

Figure 2.5: SAT_0 estimates from (a) PMIP3/CMIP5 PM simulations (1300-1700 CE) and (b) PMIP3/CMIP5 piControl simulations together with LoST temperatures. White stars show the location of the employed BTP measurements for the GIDS interpolation.

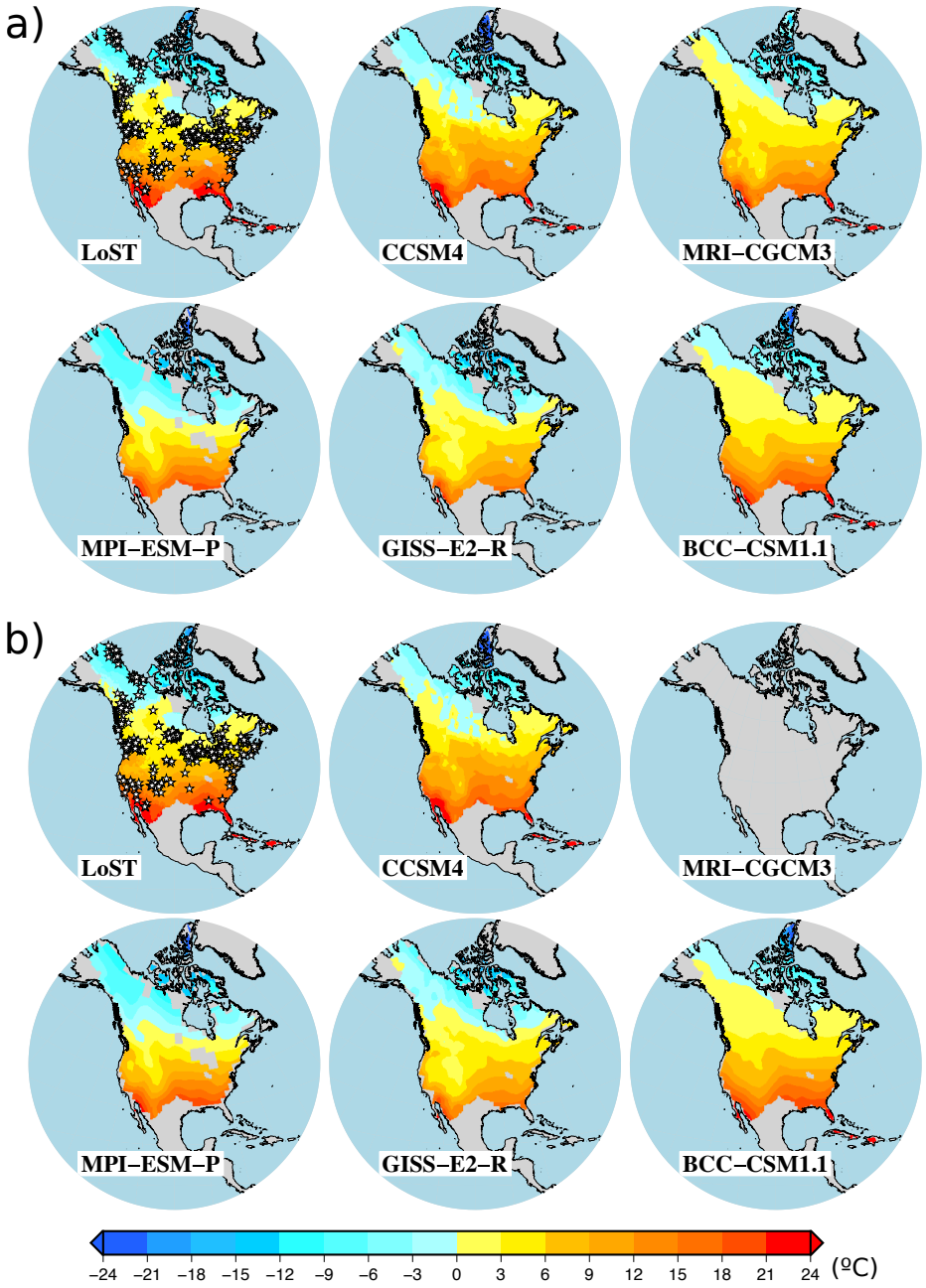

Figure 2.6: GST_0 estimates from (a) PMIP3/CMIP5 PM simulations (1300-1700 CE) and (b) PMIP3/CMIP5 piControl simulations together with T_0 temperatures. White stars shown the location of the employed BTP measurements for the GIDS interpolation.

Surface temperatures from PMIP3/CMIP5 PM and piControl simulations show similar latitudinal patterns to those from the LoST database, with lower temperatures at northern latitudes and higher temperatures at southern latitudes (Figures 2.5 and 2.6). SAT_0 estimates from the CCSM4, the MRI-CGCM3 and the BCC-CSM1.1 models show generally lower values than LoST temperatures for both piControl and PM simulations, while GST_0 estimates show higher values than LoST temperatures at high latitudes for the same CGCM simulations (Figures 2.7 and 2.8). Such results are in agreement with previous analyses of air and ground temperature relationships within CGCM simulations (González-Rouco et al., 2003; González-Rouco et al., 2006; Stieglitz et al., 2007; Koven et al., 2013; García-García et al., 2016) and meteorological observations over North America (e.g., Smerdon et al., 2003; Beltrami et al., 2003). In contrast, MPI-ESM-P and GISS-E2-R simulations present lower SAT_0 and GST_0 values than LoST temperatures, indicating lower long-term ground surface temperatures than the rest of the models (Table 2.1 and Figures 2.7 and 2.8). The comparison of the mean LoST temperature over North America with the simulated temperature evolution by each CGCM shows three different behaviors within the PMIP3/CMIP5 ensemble. The CCSM4 and the BCC-CSM1.1 simulations present lower mean air temperatures and higher mean ground temperatures than the mean LoST temperature (Figure 2.9 and Table 2.1). The similar GST_0 and mean ground surface temperatures for the CCSM4 and the BCC-CSM1.1 CGCMs in both PM and piControl simulations were expected since these models use a similar land surface model component (Wu et al., 2014) and the ground temperatures simulated by CMIP5 models are highly dependent on the employed land surface model component (Slater et al., 2013; García-García et al., 2019). In contrast, the GISS-E2-R and the MPI-ESM-P models produce lower mean GST_0 values than the mean LoST temperature and the rest of models, while simulating similar SAT_0 values to those from the rest of the PMIP3/CMIP5 CGCMs. Previous results have shown that the MPI-ESM-P PM simulation yields a high air-ground temperature coupling (García-García et al., 2016), probably due to the omission of latent heat of fusion in soil water (Koven et al., 2013). This could cause the low ground surface temperature simulated by the MPI-ESM-P model in both PM and piControl simulations in comparison with the mean LoST temperature (Fig 2.9). A strong air-ground coupling may also cause the low

ground surface temperature in the GISS-E2-R simulations, since the magnitude of the difference between GST_0 and SAT_0 is similar to that from the MPI-ESM-P simulations (Table 2.1). Finally, the MRI-CGCM3 PM simulation yields GST_0 values below the LoST climatology, but only by 0.3 °C (0.1 °C if considering the 2σ range of the LoST climatology, Figure 2.3), which are relatively small in comparison with the differences between the LoST climatology and the GST_0 values from MPI-ESM-P and GISS-E2-R simulations (>2.0 °C, Table 2.1). Thus, we can consider that three of the five PMIP3/CMIP5 CGCMs (the CCSM4, the MRI-CGCM3 and the BCC-CSM1.1) simulate a surface temperature climatology comparable to that from the LoST dataset, which is an unexpected result as none of the PMIP3/CMIP5 CGCM simulations studied here were specifically tuned to match this climatology.

2.5 Discussion

Our results demonstrate that LoST temperatures can be used as a reference for assessing the represented climatology in both PM and piControl simulations. The determination of T_0 temperatures, nevertheless, presents some uncertainties that should be discussed. The extrapolation of each quasi-equilibrium temperature profile to the surface introduces a small error in the LoST estimates, averaging less than 0.15 °C from the 514 BTPs evaluated here (see Section 2.3.1 for details about the error treatment in the LoST database). Rock heterogeneity should also be considered for estimating T_0 temperatures. We assume, nevertheless, homogenous thermal properties for all borehole profiles, which is another source of uncertainty for LoST temperatures. The ideal approach consists of estimating the thermal resistance with depth (Eq. 2.1), but the absence of thermal conductivity measurements for the employed BTPs (Jaume-Santero et al., 2016) makes that approach impractical. Additionally, measurements of thermal conductivity tend to be distributed around a central value (e.g., the measurements at the Neil Well, Beltrami et al., 1995a). If the thermal conductivity varies systematically with depth at a certain location, such variation will be reflected in the temperature profile as an unphysical signal. Such logs were removed from the database employed in this analysis, as explained in Jaume-Santero et al. (2016). Therefore, it is reasonable to assume a homogenous conductivity with

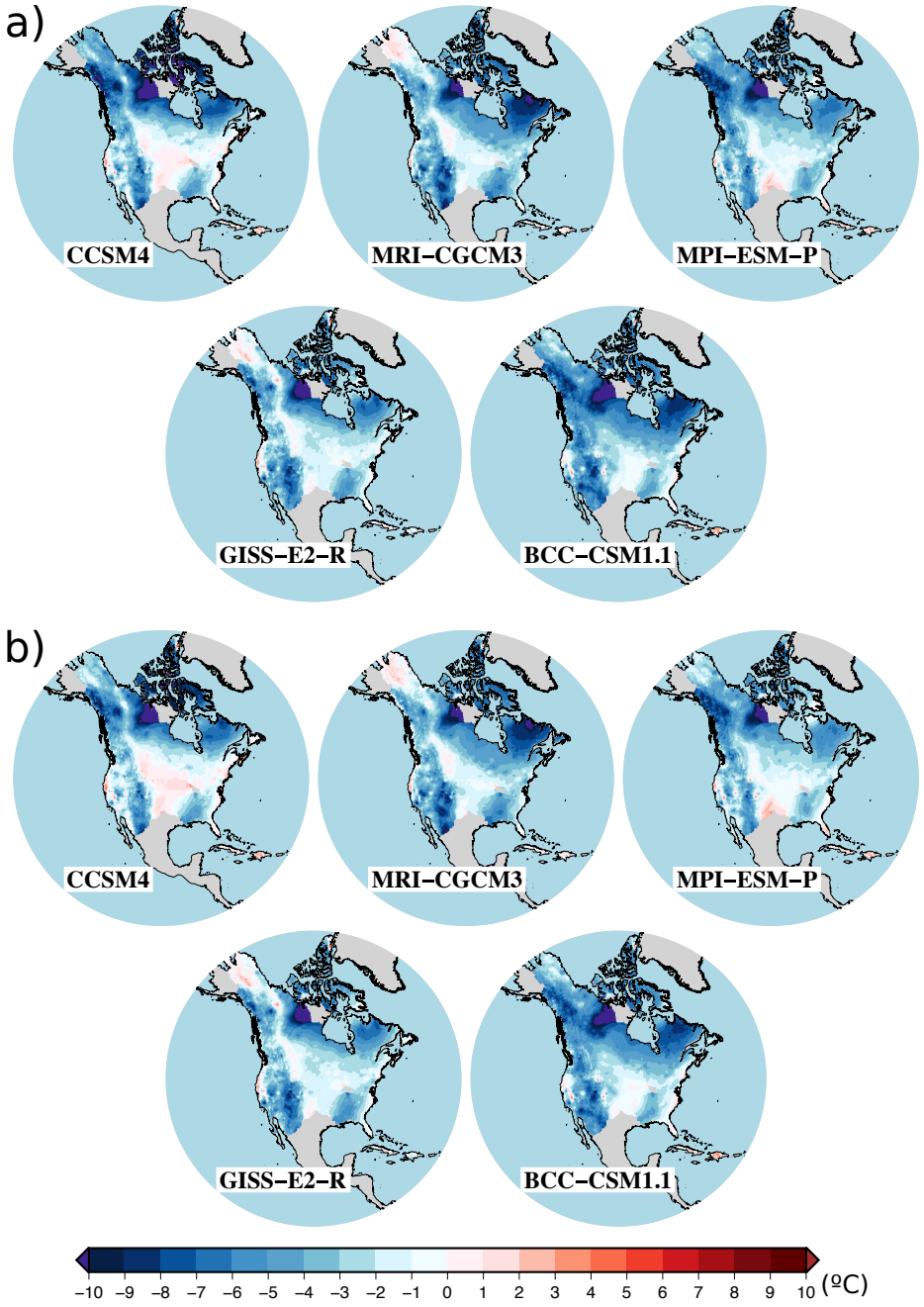

Figure 2.7: Difference between SAT_0 values from PMIP3/CMIP5 simulations and LoST temperatures. (a) Results for PM simulations (1300-1700 CE). (b) Results piControl simulations.

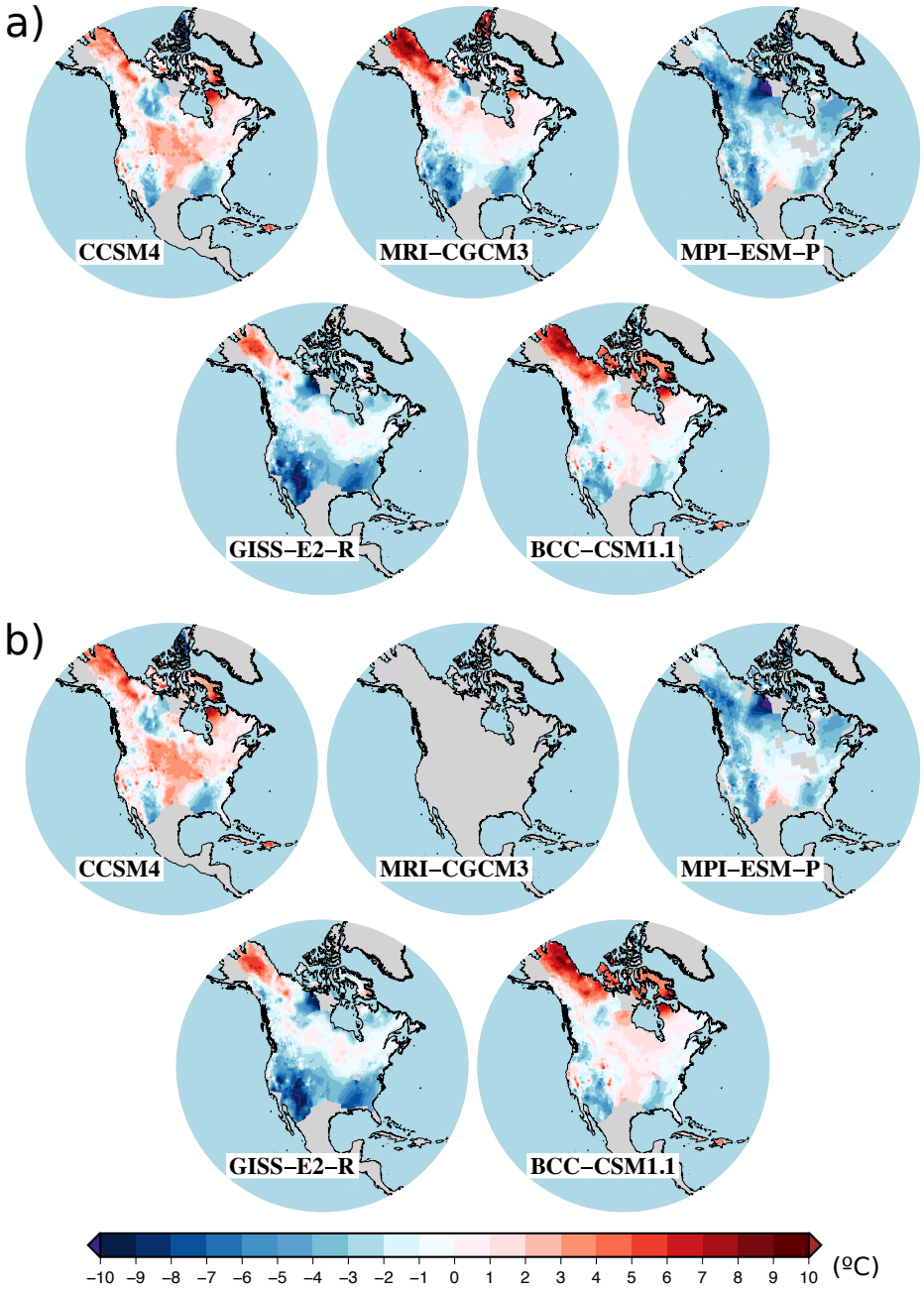

Figure 2.8: Difference between GST_0 values from PMIP3/CMIP5 simulations and LoST temperatures. (a) Results for PM simulations (1300-1700 CE). (b) Results for piControl simulations.

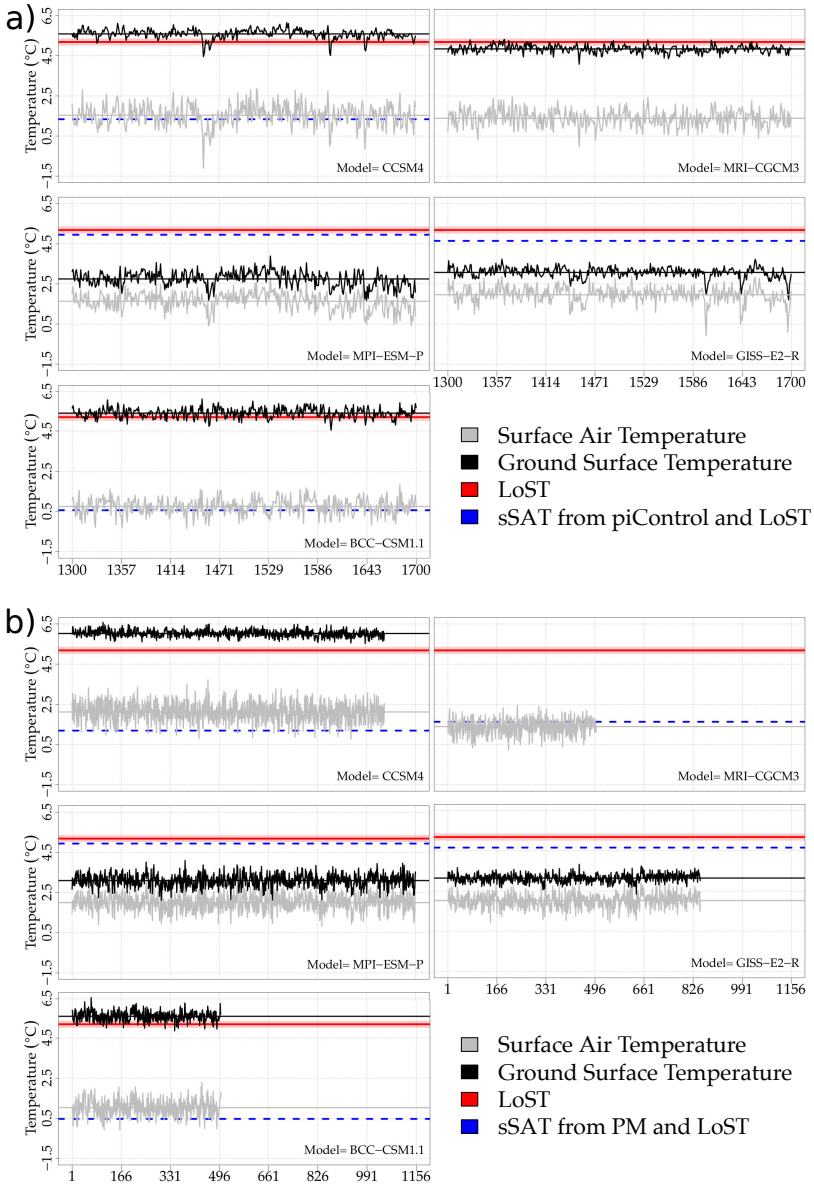

Figure 2.9: Surface air temperature evolution (gray solid line), ground surface temperature evolution (black solid line), SAT_0 (gray horizontal line) and GST_0 (black horizontal line) for (a) PMIP3/CMIP5 PM and (b) PMIP3/CMIP5 piControl simulations. Solid red lines represent the mean LoST temperature and the red shadow represents the 95% confidence interval (Section 2.3.1, Figure 2.3). Dashed blue lines represent estimated references for long-term surface air temperatures from the LoST climatology and the simulated air-ground temperature offset in (a) piControl and (b) PM simulations. Ground temperatures for the MRI-CGCM3 piControl simulation could not be retrieved from the PMIP3/CMIP5 data servers.

depth. Long-term alterations of the surface energy balance out of the 1300-1700 CE period may also affect the LoST estimates. Particularly, possible transient temperatures in BTPs due to the Little Ice Age (LIA) and the Medieval Warm Period (MWP) add a certain degree of uncertainty in the determination of T_0 values. However, the spatial extent of both LIA and MWP was not homogeneous over North America (e.g., Masson-Delmotte et al., 2013, and references therein), meaning that not all BTPs were affected by the events (Beltrami et al., 1992; Chouinard et al., 2007; Jaume-Santero et al., 2016). Additionally, the influence of the LIA and the MWP should be part of any millennial-scale transient climate simulation, and therefore the effect of such climate events is taken into account in the comparison between LoST results and transient climate simulations. The absence of these two periods in piControl simulations probably contributes to the slightly poorer agreement between LoST temperatures and piControl temperatures in comparison with results for the PM simulation (Figure 2.9). Another factor that may impact the retrieved quasi-equilibrium temperature profile is the heterogeneity of North American topography (e.g., Kohl, 1999). To our knowledge, all analyzed BTPs are located in plain terrain, and were not corrected for elevation since the employed BTP database does not provide elevation data. Therefore, we use the ETOPO2 database to assess if the altitude distribution of BTPs is sufficient for representing the topography of the LoST domain. The altitude distribution over the LoST domain and at grid cells containing boreholes sites are displayed in Figure 2.10. Both histograms present a similar shape for altitudes up to $\sim$ 430 m, showing a lack of borehole locations at altitudes between $\sim$430 m and $\sim$1013 m. The uneven latitudinal distribution of borehole sites is probably causing this gap in the distribution of altitudes, as well as a small excess of BTP locations at high altitudes. Despite these differences, both distributions are generally in agreement, indicating a sufficient altitude distribution from the borehole database to represent the North American broad-scale topography.

There are, however, two main limitations for the application of the LoST database at this stage of the study: the supplied variable and the regional character of the database. The LoST database consists of long-term estimates of ground surface temperatures, while CGCM simulations are typically evaluated against observations of Surface Air Temperature (SAT) (e.g., Mauritsen et al.,

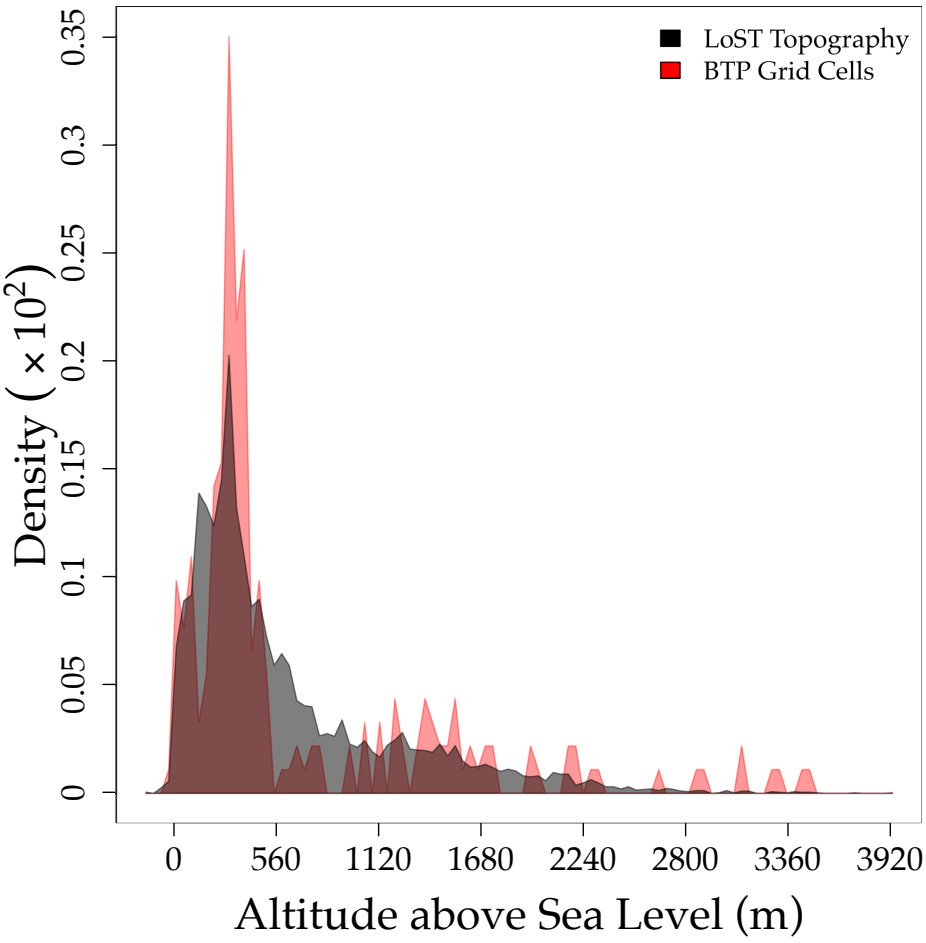

Figure 2.10: Altitude distribution over the LoST domain (black histogram) and at grid cells containing BTPs (red histogram) from the ETOPO2 product.

2012; Flato et al., 2013; Séférian et al., 2016; Schmidt et al., 2017). We can provide a reference for simulated long-term SAT by accounting for the offset between simulated air and ground temperatures and using the LoST temperatures. As an example, SAT references are estimated for the five PM and five piControl simulations employed in this study (dashed blue line in Figure 2.9). SAT references for PM simulations are estimated from the offset between air and ground temperatures in piControl simulations, while SAT references for piControl simulations are estimated from the offset between air and ground temperatures in PM simulations. Such offsets show a constant behavior in both simulations (Figure 2.11). CGCM simulations in disagreement with the estimated SAT reference (the MPI-ESM-P and the GISS-E2-R simulations) may feature a strong air-ground coupling, as discussed in Section 2.4. Therefore, although the LoST database contains estimates of ground surface temperatures, it may be also used to assess simulated long-term surface air temperatures on a first order approach.

The regional character of the presented LoST database poses some caveats for analyzing the global climatology of preindustrial simulations. Indeed, results of the simulated regional climatology cannot be globally extrapolated since the magnitude of the potential spurious drifts in control simulations varies markedly at regional scales and these regional drifts could be larger than the global-averaged drift (Sen Gupta et al., 2012, 2013). Further work exploring this concern could involve generating a global LoST database from the existing global network of BTP measurements, helping to minimize the effect of possible regional drifts on the simulated climatology. However, BTP measurements are scarce in the Southern Hemisphere, a potential burden that needs to be considered before assembling a global version of this database. Additionally, the temperature profiles employed in this study to estimate T_0 temperatures were truncated to 300 m of depth, which determines the temporal period of reference for the comparison with PM simulations. Deeper BTP measurements can retrieve the climatology of earlier time periods, although the global BTP network contains few temperature profiles deeper than 300 m (see Figure 1 in Beltrami et al., 2015).

Despite the regional character of the LoST temperatures, the northern BTPs contained in this database allow to evaluate the long-term stability of permafrost

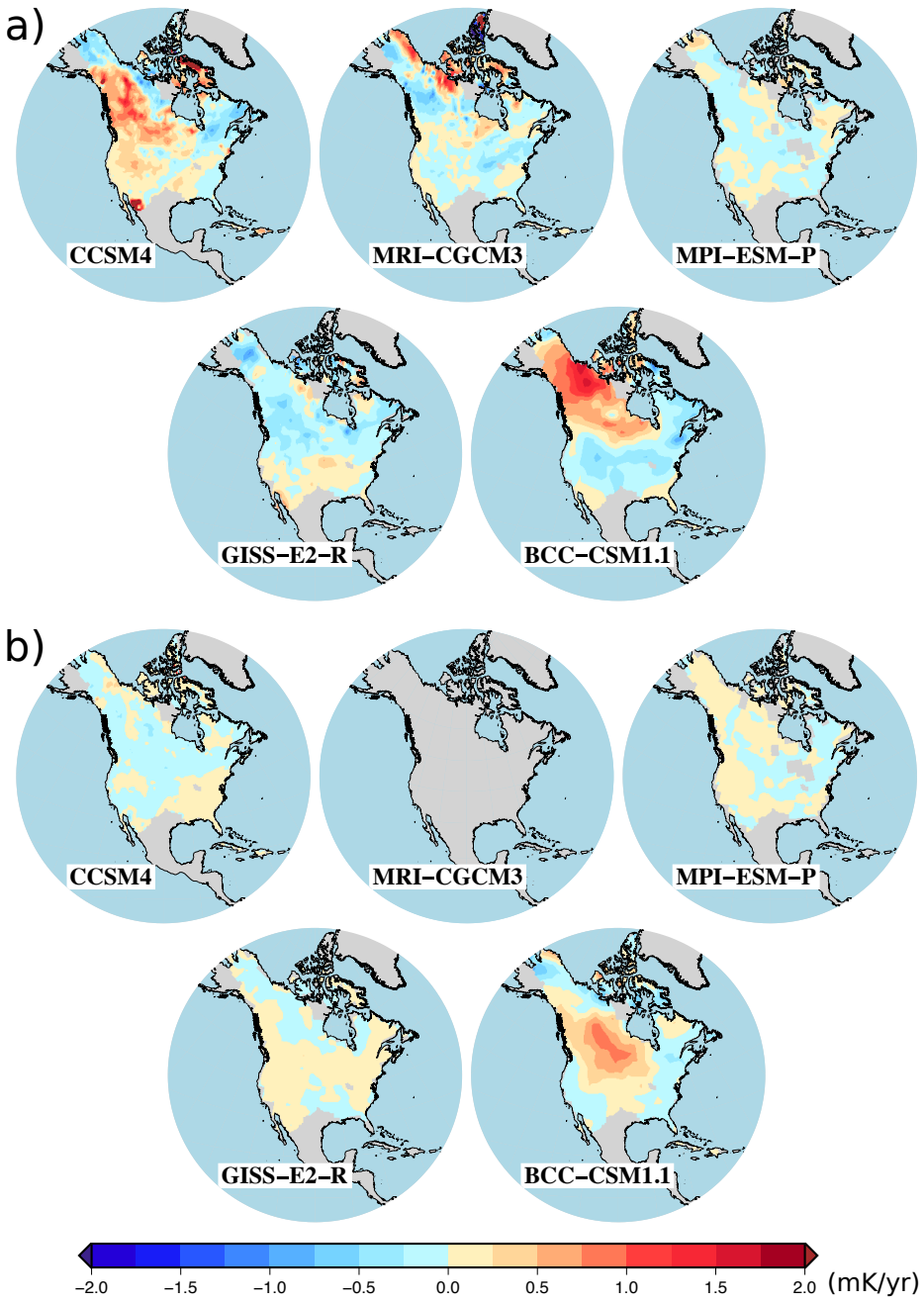

Figure 2.11: Trends of the difference between air and ground (1.0 m depth) temperatures from PMIP3/CMIP5 simulations. (a) Results for PM simulations (1300-1700 CE). (b) Results for piControl simulations.

over North America. That is, the northern temperatures in this database can be compared with regional and global simulations as a reference to the preindustrial permafrost stability. Furthermore, previous studies have found that the CMIP5 CGCM simulations have difficulty representing permafrost evolution (Koven et al., 2013; Slater et al., 2013), partially due to the broad range of simulated climate trajectories by each CGCM and the differences between the employed land surface model components (Slater et al., 2013). Using LoST temperatures to improve the surface temperature climatology of global and regional simulations may enhance the simulated long-term preindustrial 0 °C isotherm, which is necessary to correctly represent permafrost evolution.

Numerous proxy-data based reconstructions of temperature, precipitation and other climate related variables exist for North America, providing a reference for the evaluation of important aspects of past and future climate model simulations (e.g., PAGES 2k-PMIP3 Group, 2015; Cook et al., 2015). Proxy-data temperature reconstructions have already been compared against borehole temperature records of past variations in surface temperature over North America (e.g., Jaume-Santero et al., 2016). It is worth noting that proxy systems are indirect sources of climate information requiring a calibration procedure with modern meteorological data, while borehole temperature data consist of direct measurements of the thermal regime of the subsurface in the recent past. That is, the LoST database contains information derived from direct measurements of subsurface temperatures, constituting the first estimates of long-term absolute surface temperatures in North America. Another important difference between proxy and borehole reconstructions is that most proxy systems generally capture high-frequency variations of climate conditions (Moberg et al., 2005), while borehole temperature profiles record long-term changes in the surface conditions, filtering out short-period signals. In this context, LoST temperatures provide a complementary reference to the multiproxy database over North America for evaluating the performance of climate model simulations.

2.6 Conclusions

A gridded database of past long-term surface temperatures over most of continental North America has been assembled from geothermal measurements. Our

results show that this database can be used as a reference for evaluating the accuracy of CGCM preindustrial control and past millennium simulations and possibly to improve the reference climate state by adjusting key parameters or preindustrial forcings in control experiments. Thereby, spread in BTP estimates by CGCM simulations may be reduced given the relationship between control temperature climatology and long-term powerful feedbacks such as ice-albedo feedback, water vapor feedback, and permafrost carbon feedback. Future work could involve generating a global version of the LoST database using the rest of the global network of borehole temperature profile measurements and following the described methodology, as well as generating new versions of this global database including future temperature profile measurements.

2.7 References

Alexeev, V. A., Nicolsky, D. J., Romanovsky, V. E., and Lawrence, D. M. (2007). An evaluation of deep soil configurations in the CLM3 for improved representation of permafrost. *Geophysical Research Letters*, **34**(9). n/a–n/a. DOI: 10.1029/2007GL029536.

Andrews, T., Gregory, J. M., Webb, M. J., and Taylor, K. E. (2012). Forcing, feedbacks and climate sensitivity in CMIP5 coupled atmosphere-ocean climate models. *Geophysical Research Letters*, **39**(9). n/a–n/a. DOI: 10.1029/2012GL051607.

Beltrami, H. (2002). Climate from borehole data: Energy fluxes and temperatures since 1500. *Geophysical Research Letters*, **29**(23). 26–1–26–4. DOI: 10.1029/2002GL015702.

Beltrami, H. and Mareschal, J.-C. (1992). Ground temperature histories for central and eastern Canada from geothermal measurements: Little Ice Age signature. *Geophysical Research Letters*, **19**(7), 689–692. DOI: 10.1029/92GL00671.

Beltrami, H. and Taylor, A. E. (1995a). Records of climatic change in the Canadian Arctic: towards calibrating oxygen isotope data with geothermal data. *Global and Planetary Change*, **11**(3), 127 –138. DOI: https://doi.org/10.1016/0921-8181(95)00006-2.

Beltrami, H. and Mareschal, J.-C. (1995b). Resolution of ground temperature histories inverted from borehole temperature data. *Global and Planetary Change*, **11**(1-2), 57–70. DOI: https://doi.org/10.1016/0921-8181(95)00002-9.

Beltrami, H., Smerdon, J. E., Pollack, H. N., and Huang, S. (2002). Continental heat gain in the global climate system. *Geophysical Research Letters*, **29**(8), 8–1–8–3. DOI: 10.1029/2001GL014310.

Beltrami, H. and Kellman, L. (2003). An examination of short- and long-term air–ground temperature coupling. *Global and Planetary Change*, **38**(3–4), 291 –303. DOI: http://dx.doi.org/10.1016/S0921-8181(03)00112-7.

Beltrami, H. and Bourlon, E. (2004). Ground warming patterns in the Northern Hemisphere during the last five centuries. *Earth and Planetary Science Letters*, **227**(3–4), 169 –177. DOI: http://dx.doi.org/10.1016/j.epsl.2004.09.014.

Beltrami, H., Bourlon, E., Kellman, L., and González-Rouco, J. F. (2006). Spatial patterns of ground heat gain in the Northern Hemisphere. *Geophysical Research Letters*, **33**(6). n/a–n/a. DOI: 10.1029/2006GL025676.

Beltrami, H., Matharoo, G. S., and Smerdon, J. E. (2015). Impact of borehole depths on reconstructed estimates of ground surface temperature histories and energy storage. *Journal of Geophysical Research: Earth Surface*, **120**(5). 763–778. DOI: 10.1002/2014JF003382.

Bodri, L. and Cermak, V. (2007). *Borehole Climatology*. Oxford: Elsevier Science Ltd. DOI: https://doi.org/10.1016/B978-008045320-0/50001-6.

Braconnot, P., Harrison, S. P., Kageyama, M., Bartlein, P. J., Masson-Delmotte, V., Abe-Ouchi, A., Otto-Bliesner, B., and Zhao, Y. (2012). Evaluation of climate models using palaeoclimatic data. *Nature Clim. Change*, **2**(6), 417–424. DOI: 10.1038/nclimate1456.

Bullard, E. C. and Schonland, B. F. J. (1939). Heat flow in South Africa. *Proceedings of the Royal Society of London. Series A. Mathematical and Physical Sciences*, **173**(955), 474–502. DOI: 10.1098/rspa.1939.0159.

Carslaw, H. and Jaeger, J. (1959). *Conduction of Heat in Solids*. Clarendon Press, Oxford.

Cermak, V. and Rybach, L. (1982). "Thermal conductivity and specific heat of minerals and rocks". In: *Landolt Börnstein: Physical Properties of Rocks, Group V, Geophysics, Volume 1a*. Ed. by G. Angenheister. accessed 2017-06-06. Springer-Verlag Berlin Heidelberg. DOI: 10.1007/10201894_62.

Chouinard, C., Fortier, R., and Mareschal, J.-C. (2007). Recent climate variations in the subarctic inferred from three borehole temperature profiles in northern Quebec, Canada. *Earth and Planetary Science Letters*, **263**(3), 355 –369. DOI: https://doi.org/10.1016/j.epsl.2007.09.017.

Cook, B. I., Ault, T. R., and Smerdon, J. E. (2015). Unprecedented 21st century drought risk in the American Southwest and Central Plains. *Science Advances*, **1**(1). DOI: 10.1126/sciadv.1400082.

Cuesta-Valero, F. J., García-García, A., Beltrami, H., Zorita, E., and Jaume-Santero, F. (2019). Long-term Surface Temperature (LoST) database as a complement for GCM preindustrial simulations. *Climate of the Past*, **15**(3), 1099–1111. DOI: 10.5194/cp-15-1099-2019.

Cuesta-Valero, F. J., García-García, A., Beltrami, H., and Smerdon, J. E. (2016). First assessment of continental energy storage in CMIP5 simulations. *Geophysical Research Letters*. n/a–n/a. DOI: 10.1002/2016GL068496.

Demezhko, D. Y. and Gornostaeva, A. A. (2015a). Late Pleistocene–Holocene ground surface heat flux changes reconstructed from borehole temperature data (the Urals, Russia). *Climate of the Past*, **11**(4), 647–652. DOI: 10.5194/cp-11-647-2015.

Demezhko, D. Y. and Gornostaeva, A. A. (2015b). Reconstructions of ground surface heat flux variations in the urals from geothermal and meteorological data. *Izvestiya, Atmospheric and Oceanic Physics*, **51**(7), 723–736. DOI: 10.1134/S0001433815070026.

Dommenget, D. (2016). A simple model perturbed physics study of the simulated climate sensitivity uncertainty and its relation to control climate biases. *Climate Dynamics*, **46**(1), 427–447. DOI: 10.1007/s00382-015-2591-4.

Flato, G., Marotzke, J., Abiodun, B., Braconnot, P., Chou, S., Collins, W., Cox, P., Driouech, F., Emori, S., Eyring, V., Forest, C., Gleckler, P., Guilyardi, E., Jakob, C., Kattsov, V., Reason, C., and Rummukainen, M. (2013). "Evaluation of Climate Models". In: *Climate Change 2013: The Physical Science Basis. Contribution of Working Group I to the Fifth Assessment Report of the Intergovernmental Panel on Climate Change*. Ed. by T. Stocker, D. Qin, G.-K. Plattner, M. Tignor, S. Allen, J. Boschung, A. Nauels, Y. Xia, V. Bex, and P. Midgley. Cambridge, United Kingdom and New York, NY, USA: Cambridge University Press. Chap. 9, pp. 741–866. DOI: 10.1017/CBO9781107415324.020.

Forster, P. M., Andrews, T., Good, P., Gregory, J. M., Jackson, L. S., and Zelinka, M. (2013). Evaluating adjusted forcing and model spread for historical and future scenarios in the CMIP5 generation of climate models. *Journal of Geophysical Research: Atmospheres*, **118**(3), 1139–1150. DOI: 10.1002/jgrd.50174.

García-García, A, Cuesta-Valero, F. J., Beltrami, H, and Smerdon, J. E. (2016). Simulation of air and ground temperatures in PMIP3/CMIP5 last millennium simulations: implications for climate reconstructions from borehole temperature profiles. *Environmental Research Letters*, **11**(4), 044022.

García-García, A., Cuesta-Valero, F. J., Beltrami, H., and Smerdon, J. E. (2019). Characterization of Air and Ground Temperature Relationships within the CMIP5 Historical and Future Climate Simulations. *Journal of Geophysical Research: Atmospheres*, **124**(7), 3903–3929. DOI: 10.1029/2018JD030117.

Gent, P. R., Danabasoglu, G., Donner, L. J., Holland, M. M., Hunke, E. C., Jayne, S. R., Lawrence, D. M., Neale, R. B., Rasch, P. J., Vertenstein, M., Worley, P. H., Yang, Z.-L., and Zhang, M. (2011). The Community Climate System Model Version 4. *Journal of Climate*, **24**(19), 4973–4991. DOI: 10.1175/2011JCLI4083.1.

González-Rouco, F., von Storch, H., and Zorita, E. (2003). Deep soil temperature as proxy for surface air-temperature in a coupled model simulation of the last thousand years. *Geophysical Research Letters*, **30**(21). n/a–n/a. DOI: 10.1029/2003GL018264.

González-Rouco, J. F., Beltrami, H., Zorita, E., and von Storch, H. (2006). Simulation and inversion of borehole temperature profiles in surrogate climates: Spatial distribution and surface coupling. *Geophysical Research Letters*, **33**(1). n/a–n/a. DOI: 10.1029/2005GL024693.

González-Rouco, J. F., Beltrami, H., Zorita, E., and Stevens, M. B. (2009). Borehole climatology: a discussion based on contributions from climate modeling. *Climate of the Past*, **5**(1), 97–127. DOI: 10.5194/cp-5-97-2009.

Gregory, J. M., Stouffer, R. J., Raper, S. C. B., Stott, P. A., and Rayner, N. A. (2002). An Observationally Based Estimate of the Climate Sensitivity. *Journal of Climate*, **15**(22), 3117–3121. DOI: 10.1175/1520-0442(2002)015<3117:AOBEOT>2.0.CO;2.

Harris, I., Jones, P., Osborn, T., and Lister, D. (2014). Updated high-resolution grids of monthly climatic observations – the CRU TS3.10 Dataset. *International Journal of Climatology*, **34**(3), 623–642. DOI: 10.1002/joc.3711.

Harris, R. N. and Chapman, D. S. (2001). Mid-latitude (30 °–60 ° N) climatic warming inferred by combining borehole temperatures with surface air temperatures. *Geophysical Research Letters*, **28**(5), 747–750. DOI: 10.1029/2000GL012348.

Hartmann, D., Klein Tank, A., Rusticucci, M., Alexander, L., Brönnimann, S., Charabi, Y., Dentener, F., Dlugokencky, E., Easterling, D., Kaplan, A., Soden, B., Thorne, P., Wild, M., and Zhai, P. (2013). "Observations: Atmosphere and Surface". In: *Climate Change 2013: The Physical Science Basis. Contribution of Working Group I to the Fifth Assessment Report of the Intergovernmental Panel on Climate Change*. Ed. by T. Stocker, D. Qin, G.-K. Plattner, M. Tignor, S. Allen, J. Boschung, A. Nauels, Y. Xia, V. Bex, and P. Midgley. Cambridge, United Kingdom and New York, NY, USA: Cambridge University Press. Chap. 2, pp. 159–254. DOI: 10.1017/CBO9781107415324.008.

Hawkins, E., Ortega, P., Suckling, E., Schurer, A., Hegerl, G., Jones, P., Joshi, M., Osborn, T. J., Masson-Delmotte, V., Mignot, J., Thorne, P., and van Oldenborgh, G. J. (2017). Estimating Changes in Global Temperature since the Preindustrial Period. *Bulletin of the American Meteorological Society*, **98**(9), 1841–1856. DOI: 10.1175/BAMS-D-16-0007.1.

Hourdin, F., Mauritsen, T., Gettelman, A., Golaz, J.-C., Balaji, V., Duan, Q., Folini, D., Ji, D., Klocke, D., Qian, Y., Rauser, F., Rio, C., Tomassini, L., Watanabe, M., and Williamson, D. (2017). The Art and Science of Climate Model Tuning. *Bulletin of the American Meteorological Society*, **98**(3), 589–602. DOI: 10.1175/BAMS-D-15-00135.1.

Hu, X., Taylor, P. C., Cai, M., Yang, S., Deng, Y., and Sejas, S. (2017). Inter-Model Warming Projection Spread: Inherited Traits from Control Climate Diversity. *Scientific Reports*, **7**(1), 4300. DOI: 10.1038/s41598-017-04623-7.

Huang, S., Pollack, H. N., and Shen, P.-Y. (2000). Temperature trends over the past five centuries reconstructed from borehole temperatures. *Nature*, **403**(6771), 756–758.

Jaume-Santero, F., Pickler, C., Beltrami, H., and Mareschal, J.-C. (2016). North American regional climate reconstruction from ground surface temperature histories. *Climate of the Past*, **12**(12), 2181–2194. DOI: 10.5194/cp-12-2181-2016.

Jungclaus, J. H., Fischer, N., Haak, H., Lohmann, K., Marotzke, J., Matei, D., Mikolajewicz, U., Notz, D., and von Storch, J. S. (2013). Characteristics of the ocean simulations in the Max Planck Institute Ocean Model (MPIOM) the ocean component of the MPI-Earth system model. *Journal of Advances in Modeling Earth Systems*, **5**(2), 422–446. DOI: 10.1002/jame.20023.

Jungclaus, J. H., Lohmann, K., and Zanchettin, D. (2014). Enhanced 20th-century heat transfer to the Arctic simulated in the context of climate variations over the last millennium. *Climate of the Past*, **10**(6), 2201–2213. DOI: 10.5194/cp-10-2201-2014.

Knutti, R. and Sedláček, J. (2012). Robustness and uncertainties in the new CMIP5 climate model projections. *Nature Climate Change*, **3**, 369 EP –. DOI: 10.1038/nclimate1716.

Knutti, R., Rugenstein, M. A. A., and Hegerl, G. C. (2017). Beyond equilibrium climate sensitivity. *Nature Geoscience*, **10**, 727–736. DOI: 10.1038/ngeo3017.

Kohl, T. (1999). Transient thermal effects below complex topographies. *Tectonophysics*, **306**(3), 311 –324. DOI: https://doi.org/10.1016/S0040-1951(99)00063-3.

Koven, C. D., Ringeval, B., Friedlingstein, P., Ciais, P., Cadule, P., Khvorostyanov, D., Krinner, G., and Tarnocai, C. (2011). Permafrost carbon-climate feedbacks accelerate global warming. *Proceedings of the National Academy of Sciences*, **108**(36), 14769–14774. DOI: 10.1073/pnas.1103910108.

Koven, C. D., Riley, W. J., and Stern, A. (2013). Analysis of Permafrost Thermal Dynamics and Response to Climate Change in the CMIP5 Earth System Models. *Journal of Climate*, **26**(6), 1877–1900. DOI: 10.1175/JCLI-D-12-00228.1.

Landrum, L., Otto-Bliesner, B. L., Wahl, E. R., Conley, A., Lawrence, P. J., Rosenbloom, N., and Teng, H. (2013). Last Millennium Climate and Its Variability in CCSM4. *Journal of Climate*, **26**(4), 1085–1111. DOI: 10.1175/JCLI-D-11-00326.1.

Li, J. and Heap, A. D. (2011). A review of comparative studies of spatial interpolation methods in environmental sciences: Performance and impact factors. *Ecological Informatics*, **6**(3), 228 –241. DOI: http://dx.doi.org/10.1016/j.ecoinf.2010.12.003.

MacDougall, A. H., Beltrami, H., González-Rouco, J. F., Stevens, M. B., and Bourlon, E. (2010). Comparison of observed and general circulation model derived continental subsurface heat flux in the Northern Hemisphere. *Journal of Geophysical Research: Atmospheres (1984–2012)*, **115**(D12).

MacDougall, A. H., Avis, C. A., and Weaver, A. J. (2012). Significant contribution to climate warming from the permafrost carbon feedback. *Nature Geosci*, **5**(10), 719–721. DOI: 10.1038/ngeo1573.

MacDougall, A. H. and Beltrami, H. (2017). Impact of deforestation on subsurface temperature profiles: implications for the borehole paleoclimate record. *Environmental Research Letters*, **12**(7), 074014.

Mardikis, M. G., Kalivas, D. P., and Kollias, V. J. (2005). Comparison of Interpolation Methods for the Prediction of Reference Evapotranspiration—An

Application in Greece. *Water Resources Management*, **19**(3), 251–278. DOI: 10.1007/s11269-005-3179-2.

Mareschal, J.-C. and Beltrami, H. (1992). Evidence for recent warming from perturbed geothermal gradients: examples from eastern Canada. *Climate Dynamics*, **6**(3), 135–143. DOI: 10.1007/BF00193525.

Masson-Delmotte, V., Schulz, M., Abe-Ouchi, A., Beer, J., Ganopolski, A., González Rouco, J., Jansen, E., Lambeck, K., Luterbacher, J., Naish, T., Osborn, T., Otto-Bliesner, B., Quinn, T., Ramesh, R., Rojas, M., Shao, X., and Timmermann, A. (2013). "Information from Paleoclimate Archives". In: *Climate Change 2013: The Physical Science Basis. Contribution of Working Group I to the Fifth Assessment Report of the Intergovernmental Panel on Climate Change*. Ed. by T. Stocker, D. Qin, G.-K. Plattner, M. Tignor, S. Allen, J. Boschung, A. Nauels, Y. Xia, V. Bex, and P. Midgley. Cambridge, United Kingdom and New York, NY, USA: Cambridge University Press. Chap. 5, pp. 383–464. DOI: 10.1017/CBO9781107415324.013.

Mauritsen, T., Stevens, B., Roeckner, E., Crueger, T., Esch, M., Giorgetta, M., Haak, H., Jungclaus, J., Klocke, D., Matei, D., Mikolajewicz, U., Notz, D., Pincus, R., Schmidt, H., and Tomassini, L. (2012). Tuning the climate of a global model. *Journal of Advances in Modeling Earth Systems*, **4**(3). n/a–n/a. DOI: 10.1029/2012MS000154.

McCullough, I. M., Davis, F. W., Dingman, J. R., Flint, L. E., Flint, A. L., Serra-Diaz, J. M., Syphard, A. D., Moritz, M. A., Hannah, L., and Franklin, J. (2016). High and dry: high elevations disproportionately exposed to regional climate change in Mediterranean-climate landscapes. *Landscape Ecology*, **31**(5), 1063–1075. DOI: 10.1007/s10980-015-0318-x.

McFarlane, N. (2011). Parameterizations: representing key processes in climate models without resolving them. *Wiley Interdisciplinary Reviews: Climate Change*, **2**(4), 482–497. DOI: 10.1002/wcc.122.

Miller, R. L., Schmidt, G. A., Nazarenko, L. S., Tausnev, N., Bauer, S. E., DelGenio, A. D., Kelley, M., Lo, K. K., Ruedy, R., Shindell, D. T., Aleinov, I., Bauer, M., Bleck, R., Canuto, V., Chen, Y., Cheng, Y., Clune, T. L., Faluvegi, G., Hansen,

J. E., Healy, R. J., Kiang, N. Y., Koch, D., Lacis, A. A., LeGrande, A. N., Lerner, J., Menon, S., Oinas, V., Pérez García-Pando, C., Perlwitz, J. P., Puma, M. J., Rind, D., Romanou, A., Russell, G. L., Sato, M., Sun, S., Tsigaridis, K., Unger, N., Voulgarakis, A., Yao, M.-S., and Zhang, J. (2014). CMIP5 historical simulations (1850–2012) with GISS ModelE2. *Journal of Advances in Modeling Earth Systems*, **6**(2), 441–477. DOI: 10.1002/2013MS000266.

Moberg, A., Sonechkin, D. M., Holmgren, K., Datsenko, N. M., and Karlén, W. (2005). Highly variable Northern Hemisphere temperatures reconstructed from low- and high-resolution proxy data. *Nature*, **433**, 613 EP –.

Nalder, I. A. and Wein, R. W. (1998). Spatial interpolation of climatic Normals: test of a new method in the Canadian boreal forest. *Agricultural and Forest Meteorology*, **92**(4), 211 –225. DOI: http://dx.doi.org/10.1016/S0168-1923(98)00102-6.

National Geophysical Data Center (2006). *Two-minute Gridded Global Relief Data (ETOPO2) v2*. https://www.ngdc.noaa.gov/mgg/global/etopo2.html. DOI: doi:10.7289/V5J1012Q.

PAGES 2k-PMIP3 Group (2015). Continental-scale temperature variability in PMIP3 simulations and PAGES 2k regional temperature reconstructions over the past millennium. *Climate of the Past*, **11**(12), 1673–1699. DOI: 10.5194/cp-11-1673-2015.

Pickler, C., Beltrami, H., and Mareschal, J.-C. (2016). Laurentide Ice Sheet basal temperatures during the last glacial cycle as inferred from borehole data. *Climate of the Past*, **12**(1), 115–127. DOI: 10.5194/cp-12-115-2016.

Price, D. T., McKenney, D. W., Nalder, I. A., Hutchinson, M. F., and Kesteven, J. L. (2000). A comparison of two statistical methods for spatial interpolation of Canadian monthly mean climate data. *Agricultural and Forest Meteorology*, **101**(2), 81 –94. DOI: http://dx.doi.org/10.1016/S0168-1923(99)00169-0.

Schmidt, G. A., Jungclaus, J. H., Ammann, C. M., Bard, E., Braconnot, P., Crowley, T. J., Delaygue, G., Joos, F., Krivova, N. A., Muscheler, R., Otto-Bliesner, B. L., Pongratz, J., Shindell, D. T., Solanki, S. K., Steinhilber, F., and Vieira, L. E. A. (2011). Climate forcing reconstructions for use in PMIP simulations

of the last millennium (v1.0). *Geoscientific Model Development*, **4**(1), 33–45. DOI: 10.5194/gmd-4-33-2011.

Schmidt, G. A., Bader, D., Donner, L. J., Elsaesser, G. S., Golaz, J.-C., Hannay, C., Molod, A., Neale, R. B., and Saha, S. (2017). Practice and philosophy of climate model tuning across six US modeling centers. *Geoscientific Model Development*, **10**(9), 3207–3223. DOI: 10.5194/gmd-10-3207-2017.

Schmidt, G. A., Kelley, M., Nazarenko, L., Ruedy, R., Russell, G. L., Aleinov, I., Bauer, M., Bauer, S. E., Bhat, M. K., Bleck, R., Canuto, V., Chen, Y.-H., Cheng, Y., Clune, T. L., Del Genio, A., de Fainchtein, R., Faluvegi, G., Hansen, J. E., Healy, R. J., Kiang, N. Y., Koch, D., Lacis, A. A., LeGrande, A. N., Lerner, J., Lo, K. K., Matthews, E. E., Menon, S., Miller, R. L., Oinas, V., Oloso, A. O., Perlwitz, J. P., Puma, M. J., Putman, W. M., Rind, D., Romanou, A., Sato, M., Shindell, D. T., Sun, S., Syed, R. A., Tausnev, N., Tsigaridis, K., Unger, N., Voulgarakis, A., Yao, M.-S., and Zhang, J. (2014). Configuration and assessment of the GISS ModelE2 contributions to the CMIP5 archive. *Journal of Advances in Modeling Earth Systems*, **6**(1), 141–184. DOI: 10.1002/2013MS000265.

Séférian, R., Gehlen, M., Bopp, L., Resplandy, L., Orr, J. C., Marti, O., Dunne, J. P., Christian, J. R., Doney, S. C., Ilyina, T., Lindsay, K., Halloran, P. R., Heinze, C., Segschneider, J., Tjiputra, J., Aumont, O., and Romanou, A. (2016). Inconsistent strategies to spin up models in CMIP5: implications for ocean biogeochemical model performance assessment. *Geoscientific Model Development*, **9**(5), 1827–1851. DOI: 10.5194/gmd-9-1827-2016.

Sen Gupta, A., Muir, L. C., Brown, J. N., Phipps, S. J., Durack, P. J., Monselesan, D., and Wijffels, S. E. (2012). Climate Drift in the CMIP3 Models. *Journal of Climate*, **25**(13), 4621–4640. DOI: 10.1175/JCLI-D-11-00312.1.

Sen Gupta, A., Jourdain, N. C., Brown, J. N., and Monselesan, D. (2013). Climate Drift in the CMIP5 Models. *Journal of Climate*, **26**(21), 8597–8615. DOI: 10.1175/JCLI-D-12-00521.1.

Slater, A. G. and Lawrence, D. M. (2013). Diagnosing Present and Future Permafrost from Climate Models. *Journal of Climate*, **26**(15), 5608–5623. DOI: 10.1175/JCLI-D-12-00341.1.

Smerdon, J. E. (2012). Climate models as a test bed for climate reconstruction methods: pseudoproxy experiments. *Wiley Interdisciplinary Reviews: Climate Change*, **3**(1), 63–77. DOI: 10.1002/wcc.149.

Smerdon, J. E., Pollack, H. N., Enz, J. W., and Lewis, M. J. (2003). Conduction-dominated heat transport of the annual temperature signal in soil. *Journal of Geophysical Research: Solid Earth*, **108**(B9). n/a–n/a. DOI: 10.1029/2002JB002351.

Soden, B. J., Collins, W. D., and Feldman, D. R. (2018). Reducing uncertainties in climate models. *Science*, **361**(6400), 326–327. DOI: 10.1126/science.aau1864.

Stevens, M. B., González-Rouco, J. F., and Beltrami, H. (2008). North American climate of the last millennium: Underground temperatures and model comparison. *Journal of Geophysical Research: Earth Surface*, **113**(F1). n/a–n/a. DOI: 10.1029/2006JF000705.

Stieglitz, M. and Smerdon, J. E. (2007). Characterizing Land–Atmosphere Coupling and the Implications for Subsurface Thermodynamics. *Journal of Climate*, **20**(1), 21–37. DOI: 10.1175/JCLI3982.1.

Taylor, K. E., Stouffer, R. J., and Meehl, G. A. (2011). An Overview of CMIP5 and the Experiment Design. *Bulletin of the American Meteorological Society*, **93**(4), 485–498. DOI: 10.1175/BAMS-D-11-00094.1.

Vasseur, G., Bernard, P., de Meulebrouck, J. V., Kast, Y., and Jolivet, J. (1983). Holocene paleotemperatures deduced from geothermal measurements. *Palaeogeography, Palaeoclimatology, Palaeoecology*, **43**(3), 237 –259. DOI: https://doi.org/10.1016/0031-0182(83)90013-5.

Vincenty, T. (1975). Direct and Inverse Solutions of Geodesics on the Ellipsoid with Application of Nested Equations. *Survey Review*, **23**(176), 88–93. DOI: 10.1179/sre.1975.23.176.88.

Wang, J and Bras, R. (1999). Ground heat flux estimated from surface soil temperature. *Journal of Hydrology*, **216**(3), 214 –226. DOI: https://doi.org/10.1016/S0022-1694(99)00008-6.

Wu, T., Li, W., Ji, J., Xin, X., Li, L., Wang, Z., Zhang, Y., Li, J., Zhang, F., Wei, M., Shi, X., Wu, F., Zhang, L., Chu, M., Jie, W., Liu, Y., Wang, F., Liu, X., Li, Q., Dong, M., Liang, X., Gao, Y., and Zhang, J. (2013). Global carbon budgets simulated by the Beijing Climate Center Climate System Model for the last century. *Journal of Geophysical Research: Atmospheres*, **118**(10), 4326–4347. DOI: 10.1002/jgrd.50320.

Wu, T., Song, L., Li, W., Wang, Z., Zhang, H., Xin, X., Zhang, Y., Zhang, L., Li, J., Wu, F., Liu, Y., Zhang, F., Shi, X., Chu, M., Zhang, J., Fang, Y., Wang, F., Lu, Y., Liu, X., Wei, M., Liu, Q., Zhou, W., Dong, M., Zhao, Q., Ji, J., Li, L., and Zhou, M. (2014). An overview of BCC climate system model development and application for climate change studies. English. *Journal of Meteorological Research*, **28**(1), 34–56. DOI: 10.1007/s13351-014-3041-7.

Xiao-Ge, X., Tong-Wen, W., and Jie, Z. (2013). Introduction of {CMIP5} Experiments Carried out with the Climate System Models of Beijing Climate Center. *Advances in Climate Change Research*, **4**(1), 41 –49. DOI: http://dx.doi.org/10.3724/SP.J.1248.2013.041.

Yukimoto, S., Adachi, Y., Hosaka, M., Sakami, T., Yoshimura, H., Hirabara, M., Tanaka, T. Y., Shindo, E., Tsujino, H., Deushi, M., Mizuta, R., Yabu, S., Obata, A., Nakano, H., Koshiro, T., Ose, T., and Kitoh, A. (2012). A New Global Climate Model of the Meteorological Research Institute: MRI-CGCM; -Model Description and Basic Performance-. *Journal of the Meteorological Society of Japan. Ser. II*, **90A**, 23–64. DOI: 10.2151/jmsj.2012-A02.

3 Long-Term Global Ground Heat Flux and Continental Heat Storage from Geothermal Data

Reference This chapter is based on a manuscript submitted to *Climate of the Past*: Cuesta-Valero, F. J. et al. (2020). Long-Term Global Ground Heat Flux and Continental Heat Storage from Geothermal Data. *Climate of the Past Discussions*, **2020**, 1–27. DOI: 10.5194/cp-2020-65.

Abstract Energy exchanges among climate subsystems are of critical importance to determine the climate sensitivity of the Earth system to greenhouse gases, to quantify the magnitude and evolution of the Earth's radiative imbalance, and to project the evolution of future climate. Thus, ascertaining the magnitude and change of the energy distribution within climate subsystems has become urgent in recent years. Here, we provide new global estimates of changes in ground surface temperature, ground surface heat flux and continental heat storage derived from geothermal data using an expanded database and new techniques to assess uncertainties associated with borehole methodology. Results reveal markedly higher changes in ground heat flux and heat storage within the continental subsurface than previously reported, with land temperature changes of 1 K and continental heat gains of around 12 ZJ during the last part of the 20th century relative to preindustrial times. Half of the heat gain by the continental subsurface since 1960 has occurred in the last twenty years. These results reinforce the necessity of using deeper land surface model components

to correctly reproduce the Earth heat inventory within global transient climate simulations.

3.1 Introduction

Climate change is a consequence of the current radiative imbalance at the top of the atmosphere, which delivers an excess amount of energy to the Earth system in comparison with preindustrial conditions (Hansen et al., 2011; Stephens et al., 2012; Lembo et al., 2019). Nonetheless, the radiative imbalance presents an inter-hemispheric asymmetry, being larger in the southern hemisphere (Loeb et al., 2016; Irving et al., 2019). This asymmetry causes greater heat uptake by the ocean surface in the southern hemisphere in comparison to the northern hemisphere. Hence, a cross-equatorial northward transport of heat emerges to compensate this asymmetry (Lembo et al., 2019), in addition to the global meridional heat transport caused by the different incident radiation levels at the tropical and polar oceans (Trenberth et al., 2019). The hemispheric distribution of heat uptake, heat storage and heat transport is expected to change under different emission scenarios (Irving et al., 2019), meaning that characterizing where the heat enters the system (uptake), where the heat is allocated (storage), and where the heat is redistributed (transport) is of critical importance to understand the evolution of climate change.

The vast majority of excess heat due to the Earth's radiative imbalance is stored in the ocean (84-93 %), followed by the cryosphere (4-7 %) and the continental subsurface (2-5 %), with the atmosphere showing the smallest heat storage (1-4 %) (Levitus et al., 2005; Church et al., 2011). Therefore, extensive resources are devoted to monitor and understand the evolution of the ocean heat content, since it is also an indirect measure of the magnitude and variation of the radiative imbalance at the top of the atmosphere (Palmer et al., 2011; Palmer et al., 2014; Johnson et al., 2016; Riser et al., 2016; von Schuckmann et al., 2016). The rest of the components of the climate system have relevant roles in the EHI, despite their small contribution to storage (Levitus et al., 2005; Church et al., 2011; Hansen et al., 2011; von Schuckmann et al., 2016). For instance, energy-dependent processes include permafrost stability and associated permafrost carbon feedback (MacDougall et al., 2012; Hicks Pries et al., 2017),

changes in circulation patterns (Tomas et al., 2016; Screen et al., 2018) and sea level rise (Jacob et al., 2012; Vaughan et al., 2013; Dutton et al., 2015). The additional energy in the atmosphere, cryosphere and continental subsurface also affects near-surface conditions, having important consequences for society. Increases in atmospheric heat content produce warmer surface air temperatures and larger water content within the atmosphere that can impact crop yields, and consequently global food security (Lloyd et al., 2011; Rosenzweig et al., 2014; Phalkey et al., 2015; Campbell et al., 2016) as well as degrading human health due to heat stress (Sherwood et al., 2010; Matthews et al., 2017; Watts et al., 2019). Floods induced by extreme precipitation events, the frequency and intensity of which are affected by the amount of water in the atmosphere, as well as floods induced by sea level rise caused by the thermal expansion of the ocean and melting of Greenland and Antarctica ice sheets, are likely to impact human settlements (McGranahan et al., 2007; Kundzewicz et al., 2014). Furthermore, all these alterations in surface environmental conditions may enhance the spread of diseases (Levy et al., 2016; McPherson et al., 2017; Wu et al., 2016; Watts et al., 2019), among other potential risks.

Long-term global estimates of heat storage within the continental subsurface (ground heat content, GHC) have been previously estimated from Borehole Temperature Profile (BTP) measurements. Changes in the energy balance at the land surface add or remove heat from the upper continental crust, changing the long-term subsurface equilibrium temperature profile (Beltrami, 2002b). Such temperature changes propagate through the ground by conduction, and are recorded in the subsurface as perturbations on the quasi-steady state vertical temperature profile. Establishing a borehole climatology consists of estimating variations in ground surface temperature and heat flux from these recorded alterations in the subsurface thermal regime. Ground Surface Temperature Histories (GSTHs) and Ground Heat Flux Histories (GHFHs) have been retrieved from BTP measurements both at regional and at hemispheric scales for multi-century to multi-millennial time periods (Lane, 1923; Cermak, 1971; Beck, 1977; Vasseur et al., 1983; Lachenbruch et al., 1986; Huang et al., 2000; Harris et al., 2001; Roy et al., 2002; Beltrami et al., 2004; Hartmann et al., 2005; Beltrami et al., 2006; Hopcroft et al., 2007; Chouinard et al., 2009; Davis et al., 2010; Barkaoui et al., 2013; Demezhko et al., 2015; Jaume-Santero

et al., 2016; Pickler et al., 2016), constituting an useful reference for evaluating climate simulations performed by atmosphere-ocean Coupled General Circulation Models (CGCMs) beyond the observational period (González-Rouco et al., 2009; Stevens et al., 2008; MacDougall et al., 2010; Cuesta-Valero et al., 2016; García-García et al., 2016; Cuesta-Valero et al., 2019), as well as for evaluating reconstructions derived from other paleoclimate data (Fernández-Donado et al., 2013; Masson-Delmotte et al., 2013; Jaume-Santero et al., 2016; Beltrami et al., 2017).

Previous global estimates of GHC, GHFHs and GSTHs were retrieved from BTP measurements nearly two decades ago (Pollack et al., 1998; Huang et al., 2000; Beltrami et al., 2002; Beltrami, 2002a; Pollack et al., 2004), including a limited characterization of uncertainties. Since then, advances in borehole methodology allow the assessment of uncertainty in borehole reconstructions induced by a series of factors: the presence of advection and freezing phenomena, the sampling rate and the depth range used in the determination of the quasi-equilibrium profile, the depth of the profile, the different logging dates of the profiles, the noise in the measured profile, the model resolution for obtaining stable solutions, the spatial distribution of borehole measurements, and the transient variations in the subsurface thermal regime due to the end of the last glacial cycle (Bodri et al., 2005; Hartmann et al., 2005; Reiter, 2005; González-Rouco et al., 2006; Mottaghy et al., 2006; González-Rouco et al., 2009; Rath et al., 2012; Beltrami et al., 2015a,b; García-García et al., 2016; Jaume-Santero et al., 2016; Beltrami et al., 2017; Melo-Aguilar et al., 2019). These advances together with the availability of new BTP measurements necessitate an update of the global long-term evolution of ground heat content from borehole data.

Here, we use an expanded borehole database to estimate global GSTHs, GHFHs, and GHC within the continental subsurface for the last four centuries. Surface temperature and heat flux histories are retrieved from each BTP using a Singular Value Decomposition (SVD) algorithm, one of the standard borehole methodologies employed in previous analyses (Beltrami et al., 2002; Beltrami, 2002a), as well as a new approach based on generating an ensemble of inversions for each temperature profile to explore additional sources of uncertainty unaddressed in previous global borehole reconstructions.

3.2 Theory

3.2.1 Subsurface Temperature Profile

In borehole climatology, the continental subsurface is typically represented as a semi-infinite homogenous half-space without internal sources of heat, where energy exchanges at the land surface and heat flux from the Earth's interior are considered as the upper and bottom boundary conditions. I.e., the heat from natural radioactive decay of uranium, thorium and potassium in the subsurface is considered negligible at the depths used in this study (Bodri et al., 2007). The local subsurface thermal regime is, therefore, the result of a balance between the surface thermal state and the thermal conditions of the Earth's interior. If surface conditions remain stable at long time scales, the subsurface thermal regime would be in a quasi-equilibrium since the flux from the Earth's interior is constant at geological time scales (million years). Thereby, the subsurface temperature profile can be expressed as the superposition of the transient temperature due to changes in the surface conditions (T_t) relative to the long-term quasi-equilibrium state (Carslaw et al., 1959):

$$T(z) = T_0 + q_0 R(z) + T_t(z), \tag{3.1}$$

where z is depth, T_0 is the long-term surface temperature, q_0 is the heat flux from the Earth's interior, and $R(z) = \int_0^z \frac{\mathrm{d}z'}{\lambda(z')}$ is the thermal depth, which depends on the thermal conductivity (λ) of the ground (Bullard et al., 1939). Since measurements of thermal conductivity profiles are scarce and the measured profiles typically display variations around a constant value with depth, the thermal conductivity can be assumed to be constant and Equation 3.1 can be rewritten as

$$T(z) = T_0 + \Gamma \cdot z + T_t(z), \tag{3.2}$$

with $\Gamma = \frac{q_0}{\lambda}$ the equilibrium subsurface thermal gradient. The term $T_0 + \Gamma \cdot z$ in Equation 3.2 describes the quasi-equilibrium temperature profile, and can be determined from the deepest part of a BTP - that is, the least affected part of the log by recent perturbations of the energy balance at the surface.

The propagation of temperature variations in a one-dimensional, homoge-

nous, isotropic medium without internal sources of heat is governed by the heat diffusion equation

$$\frac{\partial T}{\partial t} = \kappa \frac{\partial^2 T}{\partial z^2}, \tag{3.3}$$

where T is temperature, t is time, κ is the thermal diffusivity of the medium and z is the spatial dimension. An instantaneous change in surface temperature (ΔT_0) is propagated through the ground as described in Equation 3.3, altering the quasi-equilibrium temperature profile with time following Carslaw et al. (1959)

$$T(z,t) = \Delta T_0 \cdot \operatorname{erfc}\left(\frac{z}{2\sqrt{\kappa t}}\right), \tag{3.4}$$

where erfc is the complementary error function, and t is time since the surface temperature change. A series of surface temperature perturbations will propagate through the ground as the superposition of transient variations of the long-term subsurface thermal regime:

$$T_t(z) = \sum_{i=1}^{N} \Delta T_i \left[\operatorname{erfc}\left(\frac{z}{2\sqrt{\kappa t_i}}\right) - \operatorname{erfc}\left(\frac{z}{2\sqrt{\kappa t_{i-1}}}\right)\right], \tag{3.5}$$

where ΔT_i are changes in surface temperature at i time step. Equation 3.5 is also the solution of the forward problem: given an upper (surface) boundary condition, this equation describes the perturbation of the subsurface temperature profile in response to a temporal series of ground surface temperature changes (Lesperance et al., 2010).

3.2.2 Subsurface Flux Profile

Since the conductive heat flux (q) in an isotropic medium is related to the temperature gradient of the subsurface temperature profile by Fourier's equation

$$q = -\lambda \frac{\partial T}{\partial z}, \tag{3.6}$$

the propagation of heat flux through a one-dimensional, homogenous medium without internal sources of heat satisfies:

$$\frac{\partial q}{\partial t} = \kappa \frac{\partial^2 q}{\partial z^2}. \tag{3.7}$$

That is, the propagation of both temperature and heat flux through the ground is governed by the diffusion equation (Carslaw et al., 1959; Turcotte et al., 2002). As in the case of temperature profiles, the heat flux profile can be expressed as

$$q(z) = q_0 + q_t(z), \tag{3.8}$$

where q_0 is the equilibrium geothermal flux from the Earth's interior. Therefore, alterations in the subsurface equilibrium flux profile due to an instantaneous perturbation of the long-term surface flux (Δq_0) can be expressed as

$$q(z,t) = \Delta q_0 \cdot \operatorname{erfc}\left(\frac{z}{2\sqrt{\kappa t}}\right), \tag{3.9}$$

where t is time since the perturbation. A series of perturbations of the surface flux generates a superposition of transient variations of the long-term subsurface thermal gradient as

$$q_t(z) = \sum_{i=1}^{N} \Delta q_i \left[\operatorname{erfc}\left(\frac{z}{2\sqrt{\kappa t_i}}\right) - \operatorname{erfc}\left(\frac{z}{2\sqrt{\kappa t_{i-1}}}\right)\right], \tag{3.10}$$

mirroring the forward model for surface temperature variations described in Equation 3.5 and representing the solution of the forward problem for variations in surface heat flux (Beltrami, 2001; Beltrami et al., 2006).

3.2.3 Inversion Problem

The inversion problem consists of retrieving the past ground surface temperature histories that generated the observed temperature perturbation profiles, or the ground heat flux histories that generated the heat flux anomaly profiles. A system of equations can be derived by combining Equations 3.2 and 3.5 for the temperature case, and Equations 3.8 and 3.10 for the heat flux case, with the

solution of such systems yielding an estimate of the past long-term evolution of surface temperature and surface heat flux, respectively (Vasseur et al., 1983; Beltrami et al., 1992; Mareschal et al., 1992; Shen et al., 1992; Beltrami, 2001; Hartmann et al., 2005). This system can be expressed for the temperature case as:

$$\begin{pmatrix} T_t(z_1) \\ \vdots \\ T_t(z_i) \\ \vdots \\ T_t(z_{N_z}) \end{pmatrix} = \begin{pmatrix} M_{1,1} & \cdots & M_{1,j} & \cdots & M_{1,N_t} \\ \vdots & \ddots & \vdots & \ddots & \vdots \\ M_{i,1} & \cdots & M_{i,j} & \cdots & M_{i,N_t} \\ \vdots & \ddots & \vdots & \ddots & \vdots \\ M_{N_z,1} & \cdots & M_{N_z,j} & \cdots & M_{N_z,N_t} \end{pmatrix} \begin{pmatrix} \Delta T_1 \\ \vdots \\ \Delta T_j \\ \vdots \\ \Delta T_{N_t} \end{pmatrix} \tag{3.11}$$

wrere $T_t(z_i)$ are the temperature anomalies at the depth z_i, and ΔT_i are the step change in surface temperature to be determined, that is the proposed inversion model. The elements $M_{i,j}$ are defined from the forward model (Equation 3.5)

$$M_{i,j} = \operatorname{erfc}\left(\frac{z_i}{2\sqrt{\kappa t_j}}\right) - \operatorname{erfc}\left(\frac{z_i}{2\sqrt{\kappa t_{j-1}}}\right). \tag{3.12}$$

Note that a similar system can be written in terms of heat flux using Equation 3.10. The rank of the system is given by the number of time steps in the proposed inversion model (N_t), and is generally smaller than the number of measurements in the profile (N_z). That is, there are more equations than parameters in the system, thus both the temperature and heat flux systems are overdetermined, and do not have an unique solution. Therefore, these systems are solved using a Singular Value Decomposition algorithm (Lanczos, 1961) as the one described in Mareschal et al. (1992) and Clauser et al. (1995).

The system in Equation 3.11 can be expressed as a matrix equation of the form:

$$\mathbf{T}_{obs} = \mathbf{M}\mathbf{T}_{model}, \tag{3.13}$$

where $\mathbf{T}_{obs}$ is the data vector (anomaly temperature profile of heat flux profile), $\mathbf{M}$ is the matrix containing the coefficients given by Equation 3.12 (or the equivalent expression for the case of heat flux), and $\mathbf{T}_{model}$ is a vector containing the step change model to be determined. The SVD algorithm decomposes the matrix of coefficients as

$$\mathbf{M} = \mathbf{U}\mathbf{S}\mathbf{V}^T, \tag{3.14}$$

with $\mathbf{U}$ and $\mathbf{V}$ orthonormal matrices of dimension $N_z \times N_z$ and $N_t \times N_t$, respectively, and $\mathbf{S}$ a rectangular matrix ($N_z \times N_t$) containing the eigenvalues α_j in the diagonal. Therefore, the general solution can be expressed as:

$$\mathbf{T}_{model} = \mathbf{M}^{-1}\mathbf{T}_{obs} = \mathbf{V}\mathbf{S}^{-1}\mathbf{U}^{T}\mathbf{T}_{obs}. \tag{3.15}$$

However, the solution of Equation 3.15 is dominated by noise from small eigenvalues, as the only non-zero elements of $\mathbf{S}^{-1}$ are the inverse of the eigenvalues in the diagonal of the matrix (Mareschal et al., 1992). Accordingly, small eigenvalues need to be removed from $\mathbf{S}^{-1}$ (i.e., are replaced by zeros) for stabilizing the solution, but at the cost of losing temporal resolution in the model.

3.3 Analysis

3.3.1 Borehole Data

BTPs were collected from four databases. The National Oceanic and Atmospheric Administration (NOAA) server (NOAA, 2019) contains global data; the database presented in Jaume-Santero et al. (2016) includes data for North America; logs from Tasmania were retrieved from Suman et al. (2017); and measurements from Chile were obtained from Pickler et al. (2018). Profiles from all databases were screened to avoid repetitions, resulting in 1266 independent logs in total.

Nonetheless, not all these BTPs are employed in the analysis. A process for selecting suitable logs is applied, based on trimming the maximum depth of the available BTPs and requiring a certain number of measurements at critical depth ranges. Thereby, all BTPs used here must include at least one temperature measurement between 15 m and 100 m, and between 250 m and 310 m. Profiles containing less than three measurements between 200 m and 300 m were discarded since it was impossible to perform a linear regression analysis to determine the quasi-equilibrium profile (see Section 3.3.3 below). All remaining logs were truncated from 15 m to 300 m depth, resulting in 1079 logs selected for this analysis. Thereby, we ensure that the profiles include information from the logging year to several centuries back in time and cover the same time span, since the relationship between time (t) required for a change in the surface energy balance to reach a certain depth (z) can be approximated as (Carslaw et al.,

1959; Pickler et al., 2016; Cuesta-Valero et al., 2019):

$$t \approx \frac{z^2}{4\kappa}, \tag{3.16}$$

This depth filtering constitutes the main methodological difference in comparison with previous borehole studies (including Beltrami et al., 2002; Beltrami, 2002a), since those assessments analyzed all available logs independently of their depth range, thus mixing temporal references. However, recent works have shown that using subsurface profiles with different depths affects the estimated GSTHs (González-Rouco et al., 2009; Beltrami et al., 2015b; Melo-Aguilar et al., 2019). This issue is avoided here by the selection criteria applied to the assembled BTP database. Additionally, BTPs were measured at different dates, but the logging year of the profiles had been taken intro account only in a small number of works (e.g., González-Rouco et al., 2009; Jaume-Santero et al., 2016; Melo-Aguilar et al., 2019). We aggregate the retrieved GSTHs and GHFHs from BTPs considering the logging date of each borehole profile (Figure 3.1), thus the number of borehole inversions available for analysis varies with time.

3.3.2 Surface Air Temperature Data

Meteorological measurements of surface air temperature from the Climate Research Unit (CRU) at East Anglia university are also used in this study to compare with borehole estimates. Mean global surface air temperature anomalies relative to 1961-1990 Common Era (CE) from the CRU TS 4.01 product (Harris et al., 2014) are employed to compare with GSTHs retrieved from borehole profiles. Results for the entire CRU spatial and temporal domains are provided from 1901 CE to 2016 CE, as well as results considering only locations and dates containing borehole inversions.

3.3.3 Inversion of Borehole Temperature Profiles

Standard Inversions

We invert the BTPs filtered as described in Section 3.3.1 (Figure 3.1) to obtain GSTHs while estimating the uncertainty from the determination of the equilibrium profile, as a reference to compare with the uncertainty estimates of recent

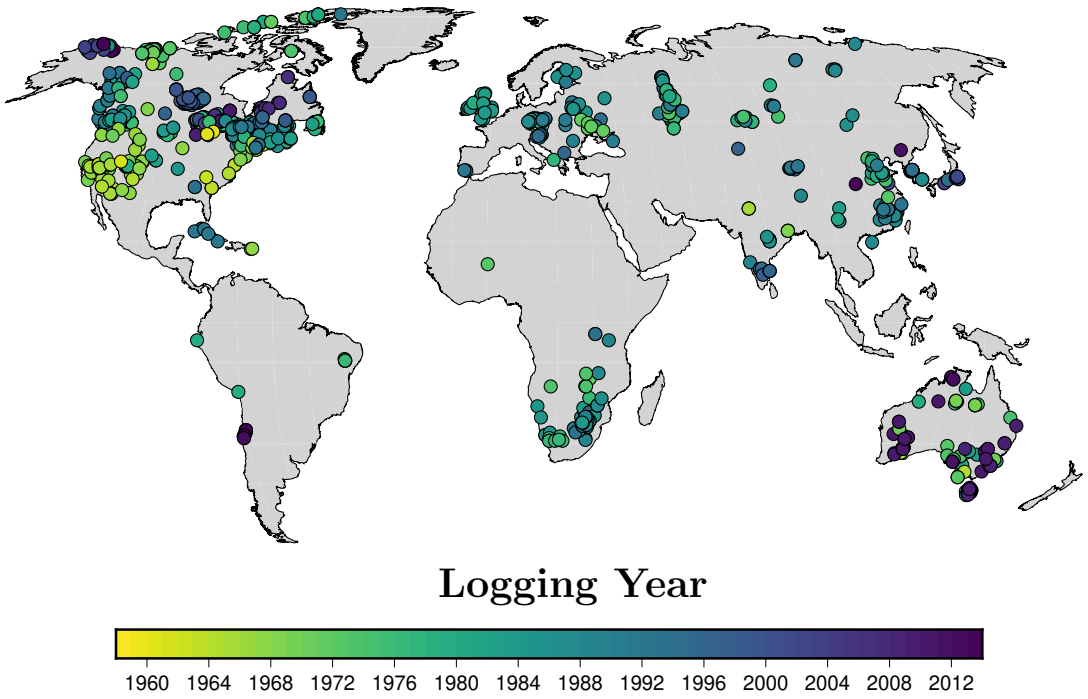

Figure 3.1: Logging years of the 1079 boreholes considered in the analysis.

works using the same SVD algorithm (Beltrami et al., 2015a; Jaume-Santero et al., 2016; Pickler et al., 2016, 2018). In this case, all logs are inverted using a model based on a thermal conductivity of $3\,\mathrm{W\,m^{-1}\,K^{-1}}$, a volumetric heat capacity of $3 \times 10^6\,\mathrm{J\,m^{-3}\,K^{-1}}$, and thus a thermal diffusion of $1 \times 10^{-6}\,\mathrm{m^2\,s^{-1}}$. The same SVD algorithm used in Beltrami (2002a) and Beltrami et al. (2002) is applied to generate the GSTHs for three step change models, since there is no preferential inversion model. All BTPs are inverted using models based on step changes of 25, 40 and 50 years to reconstruct the surface signal for 400 years preceding the logging date of the profile (i.e., inversion models of 16, 10 and 8 time steps, respectively), with all inversions including the four highest eigenvalues. We regard this as the Standard inversion approach and will serve as a reference to the new methods described below.

The equilibrium temperature profile is estimated in order to obtain the anomaly profile that is inverted by the SVD algorithm. The equilibrium profile is estimated from the deepest part of each truncated BTP, since that is the zone least affected by the recent climate change signal (grey zone in Figure 3.2a). A linear regression analysis of the lowermost 100 m of each profile (from 200 m to 300 m depth in our analysis, straight lines in Figure 3.2a) is performed to estimate the values determining the quasi-equilibrium temperature profile; that is, the long-term surface temperature (T_0) and the equilibrium geothermal gradient (Γ). We use the last hundred meters rather than a broader depth range as a compromise between the need to characterize noise and retrieve as much climatic information as possible from each log (Beltrami et al., 2015a). The anomaly profile is then retrieved by subtracting the quasi-equilibrium temperature profile from the measured log (black dots in Figure 3.2b). Additionally, the uncertainties in the slope (Γ) and intercept (T_0) values allow two extremal temperature anomaly profiles to be obtained representing the 95 % confidence interval (two standard deviations) of the anomaly profile (red and blue dots in Figure 3.2b). The inversion of these additional anomaly profiles provides the 95 % confidence interval of the retrieved GSTHs from each borehole. We do not invert the heat flux profiles using this approach, but provide surface flux estimates from the retrieved surface temperature histories to compare with Beltrami (2002a) and Beltrami et al. (2002) (see Section 3.3.4 for details).

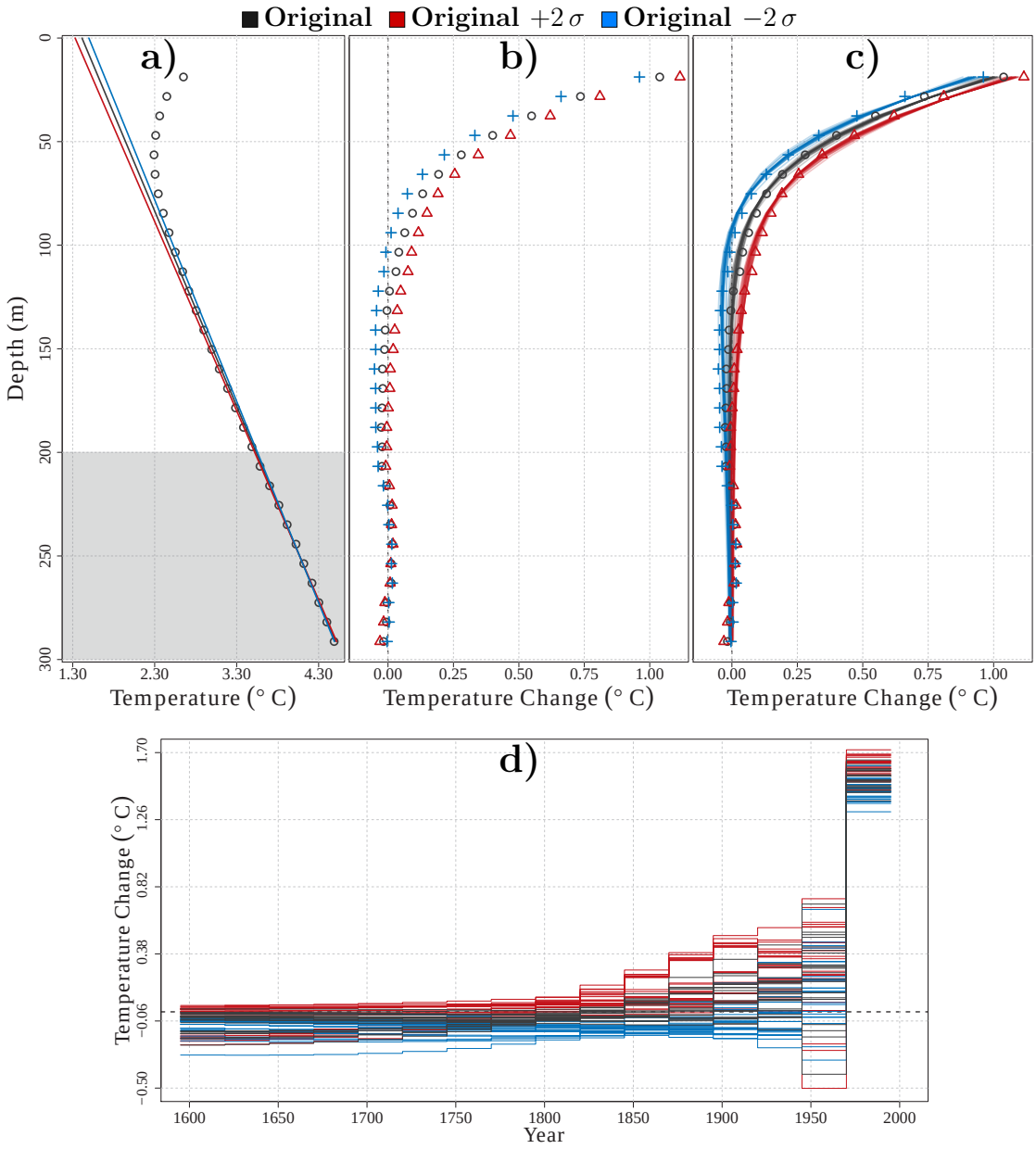

Figure 3.2: Borehole temperature profile measurements at Fox Mine (CA_9519), Manitoba (Canada) as an example to explain the inversion approaches in this study. (a) Observed original profile (black dots) as well as the estimated subsurface quasi-equilibrium temperature profile (black line) and the two extremal temperature profiles (red and blue lines) displaying the 95 % uncertainty in determining the quasi-equilibrium profile. All three equilibrium profiles were estimated from the linear regression analysis of the deepest part of the measured profile (from 200 m to 300 m, grey zone). (b) Anomaly profiles estimated by subtracting the three equilibrium profiles to the original temperature profile. (c) As in (b), but including the 243 synthetic profiles generated from the corresponding ground surface temperature histories constituting the PPI ensemble of this borehole (red, blue and black shades). (d) Final ensemble of ground surface temperature histories estimated from the 5th, 50th and 95th weighted percentiles for this borehole. Each history is weighted depending on its performance against the corresponding anomaly profile (panel c).

Perturbed Parameter Inversions

Although the inversion approach used in previous studies was successful in retrieving the past long-term evolution of ground surface temperatures and ground heat fluxes at BTP locations, several sources of uncertainty remained unaddressed. Here, we use a new approach based on generating an ensemble of inversions using the SVD algorithm described in Mareschal et al. (1992) for each borehole profile to account for as many sources of uncertainty as possible. The ensemble contains inversions retrieved by considering a range of values for the thermal properties, different number of eigenvalues in the SVD algorithm, as well as the inversions of the two additional anomaly profiles generated from the estimate of the quasi-equilibrium temperature profile. Thereby, three sources of uncertainty are considered in the analysis, expanding the methodology of previous studies based on BTP inversions performed with the same SVD algorithm (Beltrami et al., 2015a; Jaume-Santero et al., 2016; Pickler et al., 2016, 2018). Additionally, all BTPs are inverted using the three different inversion models used in the Standard approach. We name this new approach Perturbed Parameter Inversion (PPI) due to the similarities with the generation of perturbed parameter ensembles in climate modeling (e.g., Collins et al., 2011).

The PPI approach considers the three anomaly profiles estimated from the uncertainty in determining the subsurface equilibrium profile as in the Standard approach (e.g., Jaume-Santero et al., 2016, red and blue lines in Figure 3.2). Each of these anomaly profiles is inverted using different values of thermal conductivity (λ) and volumetric heat capacity (ρC). The values of thermal conductivity considered in this analysis are 2.5, 3 and 3.5 $\mathrm{W\,m^{-1}\,K^{-1}}$, while the values for volumetric heat capacity are 2.5, 3 and $3.5 \times 10^6\,\mathrm{J\,m^{-3}\,K^{-1}}$. That is, the typical values of $3\,\mathrm{W\,m^{-1}\,K^{-1}}$ and $3 \times 10^6\,\mathrm{J\,m^{-3}\,K^{-1}}$ for the conductivity and heat capacity, respectively, as well as two extremal cases to account for plausible variations of thermal properties. The combination of each pair of conductivities and heat capacities yields a series of 9 values for thermal diffusivity ranging between 0.7 and $1.4 \times 10^{-6}\,\mathrm{m^2\,s^{-1}}$. Additionally, estimates obtained for the three inversion models use different numbers of eigenvalues to retrieve the surface signal, integrating the sensitivity of the SVD algorithm to small eigenvalues and to the length of each time step into the inversion (Hartmann et al., 2005;

Melo-Aguilar et al., 2019). Thus, inversions based on the 25 yr step change model use the highest 3, 4 and 5 eigenvalues, inversions based on the 40 yr step change model use the highest 2, 3 and 4 eigenvalues, and inversions based on the 50 yr step change model use the highest 2, 3 and 4 eigenvalues.

Therefore, the PPI ensemble generated from each original borehole temperature profile consists of 243 different GSTH inversions (see the case for GHFHs below). All these inversions are then propagated using a purely conductive forward model in order to obtain synthetic BTPs as described in Equation 3.5, which are compared with the original anomaly profiles (Figure 3.2c). This allows for an evaluation of the performance of the different parameter variants in the inversion and to attribute relative weights to them. Root Mean Squared Errors (RMSEs) between the anomaly profiles and the synthetic profiles generated from the inversions are computed to assign a weight to each inversion following a gaussian function as in Knutti et al. (2017):

$$w_i = \exp\left\{\frac{-\mathrm{RMSE}_i^2}{\sigma^2}\right\}, \tag{3.17}$$

where w_i is the weight associated to the ith inversion, and σ is a parameter determining which RMSEs are deemed large and which are deemed small. We select the typical error in BTP measurements ($\sigma = 50\,\mathrm{mK}$) as criterion to assess how each inversion should be weighted, that is, to evaluate which RSMEs are large and which are small.

Thus, each inversion is classified according to the realism of its associated synthetic anomaly profile. Nevertheless, unrealistic solutions may arise as result of the broad range of parameters and inversion models considered even after weighting each inversion. Hence, we introduce here a new additional criterion to asses all the 243 inversions per BTP based on the variability of surface air temperature measurements as a guide. A temperature change in an inverted GSTH is considered unrealistic if it is larger than the maximum change obtained from the histogram of temperature variations between consecutive time steps from the CRU data. This histogram is created by aggregating temperature changes between consecutive time steps after averaging the original temperature series at each grid cell in temporal windows of 25 years (i.e, running means of 25 years,

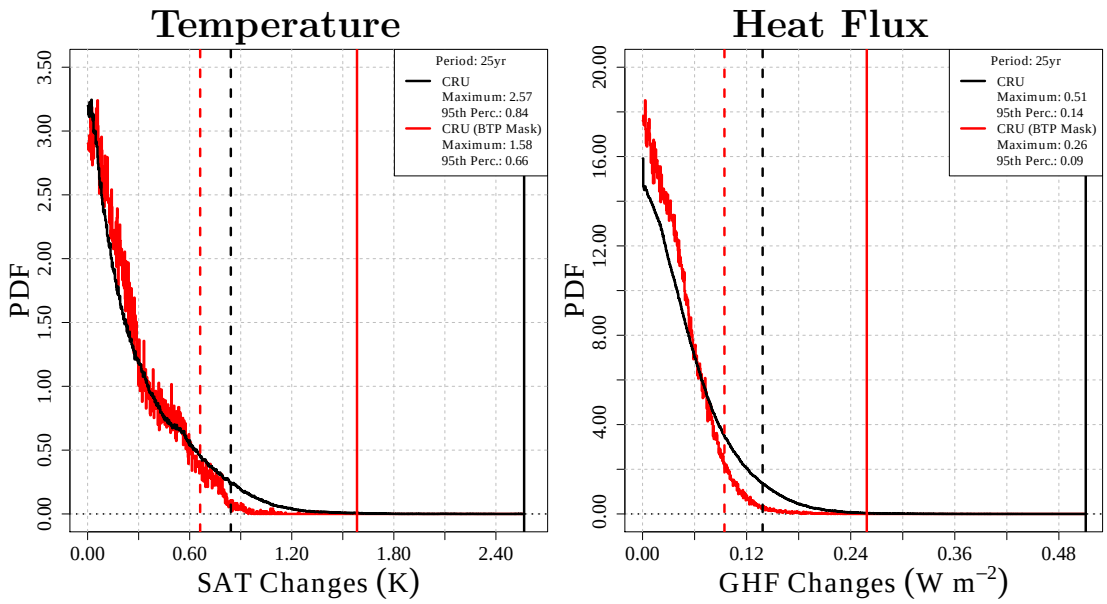

Figure 3.3: Histograms of temperature and heat flux variations between consecutive time steps from CRU temperature anomalies relative to 1961-1990 CE. The high-frequency temperature variations were filtered out by averaging the original temperature series in temporal windows of 25 years. The heat flux series were generated by applying Equation 3.19 to CRU temperatures, thus the high-frequency variability is not included in the flux histogram.

Figure 3.3). The averaging of the original temperature series is necessary to remove high-frequency variability that is not present in GSTHs from BTP inversions. That is, a GSTH is deemed as unrealistic and removed from the analysis if the temperature change between at least one pair of consecutive time steps is larger than 2.57 K for the three inversion models. The 5th, 50th, and 95th weighted percentiles are eventually estimated from the ensemble of remaining inversions (Figure 3.2d) for each borehole profile. The ensemble containing the weighted percentiles from GSTHs from all BTPs is called the PPIT ensemble hereinafter.

The same approach is applied to the corresponding heat flux profiles to retrieve ground heat flux histories from borehole data. The heat flux profiles are generated from the three estimated temperature anomaly profiles for each measured log using Fourier's equation (Equation 3.6) as

$$q_i = -\lambda \frac{T_{i+1} - Ti}{z_{i+1} - z_i}. \tag{3.18}$$

Those profiles are then inverted using the PPI approach described above. The thermal conductivity for estimating the heat flux profile is set to match the values used for each perturbed parameter inversion. Thereby, we obtain 243 heat flux histories for each original log, which are compared to the corresponding flux anomaly profile (using Equation 3.10) and weighted as in the case of temperature histories. Changes in GHFHs are compared to the histogram created by aggregating heat flux changes estimated from the CRU temperature data and Equation 3.19 in order to discard unrealistic heat flux histories. As in the case of temperature changes, heat flux changes between consecutive time steps are aggregated after averaging the original heat flux series from each grid cell over temporal windows of 25 years (Figure 3.3). Surface heat flux histories are deemed unrealistic if the difference between at least one pair of consecutive time steps is larger than $0.51\,\mathrm{W\,m^{-2}}$ for the three inversion models. The ensemble containing the 5th, 50th and 95th weighted percentiles from GHFHs from all BTPs is called the PPIF ensemble hereinafter.

Inversions of temperature profiles and from heat flux profiles using the PPI and Standard approaches need to include the same number of BTPs to obtain the same geographical representation of surface temperature and heat flux changes. This requirement reduces the number of borehole considered in the analysis to 1060, 1072 and 1074 for the 25 yr, 40 yr and 50 yr inversion models, respectively, since not all BTPs provide GSTHs and GHFHs complying with all criteria explained in this section.

3.3.4 Flux Estimates from Surface Temperatures

The relationship between surface flux (q) and a temporal series of surface temperatures can be expressed as (Wang et al., 1999; Beltrami, 2001)

$$q_{t_N} = \frac{2\lambda}{\sqrt{\pi\kappa\Delta t}} \sum_{i=1}^{N-1} \left\{ (T_i - T_{i+1}) \left(\sqrt{N-i} - \sqrt{N-i-1} \right) \right\}, \tag{3.19}$$

where Δt is the length of the time steps and T_i is surface temperature at the ith time step. We estimate ground heat flux histories at the surface from GSTHs retrieved from both the Standard and PPI approaches. Thermal properties for estimating heat fluxes from GSTHs obtained with the Standard inversion approach

are set to $\lambda = 3\,\mathrm{W\,m^{-1}\,K^{-1}}$ and $\kappa = 1 \times 10^{-6}\,\mathrm{m^2\,s^{-1}}$, while thermal properties for estimating heat fluxes from GSTHs included in the PPIT ensemble are set as those associated with the corresponding individual GSTH. Heat flux estimates are also provided using Equation 3.19 and CRU temperature data in order to create the histogram of heat flux changes displayed in Figure 3.3, considering the same thermal properties as in heat flux estimates from GSTHs retrieved by the Standard approach.

3.4 Results

Ground surface temperature histories estimated using a 25 yr inversion model together with the Standard approach and the new PPIT ensemble show temperature increases that are particularly large during the second half of the 20^{th} century in comparison with preindustrial conditions (Figure 3.4a). This is in agreement with meteorological observations of surface air temperatures (red and orange lines in the mentioned figure), as well as with previous studies using both borehole temperature profiles and proxy data (Pollack et al., 1998; Huang et al., 2000; Beltrami, 2002a; Pollack et al., 2004; Fernández-Donado et al., 2013; Masson-Delmotte et al., 2013). Both approaches used to retrieve GSTHs from temperature profiles display a remarkable agreement during the whole period, as well as similar temperature changes to those shown by CRU surface temperatures for the observational period. Global mean temperature changes between 1950-1975 CE and 1975-2000 CE reach 0.3 K for the PPIT ensemble and 0.4 K for the Standard approach (Table 3.1), with mean temperature changes from CRU data yielding approximately 0.4 K using both the entire dataset and locations and dates containing BTP inversions. GSTHs present slightly higher temperature changes since preindustrial times than previously reported, with results ranging from 1.0 ± 0.3 K to 1.2 ± 0.2 K for the last part of the 20^{th} century from the three inversion models (Tables 3.1, 3.2 and 3.3) in comparison to the ~0.9 K reported in previous works (Huang et al., 2000; Harris et al., 2001; Beltrami, 2002a; Pollack et al., 2004).

As in the case of surface temperature histories, the three approaches providing ground heat flux histories from BTP measurements are in good agreement during the entire period, although with higher uncertainties than for temper-

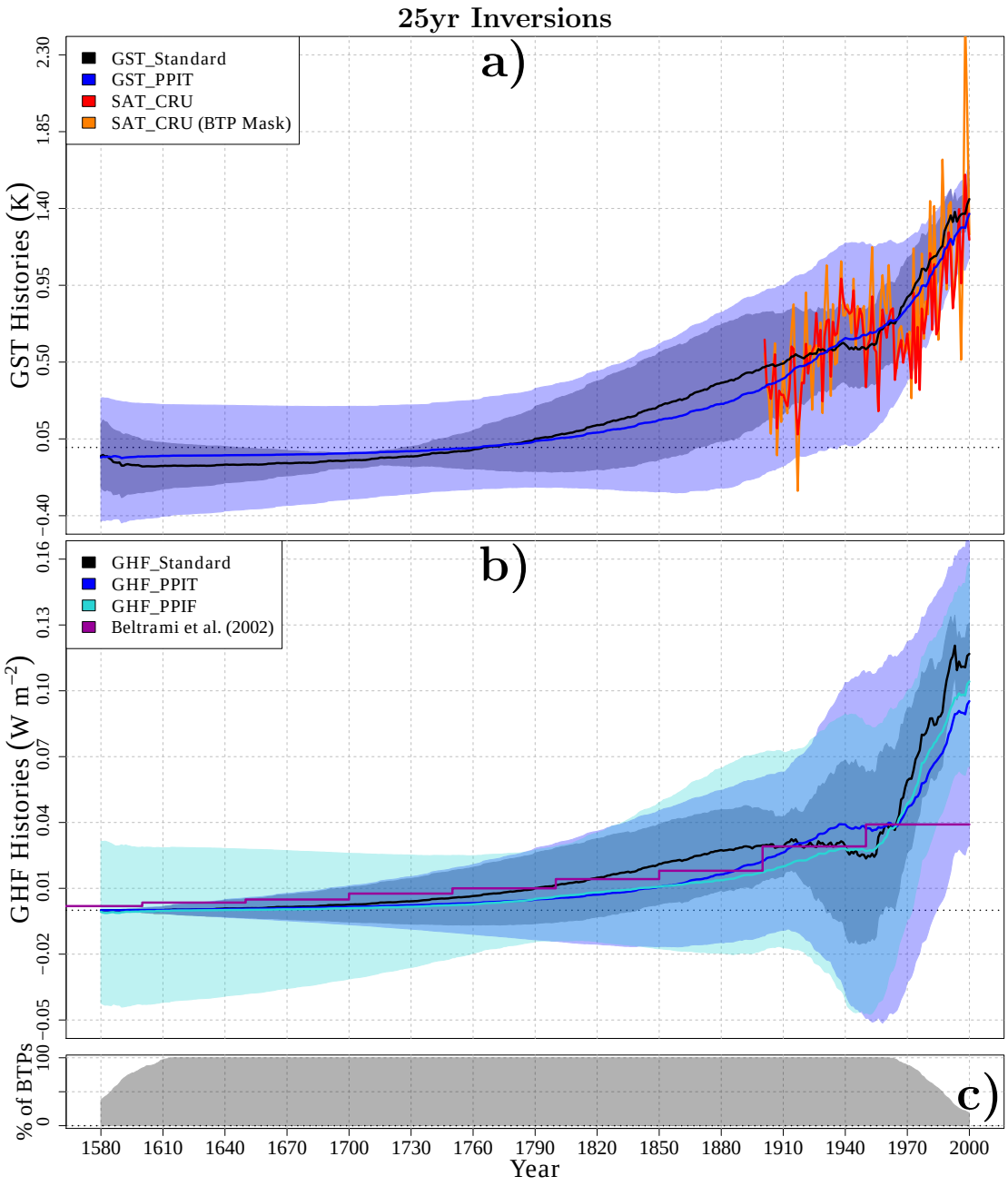

Figure 3.4: Global ground surface temperature histories (a) and global ground heat flux histories at the surface (b) from borehole temperature profiles using the Standard approach (black), the new PPI approach (PPIT, blue) and the new PPI approach applied to the corresponding heat flux profiles (PPIF, light blue). All inversions were performed using a 25 yr inversion model. (c) Percentage of total borehole inversions with time. Surface air temperature anomalies relative to 1961-1990 CE from CRU data are also displayed, including results from the entire database (red) and results from locations and dates containing borehole inversions (orange). The CRU series have been adjusted to have the same mean than the results from the Standard approach for the period 1950-1970 CE.

Table 3.1: Global mean estimates of ground surface temperature, ground heat flux at the surface and ground heat content within the continental subsurface from borehole temperature profiles. Values display the mean and 95 % confidence interval for each time period from estimates using the Standard inversion approach (Standard), the new PPI approach (PPIT) and the new PPI approach applied to subsurface flux profiles (PPIF). All the inversions were performed using a model of 25 years per time step. Temperatures in K, fluxes in $\mathrm{mW\,m^{-2}}$ and heat content in ZJ.

	Temperatures		Heat Fluxes			Heat Storage		
Period (CE)	Standard	PPIT	Standard	PPIT	PPIF	Standard	PPI	PPIF
1975-2000	1.2 ± 0.2	1.1 ± 0.3	100 ± 20	70 ± 70	80 ± 40	10 ± 2	8 ± 8	9 ± 5
1950-1975	0.8 ± 0.2	0.8 ± 0.5	40 ± 40	40 ± 80	40 ± 60	4 ± 4	4 ± 8	4 ± 6
1925-1950	0.6 ± 0.2	0.6 ± 0.6	30 ± 30	40 ± 60	30 ± 60	3 ± 4	4 ± 7	3 ± 6
1900-1925	0.5 ± 0.3	0.4 ± 0.5	30 ± 20	30 ± 40	20 ± 50	3 ± 2	3 ± 4	2 ± 5
1875-1900	0.4 ± 0.3	0.3 ± 0.5	30 ± 20	20 ± 40	20 ± 40	3 ± 2	2 ± 4	2 ± 5
1850-1875	0.3 ± 0.3	0.2 ± 0.5	20 ± 20	10 ± 30	10 ± 40	2 ± 2	1 ± 3	1 ± 4
1825-1850	0.2 ± 0.3	0.1 ± 0.4	20 ± 20	9 ± 30	10 ± 30	2 ± 2	0.9 ± 3	1 ± 3
1800-1825	0.1 ± 0.2	0.07 ± 0.3	10 ± 20	6 ± 20	7 ± 20	1 ± 2	0.7 ± 3	0.8 ± 2
1775-1800	0.04 ± 0.2	0.03 ± 0.3	10 ± 20	5 ± 20	5 ± 20	1 ± 2	0.5 ± 2	0.5 ± 2
1750-1775	-0.007 ± 0.1	0.002 ± 0.3	7 ± 10	3 ± 20	3 ± 20	0.7 ± 1	0.4 ± 2	0.3 ± 2
1725-1750	-0.04 ± 0.07	-0.02 ± 0.3	5 ± 10	3 ± 10	2 ± 20	0.5 ± 1	0.3 ± 1	0.2 ± 3
1700-1725	-0.07 ± 0.04	-0.03 ± 0.3	3 ± 9	2 ± 10	1 ± 30	0.3 ± 0.9	0.2 ± 1	0.1 ± 3
1675-1700	-0.08 ± 0.06	-0.04 ± 0.3	2 ± 7	1 ± 8	0.7 ± 30	0.2 ± 0.7	0.1 ± 0.8	0.07 ± 3
1650-1675	-0.10 ± 0.08	-0.04 ± 0.3	1 ± 5	0.9 ± 6	0.3 ± 30	0.1 ± 0.5	0.09 ± 0.6	0.03 ± 3
1625-1650	-0.1 ± 0.1	-0.05 ± 0.3	0.6 ± 4	0.5 ± 4	0.07 ± 30	0.07 ± 0.4	0.05 ± 0.4	0.007 ± 4
1600-1625	-0.1 ± 0.1	-0.05 ± 0.3	0.08 ± 2	0.2 ± 2	-0.2 ± 40	0.009 ± 0.2	0.02 ± 0.2	-0.02 ± 4

Table 3.2: Global mean estimates of ground surface temperature, ground heat flux at the surface and ground heat content within the continental subsurface from borehole temperature profiles. Values display the mean and 95 % confidence interval for each time period from estimates using the standard inversion approach (Standard), the new PPI approach (PPIT) and the new PPI approach applied to subsurface flux profiles (PPIF). All the inversions were performed using a model of 40 years per time step. Temperatures in K, fluxes in $\mathrm{mW\,m^{-2}}$ and heat content in ZJ.

	Temperatures		Heat Fluxes			Heat Storage		
Period (CE)	Standard	PPIT	Standard	PPIT	PPIF	Standard	PPIT	PPIF
1960-2000	1.1 ± 0.1	1.0 ± 0.3	80 ± 20	60 ± 40	70 ± 40	13 ± 3	11 ± 7	12 ± 6
1920-1960	0.6 ± 0.2	0.6 ± 0.4	30 ± 30	40 ± 40	30 ± 40	5 ± 5	6 ± 7	5 ± 7
1880-1920	0.4 ± 0.3	0.4 ± 0.4	20 ± 30	20 ± 30	20 ± 30	4 ± 4	4 ± 5	3 ± 5
1840-1880	0.2 ± 0.4	0.2 ± 0.3	20 ± 20	10 ± 20	10 ± 20	3 ± 3	2 ± 3	2 ± 3
1800-1840	0.1 ± 0.3	0.08 ± 0.3	10 ± 20	6 ± 10	8 ± 20	2 ± 4	1 ± 2	1 ± 3
1760-1800	0.05 ± 0.2	0.03 ± 0.3	7 ± 20	4 ± 8	6 ± 20	1 ± 3	0.6 ± 1	1 ± 3
1720-1760	0.002 ± 0.1	0.004 ± 0.2	4 ± 10	2 ± 5	5 ± 20	0.7 ± 2	0.4 ± 0.9	0.8 ± 3
1680-1720	-0.03 ± 0.09	-0.01 ± 0.2	3 ± 10	1 ± 4	4 ± 20	0.4 ± 2	0.2 ± 0.6	0.6 ± 4
1640-1680	-0.05 ± 0.2	-0.02 ± 0.2	1 ± 6	0.6 ± 2	3 ± 20	0.2 ± 1	0.1 ± 0.4	0.5 ± 4
1600-1640	-0.07 ± 0.2	-0.03 ± 0.2	0.3 ± 2	0.2 ± 0.8	3 ± 20	0.04 ± 0.4	0.03 ± 0.1	0.5 ± 3

Table 3.3: Global mean estimates of ground surface temperature, ground heat flux at the surface and ground heat content within the continental subsurface from borehole temperature profiles. Values display the mean and 95 % confidence interval for each time period from estimates using the standard inversion approach (Standard), the new PPI approach (PPIT) and the new PPI approach applied to subsurface flux profiles (PPIF). All the inversions were performed using a model of 50 years per time step. Temperatures in K, fluxes in $\mathrm{mW\,m^{-2}}$ and heat content in ZJ.

	Temperatures		Heat Fluxes			Heat Storage		
Period (CE)	Standard	PPIT	Standard	PPIT	PPIF	Standard	PPIT	PPIF
1950-2000	1.0 ± 0.1	1.0 ± 0.3	70 ± 20	60 ± 40	60 ± 30	16 ± 3	13 ± 8	14 ± 7
1900-1950	0.4 ± 0.2	0.5 ± 0.5	30 ± 30	30 ± 40	30 ± 40	5 ± 6	6 ± 8	5 ± 9
1850-1900	0.2 ± 0.4	0.2 ± 0.4	10 ± 30	20 ± 30	10 ± 30	3 ± 6	3 ± 6	2 ± 6
1800-1850	0.1 ± 0.4	0.09 ± 0.3	10 ± 30	7 ± 20	8 ± 20	2 ± 6	2 ± 3	2 ± 4
1750-1800	0.05 ± 0.3	0.02 ± 0.3	6 ± 30	4 ± 9	5 ± 20	1 ± 5	0.7 ± 2	1 ± 5
1700-1750	-0.005 ± 0.1	-0.009 ± 0.3	3 ± 20	2 ± 5	4 ± 20	0.7 ± 4	0.4 ± 1	0.9 ± 5
1650-1700	-0.03 ± 0.2	-0.03 ± 0.2	2 ± 10	0.8 ± 3	3 ± 20	0.3 ± 2	0.2 ± 0.6	0.7 ± 5
1600-1650	-0.05 ± 0.2	-0.04 ± 0.2	0.2 ± 3	0.2 ± 0.8	3 ± 20	0.05 ± 0.7	0.03 ± 0.2	0.5 ± 5

atures (Figure 3.4b and Table 3.1). Global results from Beltrami et al. (2002) are also displayed in Figure 3.4b (purple line), achieving similar values in comparison with GHFHs derived by the Standard, PPIT and PPIF approaches except for the second half of the 20th century. Global heat flux change achieves $70 \pm 20\,\mathrm{mW\,m^{-2}}$, $60 \pm 50\,\mathrm{mW\,m^{-2}}$ and $60 \pm 40\,\mathrm{mW\,m^{-2}}$ for the Standard, PPIT and PPIF ensembles, respectively (Table 3.1), in contrast to the $39 \pm 4\,\mathrm{mW\,m^{2}}$ presented in Beltrami et al. (2002) and the $\sim$33 $\mathrm{mW\,m^{-2}}$ from Beltrami (2002a). The large number of recently acquired profiles included in our analysis may explain the larger flux estimates in comparison with previous works, since BTP measurements recorded before the 1980s did not capture the large disturbances in the surface energy budget from recent decades (Stevens et al., 2008). Global changes in GHC were estimated from the Standard, PPIT and PPIF heat flux histories by scaling these fluxes to the continental areas except Antarctica and Greenland, where there are no BTP measurements. GHC changes of 15 ± 5 ZJ, 10 ± 10 ZJ and 13 ± 8 ZJ (1 ZJ = 10^{21} J) are obtained for the period 1950-2000 CE using the Standard, PPIT and PPIF approaches, respectively, in comparison with the 9 ± 1 ZJ in Beltrami et al. (2002) and the 7 ZJ in Beltrami (2002a). As expected, these estimates of continental heat storage are larger than previously reported since the heat flux histories also present higher values. The small uncertainty for heat flux histories, and therefore for estimates of continental heat storage, shown by the Standard and PPIT ensembles at the beginning of the period (Figure 3.4) is artificially imposed by Equation 3.19, since the heat flux estimate for the first temporal step is set to zero by default. Therefore, the PPIF ensemble provides a more realistic estimate of the uncertainty in the global GHFHs and GHC estimates for the first half of the period, with larger uncertainties for the three approaches in the second half of the period.

Although the borehole database used here contains BTP measurements recorded after 2000 CE, results are shown until the end of the 20th century, since the number of available logs decreases sharply afterwards and the remaining profiles are located mainly at high latitudes in North America and Australia (Figure 3.1). We use the trend for the period 1970-2000 CE to extrapolate the heat flux histories until 2018 CE, providing an estimate of the accumulated heat content in the continental subsurface from 1960 CE to the present (Figure 3.5). The global mean change of heat flux for the entire period is approxi-

mately 90 mW m^{-2} considering all inversion approaches, while the global heat flux change since 2000 CE is ~ 120 mW m^{-2}. Thus, the accumulated heat within the global continental subsurface obtained from these flux estimates reachs 20 ZJ for the entire period and ~9 ZJ for 2000-2018 CE. That is, if the global heat flux increase during the first decades of the 21st century resembled the trend of the period 1970-2000 CE, half of the total increase in energy storage within the continental subsurface in the last fifty-eight years would have occurred during the last two decades, a remarkably similar result in comparison with the accelerated ocean heat uptake in the last decades (Gleckler et al., 2016; Cheng et al., 2017, 2019).

3.5 Discussion

Ground surface temperature and ground heat flux histories retrieved by the three inversion models used here achieve similar evolutions since preindustrial times, and yield similar estimates of ground heat content for all continental areas excluding Antarctica and Greenland (Figures 3.4, 3.6 and 3.7, and Tables 3.1, 3.2 and 3.3). Nonetheless, the surface temperature, heat flux and heat storage results are larger than previous global estimates of GSTHs, GHFHs and GHC from borehole data (Pollack et al., 1998; Huang et al., 2000; Beltrami, 2002a; Beltrami et al., 2002; Pollack et al., 2004). The main reason for the higher values reported here is the inclusion of additional temperature profiles measured at more recent dates than those employed in prior literature, since logs acquired after the 1980s and 1990s recorded larger changes in the subsurface thermal regime due to larger variations in the surface energy balance (Stevens et al., 2008). That is, more than 250 high-quality logs have been measured or made available for the community since the early 2000s, including profiles from sparsely observed areas in the southern hemisphere. Additionally, there have been improvements in the aggregation and treatment of borehole profiles contributing to the differences between our estimates and previous works (Beltrami et al., 2015b). We have truncated all logs to the same depth before performing the analysis in contrast to previous studies, which used profiles including a range of bottom depths, therefore including GSTH and GHFH estimates with different periods of reference.

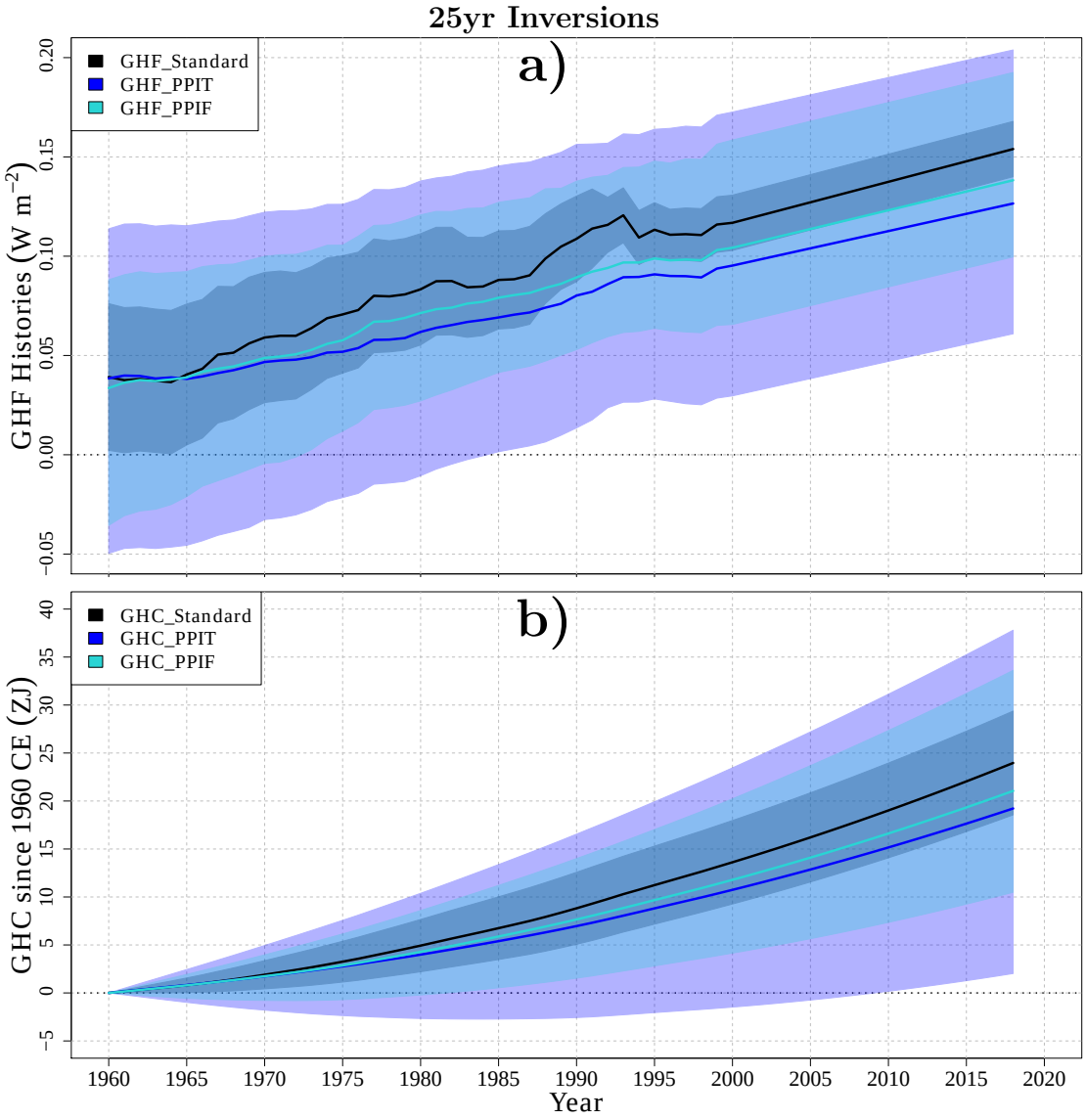

Figure 3.5: Global ground heat flux histories (a) and ground heat content accumulated since 1960 CE (b) from borehole temperature profiles using the Standard approach (black), the new PPI approach (PPIT, blue) and the new PPI approach applied to the corresponding heat flux profiles (PPIF, light blue). All inversions were performed using a 25 yr inversion model. Data since 2001 CE to 2018 CE are extrapolated using the trend for the period 1971-2000 CE.

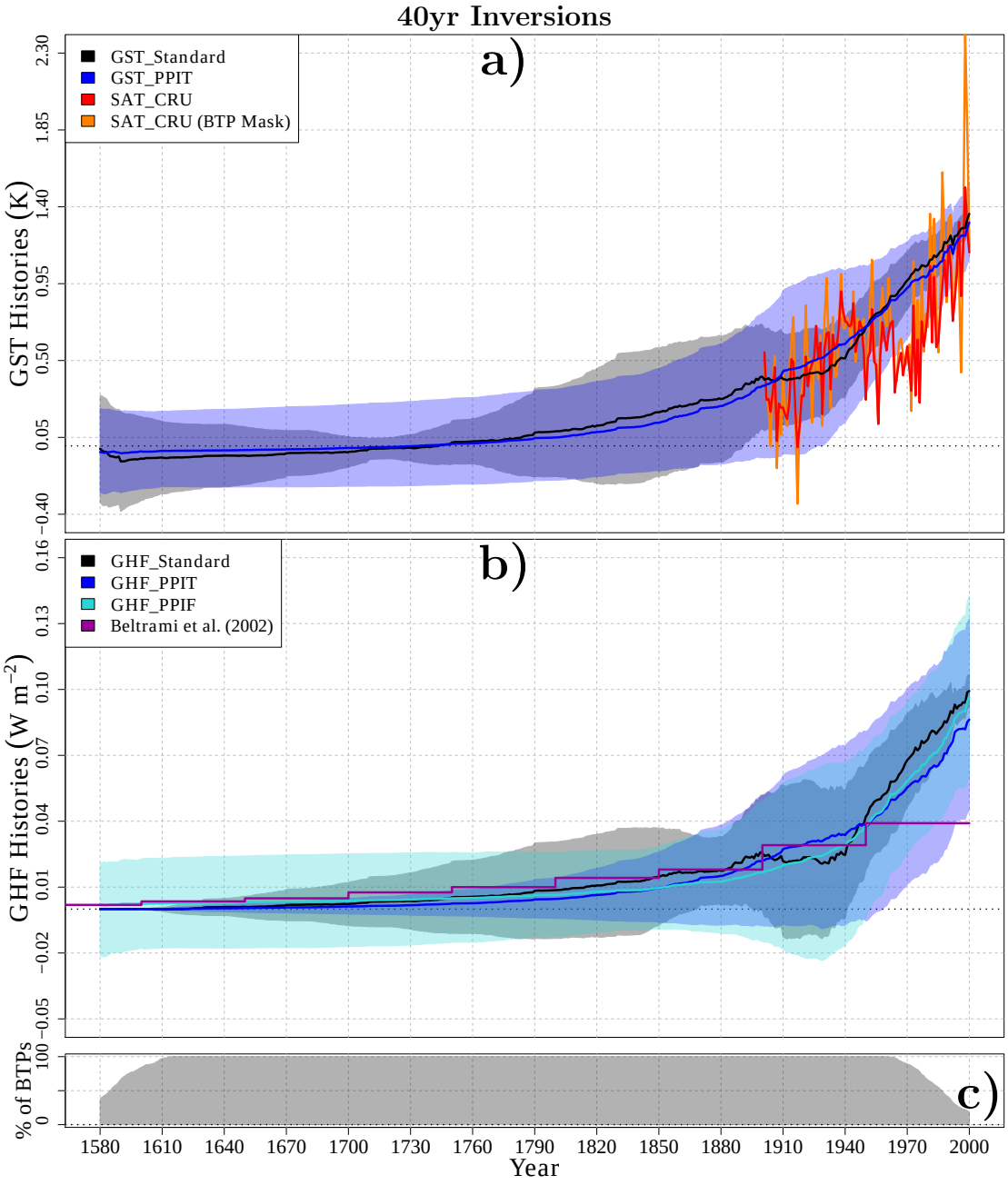

Figure 3.6: Global ground surface temperature histories (a) and global ground heat flux histories at the surface (b) from borehole temperature profiles using the Standard approach (black), the new PPI approach (PPIT, blue) and the new PPI approach applied to the corresponding heat flux profiles (PPIF, light blue). All inversions were performed using a 40 yr step change model. (c) Percentage of total borehole inversions with time. Surface air temperature anomalies relative to 1961-1990 CE from CRU data are also displayed, including results from the entire database (red) and results from locations and dates containing borehole inversions (orange). The CRU series have been adjusted to have the same mean than the results from the Standard approach for the period 1950-1970 CE.

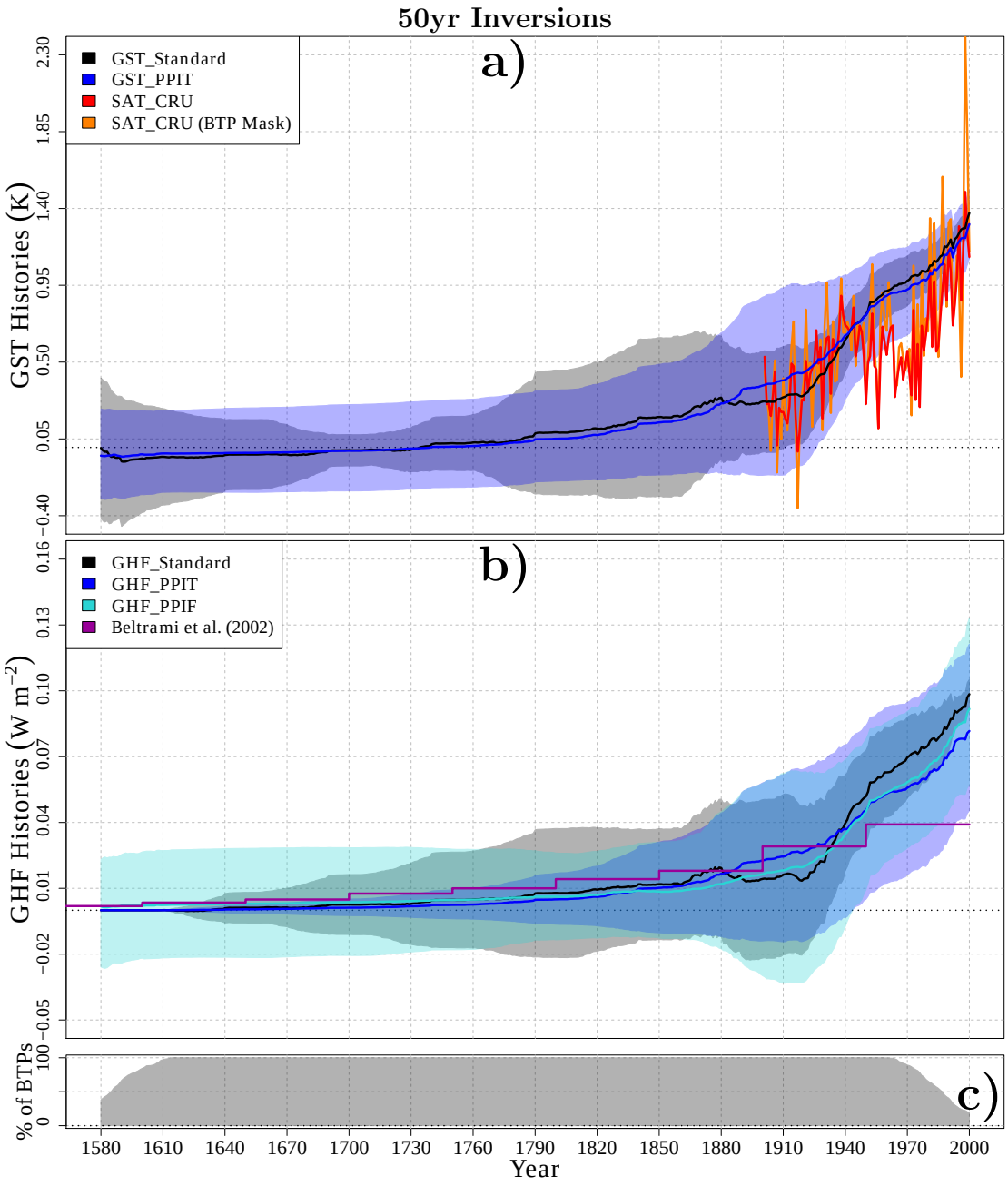

Figure 3.7: Global ground surface temperature histories (a) and global ground heat flux histories at the surface (b) from borehole temperature profiles using the Standard approach (black), the new PPI approach (PPIT, blue) and the new PPI approach applied to the corresponding heat flux profiles (PPIF, light blue). All inversions were performed using a 50 yr step change model. (c) Percentage of total borehole inversions with time. Surface air temperature anomalies relative to 1961-1990 CE from CRU data are also displayed, including results from the entire database (red) and results from locations and dates containing borehole inversions (orange). The CRU series have been adjusted to have the same mean than the results from the Standard approach for the period 1950-1970 CE.

The larger differences in uncertainties in heat flux estimates from the PPIT ensemble in comparison with those from the PPIF ensemble are caused by the criterion to discard unrealistic inversions in the PPI approach (Figures 3.4b, 3.6b and 3.7b). That is, the heat flux estimates for the PPIT ensemble were not filtered out using the flux criterion ($0.51\,\mathrm{W\,m^{-2}}$) of the PPI approach but the temperature criterion (2.57 K). Applying these different criteria is necessary since heat flux estimates from the PPIT ensemble result from applying Equation 3.19 to the previously retrieved surface temperature histories, while the heat flux histories considered in the PPIF ensemble result from direct inversions of heat flux profiles, as explained in Section 3.3.3.

Borehole temperature profiles present a unique ability to integrate multi-centennial changes in the surface energy balance (Beltrami, 2002b), which makes borehole inversions an important source of information about preindustrial conditions. The depth range considered here (from 15 m to 300 m) allows the retrieval of information from ~700 years before the logging date, i.e., several centuries before industrialization. Thus, all surface temperature histories displayed in Figures 3.4a, 3.6a and 3.7a are relative to approximately 1300-1700 CE, as the subsurface quasi-equilibrium profile is estimated here from the 200-300 m depth range for all profiles (Cuesta-Valero et al., 2019). The ground surface temperature increases relative to preindustrial conditions from the three PPIT ensembles analyzed here are ~1.0 K for the last part of the 20^{th} century (Tables 3.1, 3.2 and 3.3). This is not, however, an estimate of the global temperature change, since land temperature changes at a higher pace than the temperature at the surface of the ocean due to their different thermal properties. The ratio between land temperature change and ocean temperature change is estimated in Harrison et al. (2015) based on an ensemble of long-term CGCM simulations performed under different external forcings, resulting in land temperature changes ~2.36 times larger than ocean temperature changes. Thus, the corresponding ocean temperature change to the land temperature change retrieved from borehole temperature profiles can be approximated as ~0.4 K, which yields an approximate global surface temperature change of ~0.7 K since preindustrial times (1300-1700 CE). Such a temperature change is in good agreement with the estimates of 0.55-0.8 K discussed in Hawkins et al. (2017) using observations, CGCM simulations and proxy databases, even for a preindustrial period much

further in the past in comparison with the periods analyzed in Schurer et al. (2017).

These new estimates of continental heat storage and ground heat flux from BTP inversions have implications for the assessment of the EHI and for the comparison with CGCM simulations. Although the ocean is still the largest component of the EHI, the contribution of the continental subsurface is higher than previously reported, reinforcing the necessity of monitoring and accounting for non-ocean components. Furthermore, previous assessments have shown that CGCM simulations are unable to represent changes in continental heat storage due to their shallow land surface model components (Stevens et al., 2007; MacDougall et al., 2008; Cuesta-Valero et al., 2016). The new GHC estimates emphasize the demand for deeper subsurfaces in CGCMs in order to generate global transient simulations capable of correctly reproducing the Earth heat inventory.

The distribution of BTP measurements used in this analysis is specially scarce in zones of Africa, South America and the Middle East, which may raise doubts about the global representativity of the assembled borehole dataset. Previous works have assessed the spatial distribution of BTP measurements using transient climate simulations performed by CGCMs at millennial time scales (González-Rouco et al., 2006; González-Rouco et al., 2009; García-García et al., 2016; Melo-Aguilar et al., 2019), and borehole databases aggregated using different techniques (Beltrami et al., 2004; Pollack et al., 2004), with all studies concluding that the effects of limited regional sampling on estimates of global changes should be minor. Additionally, surface air temperatures from CRU data present markedly similar values considering both the full domain, and locations and dates containing BTP inversions (see red and orange lines in Figure 3.4), supporting the claim that borehole temporal and spatial distributions are representative of global conditions. Nevertheless, repeating measurements at borehole sites previously logged as well as obtaining new records at zones with reduced density of BTP data would improve the global estimates of ground surface temperature and ground heat flux histories from borehole temperature profiles.

3.6 Conclusions

The magnitude of the retrieved changes in ground surface temperature in this analysis supports the claim that the Earth's surface has warmed by ~0.7 K since preindustrial times. The new estimates also reveal that the continental subsurface has stored more energy during the last part of the 20th century than previously reported, reaching around 12 ZJ. This demonstrates the need for including deeper land surface model components in CGCM transient simulations in order to correctly reproduce the land component of the Earth heat inventory, as well as potentially powerful carbon feedbacks related to energy-dependent processes of the continental subsurface, such as the stability of the soil carbon pool and permafrost evolution.

3.7 References

Barkaoui, A. E., Correia, A., Zarhloule, Y., Rimi, A., Carneiro, J., Boughriba, M., and Verdoya, M. (2013). Reconstruction of remote climate change from borehole temperature measurement in the eastern part of Morocco. *Climatic Change*, **118**(2), 431–441. DOI: 10.1007/s10584-012-0638-7.

Beck, A. (1977). Climatically perturbed temperature gradients and their effect on regional and continental heat-flow means. *Tectonophysics*, **41**(1), 17 –39. DOI: https://doi.org/10.1016/0040-1951(77)90178-0.

Beltrami, H. (2001). Surface heat flux histories from inversion of geothermal data: Energy balance at the Earth's surface. *Journal of Geophysical Research: Solid Earth*, **106**(B10), 21979–21993. DOI: 10.1029/2000JB000065.

— (2002a). Climate from borehole data: Energy fluxes and temperatures since 1500. *Geophysical Research Letters*, **29**(23). 26–1–26–4. DOI: 10.1029/2002GL015702.

— (2002b). Earth's Long-Term Memory. *Science*, **297**(5579), 206–207. DOI: 10.1126/science.1074027.

Beltrami, H., Jessop, A. M., and Mareschal, J.-C. (1992). Ground temperature histories in eastern and central Canada from geothermal measurements:

evidence of climatic change. *Global and Planetary Change*, **6**(2–4). 167 –183. DOI: http://dx.doi.org/10.1016/0921-8181(92)90033-7.

Beltrami, H., Smerdon, J. E., Pollack, H. N., and Huang, S. (2002). Continental heat gain in the global climate system. *Geophysical Research Letters*, **29**(8), 8–1–8–3. DOI: 10.1029/2001GL014310.

Beltrami, H. and Bourlon, E. (2004). Ground warming patterns in the Northern Hemisphere during the last five centuries. *Earth and Planetary Science Letters*, **227**(3–4), 169 –177. DOI: http://dx.doi.org/10.1016/j.epsl.2004.09.014.

Beltrami, H., Bourlon, E., Kellman, L., and González-Rouco, J. F. (2006). Spatial patterns of ground heat gain in the Northern Hemisphere. *Geophysical Research Letters*, **33**(6). n/a–n/a. DOI: 10.1029/2006GL025676.

Beltrami, H., Matharoo, G. S., and Smerdon, J. E. (2015a). Ground surface temperature and continental heat gain: uncertainties from underground. *Environmental Research Letters*, **10**(1), 014009. DOI: 10.1088/1748-9326/10/1/014009.

Beltrami, H., Matharoo, G. S., and Smerdon, J. E. (2015b). Impact of borehole depths on reconstructed estimates of ground surface temperature histories and energy storage. *Journal of Geophysical Research: Earth Surface*, **120**(5). 763–778. DOI: 10.1002/2014JF003382.

Beltrami, H., Matharoo, G. S., Smerdon, J. E., Illanes, L., and Tarasov, L. (2017). Impacts of the Last Glacial Cycle on ground surface temperature reconstructions over the last millennium. *Geophysical Research Letters*, **44**(1), 355–364. DOI: 10.1002/2016GL071317.

Bodri, L. and Cermak, V. (2005). Borehole temperatures, climate change and the pre-observational surface air temperature mean: allowance for hydraulic conditions. *Global and Planetary Change*, **45**(4), 265 –276. DOI: https://doi.org/10.1016/j.gloplacha.2004.09.001.

— (2007). *Borehole Climatology*. Oxford: Elsevier Science Ltd. DOI: https://doi.org/10.1016/B978-008045320-0/50001-6.

Bullard, E. C. and Schonland, B. F. J. (1939). Heat flow in South Africa. *Proceedings of the Royal Society of London. Series A. Mathematical and Physical Sciences*, **173**(955), 474–502. DOI: 10.1098/rspa.1939.0159.

Campbell, B. M., Vermeulen, S. J., Aggarwal, P. K., Corner-Dolloff, C., Girvetz, E., Loboguerrero, A. M., Ramirez-Villegas, J., Rosenstock, T., Sebastian, L., Thornton, P. K., and Wollenberg, E. (2016). Reducing risks to food security from climate change. *Global Food Security*, **11**. 34 –43. DOI: https://doi.org/10.1016/j.gfs.2016.06.002.

Carslaw, H. and Jaeger, J. (1959). *Conduction of Heat in Solids*. Clarendon Press, Oxford.

Cermak, V. (1971). Underground temperature and inferred climatic temperature of the past millenium. *Palaeogeography, Palaeoclimatology, Palaeoecology*, **10**(1), 1–19. DOI: https://doi.org/10.1016/0031-0182(71)90043-5.

Cheng, L., Trenberth, K. E., Fasullo, J., Boyer, T., Abraham, J., and Zhu, J. (2017). Improved estimates of ocean heat content from 1960 to 2015. *Science Advances*, **3**(3). DOI: 10.1126/sciadv.1601545.

Cheng, L., Abraham, J., Hausfather, Z., and Trenberth, K. E. (2019). How fast are the oceans warming? *Science*, **363**(6423), 128–129. DOI: 10.1126/science.aav7619.

Chouinard, C. and Mareschal, J.-C. (2009). Ground surface temperature history in southern Canada: Temperatures at the base of the Laurentide ice sheet and during the Holocene. *Earth and Planetary Science Letters*, **277**(1), 280 –289. DOI: https://doi.org/10.1016/j.epsl.2008.10.026.

Church, J. A., White, N. J., Konikow, L. F., Domingues, C. M., Cogley, J. G., Rignot, E., Gregory, J. M., van den Broeke, M. R., Monaghan, A. J., and Velicogna, I. (2011). Revisiting the Earth's sea-level and energy budgets from 1961 to 2008. *Geophysical Research Letters*, **38**(18). n/a–n/a. DOI: 10.1029/2011GL048794.

Clauser, C. and Mareschal, J.-C. (1995). Ground temperature history in central Europe from borehole temperature data. *Geophysical Journal International*, **121**(3), 805–817. DOI: 10.1111/j.1365-246X.1995.tb06440.x.

Collins, M., Booth, B. B. B., Bhaskaran, B., Harris, G. R., Murphy, J. M., Sexton, D. M. H., and Webb, M. J. (2011). Climate model errors, feedbacks and forcings: a comparison of perturbed physics and multi-model ensembles. *Climate Dynamics*, **36**(9), 1737–1766. DOI: 10.1007/s00382-010-0808-0.

Cuesta-Valero, F. J., García-García, A., Beltrami, H., Zorita, E., and Jaume-Santero, F. (2019). Long-term Surface Temperature (LoST) database as a complement for GCM preindustrial simulations. *Climate of the Past*, **15**(3), 1099–1111. DOI: 10.5194/cp-15-1099-2019.

Cuesta-Valero, F. J., García-García, A., Beltrami, H., González-Rouco, J. F., and García-Bustamante, E. (2020). Long-Term Global Ground Heat Flux and Continental Heat Storage from Geothermal Data. *Climate of the Past Discussions*, **2020**, 1–27. DOI: 10.5194/cp-2020-65.

Cuesta-Valero, F. J., García-García, A., Beltrami, H., and Smerdon, J. E. (2016). First assessment of continental energy storage in CMIP5 simulations. *Geophysical Research Letters*. n/a–n/a. DOI: 10.1002/2016GL068496.

Davis, M. G., Harris, R. N., and Chapman, D. S. (2010). Repeat temperature measurements in boreholes from northwestern Utah link ground and air temperature changes at the decadal time scale. *Journal of Geophysical Research: Solid Earth*, **115**(B5). DOI: 10.1029/2009JB006875.

Demezhko, D. Y. and Gornostaeva, A. A. (2015). Late Pleistocene–Holocene ground surface heat flux changes reconstructed from borehole temperature data (the Urals, Russia). *Climate of the Past*, **11**(4), 647–652. DOI: 10.5194/cp-11-647-2015.

Dutton, A., Carlson, A. E., Long, A. J., Milne, G. A., Clark, P. U., DeConto, R., Horton, B. P., Rahmstorf, S., and Raymo, M. E. (2015). Sea-level rise due to polar ice-sheet mass loss during past warm periods. *Science*, **349**(6244). DOI: 10.1126/science.aaa4019.

Fernández-Donado, L., González-Rouco, J. F., Raible, C. C., Ammann, C. M., Barriopedro, D., García-Bustamante, E., Jungclaus, J. H., Lorenz, S. J., Luterbacher, J., Phipps, S. J., Servonnat, J., Swingedouw, D., Tett, S. F. B., Wagner, S., Yiou, P., and Zorita, E. (2013). Large-scale temperature response to

external forcing in simulations and reconstructions of the last millennium. *Climate of the Past*, **9**(1), 393–421. DOI: 10.5194/cp-9-393-2013.

García-García, A, Cuesta-Valero, F. J., Beltrami, H, and Smerdon, J. E. (2016). Simulation of air and ground temperatures in PMIP3/CMIP5 last millennium simulations: implications for climate reconstructions from borehole temperature profiles. *Environmental Research Letters*, **11**(4), 044022.

Gleckler, P. J., Durack, P. J., Stouffer, R. J., Johnson, G. C., and Forest, C. E. (2016). Industrial-era global ocean heat uptake doubles in recent decades. *Nature Clim. Change*, **6**(4), 394–398.

González-Rouco, J. F., Beltrami, H., Zorita, E., and von Storch, H. (2006). Simulation and inversion of borehole temperature profiles in surrogate climates: Spatial distribution and surface coupling. *Geophysical Research Letters*, **33**(1). n/a–n/a. DOI: 10.1029/2005GL024693.

González-Rouco, J. F., Beltrami, H., Zorita, E., and Stevens, M. B. (2009). Borehole climatology: a discussion based on contributions from climate modeling. *Climate of the Past*, **5**(1), 97–127. DOI: 10.5194/cp-5-97-2009.

Hansen, J., Sato, M., Kharecha, P., and Schuckmann, K. v. (2011). Earth's energy imbalance and implications. *Atmospheric Chemistry and Physics*, **11**(24), 13421–13449.

Harris, I., Jones, P., Osborn, T., and Lister, D. (2014). Updated high-resolution grids of monthly climatic observations – the CRU TS3.10 Dataset. *International Journal of Climatology*, **34**(3), 623–642. DOI: 10.1002/joc.3711.

Harris, R. N. and Chapman, D. S. (2001). Mid-latitude (30 °–60 ° N) climatic warming inferred by combining borehole temperatures with surface air temperatures. *Geophysical Research Letters*, **28**(5), 747–750. DOI: 10.1029/2000GL012348.

Harrison, S. P., Bartlein, P. J., Izumi, K., Li, G., Annan, J., Hargreaves, J., Braconnot, P., and Kageyama, M. (2015). Evaluation of CMIP5 palaeo-simulations to improve climate projections. *Nature Clim. Change*, **5**(8), 735–743.

Hartmann, A and Rath, V (2005). Uncertainties and shortcomings of ground surface temperature histories derived from inversion of temperature logs.

Journal of Geophysics and Engineering, **2**(4), 299–311. DOI: 10.1088/1742-2132/2/4/S02.

Hawkins, E., Ortega, P., Suckling, E., Schurer, A., Hegerl, G., Jones, P., Joshi, M., Osborn, T. J., Masson-Delmotte, V., Mignot, J., Thorne, P., and van Oldenborgh, G. J. (2017). Estimating Changes in Global Temperature since the Preindustrial Period. *Bulletin of the American Meteorological Society*, **98**(9), 1841–1856. DOI: 10.1175/BAMS-D-16-0007.1.

Hicks Pries, C. E., Castanha, C., Porras, R. C., and Torn, M. S. (2017). The whole-soil carbon flux in response to warming. *Science*, **355**(6332), 1420–1423. DOI: 10.1126/science.aal1319.

Hopcroft, P. O., Gallagher, K., and Pain, C. C. (2007). Inference of past climate from borehole temperature data using Bayesian Reversible Jump Markov chain Monte Carlo. *Geophysical Journal International*, **171**(3), 1430–1439. DOI: 10.1111/j.1365-246X.2007.03596.x.

Huang, S., Pollack, H. N., and Shen, P.-Y. (2000). Temperature trends over the past five centuries reconstructed from borehole temperatures. *Nature*, **403**(6771), 756–758.

Irving, D. B., Wijffels, S., and Church, J. A. (2019). Anthropogenic Aerosols, Greenhouse Gases, and the Uptake, Transport, and Storage of Excess Heat in the Climate System. *Geophysical Research Letters*, **46**(9), 4894–4903. DOI: 10.1029/2019GL082015.

Jacob, T., Wahr, J., Pfeffer, W. T., and Swenson, S. (2012). Recent contributions of glaciers and ice caps to sea level rise. *Nature*, **482**(7386), 514–518.

Jaume-Santero, F., Pickler, C., Beltrami, H., and Mareschal, J.-C. (2016). North American regional climate reconstruction from ground surface temperature histories. *Climate of the Past*, **12**(12), 2181–2194. DOI: 10.5194/cp-12-2181-2016.

Johnson, G. C., Lyman, J. M., and Loeb, N. G. (2016). Improving estimates of Earth's energy imbalance. *Nature Climate Change*, **6**, 639 EP –.

Knutti, R., Sedláček, J., Sanderson, B. M., Lorenz, R., Fischer, E. M., and Eyring, V. (2017). A climate model projection weighting scheme accounting for performance and interdependence. *Geophysical Research Letters*, **44**(4), 1909–1918. DOI: 10.1002/2016GL072012.

Kundzewicz, Z. W., Kanae, S., Seneviratne, S. I., Handmer, J., Nicholls, N., Peduzzi, P., Mechler, R., Bouwer, L. M., Arnell, N., Mach, K., Muir-Wood, R., Brakenridge, G. R., Kron, W., Benito, G., Honda, Y., Takahashi, K., and Sherstyukov, B. (2014). Flood risk and climate change: global and regional perspectives. *Hydrological Sciences Journal*, **59**(1), 1–28. DOI: 10.1080/02626667.2013.857411.

Lachenbruch, A. H. and Marshall, B. V. (1986). Changing Climate: Geothermal Evidence from Permafrost in the Alaskan Arctic. *Science*, **234**(4777), 689–696. DOI: 10.1126/science.234.4777.689.

Lanczos, C. (1961). *Linear differential operators*. New York: Van Nostrand, p. 564.

Lane, A. C. (1923). Geotherms of Lake Superior Copper Country. *GSA Bulletin*, **34**(4), 703–720. DOI: 10.1130/GSAB-34-703.

Lembo, V., Folini, D., Wild, M., and Lionello, P. (2019). Inter-hemispheric differences in energy budgets and cross-equatorial transport anomalies during the 20th century. *Climate Dynamics*, **53**(1), 115–135. DOI: 10.1007/s00382-018-4572-x.

Lesperance, M., Smerdon, J. E., and Beltrami, H. (2010). Propagation of linear surface air temperature trends into the terrestrial subsurface. *Journal of Geophysical Research: Atmospheres*, **115**(D21). n/a–n/a. DOI: 10.1029/2010JD014377.

Levitus, S., Antonov, J., and Boyer, T. (2005). Warming of the world ocean, 1955–2003. *Geophysical Research Letters*, **32**(2). n/a–n/a. DOI: 10.1029/2004GL021592.

Levy, K., Woster, A. P., Goldstein, R. S., and Carlton, E. J. (2016). Untangling the Impacts of Climate Change on Waterborne Diseases: a Systematic Review of Relationships between Diarrheal Diseases and Temperature, Rainfall, Flood-

ing, and Drought. *Environmental Science & Technology*, **50**(10). 4905–4922. DOI: 10.1021/acs.est.5b06186.

Lloyd, S. J., Kovats, R. S., and Chalabi, Z. (2011). Climate Change, Crop Yields, and Undernutrition: Development of a Model to Quantify the Impact of Climate Scenarios on Child Undernutrition. *Environmental Health Perspectives*, **119**(12), 1817–1823. DOI: 10.1289/ehp.1003311.

Loeb, N. G., Wang, H., Cheng, A., Kato, S., Fasullo, J. T., Xu, K.-M., and Allan, R. P. (2016). Observational constraints on atmospheric and oceanic cross-equatorial heat transports: revisiting the precipitation asymmetry problem in climate models. *Climate Dynamics*, **46**(9), 3239–3257. DOI: 10.1007/s00382-015-2766-z.

MacDougall, A. H., González-Rouco, J. F., Stevens, M. B., and Beltrami, H. (2008). Quantification of subsurface heat storage in a GCM simulation. *Geophysical Research Letters*, **35**(13), n/a–n/a. DOI: 10.1029/2008GL034639.

MacDougall, A. H., Beltrami, H., González-Rouco, J. F., Stevens, M. B., and Bourlon, E. (2010). Comparison of observed and general circulation model derived continental subsurface heat flux in the Northern Hemisphere. *Journal of Geophysical Research: Atmospheres (1984–2012)*, **115**(D12).

MacDougall, A. H., Avis, C. A., and Weaver, A. J. (2012). Significant contribution to climate warming from the permafrost carbon feedback. *Nature Geosci*, **5**(10), 719–721. DOI: 10.1038/ngeo1573.

Mareschal, J.-C. and Beltrami, H. (1992). Evidence for recent warming from perturbed geothermal gradients: examples from eastern Canada. *Climate Dynamics*, **6**(3), 135–143. DOI: 10.1007/BF00193525.

Masson-Delmotte, V., Schulz, M., Abe-Ouchi, A., Beer, J., Ganopolski, A., González Rouco, J., Jansen, E., Lambeck, K., Luterbacher, J., Naish, T., Osborn, T., Otto-Bliesner, B., Quinn, T., Ramesh, R., Rojas, M., Shao, X., and Timmermann, A. (2013). "Information from Paleoclimate Archives". In: *Climate Change 2013: The Physical Science Basis. Contribution of Working Group I to the Fifth Assessment Report of the Intergovernmental Panel on Climate Change*. Ed. by T. Stocker, D. Qin, G.-K. Plattner, M. Tignor, S. Allen, J. Boschung,

A. Nauels, Y. Xia, V. Bex, and P. Midgley. Cambridge, United Kingdom and New York, NY, USA: Cambridge University Press. Chap. 5, pp. 383–464. DOI: 10.1017/CBO9781107415324.013.

Matthews, T. K. R., Wilby, R. L., and Murphy, C. (2017). Communicating the deadly consequences of global warming for human heat stress. *Proceedings of the National Academy of Sciences*, **114**(15), 3861–3866. DOI: 10.1073/pnas.1617526114.

McGranahan, G., Balk, D., and Anderson, B. (2007). The rising tide: assessing the risks of climate change and human settlements in low elevation coastal zones. *Environment and Urbanization*, **19**(1), 17–37. DOI: 10.1177/0956247807076960.

McPherson, M., García-García, A., Cuesta-Valero, F. J., Beltrami, H., Hansen-Ketchum, P., MacDougall, D., and Ogden, N. H. (2017). Expansion of the Lyme Disease Vector Ixodes Scapularis in Canada Inferred from CMIP5 Climate Projections. *Environmental Health Perspectives*, **125**(5), 057008. DOI: 10.1289/EHP57.

Melo-Aguilar, C., González-Rouco, J. F., García-Bustamante, E., Steinert, N., Jungclaus, J. H., Navarro, J., and Roldan-Gómez, P. J. (2019). Methodological and physical biases in global to sub-continental borehole temperature reconstructions: an assessment from a pseudo-proxy perspective. *Climate of the Past Discussions*, **2019**, 1–31. DOI: 10.5194/cp-2019-120.

Mottaghy, D. and Rath, V. (2006). Latent heat effects in subsurface heat transport modelling and their impact on palaeotemperature reconstructions. *Geophysical Journal International*, **164**(1), 236–245. DOI: 10.1111/j.1365-246X.2005.02843.x.

NOAA (2019). *Borehole Database at National Oceanic and Atmospheric Administration's Server*. https://www.ncdc.noaa.gov/data-access/paleoclimatology-data/datasets/borehole [Last acessed September 2019].

Palmer, M. D. and McNeall, D. J. (2014). Internal variability of Earth's energy budget simulated by CMIP5 climate models. *Environmental Research Letters*, **9**(3), 034016.

Palmer, M. D., McNeall, D. J., and Dunstone, N. J. (2011). Importance of the deep ocean for estimating decadal changes in Earth's radiation balance. *Geophysical Research Letters*, **38**(13). n/a–n/a. DOI: 10.1029/2011GL047835.

Phalkey, R. K., Aranda-Jan, C., Marx, S., Höfle, B., and Sauerborn, R. (2015). Systematic review of current efforts to quantify the impacts of climate change on undernutrition. *Proceedings of the National Academy of Sciences*, **112**(33), E4522–E4529. DOI: 10.1073/pnas.1409769112.

Pickler, C., Beltrami, H., and Mareschal, J.-C. (2016). Laurentide Ice Sheet basal temperatures during the last glacial cycle as inferred from borehole data. *Climate of the Past*, **12**(1), 115–127. DOI: 10.5194/cp-12-115-2016.

Pickler, C., Gurza Fausto, E., Beltrami, H., Mareschal, J.-C., Suárez, F., Chacon-Oecklers, A., Blin, N., Cortés Calderón, M. T., Montenegro, A., Harris, R., and Tassara, A. (2018). Recent climate variations in Chile: constraints from borehole temperature profiles. *Climate of the Past*, **14**(4), 559–575. DOI: 10.5194/cp-14-559-2018.

Pollack, H. N., Huang, S., and Shen, P.-Y. (1998). Climate Change Record in Subsurface Temperatures: A Global Perspective. *Science*, **282**(5387), 279–281. DOI: 10.1126/science.282.5387.279.

Pollack, H. N. and Smerdon, J. E. (2004). Borehole climate reconstructions: Spatial structure and hemispheric averages. *Journal of Geophysical Research: Atmospheres*, **109**(D11). n/a–n/a. DOI: 10.1029/2003JD004163.

Rath, V., González Rouco, J. F., and Goosse, H. (2012). Impact of postglacial warming on borehole reconstructions of last millennium temperatures. *Climate of the Past*, **8**(3), 1059–1066. DOI: 10.5194/cp-8-1059-2012.

Reiter, M. (2005). Possible Ambiguities in Subsurface Temperature Logs: Consideration of Ground-water Flow and Ground Surface Temperature Change. *pure and applied geophysics*, **162**(2), 343–355. DOI: 10.1007/s00024-004-2604-4.

Riser, S. C., Freeland, H. J., Roemmich, D., Wijffels, S., Troisi, A., Belbéoch, M., Gilbert, D., Xu, J., Pouliquen, S., Thresher, A., Le Traon, P.-Y., Maze, G., Klein, B., Ravichandran, M., Grant, F., Poulain, P.-M., Suga, T., Lim, B.,

Sterl, A., Sutton, P., Mork, K.-A., Vélez-Belchí, P. J., Ansorge, I., King, B., Turton, J., Baringer, M., and Jayne, S. R. (2016). Fifteen years of ocean observations with the global Argo array. *Nature Climate Change*, **6**, 145–153. DOI: 10.1038/nclimate2872.

Rosenzweig, C., Elliott, J., Deryng, D., Ruane, A. C., Müller, C., Arneth, A., Boote, K. J., Folberth, C., Glotter, M., Khabarov, N., Neumann, K., Piontek, F., Pugh, T. A. M., Schmid, E., Stehfest, E., Yang, H., and Jones, J. W. (2014). Assessing agricultural risks of climate change in the 21st century in a global gridded crop model intercomparison. *Proceedings of the National Academy of Sciences*, **111**(9), 3268–3273. DOI: 10.1073/pnas.1222463110.

Roy, S., Harris, R. N., Rao, R. U. M., and Chapman, D. S. (2002). Climate change in India inferred from geothermal observations. *Journal of Geophysical Research: Solid Earth*, **107**(B7), ETG 5–1–ETG 5–16. DOI: 10.1029/2001JB000536.

Schurer, A. P., Mann, M. E., Hawkins, E., Tett, S. F. B., and Hegerl, G. C. (2017). Importance of the pre-industrial baseline for likelihood of exceeding Paris goals. *Nature Climate Change*, **7**(8), 563–567. DOI: 10.1038/nclimate3345.

Screen, J. A., Deser, C., Smith, D. M., Zhang, X., Blackport, R., Kushner, P. J., Oudar, T., McCusker, K. E., and Sun, L. (2018). Consistency and discrepancy in the atmospheric response to Arctic sea-ice loss across climate models. *Nature Geoscience*, **11**(3), 155–163. DOI: 10.1038/s41561-018-0059-y.

Shen, P., Wang, K., Beltrami, H., and Mareschal, J.-C. (1992). A comparative study of inverse methods for estimating climatic history from borehole temperature data. *Global and Planetary Change*, **6**(2). 113 –127. DOI: https://doi.org/10.1016/0921-8181(92)90030-E.

Sherwood, S. C. and Huber, M. (2010). An adaptability limit to climate change due to heat stress. *Proceedings of the National Academy of Sciences*, **107**(21), 9552–9555. DOI: 10.1073/pnas.0913352107.

Stephens, G. L., Li, J., Wild, M., Clayson, C. A., Loeb, N., Kato, S., L'Ecuyer, T., Stackhouse, P. W., Lebsock, M., and Andrews, T. (2012). An update on Earth's

energy balance in light of the latest global observations. *Nature Geoscience*, **5**(10), 691–696. DOI: 10.1038/ngeo1580.

Stevens, M. B., Smerdon, J. E., González-Rouco, J. F., Stieglitz, M., and Beltrami, H. (2007). Effects of bottom boundary placement on subsurface heat storage: Implications for climate model simulations. *Geophysical Research Letters*, **34**(2). n/a–n/a. DOI: 10.1029/2006GL028546.

Stevens, M. B., González-Rouco, J. F., and Beltrami, H. (2008). North American climate of the last millennium: Underground temperatures and model comparison. *Journal of Geophysical Research: Earth Surface*, **113**(F1). n/a–n/a. DOI: 10.1029/2006JF000705.

Suman, A., Dyer, F., and White, D. (2017). Late Holocene temperature variability in Tasmania inferred from borehole temperature data. *Climate of the Past*, **13**(6), 559–572. DOI: 10.5194/cp-13-559-2017.

Tomas, R. A., Deser, C., and Sun, L. (2016). The Role of Ocean Heat Transport in the Global Climate Response to Projected Arctic Sea Ice Loss. *Journal of Climate*, **29**(19), 6841–6859. DOI: 10.1175/JCLI-D-15-0651.1.

Trenberth, K. E., Zhang, Y., Fasullo, J. T., and Cheng, L. (2019). Observation-Based Estimates of Global and Basin Ocean Meridional Heat Transport Time Series. *Journal of Climate*, **32**(14), 4567–4583. DOI: 10.1175/JCLI-D-18-0872.1.

Turcotte, D. L. and Schubert, G. (2002). *Geodynamics*. 2nd Edition. Cambridge University Press.

Vasseur, G., Bernard, P., de Meulebrouck, J. V., Kast, Y., and Jolivet, J. (1983). Holocene paleotemperatures deduced from geothermal measurements. *Palaeogeography, Palaeoclimatology, Palaeoecology*, **43**(3), 237 –259. DOI: https://doi.org/10.1016/0031-0182(83)90013-5.

Vaughan, D., Comiso, J., Allison, I., Carrasco, J., Kaser, G., Kwok, R., Mote, P., Murray, T., Paul, F., Ren, J., Rignot, E., Solomina, O., Steffen, K., and Zhang, T. (2013). "Observations: Cryosphere". In: *Climate Change 2013: The Physical Science Basis. Contribution of Working Group I to the Fifth Assessment Report of the Intergovernmental Panel on Climate Change*. Ed. by T. Stocker, D. Qin,

G.-K. Plattner, M. Tignor, S. Allen, J. Boschung, A. Nauels, Y. Xia, V. Bex, and P. Midgley. Cambridge, United Kingdom and New York, NY, USA: Cambridge University Press. Chap. 4, pp. 317–382. DOI: 10.1017/CBO9781107415324.012.

Von Schuckmann, K., Palmer, M. D., Trenberth, K. E., Cazenave, A., Chambers, D., Champollion, N., Hansen, J., Josey, S. A., Loeb, N., Mathieu, P. P., Meyssignac, B., and Wild, M. (2016). An imperative to monitor Earth's energy imbalance. *Nature Climate Change*, **6**, 138 EP –.

Wang, J and Bras, R. (1999). Ground heat flux estimated from surface soil temperature. *Journal of Hydrology*, **216**(3), 214 –226. DOI: https://doi.org/10.1016/S0022-1694(99)00008-6.

Watts, N., Amann, M., Arnell, N., Ayeb-Karlsson, S., Belesova, K., Boykoff, M., Byass, P., Cai, W., Campbell-Lendrum, D., Capstick, S., Chambers, J., Dalin, C., Daly, M., Dasandi, N., Davies, M., Drummond, P., Dubrow, R., Ebi, K. L., Eckelman, M., Ekins, P., Escobar, L. E., Fernandez Montoya, L., Georgeson, L., Graham, H., Haggar, P., Hamilton, I., Hartinger, S., Hess, J., Kelman, I., Kiesewetter, G., Kjellstrom, T., Kniveton, D., Lemke, B., Liu, Y., Lott, M., Lowe, R., Sewe, M. O., Martinez-Urtaza, J., Maslin, M., McAllister, L., McGushin, A., Jankin Mikhaylov, S., Milner, J., Moradi-Lakeh, M., Morrissey, K., Murray, K., Munzert, S., Nilsson, M., Neville, T., Oreszczyn, T., Owfi, F., Pearman, O., Pencheon, D., Phung, D., Pye, S., Quinn, R., Rabbaniha, M., Robinson, E., Rocklöv, J., Semenza, J. C., Sherman, J., Shumake-Guillemot, J., Tabatabaei, M., Taylor, J., Trinanes, J., Wilkinson, P., Costello, A., Gong, P., and Montgomery, H. (2019). The 2019 report of The Lancet Countdown on health and climate change: ensuring that the health of a child born today is not defined by a changing climate. *The Lancet*, **394**(10211), 1836–1878. DOI: 10.1016/S0140-6736(19)32596-6.

Wu, X., Lu, Y., Zhou, S., Chen, L., and Xu, B. (2016). Impact of climate change on human infectious diseases: Empirical evidence and human adaptation. *Environment International*, **86**, 14 –23. DOI: https://doi.org/10.1016/j.envint.2015.09.007.

4 Assessment of the Earth's Heat Inventory Within CMIP5 CGCM Simulations

Reference This chapter is based on the manuscript Cuesta-Valero F.J., García-García A., Beltrmi H. and Finnis J. (2020). Assessment of the Earth's Heat Inventory Within CMIP5 CGCM Simulations. *In preparation*.

Abstract The energy imbalance at the top of the atmosphere over the last century has caused an accumulation of heat within the ocean, the continental subsurface, the atmosphere and the cryosphere. Although ~90 % of the energy gained by the climate system has been stored in the ocean, the other components of the climate system cannot be neglected due to their influence on associated climate feedback processes dependent on heat storage, such as sea level rise and permafrost stability. However, there has not yet been a comprehensive assessment of the heat inventory within global climate simulations. Here, we explore the ability of thirty atmosphere-ocean Coupled General Circulation Models (CGCMs) from the fifth phase of the Coupled Model Intercomparison Project (CMIP5) to simulate the distribution of heat within the Earth's energy reservoirs in their Historical simulations. The CMIP5 CGCMs present net heat gains in all subsystems during the last three decades of the 20th century, with ensemble averages overestimating the ocean heat content and underestimating the heat content in the cryosphere and the continental subsurface in comparison with observations. The CMIP5 ensemble presents a large inter-model spread for

all energy reservoirs, which is reduced in the simulated partition of heat among the different climate subsystems. The representation of terrestrial ice masses and the continental subsurface, as well as the response of each model to the external forcing within these CGCM simulations, should be improved in order to obtain better representations of the Earth heat inventory and the partition of heat among climate subsystems in global transient climate simulations.

4.1 Introduction

Sustained net radiative imbalance at the top of the atmosphere is increasing heat storage within the climate subsystems –the ocean, the continental subsurface, the atmosphere and the cryosphere (Hansen et al., 2011). The ocean is the largest component of the EHI, accounting for around 90 % of the total heat in the climate system (Rhein et al., 2013; Gleckler et al., 2016; von Schuckmann et al., 2016, 2020). Nonetheless, it is imperative to measure the distribution of heat storage within the four components of the climate system, since the evolution of several physical processes that are critical to understand climate change and quantify future impacts of climate change on society are strongly dependent on the partition of heat among all climate components.

The evolution of ocean heat content determines the thermosteric component of sea level rise (Church et al., 2011; Kuhlbrodt et al., 2012; Levitus et al., 2012), affects the total precipitation and intensity of hurricanes (Mainelli et al., 2008; Wada et al., 2008; Lin et al., 2013; Trenberth et al., 2018), and influences regional cyclonic activity (Bhowmick et al., 2016). The increase in ground heat content leads to the warming of the continental subsurface and to permafrost thawing in the Northern Hemisphere (Koven et al., 2013; Cuesta-Valero et al., 2016; Soong et al., 2020). Thus, the increase in continental heat storage threatens the stability of the global soil carbon pool, potentially facilitating the release of large amounts of greenhouse gasses from the decomposition of soil organic matter in northern soils (Koven et al., 2011; MacDougall et al., 2012; Schädel et al., 2014; Schuur et al., 2015; Hicks Pries et al., 2017). Melting of ice sheets in Greenland and Antarctica as well as glacier degradation at all latitudes contribute to sea level rise (Jacob et al., 2012; Hanna et al., 2013; Vaughan et al., 2013;

Dutton et al., 2015), and together with changes in the extension and volume of sea ice may disturb deep water formation zones and alter ocean circulation and large scale heat distribution (Hu et al., 2013; Jahn et al., 2013; Ferrari et al., 2014). The evolution of the atmosphere heat content constrains the projected change in total global precipitation due to atmospheric warming (Pendergrass et al., 2014b; Hegerl et al., 2015), and the additional moisture in a warmer atmosphere increases the frequency of extreme precipitation events (Pendergrass et al., 2014a). The intensity of cyclones and hurricanes is also expected to increase in the future due to the higher energy available in the atmosphere (Pan et al., 2017).

Therefore, the partition of heat within these subsystems have long-term impacts on society, as the heat content of each subsystem is related to processes altering near-surface conditions. Higher surface temperatures together with changes in precipitation regimes and sea level rise threaten global food security (Lloyd et al., 2011; Rosenzweig et al., 2014; Phalkey et al., 2015; Campbell et al., 2016), and may result in an increase in the frequency of floods and storm surges (McGranahan et al., 2007; Lin et al., 2013; Kundzewicz et al., 2014). The combination of high temperature and moisture, and changes in precipitation patterns also affect human health, particularly for the populations least responsible for climate change (Patz et al., 2007). These changes in near-surface conditions increase the risk of high levels of heat stress (Sherwood et al., 2010; Matthews et al., 2017) and the spread of infectious diseases (Levy et al., 2016; Wu et al., 2016; McPherson et al., 2017), among others risks for human health (McMichael et al., 2006).

Atmosphere-ocean Coupled General Circulation Model (CGCM) simulations are the main source of information about the possible evolution of the climate system, which is critical for society's adaptation to future risks posed by climate change. Modeling experiments performed for the fifth phase of the Coupled Model Intercomparison Project (CMIP5) have provided several insights into the long-term evolution of the net radiative imbalance at the top of the atmosphere (Allan et al., 2014; Smith et al., 2015), the evolution of ocean heat content since preindustrial times (Gleckler et al., 2016), and the relationship between these two changes (Palmer et al., 2011; Palmer et al., 2014; Smith et al., 2015). The same CGCM simulations, nevertheless, do not simulate other aspects of the

Earth heat inventory successfully. CMIP5 CGCMs are unable to accurately represent heat storage within the continental subsurface over the second half of the 20th century (Cuesta-Valero et al., 2016); many do not conserve atmospheric water (Liepert et al., 2013) nor subsurface water (Krakauer et al., 2013; Trenberth et al., 2016), which leads to non-conservation of total heat content (Hobbs et al., 2016). Furthermore, there has not yet been an assessment of the ability of CMIP5 CGCMs to reproduce heat storage within the atmosphere and the cryosphere, despite their impact on a variety of phenomena of critical interest to both society and the scientific community.

Here, we assess the ability of thirty CMIP5 CGCM Historical simulations to reproduce the Earth heat inventory and the partition of heat within the ocean, continental subsurface, atmosphere and cryosphere. Results are compared with estimates from observations for the period 1972-2005 of the Common Era (CE). Our analysis reveals the importance of the simulated terrestrial ice masses and continental subsurface for achieving a realistic distribution of the total Earth heat content within CGCM simulations, and thus reinforces the need to reduce the spread in model responses to external forcing.

4.2 Data and Methods

Thirty different CGCM Historical simulations were retrieved from the fifth phase of the Coupled Model Intercomparison Project (CMIP5) archive (Taylor et al., 2011). Our analysis focuses on Historical simulations, which attempt to represent the evolution of global climate from the Industrial Revolution to the present (1850-2005 CE) using estimates of natural and anthropogenic emissions of greenhouse gases and aerosols, as well as changes in land cover and land use (Mieville et al., 2010; Hurtt et al., 2011). We analyzed the simulated evolution of heat storage in each climate subsystem as well as in the entire climate system for the period 1972-2005 CE, consistently with observations from Church et al. (2011) and von Schuckmann et al. (2020).

Global averages of Ocean Heat Content (OHC), heat content within the continental subsurface (ground heat content, GHC), Atmosphere Heat Content (AHC) and heat absorbed by ice masses (cryosphere heat content, CHC) were derived from the CMIP5 Historical experiments. The OHC values were estimated us-

ing the formulation for potential enthalpy described in McDougall (2003) and Griffies (2004) from simulated seawater potential temperature and salinity profiles (Table 4.1 contains the list of variables employed for estimating each term of the EHI from CMIP5 simulations). Once the potential enthalpy has been determined, estimates of seawater density (McDougall et al., 2003) and pressure profiles (Smith et al., 2010) allowed simulated heat content in the ocean to be calculated as:

$$Q_{Ocean}(S,\theta) = \sum_{i=z_0}^{z_f} \rho_i(S,\theta,p(z_i)) \cdot \mathcal{H}_i^{\circ}(S,\theta), \cdot \Delta z_i, \tag{4.1}$$

where Q_{Ocean} is the ocean heat per surface unit (in $\mathrm{J\,m^{-2}}$), S is salinity (in psu), θ is potential temperature (in °C), p is pressure (in bar), z_i, ρ_i, $\mathcal{H}_i^{\circ}$ and Δz_i are depth (in m), density (in $\mathrm{kg\,m^{-3}}$), potential enthalpy (in $\mathrm{J\,kg^{-1}}$) and thickness (in m) of the i-th ocean layer, respectively.

The GHC series were estimated as in Cuesta-Valero et al. (2016) for all terrestrial grid cells. Subsurface thermal properties were computed taking into account spatial variations of soil composition (% of sand, clay and bedrock) and simulated subsurface water and ice amounts (Van Wijk et al., 1963; Oleson et al., 2010). The subsurface temperature profile was then integrated following

$$Q_{Ground} = \sum_{i=z_0}^{z_f} \rho C_i \cdot T_i \cdot \Delta z_i, \tag{4.2}$$

where Q_{Ground} is the subsurface heat storage per surface unit (in $\mathrm{J\,m^{-2}}$) and ρC_i, T_i and Δz_i are the volumetric heat capacity (in $\mathrm{J\,m^{-3}\,K^{-1}}$), the temperature (in K) and the thickness (in m) of the i-th soil layer, respectively. All CMIP5 CGCMs present outputs for subsurface temperature, but not all models provide outputs for subsurface water and ice content in the same format (Table 4.1), hampering the estimate of thermal properties (ρC) in Equation 4.2. Indeed, two thirds of the CGCMs provide the joint content of water and ice for each soil layer (*mrlsl* variable in CMIP5 notation), while the remaining third provide the total water and ice content in the entire soil column (*mrso* variable). As in Cuesta-Valero et al. (2016), we considered water to be frozen in layers with temperatures below 0 °C and liquid water otherwise for models providing the *mrlsl* variable. For

Table 4.1: Variables from the CMIP5 archive employed to estimate the heat content within each climate subsystem (Section 4.2) by each CGCM. References for each CGCM Historical experiment are also provided. All variables correspond with the r1i1p1 realization of the Historical experiment. A description of all listed variables can be found at the dedicated webpage of the Lawrence Livermore National Laboratory (LLNL, 2010).

Model	Ocean	Land	Atmosphere	Cryosphere	TOA Imbalance	References
CCSM4	*so, thetao*	*mrlsl, tsl*	*hus, ps, ta, ua, va*	*mrfso, sic, sit, snw*	*rlut, rsdt, rsut*	Gent et al. (2011)
CESM1-BGC	*so, thetao*	*mrlsl, tsl*	*hus, ps, ta, ua, va*	*mrfso, sic, sit, snw*	*rlut, rsdt, rsut*	Long et al. (2013)
CESM1-CAM5	*so, thetao*	*mrlsl, tsl*	*hus, ps, ta, ua, va*	*mrfso, sic, sit, snw*	*rlut, rsdt, rsut*	Meehl et al. (2013)
CESM1-FASTCHEM	*so, thetao*	*mrlsl, tsl*	*hus, ps, ta, ua, va*	*mrfso, sic, sit, snw*	*rlut, rsdt, rsut*	Hurrell et al. (2013)
CESM1-WACCM	*so, thetao*	*mrlsl, tsl*	*hus, ps, ta, ua, va*	*mrfso, sic, sit, snw*	*rlut, rsdt, rsut*	Marsh et al. (2013)
NOR-ESM1-M	*so, thetao*	*mrlsl, tsl*	*hus, ps, ta, ua, va*	*mrfso, sic, sit, snw*	*rlut, rsdt, rsut*	Iversen et al. (2013)
NOR-ESM1-ME	*so, thetao*	*mrlsl, tsl*	*hus, ps, ta, ua, va*	*mrfso, sic, sit, snw*	*rlut, rsdt, rsut*	Tjiputra et al. (2013)
INM-CM4	*so, thetao*	*mrlsl, tsl*	*hus, ps, ta, ua, va*	*sic, sit, snw*	*rlut, rsdt, rsut*	Volodin et al. (2010)
MIROC-ESM	*so, thetao*	*mrlsl, tsl*	*hus, ps, ta, ua, va*	*mrfso, sic, sit, snw*	*rlut, rsdt, rsut*	Watanabe et al. (2011)
MIROC-ESM-CHEM	*so, thetao*	*mrlsl, tsl*	*hus, ps, ta, ua, va*	*mrfso, sic, sit, snw*	*rlut, rsdt, rsut*	Watanabe et al. (2011)
MIROC5	*so, thetao*	*mrlsl, tsl*	*hus, ps, ta, ua, va*	*mrfso, sic, sit, snw*	*rlut, rsdt, rsut*	Watanabe et al. (2010)
GFDL-CM3	*so, thetao*	*mrlsl, tsl*	*hus, ps, ta, ua, va*	*mrfso, sic, sit, snw*	*rlut, rsdt, rsut*	Donner et al. (2011)
GFDL-ESM2G	*so, thetao*	*mrlsl, tsl*	*hus, ps, ta, ua, va*	*mrfso, sic, sit, snw*	*rlut, rsdt, rsut*	Dunne et al. (2012)
GFDL-ESM2M	*so, thetao*	*mrlsl, tsl*	*hus, ps, ta, ua, va*	*mrfso, sic, sit, snw*	*rlut, rsdt, rsut*	Dunne et al. (2012)
MRI-CGCM3	*so, thetao*	*mrso, tsl*	*hus, ps, ta, ua, va*	*mrfso, sic, sit, snw*	*rlut, rsdt, rsut*	Yukimoto et al. (2012)
MRI-ESM1	*so, thetao*	*mrso, tsl*	*hus, ps, ta, ua, va*	*mrfso, sic, sit, snw*	*rlut, rsdt, rsut*	Adachi et al. (2013)
MPI-ESM-LR	*so, thetao*	*mrso, tsl*	*hus, ps, ta, ua, va*	*sic, sit, snw*	*rlut, rsdt, rsut*	Giorgetta et al. (2013)
MPI-ESM-MR	*so, thetao*	*mrso, tsl*	*hus, ps, ta, ua, va*	*sic, sit, snw*	*rlut, rsdt, rsut*	Giorgetta et al. (2013)
MPI-ESM-P	*so, thetao*	*mrso, tsl*	*hus, ps, ta, ua, va*	*sic, sit, snw*	*rlut, rsdt, rsut*	Jungclaus et al. (2014)
CMCC-CM	*so, thetao*	*mrso, tsl*	*hus, ps, ta, ua, va*	*sic, sit, snw*	*rlut, rsdt, rsut*	Scoccimarro et al. (2011)
CMCC-CMS	*so, thetao*	*mrso, tsl*	*hus, ps, ta, ua, va*	*sic, sit, snw*	*rlut, rsdt, rsut*	Scoccimarro et al. (2011)
CANESM2	*so, thetao*	*mrlsl, tsl*	*hus, ps, ta, ua, va*	*mrfso, sic, sit, snw*	*rlut, rsdt, rsut*	Arora et al. (2011)
IPSL-CM5A-LR	*so, thetao*	*mrso, tsl*	*hus, ps, ta, ua, va*	*sic, sit*	*rlut, rsdt, rsut*	Dufresne et al. (2013)
IPSL-CM5A-MR	*so, thetao*	*mrso, tsl*	*hus, ps, ta, ua, va*	*sic, sit*	*rlut, rsdt, rsut*	Dufresne et al. (2013)
IPSL-CM5B-LR	*so, thetao*	*mrso, tsl*	*hus, ps, ta, ua, va*	*sic, sit*	*rlut, rsdt, rsut*	Dufresne et al. (2013)
GISS-E2-H	*so, thetao*	*mrlsl, tsl*	*hus, ps, ta, ua, va*	*mrfso, sic, sit, snw*	*rlut, rsdt, rsut*	Miller et al. (2014)
GISS-E2-R	*so, thetao*	*mrlsl, tsl*	*hus, ps, ta, ua, va*	*mrfso, sic, sit, snw*	*rlut, rsdt, rsut*	Miller et al. (2014)
BCC-CSM1.1	*so, thetao*	*mrlsl, tsl*	*hus, ps, ta, ua, va*	*mrfso, sic, sit, snw*	*rlut, rsdt, rsut*	Wu et al. (2014)
BCC-CSM1.1-M	*so, thetao*	*mrlsl,tsl*	*hus, ps, ta, ua, va*	*mrfso, sic, sit, snw*	*rlut, rsdt, rsut*	Wu et al. (2014)
HADGEM2-CC	*so, thetao*	*mrlsl, tsl*	*hus, ps, ta, ua, va*	*mrfso, sic, sit, snw*	*rlut, rsdt, rsut*	Collins et al. (2011)

models providing the *mrso* variable, we distributed the water and ice content among the soil layers proportionally with thickness, considering ice in soil layers with temperature below 0 °C and liquid water otherwise.

The AHC series were estimated as in Trenberth (1997), Previdi et al. (2015) and von Schuckmann et al. (2020). The simulated air temperature profile was integrated for all atmospheric grid cells together with estimates of wind kinetic energy, latent heat of vaporization and surface geopotential, which was determined as in Dutton (2002). Vertical atmospheric profiles were integrated in pressure coordinates as:

$$Q_{Atmosphere} = \frac{1}{g} \sum_{i=0}^{p_s} \left(c_p \cdot T_i + k_i + L \cdot q_i + \Phi_s \right) \Delta p_i, \tag{4.3}$$

where $Q_{Atmosphere}$ is atmospheric heat per surface unit (in $\mathrm{J\,m^{-2}}$), g is apparent acceleration due to gravity (in $\mathrm{m\,s^{-2}}$), p_s is surface pressure (in Pa), $c_p = 1000\,\mathrm{J\,kg^{-1}\,K^{-1}}$ is the specific heat of air at constant pressure, $L = 2260\,\mathrm{J\,kg^{-1}}$ is the latent heat of vaporization, Φ_s is the surface geopotential estimated from orography (in $\mathrm{m^2\,s^{-2}}$), T_i, k_i, q_i and Δp_i are the air temperature (in K), specific kinetic energy (in $\mathrm{J\,kg^{-1}}$), specific humidity (in $\mathrm{kg\,kg^{-1}}$) and thickness (in Pa) of the i-th atmospheric layer, respectively.

For estimating the CHC series, the simulated cryosphere was divided into three terms: sea ice, subsurface ice and glaciers. Variations in the mass of simulated sea ice and subsurface ice were multiplied by the latent heat of fusion ($L_f = 3.34 \times 10^5\,\mathrm{J\,kg^{-1}}$, Rhein et al., 2013) to obtain the heat absorbed in the melting process. The same method was applied to the change in snow mass in grid cells containing land ice within each CMIP5 CGCM (glaciers or ice sheets, *sftgif* variable in the CMIP5 archive). Therefore, the cryosphere heat content was estimated as

$$Q_{Cryosphere} = L_f \cdot (\Delta\omega + \rho \cdot \Delta p \cdot \Delta z + \Delta\Omega), \tag{4.4}$$

where $Q_{Cryosphere}$ is absorbed heat per surface unit (in $\mathrm{J\,m^{-2}}$), $\rho = 920\,\mathrm{kg\,m^{-3}}$ is ice density (Rhein et al., 2013), $\Delta\omega$ is the change in subsurface ice mass per surface unit (in $\mathrm{kg\,m^{-2}}$), Δp is the change in the proportion of sea ice at each ocean grid cell, Δz is the change in thickness of sea ice at each ocean grid cell

(in m), and $\Delta\Omega$ is the change in snow amount at each cell containing land ice (in $\mathrm{kg\,m^{-2}}$). It is important to note that nine of the CMIP5 CGCMs did not provide outputs for the subsurface ice amount (*mrfso* variable) and that three of the models did not provide outputs for snow amount (*snw* variable, see Table 4.1), and thus these terms are missing in the CHC estimates from those models. We were unable to retrieve the file indicating the cells containing land ice (*sftgif* file) for the HADGEM2-CC CGCM, thus we used the CMCC-CMS *sftgif* file interpolated to the HADGEM2-CC grid, since the grid for both models have a similar spatial resolution (1.25°×1.875° for HADGEM2-CC, 1.875°×1.875° for CMCC-CMS).

Estimates of total heat in the climate system from each CMIP5 model are required to determine the simulated partition of heat among each climate subsystem. The total heat content can be determined as the sum of the heat storage within the different climate subsystems (Earth heat content, EHC) or as the integration of the radiative imbalance at the top of the atmosphere (N) during the period of interest. Both approximations have been used in the literature and are considered equivalent (Rhein et al., 2013; Palmer et al., 2014; Trenberth et al., 2014; von Schuckmann et al., 2016). That is, if a model does not produce artificial sources or leakages of energy or mass (i.e., if the model conserves the total heat content in the system), the change in N and in EHC should be almost identical (Hobbs et al., 2016). Nevertheless, CMIP5 CGCM simulations are prone to drift, particularly the ocean component due to incomplete model spin-up procedures (Sen Gupta et al., 2013; Séférian et al., 2016). For this reason, potential drifts in estimates of heat content and the components of the radiative budget at the top of the atmosphere were removed by subtracting the trend of the corresponding preindustrial control simulation from the Historical simulations, which should correct artificial drifts in the simulated heat content within each climate subsystem (Hobbs et al., 2016). N estimates from the CESM1-CAM5 CGCM constitutes a particular case, since a large, unrealistic trend remained in the Historical experiment in comparison with other CMIP5 CGCMs after removing the drift using data from the corresponding control simulation (Figure 4.1). The rest of variables from this CGCM were dedrifted using the trend estimated from the preindustrial control simulation as in the other CMIP5 simulations, but the drift in the outgoing shortwave radiation and the outgoing longwave

radiation at the top of the atmosphere could not be removed using the trend of the control simulation. Therefore, we used the trend estimated from the first five decades of the Historical simulation (1861-1911 CE) to remove the drift in N estimates, achieving a better comparison with the other CMIP5 CGCMs (Figure 4.1).

As a complement to the estimates of the EHI detailed above, we also estimated the partition of the simulated total heat content among the ocean, the continental subsurface, the atmosphere and the cryosphere. A linear regression analysis was performed between the evolution of the simulated heat storage within each climate subsystem and the estimates of accumulated heat content in the entire climate system to estimate the partition of heat within the four subsystems (Figure 4.2). The slope of the linear fit was assumed to be an estimate of the simulated proportion of heat in the corresponding subsystem, obtaining estimates of OHC/N and OHC/EHC for the simulated proportion of heat in the ocean, GHC/N and GHC/EHC for the simulated proportion of heat in the continental subsurface, AHC/N and AHC/EHC for the simulated proportion of heat in the atmosphere, and CHC/N and CHC/EHC for the simulated proportion of heat absorbed by the cryosphere.

4.3 Results

4.3.1 Earth's Heat Inventory

Although the majority of the CMIP5 CGCMs are able to reproduce the atmosphere heat content for the period 1972-2005 CE, the ensemble mean is higher than observations for the ocean and lower than observations for the continental subsurface and the cryosphere (Figure 4.3). Additionally, the multimodel mean yields higher total heat in the climate system than observations, as expected due to the high OHC values reached by these simulations (Figure 4.3a). Indeed, the CMIP5 multimodel mean yields an OHC increase of 247 ± 172 ZJ (mean $\pm$ two standard deviations, $1\,\mathrm{ZJ} = 10^{21}$ J) for 1971-2005 CE, higher than the observational estimates in Church et al. (2011) ($\sim$199 ZJ) and von Schuckmann et al. (2020) (175 ± 35 ZJ, Table 4.2). These OHC estimates are the cause of the large Earth heat content displayed by the CMIP5 ensemble, since the EHC estimates

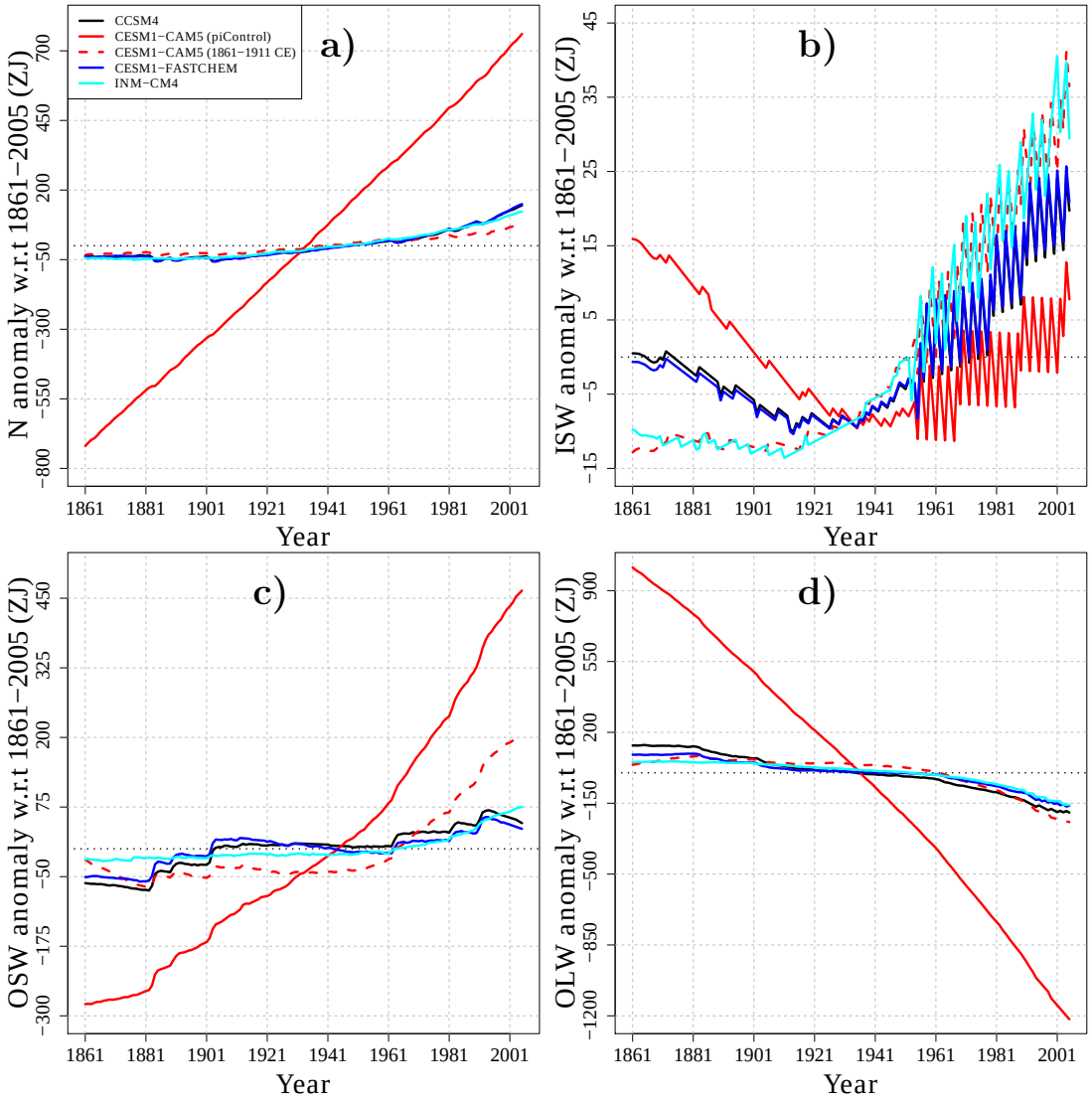

Figure 4.1: (a) Integrated total radiative imbalance (N), (b) incoming shortwave radiation (ISW), (c) outgoing shortwave radiation (OSW) and (d) outgoing longwave radiation (OLW) at the top of the atmosphere for the CCSM4, CESM1-CAM5, CESM1-FASTCHEM and INM-CM4 Historical simulations. Data from the CESM1-CAM5 are dedrifted using the preindustrial control simulation (solid red line) or the first five decades of the Historical simulation (dashed red line). Data from the rest of models are dedrifted using the corresponding preindustrial control simulation.

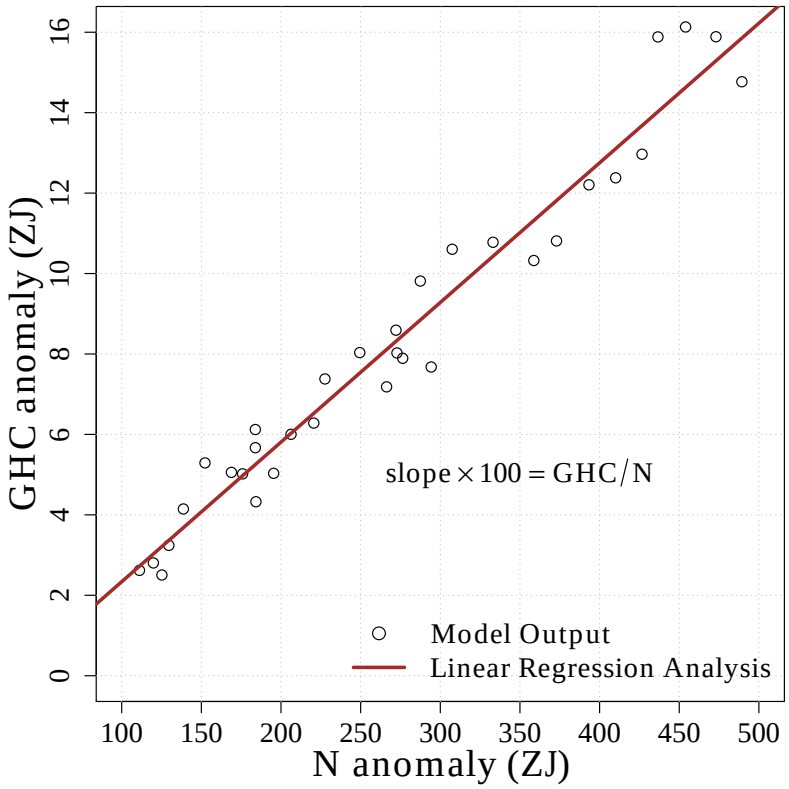

Figure 4.2: Example to illustrate the process to estimate heat proportions using data from the CCSM4 Historical simulation. In this case, the proportion of heat within the continental subsurface (GHC/N) is estimated as the slope from the linear regression analysis (solid line) between the simulated GHC and N anomalies (dots) for the period 1972-2005 CE multiplied by 100. The proportion of heat in the rest of climate subsystems is estimated replacing the GHC anomaly with the corresponding heat content anomaly. The EHC anomaly is also used as metric for the total heat content in the system by replacing the N anomaly in the regression analysis.

result from the cumulative heat storage in the four climate subsystems, and the ocean accounts for around 90 % of the total heat storage (Church et al., 2011; Hansen et al., 2011; Rhein et al., 2013; Gleckler et al., 2016; von Schuckmann et al., 2016, 2020). The integration of the radiative imbalance at the top of the atmosphere for the period 1972-2005 CE should yield similar values to those of EHC and OHC over the same period, as the radiative imbalance causes the heat storage within the different climate subsystems. Nevertheless, EHC and OHC estimates are generally similar within each model, while N values diverge from those for the Earth heat content in some models, suggesting that these models may have biases in their represented energy budget. Furthermore, the inter-model spread obtained for these three magnitudes is excessively large, given that all Historical simulations were forced using the same boundary conditions –i.e., the same external forcing.

Table 4.2: Earth heat inventory and heat partition estimated from the 30 CMIP5 CGCMs analyzed here (MMM), and observations from Church et al. (2011) (Ch11) and von Schuckmann et al. (2020) (vS20). Heat storage in ZJ, heat partition in %.

Magnitude	MMM	Ch11	vS20
N	264 ± 171	–	–
EHC	256 ± 177	212	197 ± 36
OHC	247 ± 172	199	175 ± 35
GHC	5 ± 9	4	14 ± 3
AHC	2 ± 2	2	1.8 ± 0.5
CHC	2 ± 3	7	7.1 ± 0.9
CHC (only sea ice)	2 ± 2	2	2.1 ± 0.4
OHC/N	93 ± 25	–	–
OHC/EHC	96 ± 4	94	90 ± 24
OHC/EHC (only sea ice)	96 ± 4	96	92 ± 25
GHC/N	2 ± 3	–	–
GHC/EHC	2 ± 3	2	6 ± 2
GHC/EHC (only sea ice)	2 ± 3	2	7 ± 2
AHC/N	1.0 ± 0.9	–	–
AHC/EHC	1 ± 1	1	0.7 ± 0.2
AHC/EHC (only sea ice)	1 ± 1	1	0.7 ± 0.2
CHC/N	0.9 ± 1	–	–
CHC/EHC	1 ± 1	3	3.4 ± 0.7
CHC/EHC (only sea ice)	1 ± 1	1	1.1 ± 0.2

A different situation is found for the magnitude of the simulated heat storage

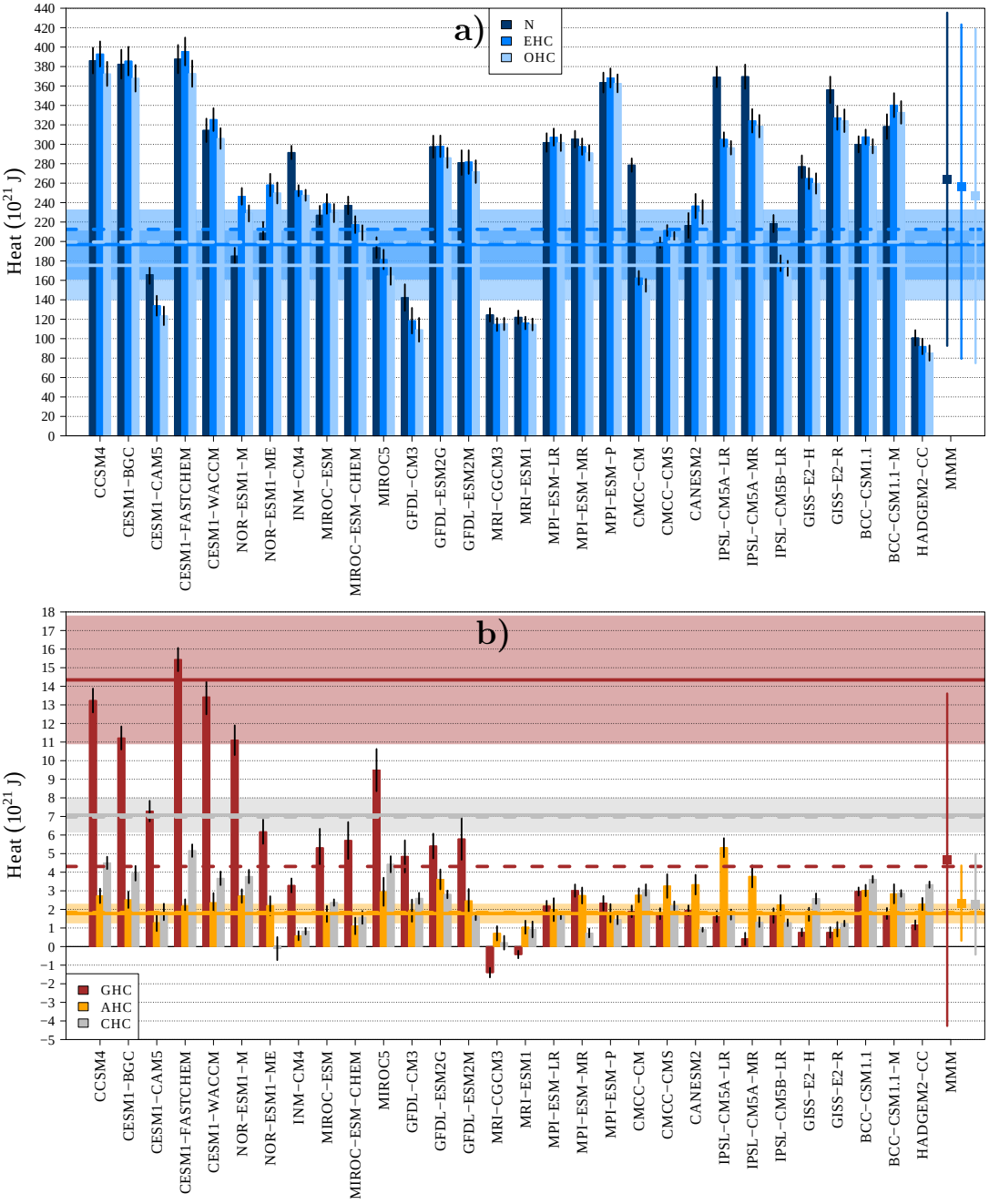

Figure 4.3: Simulated heat storage for 1972-2005 CE from 30 CMIP5 CGCM Historical simulations. (upper panel) Results for N (dark blue bars), EHC (blue bars) and OHC (light blue bars). (bottom panel) Results for GHC (brown bars), AHC, (orange bars) and CHC (gray bars). Black lines at the top of the bars indicate the 95 % confidence interval for each model. Observations from von Schuckmann et al. (2020) are shown as solid horizontal lines and shadows (mean and 95 % confidence intervals), and observations from Church et al. (2011) are displayed as dashed horizontal lines. Multimodel means and 95 % confidence intervals are indicated in the right side of the panel (MMM).

within the continental subsurface, with the CMIP5 ensemble yielding generally lower estimates of GHC than the observations (Figure 4.3b). The multimodel mean achieves a GHC change of 5 ± 9 ZJ for 1972-2005 CE, which is lower than the 14 ± 3 ZJ in von Schuckmann et al. (2020) but similar to the ~4 ZJ in Church et al. (2011) (Table 4.2). However, the difference between the GHC estimates in Church et al. (2011) and in von Schuckmann et al. (2020) is large, with the value from Church et al. (2011) out of the uncertainty range presented in von Schuckmann et al. (2020), which does not occur for the other components of the Earth heat inventory (Figure 4.3). This discrepancy is probably caused by the higher number of recent geothermal measurements considered in von Schuckmann et al. (2020), which include the most recent warming of the continental subsurface in the GHC estimates in comparison with earlier studies (see Chapter 3 for a discussion). Additionally, the representation of GHC in the CMIP5 CGCMs is markedly limited by the simulated subsurface volume, which is determined by the depth of the Land Surface Model (LSM) component (Stevens et al., 2007; MacDougall et al., 2008; Cuesta-Valero et al., 2016). Indeed, five of the seven CGCMs using LSM components deeper than 40 m yield GHC estimates in agreement with the 95 % confidence interval of observations from von Schuckmann et al. (2020), suggesting that the underestimated continental heat storage and the large spread in the CMIP5 ensemble are direct consequences of the different bottom boundary depths used by each model (see Cuesta-Valero et al., 2016, for a complete list of bottom boundary depths). The negative GHC estimates for both MRI simulations in Figure 4.3b are caused by an unrealistic and sharp decrease of the total water content in the subsurface along these Historical simulations (see Cuesta-Valero et al., 2016, for more details).

The CMIP5 ensemble constantly underestimates the cryosphere heat content in comparison with observations (Figure 4.3b). The ensemble estimates a 2 ± 3 ZJ change in the cryosphere heat content for the period 1972-2005 CE, which is much lower than the observed CHC in Church et al. (2011) (7 ZJ) and in von Schuckmann et al. (2020) (7.1 ± 0.9 ZJ, Table 4.2). Figure 4.4 examines the three components contributing to the cryosphere heat content in this analysis for each CMIP5 model (i.e, sea ice, subsurface ice and glaciers), in order to understand the reason for the disagreement between simulated and observed CHC estimates. Melting of sea ice is the main contributor to the cryosphere heat

content in all models, followed by the melting of subsurface ice. Nevertheless, neither Church et al. (2011) nor von Schuckmann et al. (2020) include observations of the change in subsurface ice, and not all CMIP5 CGCMs include a representation of subsurface ice, thus we cannot assess the ability of the CMIP5 CGCMs to reproduce this term of the cryosphere heat content. Furthermore, the approach used in this study to estimate the heat absorbed by glaciers (see Section 4.2) is just an approximation given the available variables from the models, yielding a much smaller value from all models than from observations (~2.8 ZJ in Church et al., 2011 and ~1.4 ZJ in von Schuckmann et al., 2020). Therefore, the only component of the cryosphere properly represented in all models and considered in both observational studies is sea ice volume. The simulated absorbed heat due to the decrease in sea ice volume is in agreement with observations, with a multimodel mean of 2 ± 2 ZJ, while observations reach ~2.3 ZJ and 2.1 ± 0.4 ZJ in Church et al. (2011) and von Schuckmann et al. (2020), respectively (Table 4.2). However, the spread in the CMIP5 results is still large, with the difference between the highest and the lowest estimates of heat storage due to sea ice melting being more than double the value of the ensemble mean (5 ZJ).

The heat storage within the atmosphere yields the best results for the CMIP5 CGCMs in comparison with observations (Figure 4.3b). The CMIP5 ensemble mean achieves an atmosphere heat content of 2 ± 2 ZJ, in agreement with observations from Church et al. (2011) (2 ZJ) and von Schuckmann et al. (2020) (1.8 ± 0.5 ZJ). Additionally, one third of the models displays AHC estimates similar to the observed atmosphere heat content. Despite the similarity between the multimodel mean and observations, the inter-model spread is large, with the difference between the maximum and minimum AHC from CMIP5 models reaching 5 ZJ, which corresponds to more than double the value of the multimodel mean and the observational estimate.

4.3.2 Heat Partition Within Climate Subsystems

Although the assessment of the heat storage within each climate subsystem is important, the represented Earth's heat inventory within CMIP5 CGCMs depends on the total heat content simulated by each model. The CMIP5 ensemble has shown a large inter-model spread for N and EHC estimates, nevertheless, models may be distributing the total heat content among the four climate subsys-

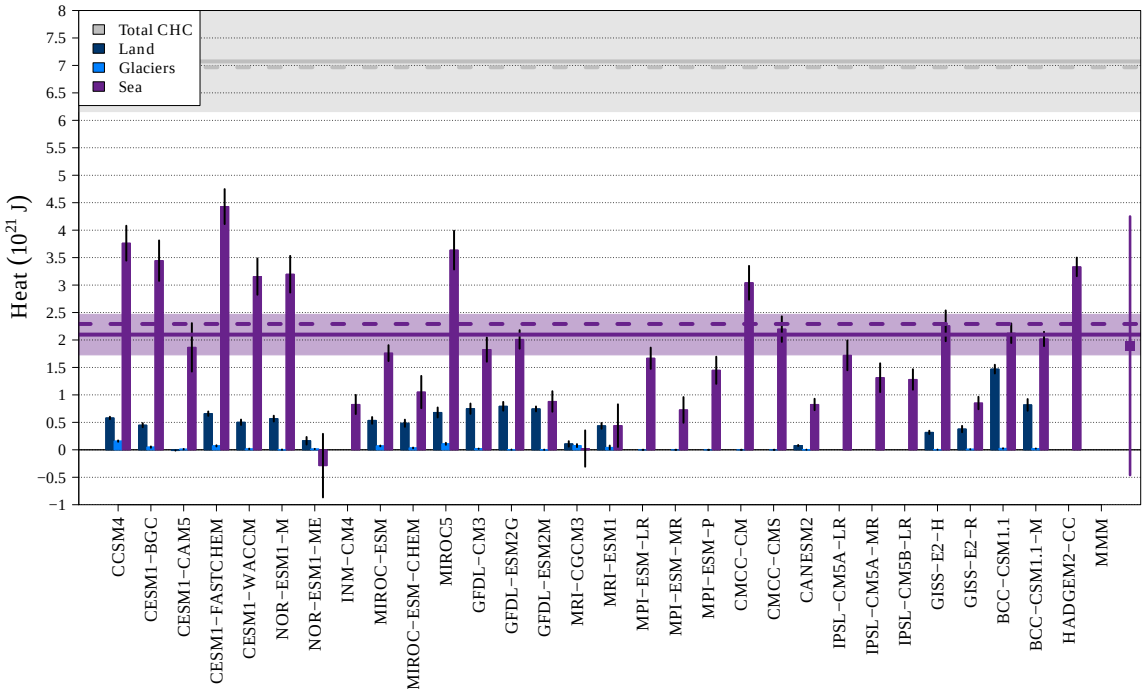

Figure 4.4: Simulated CHC for 1972-2005 CE. Dark blue bars indicate the heat absorbed by changes in subsurface ice mass, blue bars indicate the heat absorbed by changes in glacier mass, and purple bars indicate the heat absorbed by changes in sea ice volume (see Section 4.2 for details). Black lines at the top of the bars indicate the 95 % confidence interval for each model. The multimodel mean and 95 % confidence interval for the heat absorbed by changes in sea ice volume are indicated in the right side of the panel (MMM). Observations from von Schuckmann et al. (2020) are shown as solid horizontal lines and shadows (means and 95 % confidence intervals), and observations from Church et al. (2011) are displayed as dashed horizontal lines.

tems similarly. Therefore, we evaluate the partition of heat among climate subsystems within each CMIP5 CGCM, testing whether models simulating higher values of N and EHC distribute this energy in the same proportions as models simulating lower values of total heat content.

The simulated heat partitions by the thirty CMIP5 CGCMs achieve a lower inter-model spread in comparison with the simulated EHI, particularly for the ocean component (Figures 4.5 and 4.6). Nevertheless, the ensemble mean presents a partition of heat in each climate subsystem similar to the results for the Earth heat inventory. That is, the simulated proportion of energy in the ocean is larger than observations, the proportion of heat in the continental subsurface and in the cryosphere is lower than observations, and the proportion of heat in the atmosphere is slightly higher than the 95 % confidence interval of the observations. Additionally, results vary depending on the metric used to indicate total heat in the system, especially for the ocean.

The thirty CMIP5 CGCM simulations generally agree with the observed proportion of heat stored in the ocean considering EHC as metric for total energy in the climate system (OHC/EHC, blue dots in Figure 4.5a), achieving a multimodel mean just 2 % higher than Church et al. (2011) and 6 % higher than von Schuckmann et al. (2020) (Table 4.2). The spread of OHC/EHC estimates is small, with values ranging from 91 ± 2 % (MIROC5) to 100 ± 1 % (MRI-CGCM3). Nevertheless, the simulated proportion of energy in the ocean presents disagreements for some models when considering the integration of the radiative imbalance at the top of the atmosphere as metric for total heat in the climate system (OHC/N, black dots in Figure 4.5a). The model spread is much larger for OHC/N estimates than for OHC/EHC estimates, ranging from 56 ± 2 % (CMCC-CM) to 122 ± 4 % (NOR-ESM1-M). These different estimates are related to the differences between N and EHC values displayed in Figure 4.3. That is, some CMIP5 models yield excessively different values of N and EHC, suggesting the presence of non-conservation terms in the simulated energy budget. Six models obtain OHC/N estimates above 100 %, which indicates that the simulated N in those models are much lower than EHC estimates (Figure 4.5a). The opposite behavior occurs in other five models that simulate OHC/N values below 80 %, which is probably a excessively small proportion of heat stored in the ocean in comparison with observations (Hansen et al., 2011; Palmer et al., 2011; Rhein et al., 2013; Palmer

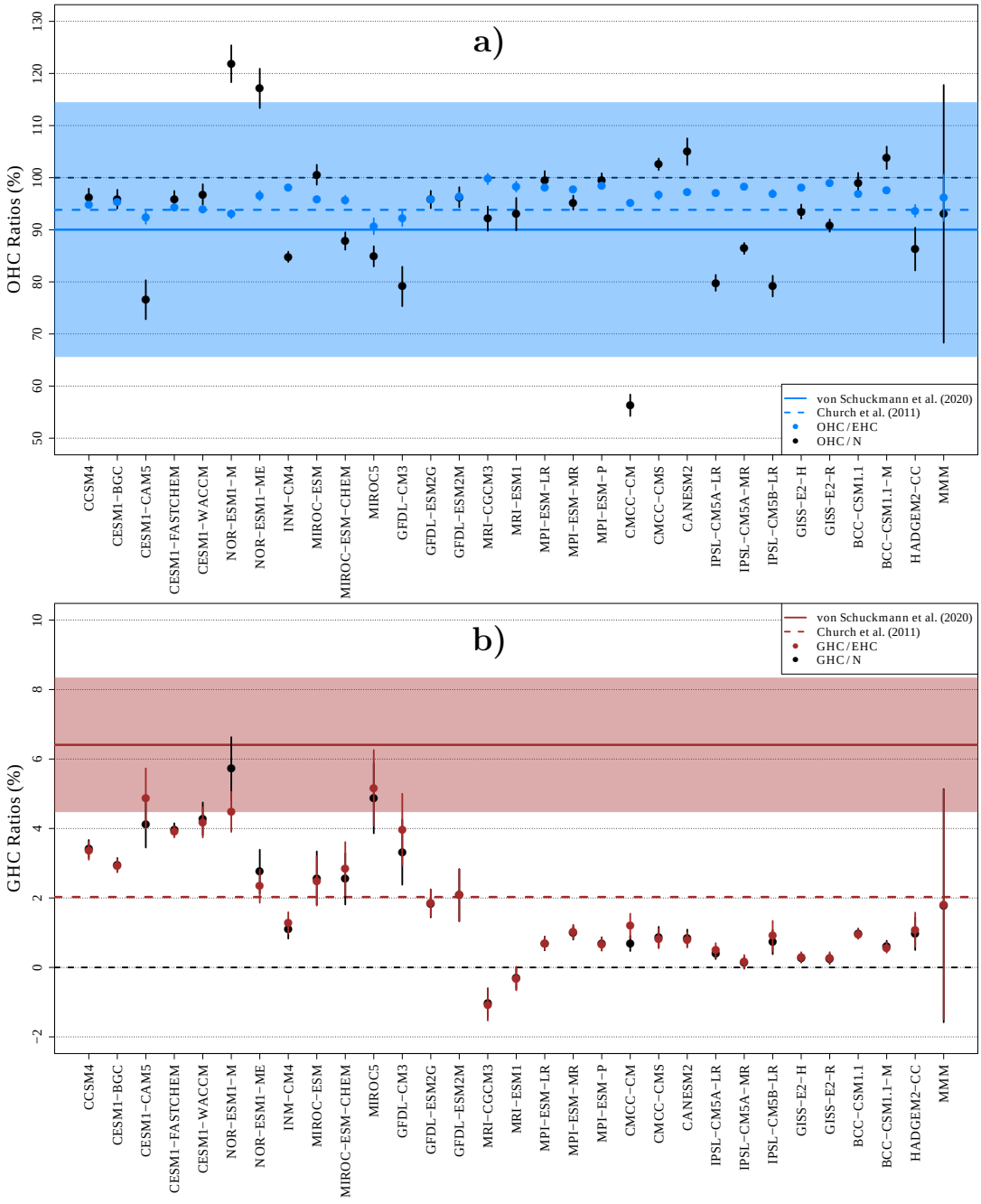

Figure 4.5: (a) Proportion of energy within the ocean for the period 1972-2005 CE using EHC (blue dots) and N (black dots) as estimates of total heat content in the climate system. (b) Proportion of energy within the continental subsurface for the period 1972-2005 CE using EHC (red dots) and N (black dots) as estimates of total heat content in the climate system. Observations from von Schuckmann et al. (2020) are shown as solid horizontal lines and shadows (means and 95 % confidence intervals), and observations from Church et al. (2011) are displayed as dashed horizontal lines. Multimodel means and 95 % confidence intervals are indicated in the right side of the panels (MMM). Black dashed lines indicate the 0 % and 100 % values.

et al., 2014; Trenberth et al., 2014; Hobbs et al., 2016; von Schuckmann et al., 2016, 2020). Although OHC/N values of 80 % are contained in the estimated uncertainty range from von Schuckmann et al. (2020), this 95 % confidence interval is large, as it includes values higher than 100 %. This is caused by the large uncertainties in OHC and EHC, since the 95 % confidence interval for observations is obtained from the uncertainties in both magnitudes (Table 4.2).

Estimates of the proportion of heat in the ground show smaller differences between GHC/N and GHC/EHC than in the case of the proportion of heat in the ocean (Figure 4.5b). Both GHC/N and GHC/EHC estimates have a multi-model mean and 95 % confidence interval of 2 ± 3 %, which is in agreement with estimates derived from Church et al. (2011) (~2 %), but excessively low in comparison with results from von Schuckmann et al. (2020) (6 ± 2 %). As in the case of the simulated ground heat content, the relatively large inter-model spread in the simulated proportion of heat stored in the continental subsurface is caused by the depth of the used LSM component. Thus, deeper models reach higher proportions of heat in the ground than shallower models using either EHC or N as metric for total heat in the climate system. This marked dependence on the depth of the represented subsurface is apparent in a covariance analysis, with high correlation coefficients between the depth of the LSM component and the GHC/N and GHC/EHC estimates (Figure 4.7).

As in the case of the continental subsurface, CMIP5 CGCMs consistently underestimate the observed proportion of heat absorbed by the cryosphere. Both metrics of total heat content in the system yield similar ratios (CHC/N and CHC/EHC), with only one model (the HADGEM2-CC) reaching the 95 % confidence interval from von Schuckmann et al. (2020) (Figure 4.6). This disagreement between observations and CMIP5 simulations is expected given the large differences in the simulated and observed cryosphere heat content (Figure 4.3b). Since CMIP5 CGCMs represent neither ice sheets nor glaciers (Figure 4.4), the partial agreement between the HADGEM2-CC and the observations in the CHC/EHC and CHC/N estimates is likely just the result of the low EHC and N values simulated by this model (Figure 4.3a).

The CMIP5 CGCMs also show similar estimates for the proportion of heat in the atmosphere using both EHC and N metrics. A large proportion of the models achieve AHC/N and AHC/EHC ratios within the 95 % confidence interval from

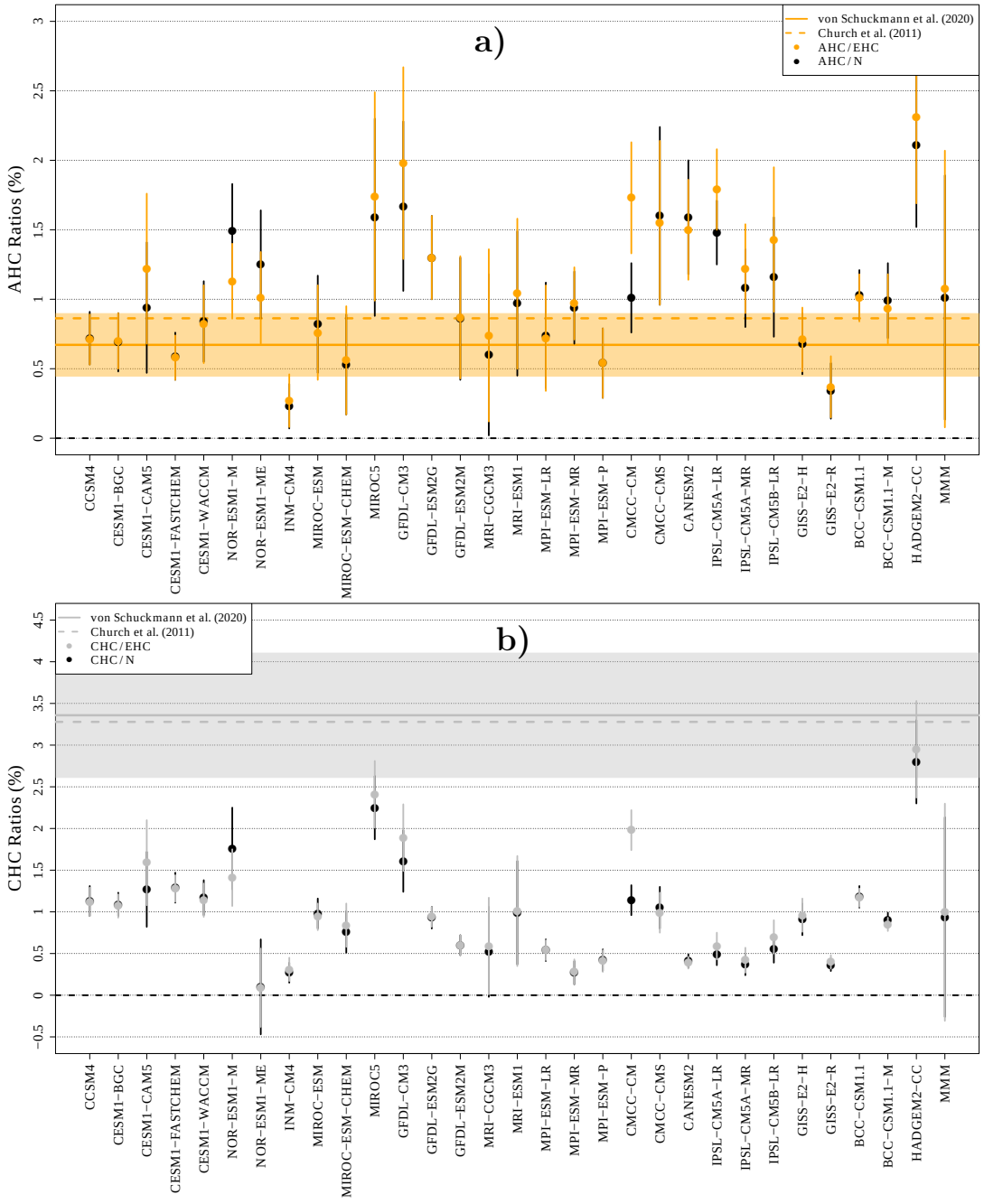

Figure 4.6: (a) Proportion of energy within the atmosphere for the period 1972-2005 CE using EHC (orange dots) and N (black dots) as estimates of total heat content in the climate system. (b) Proportion of energy within the continental subsurface for the period 1972-2005 CE using EHC (light blue dots) and N (black dots) as estimates of total heat content within the climate system. Observations from von Schuckmann et al. (2020) are shown as solid horizontal lines and shadows (means and 95 % confidence intervals), and observations from Church et al. (2011) are displayed as dashed horizontal lines. Multimodel means and 95 % confidence intervals are indicated in the right side of the panels (MMM). Black dashed lines indicate the 0 % value.

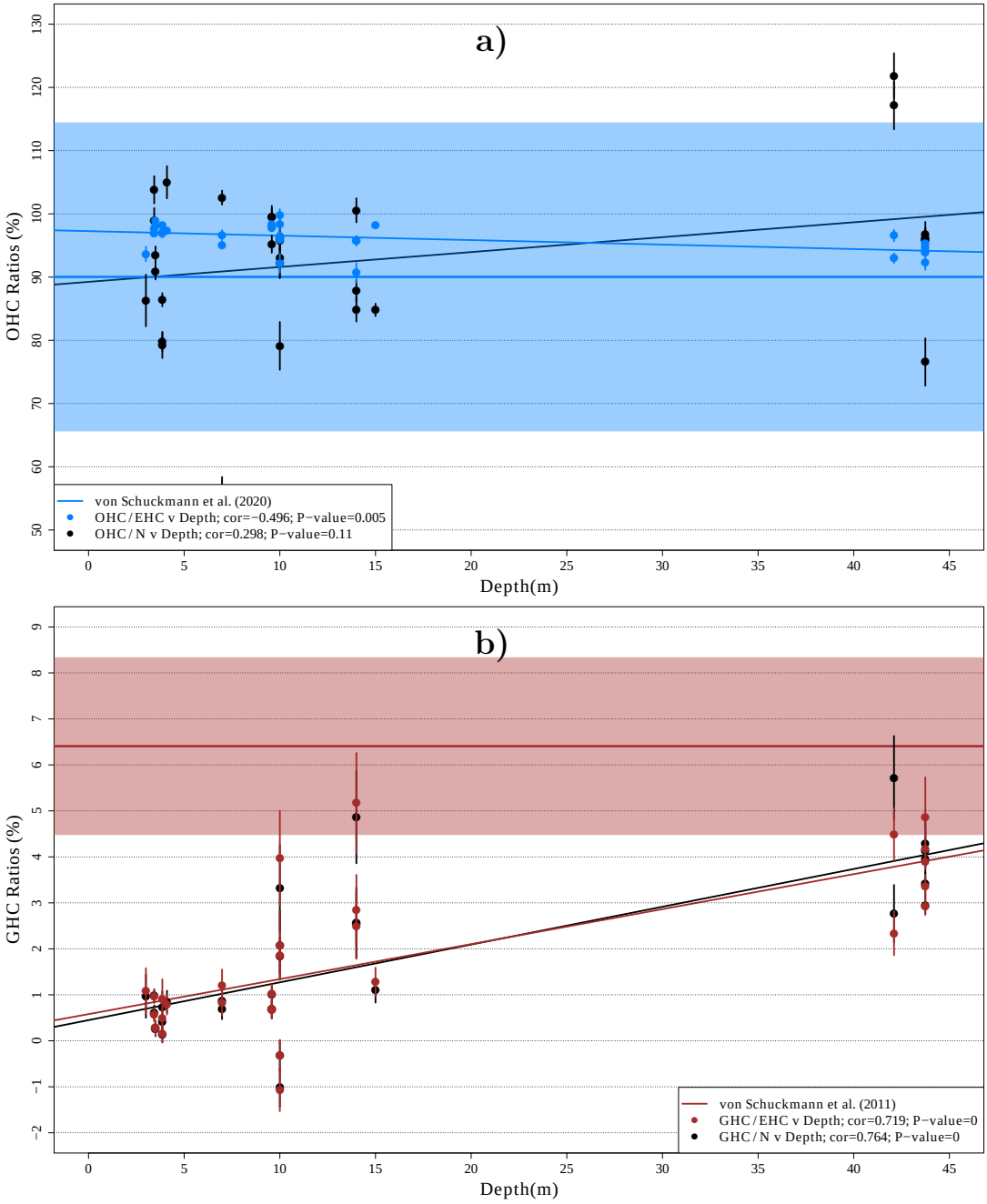

Figure 4.7: (a) Relationship between the proportion of energy within the ocean and the depth of the used LSM component for the period 1972-2005 CE using EHC (blue dots) and N (black dots) as estimates for the total heat content in the climate system. (b) Relationship between the proportion of energy within the continental subsurface and the depth of the used LSM component for the period 1972-2005 CE using EHC (red dots) and N (black dots) as estimates for the total heat content in the climate system. Observations from von Schuckmann et al. (2020) are shown as solid horizontal lines and shadows (means and 95 % confidence intervals).

von Schuckmann et al. (2020), and contain the observational estimates from Church et al. (2011) within the limits of their confidence intervals (Figure 4.6). The ensemble average yields a proportion of heat in the atmosphere of around $1 \pm 1\,\%$, with observations reporting $\sim 1\,\%$ (Church et al., 2011) and $0.7 \pm 0.2\,\%$, which is a reassuring result for the CMIP5 models (von Schuckmann et al., 2020, Table 4.2).

4.4 Discussion

The thirty CMIP5 CGCMs analyzed here simulate markedly different total heat contents within the climate system, independently of the metric for total heat (N, EHC and OHC values in Figure 4.3a), probably because the different response from each model to the common Historical forcing. Forster et al. (2013) assessed the response to the common Historical forcing of a large ensemble of CMIP5 CGCMs in terms of climate sensitivity, feedbacks and adjusted radiative forcings, showing that these models yielded a broad range of responses to the common external forcing. Furthermore, we find that CMIP5 models obtaining high adjusted radiative forcings in the analysis of Forster et al. (2013) also yield large estimates of N, EHC and OHC, which is reasonable since a stronger response to the same forcing should involve a higher radiative imbalance at the top of the atmosphere, and thus a larger heat content in the climate system.

The simulated proportion of heat in the ocean for some models shows markedly different results depending on the used metric for total heat content in the climate system (Figure 4.5a). The different heat partition is caused by the discrepancies between estimates of N and EHC within each CGCM simulation (Figure 4.3a), which are probably related to non-conservation terms in the simulated energy budget by each CGCM as discussed in Hobbs et al. (2016). That is, small numerical inconsistencies, insufficient spin up time, or the amount of water leaving the LSM component at the bottom of the soil column may prevent the conservation of energy in CGCM simulations (Sen Gupta et al., 2013; Hobbs et al., 2016; Séférian et al., 2016; Trenberth et al., 2016). We applied a drift-removal technique to each variable considered in this study in order to minimize the effect of possible non-conservation terms in our results (see Section 4.2). This method has shown good results in previous analyses including

several CMIP5 experiments (Hobbs et al., 2016), although no perfect solution is available and therefore this point requires further investigation.

The low ground heat content achieved by the shallow LSM components (Figure 4.3b) alters the distribution of heat within models, mainly because a higher proportion of heat is stored in the ocean for models with shallower subsurfaces if considering EHC as metric for total heat content. That is, OHC/EHC values show a strong covariance with the depth of the LSM component in the analyzed CMIP5 simulations (Figure 4.7). The shallow depth of the LSM components included in the CMIP5 CGCMs affects the GHC estimates and the obtained GHC/EHC and GHC/N ratios (Figures 4.3b and 4.5b), as the shallow subsurface limits the represented amount of continental heat storage within each simulation (Stevens et al., 2007; MacDougall et al., 2008; Cuesta-Valero et al., 2016; Hermoso de Mendoza et al., 2020). Simulated OHC/N values, nevertheless, do not present such covariance with the depth of the LSM component, nor the simulated proportion of heat in the atmosphere and the cryosphere (Figure 4.8).

The simulated cryosphere heat content is in better agreement with observations when omitting the heat absorbed by ice sheets and glaciers from the assessment (Figure 4.4 and Table 4.2), and the same can be said about the simulated proportion of heat in the cryosphere (Figure 4.9 and Table 4.2). Nevertheless, the observed proportion of heat in the ocean presents different results if considering the whole cryosphere for estimating EHC o if considering only the change in sea ice volume (Figure 4.9 and Table 4.2). Therefore, the representation of the melting of terrestrial ice sheets and glaciers is probably important to improve the simulated EHI and the partition of heat within CGCM simulations. CMIP5 CGCMs currently include modules representing glaciers and ice sheets, but such model components were not activated for generating the CMIP5 simulations analyzed here, probably due to issues with computational resources and technical challenges of coupling the ice sheet grids with the rest of subsystems (Flato et al., 2013). New experiments are planned to assess the ability of the latest generation of CGCMs to reproduce the ice sheets of Greenland and Antarctica within the sixth phase of the Coupled Model Intercomparison Project (CMIP6) (Nowicki et al., 2016), which could be also useful to test if including land ice masses enhances the representation of the Earth heat inventory within CGCM simulations.

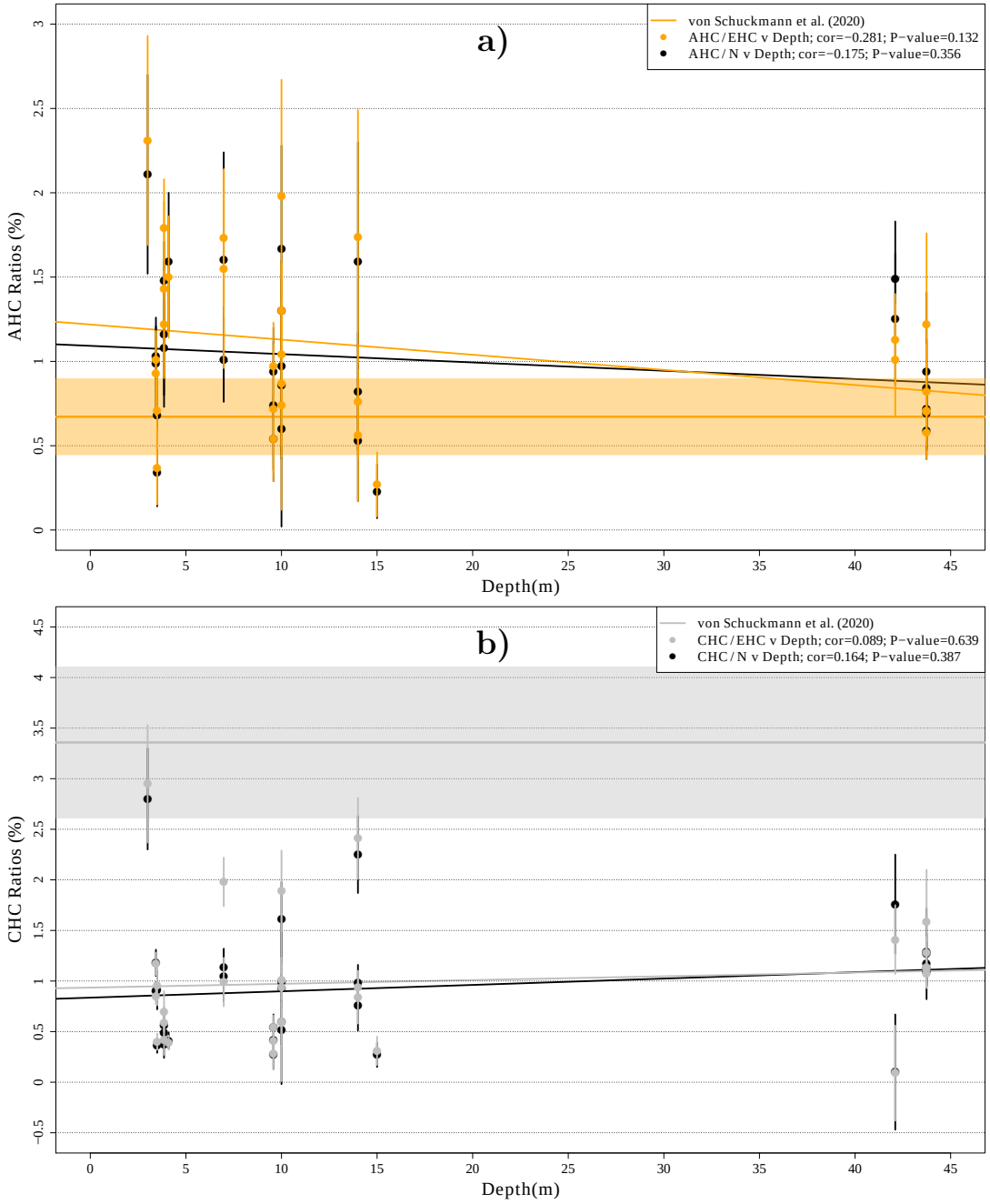

Figure 4.8: (a) Relationship between the proportion of energy within the atmosphere and the depth of the used LSM component for the period 1972-2005 CE using EHC (orange dots) and N (black dots) as estimates for the total heat content in the climate system. (b) Relationship between the proportion of energy within the cryosphere and the depth of the used LSM component for the period 1972-2005 CE using EHC (light blue dots) and N (black dots) as estimates for the total heat content in the climate system. Observations from von Schuckmann et al. (2020) are shown as solid horizontal lines and shadows (means and 95 % confidence intervals).

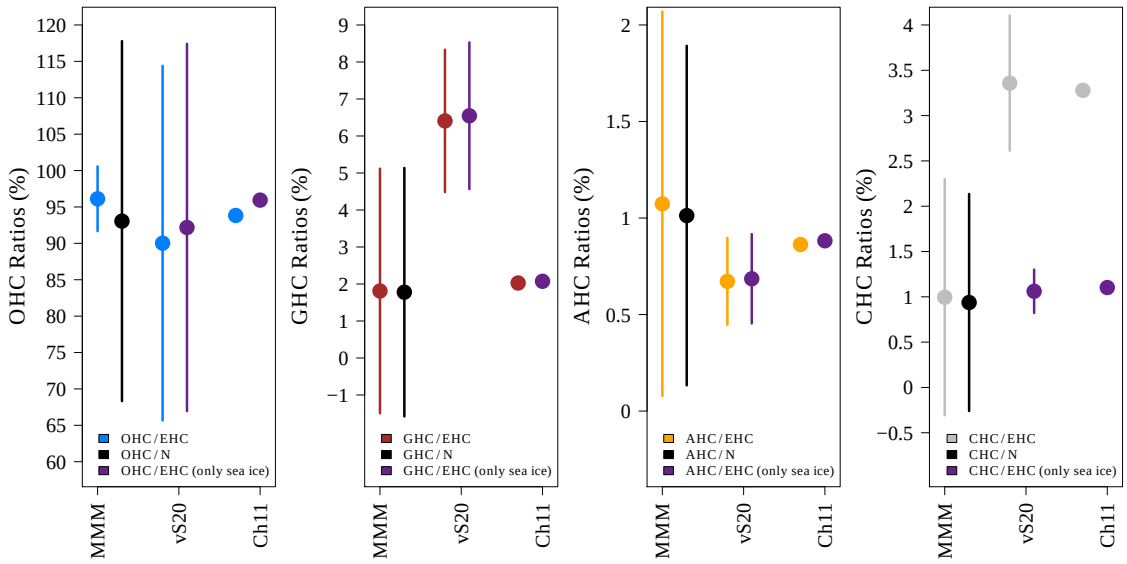

Figure 4.9: Mean and 95 % confidence interval for estimates of the heat partition among climate subsystems from the 30 CMIP5 Historical simulations used here (MMM) and observations from von Schuckmann et al. (2020) (vS20) and Church et al. (2011) (Ch11). Purple dots represent estimates considering only sea ice within the cryosphere.

4.5 Conclusions

The thirty CMIP5 CGCMs analyzed here are not able to reproduce the observed Earth heat inventory due to the different response to the common external forcing of each model, the excessively shallow continental subsurfaces included in the CGCMs, and the lack of an adequate representation of continental ice masses. These last two factors limit the simulated ground heat content and cryosphere heat content, respectively, affecting the partition of heat among climate subsystems. The different response of each CGCM to a common external forcing is probably responsible for the broad range of estimates of ocean heat content, as well as the large spread in the simulated total heat content in the climate system. Evaluating the heat partition avoids the difficulties posed by these different estimates of total heat content, but the missing terms in the simulated energy budget hampers the assessment of the proportion of heat stored in the ocean. Our results suggests that incorporating a representation of glaciers and ice sheets, as well as deeper continental subsurfaces, will probably improve the accuracy of the simulated Earth's heat inventory and the partition of heat

among the different climate components.

4.6 References

Adachi, Y., Yukimoto, S., Deushi, M., Obata, A., Nakano, H., Tanaka, T. Y., Hosaka, M., Sakami, T., Yoshimura, H., Hirabara, M., Shindo, E., Tsujino, H., Mizuta, R., Yabu, S., Koshiro, T., Ose, T., and Kitoh, A. (2013). Basic performance of a new earth system model of the Meteorological Research Institute (MRI-ESM1). *Papers in Meteorology and Geophysics*, **64**, 1–19. DOI: 10.2467/mripapers.64.1.

Allan, R. P., Liu, C., Loeb, N. G., Palmer, M. D., Roberts, M., Smith, D., and Vidale, P.-L. (2014). Changes in global net radiative imbalance 1985–2012. *Geophysical Research Letters*, **41**(15), 5588–5597. DOI: 10.1002/2014GL060962.

Arora, V. K., Scinocca, J. F., Boer, G. J., Christian, J. R., Denman, K. L., Flato, G. M., Kharin, V. V., Lee, W. G., and Merryfield, W. J. (2011). Carbon emission limits required to satisfy future representative concentration pathways of greenhouse gases. *Geophysical Research Letters*, **38**(5). DOI: 10.1029/2010GL046270.

Bhowmick, S. A., Agarwal, N., Ali, M. M., Kishtawal, C. M., and Sharma, R. (2016). Role of ocean heat content in boosting post-monsoon tropical storms over Bay of Bengal during La-Niña events. *Climate Dynamics*, 1–10. DOI: 10.1007/s00382-016-3428-5.

Campbell, B. M., Vermeulen, S. J., Aggarwal, P. K., Corner-Dolloff, C., Girvetz, E., Loboguerrero, A. M., Ramirez-Villegas, J., Rosenstock, T., Sebastian, L., Thornton, P. K., and Wollenberg, E. (2016). Reducing risks to food security from climate change. *Global Food Security*, **11**. 34 –43. DOI: https://doi.org/10.1016/j.gfs.2016.06.002.

Church, J. A., White, N. J., Konikow, L. F., Domingues, C. M., Cogley, J. G., Rignot, E., Gregory, J. M., van den Broeke, M. R., Monaghan, A. J., and Velicogna, I. (2011). Revisiting the Earth's sea-level and energy budgets from

1961 to 2008. *Geophysical Research Letters*, **38**(18). n/a–n/a. DOI: 10.1029/2011GL048794.

Collins, W. J., Bellouin, N., Doutriaux-Boucher, M., Gedney, N., Halloran, P., Hinton, T., Hughes, J., Jones, C. D., Joshi, M., Liddicoat, S., Martin, G., O'Connor, F., Rae, J., Senior, C., Sitch, S., Totterdell, I., Wiltshire, A., and Woodward, S. (2011). Development and evaluation of an Earth-System model – HadGEM2. *Geoscientific Model Development*, **4**(4), 1051–1075. DOI: 10.5194/gmd-4-1051-2011.

Cuesta-Valero, F. J., García-García, A., Beltrami, H., and Smerdon, J. E. (2016). First assessment of continental energy storage in CMIP5 simulations. *Geophysical Research Letters*. n/a–n/a. DOI: 10.1002/2016GL068496.

Donner, L. J., Wyman, B. L., Hemler, R. S., Horowitz, L. W., Ming, Y., Zhao, M., Golaz, J.-C., Ginoux, P., Lin, S. J., Schwarzkopf, M. D., Austin, J., Alaka, G., Cooke, W. F., Delworth, T. L., Freidenreich, S. M., Gordon, C. T., Griffies, S. M., Held, I. M., Hurlin, W. J., Klein, S. A., Knutson, T. R., Langenhorst, A. R., Lee, H.-C., Lin, Y., Magi, B. I., Malyshev, S. L., Milly, P. C. D., Naik, V., Nath, M. J., Pincus, R., Ploshay, J. J., Ramaswamy, V., Seman, C. J., Shevliakova, E., Sirutis, J. J., Stern, W. F., Stouffer, R. J., Wilson, R. J., Winton, M., Wittenberg, A. T., and Zeng, F. (2011). The Dynamical Core, Physical Parameterizations, and Basic Simulation Characteristics of the Atmospheric Component AM3 of the GFDL Global Coupled Model CM3. *Journal of Climate*, **24**(13), 3484–3519. DOI: 10.1175/2011JCLI3955.1.

Dufresne, J.-L., Foujols, M.-A., Denvil, S., Caubel, A., Marti, O., Aumont, O., Balkanski, Y., Bekki, S., Bellenger, H., Benshila, R., Bony, S., Bopp, L., Braconnot, P., Brockmann, P., Cadule, P., Cheruy, F., Codron, F., Cozic, A., Cugnet, D., de Noblet, N., Duvel, J.-P., Ethé, C., Fairhead, L., Fichefet, T., Flavoni, S., Friedlingstein, P., Grandpeix, J.-Y., Guez, L., Guilyardi, E., Hauglustaine, D., Hourdin, F., Idelkadi, A., Ghattas, J., Joussaume, S., Kageyama, M., Krinner, G., Labetoulle, S., Lahellec, A., Lefebvre, M.-P., Lefevre, F., Levy, C., Li, Z., Lloyd, J., Lott, F., Madec, G., Mancip, M., Marchand, M., Masson, S., Meurdesoif, Y., Mignot, J., Musat, I., Parouty, S., Polcher, J., Rio, C., Schulz, M., Swingedouw, D., Szopa, S., Talandier, C., Terray, P., Viovy, N., and Vuichard,

N. (2013). Climate change projections using the IPSL-CM5 Earth System Model: from CMIP3 to CMIP5. English. *Climate Dynamics*, **40**(9-10), 2123–2165. DOI: 10.1007/s00382-012-1636-1.

Dunne, J. P., John, J. G., Adcroft, A. J., Griffies, S. M., Hallberg, R. W., Shevliakova, E., Stouffer, R. J., Cooke, W., Dunne, K. A., Harrison, M. J., Krasting, J. P., Malyshev, S. L., Milly, P. C. D., Phillipps, P. J., Sentman, L. T., Samuels, B. L., Spelman, M. J., Winton, M., Wittenberg, A. T., and Zadeh, N. (2012). GFDL's ESM2 Global Coupled Climate–Carbon Earth System Models. Part I: Physical Formulation and Baseline Simulation Characteristics. *Journal of Climate*, **25**(19), 6646–6665. DOI: 10.1175/JCLI-D-11-00560.1.

Dutton, A., Carlson, A. E., Long, A. J., Milne, G. A., Clark, P. U., DeConto, R., Horton, B. P., Rahmstorf, S., and Raymo, M. E. (2015). Sea-level rise due to polar ice-sheet mass loss during past warm periods. *Science*, **349**(6244). DOI: 10.1126/science.aaa4019.

Dutton, J. A. (2002). *The Ceaseless Wind: An Introduction to the Theory of Atmospheric Motion*. Mineola, New York: Dover Publications.

Ferrari, R., Jansen, M. F., Adkins, J. F., Burke, A., Stewart, A. L., and Thompson, A. F. (2014). Antarctic sea ice control on ocean circulation in present and glacial climates. *Proceedings of the National Academy of Sciences*, **111**(24), 8753–8758. DOI: 10.1073/pnas.1323922111.

Flato, G., Marotzke, J., Abiodun, B., Braconnot, P., Chou, S., Collins, W., Cox, P., Driouech, F., Emori, S., Eyring, V., Forest, C., Gleckler, P., Guilyardi, E., Jakob, C., Kattsov, V., Reason, C., and Rummukainen, M. (2013). "Evaluation of Climate Models". In: *Climate Change 2013: The Physical Science Basis. Contribution of Working Group I to the Fifth Assessment Report of the Intergovernmental Panel on Climate Change*. Ed. by T. Stocker, D. Qin, G.-K. Plattner, M. Tignor, S. Allen, J. Boschung, A. Nauels, Y. Xia, V. Bex, and P. Midgley. Cambridge, United Kingdom and New York, NY, USA: Cambridge University Press. Chap. 9, pp. 741–866. DOI: 10.1017/CBO9781107415324.020.

Forster, P. M., Andrews, T., Good, P., Gregory, J. M., Jackson, L. S., and Zelinka, M. (2013). Evaluating adjusted forcing and model spread for historical and

future scenarios in the CMIP5 generation of climate models. *Journal of Geophysical Research: Atmospheres*, **118**(3), 1139–1150. DOI: 10.1002/jgrd.50174.

Gent, P. R., Danabasoglu, G., Donner, L. J., Holland, M. M., Hunke, E. C., Jayne, S. R., Lawrence, D. M., Neale, R. B., Rasch, P. J., Vertenstein, M., Worley, P. H., Yang, Z.-L., and Zhang, M. (2011). The Community Climate System Model Version 4. *Journal of Climate*, **24**(19), 4973–4991. DOI: 10.1175/2011JCLI4083.1.

Giorgetta, M. A., Jungclaus, J., Reick, C. H., Legutke, S., Bader, J., Böttinger, M., Brovkin, V., Crueger, T., Esch, M., Fieg, K., Glushak, K., Gayler, V., Haak, H., Hollweg, H.-D., Ilyina, T., Kinne, S., Kornblueh, L., Matei, D., Mauritsen, T., Mikolajewicz, U., Mueller, W., Notz, D., Pithan, F., Raddatz, T., Rast, S., Redler, R., Roeckner, E., Schmidt, H., Schnur, R., Segschneider, J., Six, K. D., Stockhause, M., Timmreck, C., Wegner, J., Widmann, H., Wieners, K.-H., Claussen, M., Marotzke, J., and Stevens, B. (2013). Climate and carbon cycle changes from 1850 to 2100 in MPI-ESM simulations for the Coupled Model Intercomparison Project phase 5. *Journal of Advances in Modeling Earth Systems*, **5**(3), 572–597. DOI: 10.1002/jame.20038.

Gleckler, P. J., Durack, P. J., Stouffer, R. J., Johnson, G. C., and Forest, C. E. (2016). Industrial-era global ocean heat uptake doubles in recent decades. *Nature Clim. Change*, **6**(4), 394–398.

Griffies, S. M. (2004). *Fundamentals of Ocean Climate Models*. Princeton, New Jersey: Princeton University Press.

Hanna, E., Navarro, F. J., Pattyn, F., Domingues, C. M., Fettweis, X., Ivins, E. R., Nicholls, R. J., Ritz, C., Smith, B., Tulaczyk, S., Whitehouse, P. L., and Zwally, H. J. (2013). Ice-sheet mass balance and climate change. *Nature*, **498**, 51 EP –.

Hansen, J., Sato, M., Kharecha, P., and Schuckmann, K. v. (2011). Earth's energy imbalance and implications. *Atmospheric Chemistry and Physics*, **11**(24), 13421–13449.

Hegerl, G. C., Black, E., Allan, R. P., Ingram, W. J., Polson, D., Trenberth, K. E., Chadwick, R. S., Arkin, P. A., Sarojini, B. B., Becker, A., Dai, A., Durack, P. J., Easterling, D., Fowler, H. J., Kendon, E. J., Huffman, G. J., Liu, C., Marsh, R., New, M., Osborn, T. J., Skliris, N., Stott, P. A., Vidale, P.-L., Wijffels, S. E., Wilcox, L. J., Willett, K. M., and Zhang, X. (2015). Challenges in Quantifying Changes in the Global Water Cycle. *Bulletin of the American Meteorological Society*, **96**(7), 1097–1115. DOI: 10.1175/BAMS-D-13-00212.1.

Hermoso de Mendoza, I., Beltrami, H., MacDougall, A. H., and Mareschal, J.-C. (2020). Lower boundary conditions in land surface models – effects on the permafrost and the carbon pools: a case study with CLM4.5. *Geoscientific Model Development*, **13**(3), 1663–1683. DOI: 10.5194/gmd-13-1663-2020.

Hicks Pries, C. E., Castanha, C., Porras, R. C., and Torn, M. S. (2017). The whole-soil carbon flux in response to warming. *Science*, **355**(6332), 1420–1423. DOI: 10.1126/science.aal1319.

Hobbs, W., Palmer, M. D., and Monselesan, D. (2016). An Energy Conservation Analysis of Ocean Drift in the CMIP5 Global Coupled Models. *Journal of Climate*, **29**(5), 1639–1653. DOI: 10.1175/JCLI-D-15-0477.1.

Hu, A., Meehl, G. A., Han, W., Yin, J., Wu, B., and Kimoto, M. (2013). Influence of Continental Ice Retreat on Future Global Climate. *Journal of Climate*, **26**(10), 3087–3111. DOI: 10.1175/JCLI-D-12-00102.1.

Hurrell, J. W., Holland, M. M., Gent, P. R., Ghan, S., Kay, J. E., Kushner, P. J., Lamarque, J.-F., Large, W. G., Lawrence, D., Lindsay, K., Lipscomb, W. H., Long, M. C., Mahowald, N., Marsh, D. R., Neale, R. B., Rasch, P., Vavrus, S., Vertenstein, M., Bader, D., Collins, W. D., Hack, J. J., Kiehl, J., and Marshall, S. (2013). The Community Earth System Model: A Framework for Collaborative Research. *Bulletin of the American Meteorological Society*, **94**(9), 1339–1360. DOI: 10.1175/BAMS-D-12-00121.1.

Hurtt, G., Chini, L., Frolking, S., Betts, R., Feddema, J., Fischer, G., Fisk, J., Hibbard, K., Houghton, R., Janetos, A., Jones, C., Kindermann, G., Kinoshita, T., Klein Goldewijk, K., Riahi, K., Shevliakova, E., Smith, S., Stehfest, E., Thomson, A., Thornton, P., van Vuuren, D., and Wang, Y. (2011). Harmo-

nization of land-use scenarios for the period 1500–2100: 600 years of global gridded annual land-use transitions, wood harvest, and resulting secondary lands. English. *Climatic Change*, **109**(1-2), 117–161. DOI: 10.1007/s10584-011-0153-2.

Iversen, T., Bentsen, M., Bethke, I., Debernard, J. B., Kirkevåg, A., Seland, Ø., Drange, H., Kristjansson, J. E., Medhaug, I., Sand, M., and Seierstad, I. A. (2013). The Norwegian Earth System Model, NorESM1-M – Part 2: Climate response and scenario projections. *Geoscientific Model Development*, **6**(2), 389–415. DOI: 10.5194/gmd-6-389-2013.

Jacob, T., Wahr, J., Pfeffer, W. T., and Swenson, S. (2012). Recent contributions of glaciers and ice caps to sea level rise. *Nature*, **482**(7386), 514–518.

Jahn, A. and Holland, M. M. (2013). Implications of Arctic sea ice changes for North Atlantic deep convection and the meridional overturning circulation in CCSM4-CMIP5 simulations. *Geophysical Research Letters*, **40**(6), 1206–1211. DOI: 10.1002/grl.50183.

Jungclaus, J. H., Lohmann, K., and Zanchettin, D. (2014). Enhanced 20th-century heat transfer to the Arctic simulated in the context of climate variations over the last millennium. *Climate of the Past*, **10**(6), 2201–2213. DOI: 10.5194/cp-10-2201-2014.

Koven, C. D., Ringeval, B., Friedlingstein, P., Ciais, P., Cadule, P., Khvorostyanov, D., Krinner, G., and Tarnocai, C. (2011). Permafrost carbon-climate feedbacks accelerate global warming. *Proceedings of the National Academy of Sciences*, **108**(36), 14769–14774. DOI: 10.1073/pnas.1103910108.

Koven, C. D., Riley, W. J., and Stern, A. (2013). Analysis of Permafrost Thermal Dynamics and Response to Climate Change in the CMIP5 Earth System Models. *Journal of Climate*, **26**(6), 1877–1900. DOI: 10.1175/JCLI-D-12-00228.1.

Krakauer, N. Y., Puma, M. J., and Cook, B. I. (2013). Impacts of soil–aquifer heat and water fluxes on simulated global climate. *Hydrology and Earth System Sciences*, **17**(5), 1963–1974. DOI: 10.5194/hess-17-1963-2013.

Kuhlbrodt, T. and Gregory, J. M. (2012). Ocean heat uptake and its consequences for the magnitude of sea level rise and climate change. *Geophysical Research Letters*, **39**(18). DOI: 10.1029/2012GL052952.

Kundzewicz, Z. W., Kanae, S., Seneviratne, S. I., Handmer, J., Nicholls, N., Peduzzi, P., Mechler, R., Bouwer, L. M., Arnell, N., Mach, K., Muir-Wood, R., Brakenridge, G. R., Kron, W., Benito, G., Honda, Y., Takahashi, K., and Sherstyukov, B. (2014). Flood risk and climate change: global and regional perspectives. *Hydrological Sciences Journal*, **59**(1), 1–28. DOI: 10.1080/02626667.2013.857411.

Levitus, S., Antonov, J. I., Boyer, T. P., Baranova, O. K., Garcia, H. E., Locarnini, R. A., Mishonov, A. V., Reagan, J. R., Seidov, D., Yarosh, E. S., and Zweng, M. M. (2012). World ocean heat content and thermosteric sea level change (0–2000 m), 1955–2010. *Geophysical Research Letters*, **39**(10). n/a–n/a. DOI: 10.1029/2012GL051106.

Levy, K., Woster, A. P., Goldstein, R. S., and Carlton, E. J. (2016). Untangling the Impacts of Climate Change on Waterborne Diseases: a Systematic Review of Relationships between Diarrheal Diseases and Temperature, Rainfall, Flooding, and Drought. *Environmental Science & Technology*, **50**(10). 4905–4922. DOI: 10.1021/acs.est.5b06186.

Liepert, B. G. and Lo, F. (2013). CMIP5 update of 'Inter-model variability and biases of the global water cycle in CMIP3 coupled climate models'. *Environmental Research Letters*, **8**(2), 029401.

Lin, I. I., Goni, G. J., Knaff, J. A., Forbes, C., and Ali, M. M. (2013). Ocean heat content for tropical cyclone intensity forecasting and its impact on storm surge. *Natural Hazards*, **66**(3), 1481–1500. DOI: 10.1007/s11069-012-0214-5.

LLNL (2010). *CMIP5 Data Description*. https://pcmdi.llnl.gov/mips/cmip5/docs/standard_output.pdf?id=14 [Last acessed May 2020].

Lloyd, S. J., Kovats, R. S., and Chalabi, Z. (2011). Climate Change, Crop Yields, and Undernutrition: Development of a Model to Quantify the Impact of Cli-

mate Scenarios on Child Undernutrition. *Environmental Health Perspectives*, **119**(12), 1817–1823. DOI: 10.1289/ehp.1003311.

Long, M. C., Lindsay, K., Peacock, S., Moore, J. K., and Doney, S. C. (2013). Twentieth-Century Oceanic Carbon Uptake and Storage in CESM1(BGC)*. *Journal of Climate*, **26**(18), 6775–6800. DOI: 10.1175/JCLI-D-12-00184.1.

MacDougall, A. H., González-Rouco, J. F., Stevens, M. B., and Beltrami, H. (2008). Quantification of subsurface heat storage in a GCM simulation. *Geophysical Research Letters*, **35**(13), n/a–n/a. DOI: 10.1029/2008GL034639.

MacDougall, A. H., Avis, C. A., and Weaver, A. J. (2012). Significant contribution to climate warming from the permafrost carbon feedback. *Nature Geosci*, **5**(10), 719–721. DOI: 10.1038/ngeo1573.

Mainelli, M., DeMaria, M., Shay, L. K., and Goni, G. (2008). Application of Oceanic Heat Content Estimation to Operational Forecasting of Recent Atlantic Category 5 Hurricanes. *Weather and Forecasting*, **23**(1), 3–16. DOI: 10.1175/2007WAF2006111.1.

Marsh, D. R., Mills, M. J., Kinnison, D. E., Lamarque, J.-F., Calvo, N., and Polvani, L. M. (2013). Climate Change from 1850 to 2005 Simulated in CESM1(WACCM). *Journal of Climate*, **26**(19), 7372–7391. DOI: 10.1175/JCLI-D-12-00558.1.

Matthews, T. K. R., Wilby, R. L., and Murphy, C. (2017). Communicating the deadly consequences of global warming for human heat stress. *Proceedings of the National Academy of Sciences*, **114**(15), 3861–3866. DOI: 10.1073/pnas.1617526114.

McDougall, T. J. (2003). Potential Enthalpy: A Conservative Oceanic Variable for Evaluating Heat Content and Heat Fluxes. *Journal of Physical Oceanography*, **33**(5), 945–963. DOI: 10.1175/1520-0485(2003)033<0945:PEACOV>2.0.CO;2.

McDougall, T. J., Jackett, D. R., Wright, D. G., and Feistel, R. (2003). Accurate and Computationally Efficient Algorithms for Potential Temperature and Density of Seawater. *Journal of Atmospheric and Oceanic Technology*, **20**(5), 730–741. DOI: 10.1175/1520-0426(2003)20<730:AACEAF>2.0.CO;2.

McGranahan, G., Balk, D., and Anderson, B. (2007). The rising tide: assessing the risks of climate change and human settlements in low elevation coastal zones. *Environment and Urbanization*, **19**(1), 17–37. DOI: 10.1177/0956247807076960.

McMichael, A. J., Woodruff, R. E., and Hales, S. (2006). Climate change and human health: present and future risks. *The Lancet*, **367**(9513), 859 –869. DOI: https://doi.org/10.1016/S0140-6736(06)68079-3.

McPherson, M., García-García, A., Cuesta-Valero, F. J., Beltrami, H., Hansen-Ketchum, P., MacDougall, D., and Ogden, N. H. (2017). Expansion of the Lyme Disease Vector Ixodes Scapularis in Canada Inferred from CMIP5 Climate Projections. *Environmental Health Perspectives*, **125**(5), 057008. DOI: 10.1289/EHP57.

Meehl, G. A., Washington, W. M., Arblaster, J. M., Hu, A., Teng, H., Kay, J. E., Gettelman, A., Lawrence, D. M., Sanderson, B. M., and Strand, W. G. (2013). Climate Change Projections in CESM1(CAM5) Compared to CCSM4. *Journal of Climate*, **26**(17), 6287–6308. DOI: 10.1175/JCLI-D-12-00572.1.

Mieville, A., Granier, C., Liousse, C., Guillaume, B., Mouillot, F., Lamarque, J.-F., Grégoire, J.-M., and Pétron, G. (2010). Emissions of gases and particles from biomass burning during the 20th century using satellite data and an historical reconstruction. *Atmospheric Environment*, **44**(11), 1469 –1477. DOI: http://dx.doi.org/10.1016/j.atmosenv.2010.01.011.

Miller, R. L., Schmidt, G. A., Nazarenko, L. S., Tausnev, N., Bauer, S. E., DelGenio, A. D., Kelley, M., Lo, K. K., Ruedy, R., Shindell, D. T., Aleinov, I., Bauer, M., Bleck, R., Canuto, V., Chen, Y., Cheng, Y., Clune, T. L., Faluvegi, G., Hansen, J. E., Healy, R. J., Kiang, N. Y., Koch, D., Lacis, A. A., LeGrande, A. N., Lerner, J., Menon, S., Oinas, V., Pérez García-Pando, C., Perlwitz, J. P., Puma, M. J., Rind, D., Romanou, A., Russell, G. L., Sato, M., Sun, S., Tsigaridis, K., Unger, N., Voulgarakis, A., Yao, M.-S., and Zhang, J. (2014). CMIP5 historical simulations (1850–2012) with GISS ModelE2. *Journal of Advances in Modeling Earth Systems*, **6**(2), 441–477. DOI: 10.1002/2013MS000266.

Nowicki, S. M. J., Payne, A., Larour, E., Seroussi, H., Goelzer, H., Lipscomb, W., Gregory, J., Abe-Ouchi, A., and Shepherd, A. (2016). Ice Sheet Model Intercomparison Project (ISMIP6) contribution to CMIP6. *Geoscientific Model Development*, **9**(12), 4521–4545. DOI: 10.5194/gmd-9-4521-2016.

Oleson, K. W., Lawrence, D. M., Bonan, G. B., Flanner, E. K., Lawrence, P. J., Levis, S, Swenson, S. C., Thornton, P. E., Dai, A, Decker, M, Dickinson, R, Feddema, J, Heald, C. L., Hoffman, F, Lamarque, J.-F., Mahowald, N, Niu, G.-Y., Qian, T, Randerson, J, Running, S, Sakaguchi, K, Slater, A, Stockli, R, Wang, A, Yang, Z.-L., Zeng, X., and Zeng, X. (2010). *Technical description of version 4.0 of the Community Land Model (CLM)*. Tech. rep. NCAR Technical Note NCAR/TN-478+STR. National Center for Atmospheric Research, Boulder, CO.

Palmer, M. D. and McNeall, D. J. (2014). Internal variability of Earth's energy budget simulated by CMIP5 climate models. *Environmental Research Letters*, **9**(3), 034016.

Palmer, M. D., McNeall, D. J., and Dunstone, N. J. (2011). Importance of the deep ocean for estimating decadal changes in Earth's radiation balance. *Geophysical Research Letters*, **38**(13). n/a–n/a. DOI: 10.1029/2011GL047835.

Pan, Y., Li, L., Jiang, X., Li, G., Zhang, W., Wang, X., and Ingersoll, A. P. (2017). Earth's changing global atmospheric energy cycle in response to climate change. *Nature Communications*, **8**, 14367 EP –.

Patz, J. A., Gibbs, H. K., Foley, J. A., Rogers, J. V., and Smith, K. R. (2007). Climate Change and Global Health: Quantifying a Growing Ethical Crisis. *EcoHealth*, **4**(4), 397–405. DOI: 10.1007/s10393-007-0141-1.

Pendergrass, A. G. and Hartmann, D. L. (2014a). Changes in the Distribution of Rain Frequency and Intensity in Response to Global Warming. *Journal of Climate*, **27**(22), 8372–8383. DOI: 10.1175/JCLI-D-14-00183.1.

— (2014b). The Atmospheric Energy Constraint on Global-Mean Precipitation Change. *Journal of Climate*, **27**(2), 757–768. DOI: 10.1175/JCLI-D-13-00163.1.

Phalkey, R. K., Aranda-Jan, C., Marx, S., Höfle, B., and Sauerborn, R. (2015). Systematic review of current efforts to quantify the impacts of climate change on undernutrition. *Proceedings of the National Academy of Sciences*, **112**(33), E4522–E4529. DOI: 10.1073/pnas.1409769112.

Previdi, M., Smith, K. L., and Polvani, L. M. (2015). How Well Do the CMIP5 Models Simulate the Antarctic Atmospheric Energy Budget? *Journal of Climate*, **28**(20), 7933–7942. DOI: 10.1175/JCLI-D-15-0027.1.

Rhein, M., Rintoul, S., Aoki, S., Campos, E., Chambers, D., Feely, R., Gulev, S., Johnson, G., Josey, S., Kostianoy, A., Mauritzen, C., Roemmich, D., Talley, L., and Wang, F. (2013). "Observations: Ocean". In: *Climate Change 2013: The Physical Science Basis. Contribution of Working Group I to the Fifth Assessment Report of the Intergovernmental Panel on Climate Change*. Ed. by T. Stocker, D. Qin, G.-K. Plattner, M. Tignor, S. Allen, J. Boschung, A. Nauels, Y. Xia, V. Bex, and P. Midgley. Cambridge, United Kingdom and New York, NY, USA: Cambridge University Press. Chap. 3, pp. 255–316. DOI: 10.1017/CBO9781107415324.010.

Rosenzweig, C., Elliott, J., Deryng, D., Ruane, A. C., Müller, C., Arneth, A., Boote, K. J., Folberth, C., Glotter, M., Khabarov, N., Neumann, K., Piontek, F., Pugh, T. A. M., Schmid, E., Stehfest, E., Yang, H., and Jones, J. W. (2014). Assessing agricultural risks of climate change in the 21st century in a global gridded crop model intercomparison. *Proceedings of the National Academy of Sciences*, **111**(9), 3268–3273. DOI: 10.1073/pnas.1222463110.

Schädel, C., Schuur, E. A. G., Bracho, R., Elberling, B., Knoblauch, C., Lee, H., Luo, Y., Shaver, G. R., and Turetsky, M. R. (2014). Circumpolar assessment of permafrost C quality and its vulnerability over time using long-term incubation data. *Global Change Biology*, **20**(2), 641–652. DOI: 10.1111/gcb.12417.

Schuur, E. A. G., McGuire, A. D., Schadel, C., Grosse, G., Harden, J. W., Hayes, D. J., Hugelius, G., Koven, C. D., Kuhry, P., Lawrence, D. M., Natali, S. M., Olefeldt, D., Romanovsky, V. E., Schaefer, K., Turetsky, M. R., Treat, C. C., and Vonk, J. E. (2015). Climate change and the permafrost carbon feedback. *Nature*, **520**(7546), 171–179. DOI: 10.1038/nature14338.

Scoccimarro, E., Gualdi, S., Bellucci, A., Sanna, A., Giuseppe Fogli, P., Manzini, E., Vichi, M., Oddo, P., and Navarra, A. (2011). Effects of Tropical Cyclones on Ocean Heat Transport in a High-Resolution Coupled General Circulation Model. *Journal of Climate*, **24**(16), 4368–4384. DOI: 10.1175/2011JCLI4104.1.

Séférian, R., Gehlen, M., Bopp, L., Resplandy, L., Orr, J. C., Marti, O., Dunne, J. P., Christian, J. R., Doney, S. C., Ilyina, T., Lindsay, K., Halloran, P. R., Heinze, C., Segschneider, J., Tjiputra, J., Aumont, O., and Romanou, A. (2016). Inconsistent strategies to spin up models in CMIP5: implications for ocean biogeochemical model performance assessment. *Geoscientific Model Development*, **9**(5), 1827–1851. DOI: 10.5194/gmd-9-1827-2016.

Sen Gupta, A., Jourdain, N. C., Brown, J. N., and Monselesan, D. (2013). Climate Drift in the CMIP5 Models. *Journal of Climate*, **26**(21), 8597–8615. DOI: 10.1175/JCLI-D-12-00521.1.

Sherwood, S. C. and Huber, M. (2010). An adaptability limit to climate change due to heat stress. *Proceedings of the National Academy of Sciences*, **107**(21), 9552–9555. DOI: 10.1073/pnas.0913352107.

Smith, D. M., Allan, R. P., Coward, A. C., Eade, R., Hyder, P., Liu, C., Loeb, N. G., Palmer, M. D., Roberts, C. D., and Scaife, A. A. (2015). Earth's energy imbalance since 1960 in observations and CMIP5 models. *Geophysical Research Letters*, **42**(4), 1205–1213. DOI: 10.1002/2014GL062669.

Smith, R, Jones, P, Briegleb, B, Bryan, F, Danabasoglu, G, Dennis, J, Dukowicz, J, Eden, C, Fox-Kemper, B, Gent, P, Hecht, M, Jayne, S, Jochum, M, Large, W, Lindsay, K, Maltrud, M, Norton, N, Peacock, S, Vertenstein, M, and Yeager, S (2010). *The Parallel Ocean Program (POP) Reference Manual. Ocean Component of the Community Climate System Model (CCSM) and Community Earth System Model (CESM)*. Tech. rep. LAUR-01853. National Center for Atmospheric Research, Boulder, CO, p. 141.

Soong, J. L., Phillips, C. L., Ledna, C., Koven, C. D., and Torn, M. S. (2020). CMIP5 Models Predict Rapid and Deep Soil Warming Over the 21st Century.

Journal of Geophysical Research: Biogeosciences, **125**(2). e2019JG005266. DOI: 10.1029/2019JG005266.

Stevens, M. B., Smerdon, J. E., González-Rouco, J. F., Stieglitz, M., and Beltrami, H. (2007). Effects of bottom boundary placement on subsurface heat storage: Implications for climate model simulations. *Geophysical Research Letters*, **34**(2). n/a–n/a. DOI: 10.1029/2006GL028546.

Taylor, K. E., Stouffer, R. J., and Meehl, G. A. (2011). An Overview of CMIP5 and the Experiment Design. *Bulletin of the American Meteorological Society*, **93**(4), 485–498. DOI: 10.1175/BAMS-D-11-00094.1.

Tjiputra, J. F., Roelandt, C., Bentsen, M., Lawrence, D. M., Lorentzen, T., Schwinger, J., Seland, Ø., and Heinze, C. (2013). Evaluation of the carbon cycle components in the Norwegian Earth System Model (NorESM). *Geoscientific Model Development*, **6**(2), 301–325. DOI: 10.5194/gmd-6-301-2013.

Trenberth, K. E. (1997). Using Atmospheric Budgets as a Constraint on Surface Fluxes. *Journal of Climate*, **10**(11), 2796–2809. DOI: 10.1175/1520-0442(1997)010<2796:UABAAC>2.0.CO;2.

Trenberth, K. E., Fasullo, J. T., and Balmaseda, M. A. (2014). Earth's Energy Imbalance. *Journal of Climate*, **27**(9), 3129–3144. DOI: 10.1175/JCLI-D-13-00294.1.

Trenberth, K. E., Fasullo, J. T., von Schuckmann, K., and Cheng, L. (2016). Insights into Earth's Energy Imbalance from Multiple Sources. *Journal of Climate*, **29**(20), 7495–7505. DOI: 10.1175/JCLI-D-16-0339.1.

Trenberth, K. E., Cheng, L., Jacobs, P., Zhang, Y., and Fasullo, J. (2018). Hurricane Harvey Links to Ocean Heat Content and Climate Change Adaptation. *Earth's Future*, **6**(5), 730–744. DOI: 10.1029/2018EF000825.

Van Wijk, W. R., Borghrst, A. J. W., Businger, J. A., Derksen, W. J., Schmidt, F. H., Scholte Ubing, D. W., and De Vries, D. A. (1963). *Physics of Plant Environment*. North-Holland Publishing Company - Amsterdam.

Vaughan, D., Comiso, J., Allison, I., Carrasco, J., Kaser, G., Kwok, R., Mote, P., Murray, T., Paul, F., Ren, J., Rignot, E., Solomina, O., Steffen, K., and Zhang, T.

(2013). “Observations: Cryosphere”. In: *Climate Change 2013: The Physical Science Basis. Contribution of Working Group I to the Fifth Assessment Report of the Intergovernmental Panel on Climate Change*. Ed. by T. Stocker, D. Qin, G.-K. Plattner, M. Tignor, S. Allen, J. Boschung, A. Nauels, Y. Xia, V. Bex, and P. Midgley. Cambridge, United Kingdom and New York, NY, USA: Cambridge University Press. Chap. 4, pp. 317–382. DOI: 10.1017/CBO9781107415324.012.

Volodin, E., Dianskii, N., and Gusev, A. (2010). Simulating present-day climate with the INMCM4.0 coupled model of the atmospheric and oceanic general circulations. English. *Izvestiya, Atmospheric and Oceanic Physics*, **46**(4), 414–431. DOI: 10.1134/S000143381004002X.

Von Schuckmann, K., Palmer, M. D., Trenberth, K. E., Cazenave, A., Chambers, D., Champollion, N., Hansen, J., Josey, S. A., Loeb, N., Mathieu, P. P., Meyssignac, B., and Wild, M. (2016). An imperative to monitor Earth’s energy imbalance. *Nature Climate Change*, **6**, 138 EP –.

Von Schuckmann, K., Cheng, L., Palmer, M. D., Hansen, J., Tassone, C., Aich, V., Adusumilli, S., Beltrami, H., Boyer, T., Cuesta-Valero, F. J., Desbruyères, D., Domingues, C., García-García, A., Gentine, P., Gilson, J., Gorfer, M., Haimberger, L., Ishii, M., Johnson, G. C., Killick, R., King, B. A., Kirchengast, G., Kolodziejczyk, N., Lyman, J., Marzeion, B., Mayer, M., Monier, M., Monselesan, D. P., Purkey, S., Roemmich, D., Schweiger, A., Seneviratne, S. I., Shepherd, A., Slater, D. A., Steiner, A. K., Straneo, F., Timmermans, M.-L., and Wijffels, S. E. (2020). Heat stored in the Earth system: where does the energy go? *Earth System Science Data*, **12**(3), 2013–2041. DOI: 10.5194/essd-12-2013-2020.

Wada, A. and Chan, J. C. L. (2008). Relationship between typhoon activity and upper ocean heat content. *Geophysical Research Letters*, **35**(17). DOI: 10.1029/2008GL035129.

Watanabe, M., Suzuki, T., O’ishi, R., Komuro, Y., Watanabe, S., Emori, S., Takemura, T., Chikira, M., Ogura, T., Sekiguchi, M., Takata, K., Yamazaki, D., Yokohata, T., Nozawa, T., Hasumi, H., Tatebe, H., and Kimoto, M. (2010). Improved Climate Simulation by MIROC5: Mean States, Variability, and

Climate Sensitivity. *Journal of Climate*, **23**(23), 6312–6335. DOI: 10.1175/2010JCLI3679.1.

Watanabe, S., Hajima, T., Sudo, K., Nagashima, T., Takemura, T., Okajima, H., Nozawa, T., Kawase, H., Abe, M., Yokohata, T., Ise, T., Sato, H., Kato, E., Takata, K., Emori, S., and Kawamiya, M. (2011). MIROC-ESM 2010: model description and basic results of CMIP5-20c3m experiments. *Geoscientific Model Development*, **4**(4), 845–872. DOI: 10.5194/gmd-4-845-2011.

Wu, T., Song, L., Li, W., Wang, Z., Zhang, H., Xin, X., Zhang, Y., Zhang, L., Li, J., Wu, F., Liu, Y., Zhang, F., Shi, X., Chu, M., Zhang, J., Fang, Y., Wang, F., Lu, Y., Liu, X., Wei, M., Liu, Q., Zhou, W., Dong, M., Zhao, Q., Ji, J., Li, L., and Zhou, M. (2014). An overview of BCC climate system model development and application for climate change studies. English. *Journal of Meteorological Research*, **28**(1), 34–56. DOI: 10.1007/s13351-014-3041-7.

Wu, X., Lu, Y., Zhou, S., Chen, L., and Xu, B. (2016). Impact of climate change on human infectious diseases: Empirical evidence and human adaptation. *Environment International*, **86**, 14 –23. DOI: https://doi.org/10.1016/j.envint.2015.09.007.

Yukimoto, S., Adachi, Y., Hosaka, M., Sakami, T., Yoshimura, H., Hirabara, M., Tanaka, T. Y., Shindo, E., Tsujino, H., Deushi, M., Mizuta, R., Yabu, S., Obata, A., Nakano, H., Koshiro, T., Ose, T., and Kitoh, A. (2012). A New Global Climate Model of the Meteorological Research Institute: MRI-CGCM; -Model Description and Basic Performance-. *Journal of the Meteorological Society of Japan. Ser. II*, **90A**, 23–64. DOI: 10.2151/jmsj.2012-A02.

5 General Conclusions

5.1 Summary

Determining the magnitude of the Earth's radiative imbalance at the top of the atmosphere is fundamental to understand the evolution of climate change. Such imbalance is the result of alterations in the climate system –both natural an anthropogenic, causing a disturbance in heat exchanges between the different climate subsystems until a new equilibrium state is reached. These changes are called forcings, and typically involve changes in shortwave and longwave radiative fluxes that can be measured at the top of the atmosphere. Direct observations of the shortwave and longwave radiative fluxes using satellite data allow to estimate the Earth's radiative imbalance as the difference between the incoming and outgoing radiative fluxes. However, this method yields large uncertainties, since the radiative imbalance is small in comparison with the observed fluxes, thus an indirect approach is required to characterize the imbalance. An observable effect of this radiative imbalance at the top of the atmosphere is the storage of heat within the ocean, the atmosphere, the cryosphere and the continental subsurface. Nevertheless, quantifying the magnitude of heat storage within the climate system with a reasonable degree of accuracy has been challenging and only possible since the early 2000s. The main issue is the scarcity of observations, beacause estimates of the Earth Heat Inventory (EHI) require the characterization of several magnitudes at a global scale, which are hard to measure. Additionally, the evolution of the EHI before the Industrial Revolution is poorly known, hampering the assessment of its long-term variability. Climate simulations performed by advanced atmosphere-ocean Coupled General Circulation Models (CGCMs) have been used to fill the temporal gap in estimates of

heat storage and transport between climate subsystems obtaining mixed results. This thesis contributes to the understanding of the EHI from both observational and modeling perspectives.

Chapter 2 in this dissertation introduces a preindustrial, long-term surface temperature climatology (the Long-term Surface Temperature database, LoST) for the period ~1300-1700 Common Era (CE) over North America based on Borehole Temperature Profile (BTP) measurements. The magnitude and spatial pattern of the retrieved temperature climatology is consistent with features present in meteorological observations, which is a reassuring result. The LoST climatology is also used to assess an ensemble of preindustrial simulations from the fifth phase of the Coupled Model Intercomparison Project (CMIP5) project, the same simulations that informed the fifth Assessment Report of the Intergovernmental Panel on Climate Change (IPCC-AR5). Part of the CGCM simulations agree with the LoST temperatures, although these models were not tuned to match this climatology. Nevertheless, the rest of the models achieve poor climatologies in comparison with the LoST database, probably due to an excessively strong coupling between near-surface atmospheric and subsurface temperatures over North America.

New estimates of global surface temperature evolution and Ground Heat Content (GHC) for the period 1600-2018 CE based on BTP data are presented in this dissertation (Chapter 3). The retrieved surface temperatures histories are in agreement with meteorological observations both globally and using only BTP locations, which suggests that the density and distribution of BTP measurements is enough to represent long-term global conditions. The obtained surface temperatures, nevertheless, are slightly higher than previous BTP reconstructions, while the obtained GHC values are markedly higher than previous estimates for the second half of the 20^{th} century. This is mainly caused by the number of new borehole temperature profiles used in this dissertation in comparison with previous studies, which results in a better description of the subsurface warming since the 1980s. The new temperature and flux histories provided here also include a more comprehensive estimate of uncertainties comparing with previous BTP reconstructions.

The estimates of GHC presented in Chapter 3 are used to assess the ability of an ensemble of CMIP5 CGCM simulations to reproduce the observed Earth heat

inventory for the last decades of the 20^{th} century (Chapter 4). CMIP5 models underestimate the observed continental heat storage in agreement with previous results, particularly after considering the new GHC estimates from BTP measurements presented in this dissertation. The model ensemble also overestimates the observed ocean heat content, while reaching reasonable values for atmosphere heat content and Cryosphere Heat Content (CHC) in comparison with observations. Nevertheless, the CMIP5 ensemble reaches high inter-model spread, particularly for the estimates of ocean heat content and total heat storage in the system. Such spread in the simulated total heat content may be associated with the broad range of responses to the common external forcing achieved by CMIP5 models.

5.2 Significance

The simulated response of CMIP5 CGCMs to the same prescribed forcings has shown a large inter-model spread, resulting in large uncertainties in the projected evolution of climate change. This different response is caused by several factors, mainly the parameterization of processes that cannot be resolved in the models, tuning practices, and the spread in the simulated climatologies. Temperature climatologies affect the representation of feedback processes depending on absolute temperatures, such as ice-albedo and water vapor feedbacks, which determine the model response to the external forcing. The LoST temperature database (Chapter 2) is the first observational reference available to constrain the climatology in preindustrial CGCM simulations. Assessing the climatology in Preindustrial Control (piControl) simulations should improve the represented processes depending on absolute temperature in transient climate simulations started from the piControl experiment, reducing the uncertainties in the response of the models to the external forcing. Another physical magnitude determined by the surface temperature climatology is the permafrost extension, that is, the extension of soil perennially frozen. Permafrost stability is important to project the evolution of climate change since permafrost soils contain large amounts of organic matter, which could be released into the atmosphere as greenhouse gases if permafrost thaws. The permafrost extension in North America can be derived from the LoST database just by evaluating the area with

temperatures below 0 °C, providing an additional observational estimate in a field with limited observations due to the large areas to be sampled.

Estimating the long-term evolution of the climate system is fundamental to understand the internal variability of the climate system, as well as to detect and attribute the role of anthropogenic activities in climate change. Also, the Paris Agreement, reached during the 21st Conference of the Parties (COP21) in 2015, declared the establishment of an international common target to limit the increase in global surface temperature, aiming to keep the temperature change relative to preindustrial conditions below 2 °C. Nevertheless, the determination of preindustrial temperatures is a complex challenge that requires of paleoreconstruction techniques in order to be achieved. Borehole temperature profiles present a unique ability to integrate multi-centennial changes in surface temperature, deeming borehole measurements an important source of information about preindustrial conditions. Indeed, surface temperature reconstructions in Chapter 3 suggest a global temperature increase of 0.7 °C since 1300-1700 CE, in agreement with other studies using proxy reconstructions and paleosimulations.

Another fundamental magnitude to quantify the EHI estimated from BTP measurements is continental heat storage. The radiative imbalance at the top of the atmosphere causes an increase in the amount of heat stored within the oceans, the atmosphere, the cryosphere and the continental subsurface. The partition of heat within each climate subsystem is of crucial importance to project future climate change, since alterations in the heat content of each subsystem affects the dynamics of associated physical phenomena. For example, sea level rise is related to the heat absorbed by the cryosphere and the ocean, permafrost thawing is related to the continental heat storage, and extreme precipitation events are related to the atmosphere heat content. Reconstructions from borehole temperature profiles are the only source of information about ground heat content. Changes in continental heat storage obtained in this dissertation (Chapter 3) are higher than the values previously reported for the period 1950-2000 CE. This means that the proportion of heat storage in the continental subsurface raises from 2 % to 6 % of the total heat content in the climate system, the second largest term only after the ocean (90 %).

Climate simulations performed by CGCMs have greatly advanced our knowledge about the Earth system, contributing to the understanding of large scale

processes such as the heat distribution within the atmosphere and the ocean as well as the evolution of the global carbon cycle. Projections of future climate change are a type of simulations particularly important, as these tools are essential to inform decisions about climate change mitigation and adaptation, and to understand the possible risks to society and ecosystems. Nevertheless, these climate projections present large uncertainties due to several limitations in climate models, including structural differences among models, sensitivity to initial conditions, the use of parameterizations to represent certain processes, and tuning practices. Model tuning is particularly important for evaluating climate simulations, because model calibration reduces the available climate variables that can be used to check the realism of models. Assessment of observed magnitudes that are not considered in tuning practices, such as the EHI, are therefore critical to gain confidence in projections of future climate change performed by CGCMs, as well as to identify potential sources of uncertainty in climate simulations. Despite the continuous efforts of the modelling community to create CGCMs as realistic as possible, advanced models contributing to the CMIP5 project still present problems to reproduce the observed Earth heat inventory (Chapter 4). Therefore, CGCM issues affecting the simulation of these key aspects of physical climate should be corrected in future versions of climate models to reduce the large uncertainties in the projected evolution of climate change, as well as to improve the representation of heat-dependent processes within climate models, such as sea level rise, permafrost thawing or the water vapor feedback, among others.

5.3 Future Work

The LoST database has been useful to assess the preindustrial surface temperature climatology over North America within CGCM simulations. This dataset can be expanded to estimate a long-term global land surface temperature climatology by applying the methodology developed in Chapter 2 to the entire borehole network (Figure 3.1). Thereby, the assessment of CGCM simulations would be more comprehensive, allowing both global and regional evaluations. Temperature climatologies for other periods of time can also be derived, although the number of suitable borehole temperature profiles is reduced. This is because

estimating temperature climatologies for past periods of time requires deeper profiles, and there are fewer deep profiles than shallow profiles in the global borehole database.

The global network of borehole temperature profiles has been used in this dissertation to reconstruct the continental heat storage for the last four centuries. Although this estimate constitutes the most recent estimate of the land component of the Earth heat inventory, additional sources of information are desirable in order to gain confidence in the magnitude an evolution of the retrieved ground heat content. Fortunately, new surface heat flux measurements using other observational techniques have been made available recently as an outcome of the FluxNet project. The FluxNet project (Baldocchi et al., 2001) consists in a global network of micrometeorological flux measurements that includes observations of surface heat flux. Therefore, an interesting continuation of Chapter 3 would be to reconcile estimates of continental heat storage from both the global borehole network and from the FluxNet database. A collaboration of scientists, in which I am participating, is currently comparing surface heat fluxes estimates from both datasets and an advanced Land Surface Model (LSM) component used by several CGCMs, displaying promising preliminary results (Gentine et al., 2019).

Both LoST temperatures and continental heat storage estimates from BTPs have been used to assess piControl, Past Millennium (PM) and Historical simulations from the CMIP5 archive. During the time for completing this dissertation, nevertheless, a new generation of models and climate experiments have been performed, the sixth phase of the Coupled Model Intercomparison Project (CMIP6). Therefore, an important continuation of the work performed here would be to repeat the assessment of the EHI using CMIP6 simulations, and to compare the results with those for CMIP5 models. Thereby, we could be able to identify improvements and persistent caveats in the new generation of CGCMs, and the experiments performed for the first time within the CMIP6 project will allow to explore other questions. For example, nine new future scenarios named Shared Socioeconomic Pathways (SSPs) would be available to investigate climate evolution under plausible developments of socio-economic conditions. These experiments can be used to determine if the simulated EHI depends on the concentration of greenhouse gases, or if the partition of heat among climate subsystems remains constant with time.

Results in Chapter 4 and the literature have shown that the represented EHI in CMIP5 simulations is affected by the depth of the used LSM component in each coupled general circulation model. Shallow LSM components reduce the subsurface volume available for storing heat, and represent higher soil temperatures at shallow depths than models including sufficiently deep subsurfaces. Thereby, other energy dependent processes occurring in the ground depend on the depth of the LSM component, such as permafrost extension and evolution. Nevertheless, the role of the subsurface's depth has not been assessed in other processes relevant for projecting future climate change. Therefore, I propose to investigate whether soil respiration in climate simulations is affected by the depth of the represented subsurface in LSM components. CGCMs represent continental heat storage and soil respiration as a function of the simulated soil water content and soil temperature profile, thus both magnitudes may share biases imposed by very shallow LSM components. Thereby, this research line can help to understand the future evolution of the global soil carbon pool, including the possible change of the terrestrial biosphere from a net carbon sink to a source of additional greenhouse gases during this century.

5.4 References

Baldocchi, D., Falge, E., Gu, L., Olson, R., Hollinger, D., Running, S., Anthoni, P., Bernhofer, C., Davis, K., Evans, R., Fuentes, J., Goldstein, A., Katul, G., Law, B., Lee, X., Malhi, Y., Meyers, T., Munger, W., Oechel, W., Paw U, K. T., Pilegaard, K., Schmid, H. P., Valentini, R., Verma, S., Vesala, T., Wilson, K., and Wofsy, S. (2001). FLUXNET: A New Tool to Study the Temporal and Spatial Variability of Ecosystem-Scale Carbon Dioxide, Water Vapor, and Energy Flux Densities. *Bulletin of the American Meteorological Society*, **82**(11), 2415–2434. DOI: 10.1175/1520-0477(2001)082<2415:FANTTS>2.3.CO;2.

Gentine, P., García-García, A., Meier, R., Cuesta-Valero, F., Beltrami, H., Davin, E., and Seneviratne, S. (2019). "Large recent continental heat storage". Submitted to Nature.

General Bibliography

Adachi, Y., Yukimoto, S., Deushi, M., Obata, A., Nakano, H., Tanaka, T. Y., Hosaka, M., Sakami, T., Yoshimura, H., Hirabara, M., Shindo, E., Tsujino, H., Mizuta, R., Yabu, S., Koshiro, T., Ose, T., and Kitoh, A. (2013). Basic performance of a new earth system model of the Meteorological Research Institute (MRI-ESM1). *Papers in Meteorology and Geophysics*, **64**, 1–19. DOI: 10.2467/mripapers.64.1.

Alexeev, V. A., Nicolsky, D. J., Romanovsky, V. E., and Lawrence, D. M. (2007). An evaluation of deep soil configurations in the CLM3 for improved representation of permafrost. *Geophysical Research Letters*, **34**(9). n/a–n/a. DOI: 10.1029/2007GL029536.

Allan, R. P., Liu, C., Loeb, N. G., Palmer, M. D., Roberts, M., Smith, D., and Vidale, P.-L. (2014). Changes in global net radiative imbalance 1985–2012. *Geophysical Research Letters*, **41**(15), 5588–5597. DOI: 10.1002/2014GL060962.

Andrews, T., Gregory, J. M., Webb, M. J., and Taylor, K. E. (2012). Forcing, feedbacks and climate sensitivity in CMIP5 coupled atmosphere-ocean climate models. *Geophysical Research Letters*, **39**(9). n/a–n/a. DOI: 10.1029/2012GL051607.

Arora, V. K., Scinocca, J. F., Boer, G. J., Christian, J. R., Denman, K. L., Flato, G. M., Kharin, V. V., Lee, W. G., and Merryfield, W. J. (2011). Carbon emission limits required to satisfy future representative concentration pathways of greenhouse gases. *Geophysical Research Letters*, **38**(5). DOI: 10.1029/2010GL046270.

Arora, V. K., Boer, G. J., Friedlingstein, P., Eby, M., Jones, C. D., Christian, J. R., Bonan, G., Bopp, L., Brovkin, V., Cadule, P., Hajima, T., Ilyina, T., Lindsay,

K., Tjiputra, J. F., and Wu, T. (2013). Carbon–Concentration and Carbon–Climate Feedbacks in CMIP5 Earth System Models. *Journal of Climate*, **26**(15), 5289–5314. DOI: 10.1175/JCLI-D-12-00494.1.

Baldocchi, D., Falge, E., Gu, L., Olson, R., Hollinger, D., Running, S., Anthoni, P., Bernhofer, C., Davis, K., Evans, R., Fuentes, J., Goldstein, A., Katul, G., Law, B., Lee, X., Malhi, Y., Meyers, T., Munger, W., Oechel, W., Paw U, K. T., Pilegaard, K., Schmid, H. P., Valentini, R., Verma, S., Vesala, T., Wilson, K., and Wofsy, S. (2001). FLUXNET: A New Tool to Study the Temporal and Spatial Variability of Ecosystem-Scale Carbon Dioxide, Water Vapor, and Energy Flux Densities. *Bulletin of the American Meteorological Society*, **82**(11), 2415–2434. DOI: 10.1175/1520-0477(2001)082<2415:FANTTS>2.3.CO;2.

Barkaoui, A. E., Correia, A., Zarhloule, Y., Rimi, A., Carneiro, J., Boughriba, M., and Verdoya, M. (2013). Reconstruction of remote climate change from borehole temperature measurement in the eastern part of Morocco. *Climatic Change*, **118**(2), 431–441. DOI: 10.1007/s10584-012-0638-7.

Barnett, T. P., Pierce, D. W., and Schnur, R. (2001). Detection of Anthropogenic Climate Change in the World's Oceans. *Science*, **292**(5515), 270–274. DOI: 10.1126/science.1058304.

Baumberger, C., Knutti, R., and Hirsch Hadorn, G. (2017). Building confidence in climate model projections: an analysis of inferences from fit. *Wiley Interdisciplinary Reviews: Climate Change*, **8**(3). e454–n/a. DOI: 10.1002/wcc.454.

Beck, A. (1977). Climatically perturbed temperature gradients and their effect on regional and continental heat-flow means. *Tectonophysics*, **41**(1), 17 –39. DOI: https://doi.org/10.1016/0040-1951(77)90178-0.

Beltrami, H. (2001). Surface heat flux histories from inversion of geothermal data: Energy balance at the Earth's surface. *Journal of Geophysical Research: Solid Earth*, **106**(B10), 21979–21993. DOI: 10.1029/2000JB000065.

— (2002a). Climate from borehole data: Energy fluxes and temperatures since 1500. *Geophysical Research Letters*, **29**(23). 26–1–26–4. DOI: 10.1029/2002GL015702.

— (2002b). Earth's Long-Term Memory. *Science*, **297**(5579), 206–207. DOI: 10.1126/science.1074027.

Beltrami, H. and Mareschal, J.-C. (1992a). Ground temperature histories for central and eastern Canada from geothermal measurements: Little Ice Age signature. *Geophysical Research Letters*, **19**(7), 689–692. DOI: 10.1029/92GL00671.

Beltrami, H., Jessop, A. M., and Mareschal, J.-C. (1992b). Ground temperature histories in eastern and central Canada from geothermal measurements: evidence of climatic change. *Global and Planetary Change*, **6**(2–4). 167 –183. DOI: http://dx.doi.org/10.1016/0921-8181(92)90033-7.

Beltrami, H. and Taylor, A. E. (1995a). Records of climatic change in the Canadian Arctic: towards calibrating oxygen isotope data with geothermal data. *Global and Planetary Change*, **11**(3), 127 –138. DOI: https://doi.org/10.1016/0921-8181(95)00006-2.

Beltrami, H. and Mareschal, J.-C. (1995b). Resolution of ground temperature histories inverted from borehole temperature data. *Global and Planetary Change*, **11**(1-2), 57–70. DOI: https://doi.org/10.1016/0921-8181(95)00002-9.

Beltrami, H., Smerdon, J. E., Pollack, H. N., and Huang, S. (2002). Continental heat gain in the global climate system. *Geophysical Research Letters*, **29**(8), 8–1–8–3. DOI: 10.1029/2001GL014310.

Beltrami, H. and Kellman, L. (2003). An examination of short- and long-term air–ground temperature coupling. *Global and Planetary Change*, **38**(3–4), 291 –303. DOI: http://dx.doi.org/10.1016/S0921-8181(03)00112-7.

Beltrami, H. and Bourlon, E. (2004). Ground warming patterns in the Northern Hemisphere during the last five centuries. *Earth and Planetary Science Letters*, **227**(3–4), 169 –177. DOI: http://dx.doi.org/10.1016/j.epsl.2004.09.014.

Beltrami, H., Bourlon, E., Kellman, L., and González-Rouco, J. F. (2006). Spatial patterns of ground heat gain in the Northern Hemisphere. *Geophysical Research Letters*, **33**(6). n/a–n/a. DOI: 10.1029/2006GL025676.

Beltrami, H., Matharoo, G. S., and Smerdon, J. E. (2015a). Ground surface temperature and continental heat gain: uncertainties from underground.

Environmental Research Letters, **10**(1), 014009. DOI: 10.1088/1748-9326/10/1/014009.

Beltrami, H., Matharoo, G. S., and Smerdon, J. E. (2015b). Impact of borehole depths on reconstructed estimates of ground surface temperature histories and energy storage. *Journal of Geophysical Research: Earth Surface*, **120**(5). 763–778. DOI: 10.1002/2014JF003382.

Beltrami, H., Matharoo, G. S., Smerdon, J. E., Illanes, L., and Tarasov, L. (2017). Impacts of the Last Glacial Cycle on ground surface temperature reconstructions over the last millennium. *Geophysical Research Letters*, **44**(1), 355–364. DOI: 10.1002/2016GL071317.

Bhowmick, S. A., Agarwal, N., Ali, M. M., Kishtawal, C. M., and Sharma, R. (2016). Role of ocean heat content in boosting post-monsoon tropical storms over Bay of Bengal during La-Niña events. *Climate Dynamics*, 1–10. DOI: 10.1007/s00382-016-3428-5.

Bibring, J.-P., Langevin, Y., Poulet, F., Gendrin, A., Gondet, B., Berthé, M., Soufflot, A., Drossart, P., Combes, M., Bellucci, G., Moroz, V., Mangold, N., Schmitt, B., and OMEGA team, t. (2004). Perennial water ice identified in the south polar cap of Mars. *Nature*, **428**(6983), 627–630. DOI: 10.1038/nature02461.

Bodri, L. and Cermak, V. (2005). Borehole temperatures, climate change and the pre-observational surface air temperature mean: allowance for hydraulic conditions. *Global and Planetary Change*, **45**(4), 265 –276. DOI: https://doi.org/10.1016/j.gloplacha.2004.09.001.

— (2007). *Borehole Climatology*. Oxford: Elsevier Science Ltd. DOI: https://doi.org/10.1016/B978-008045320-0/50001-6.

Braconnot, P., Harrison, S. P., Kageyama, M., Bartlein, P. J., Masson-Delmotte, V., Abe-Ouchi, A., Otto-Bliesner, B., and Zhao, Y. (2012). Evaluation of climate models using palaeoclimatic data. *Nature Clim. Change*, **2**(6), 417–424. DOI: 10.1038/nclimate1456.

Bryan, K. and Cox, M. D. (1967). A numerical investigation of the oceanic general circulation. *Tellus*, **19**(1), 54–80. DOI: 10.3402/tellusa.v19i1.9761.

Bryan, K., Manabe, S., and Pacanowski, R. C. (1975). A Global Ocean-Atmosphere Climate Model. Part II. The Oceanic Circulation. *Journal of Physical Oceanography*, **5**(1), 30–46. DOI: 10.1175/1520-0485(1975)005<0030:AGOACM>2.0.CO;2.

Bullard, E. C. and Schonland, B. F. J. (1939). Heat flow in South Africa. *Proceedings of the Royal Society of London. Series A. Mathematical and Physical Sciences*, **173**(955), 474–502. DOI: 10.1098/rspa.1939.0159.

Campbell, B. M., Vermeulen, S. J., Aggarwal, P. K., Corner-Dolloff, C., Girvetz, E., Loboguerrero, A. M., Ramirez-Villegas, J., Rosenstock, T., Sebastian, L., Thornton, P. K., and Wollenberg, E. (2016). Reducing risks to food security from climate change. *Global Food Security*, **11**. 34 –43. DOI: https://doi.org/10.1016/j.gfs.2016.06.002.

Carslaw, H. and Jaeger, J. (1959). *Conduction of Heat in Solids*. Clarendon Press, Oxford.

Cermak, V. and Rybach, L. (1982a). "Thermal conductivity and specific heat of minerals and rocks". In: *Landolt Börnstein: Physical Properties of Rocks, Group V, Geophysics, Volume 1a*. Ed. by G. Angenheister. accessed 2017-06-06. Springer-Verlag Berlin Heidelberg. DOI: 10.1007/10201894_62.

Cermak, V. (1971). Underground temperature and inferred climatic temperature of the past millenium. *Palaeogeography, Palaeoclimatology, Palaeoecology*, **10**(1), 1–19. DOI: https://doi.org/10.1016/0031-0182(71)90043-5.

Charney, J. G., Arakawa, A., Baker, D. J., Bolin, B., Dickinson, R. E., Goody, R. M., Leith, C. E., Stommel, H. M., and Wunsch, C. I. (1979). *Carbon dioxide and climate: a scientific assessment*. National Academy of Sciences, Washington, DC.

Cheng, L., Trenberth, K. E., Fasullo, J., Boyer, T., Abraham, J., and Zhu, J. (2017). Improved estimates of ocean heat content from 1960 to 2015. *Science Advances*, **3**(3). DOI: 10.1126/sciadv.1601545.

Cheng, L., Abraham, J., Hausfather, Z., and Trenberth, K. E. (2019). How fast are the oceans warming? *Science*, **363**(6423), 128–129. DOI: 10.1126/science.aav7619.

Chouinard, C., Fortier, R., and Mareschal, J.-C. (2007). Recent climate variations in the subarctic inferred from three borehole temperature profiles in northern Quebec, Canada. *Earth and Planetary Science Letters*, **263**(3), 355 –369. DOI: https://doi.org/10.1016/j.epsl.2007.09.017.

Chouinard, C. and Mareschal, J.-C. (2009). Ground surface temperature history in southern Canada: Temperatures at the base of the Laurentide ice sheet and during the Holocene. *Earth and Planetary Science Letters*, **277**(1), 280 –289. DOI: https://doi.org/10.1016/j.epsl.2008.10.026.

Church, J. A., White, N. J., Konikow, L. F., Domingues, C. M., Cogley, J. G., Rignot, E., Gregory, J. M., van den Broeke, M. R., Monaghan, A. J., and Velicogna, I. (2011). Revisiting the Earth's sea-level and energy budgets from 1961 to 2008. *Geophysical Research Letters*, **38**(18). n/a–n/a. DOI: 10.1029/2011GL048794.

Clauser, C. and Mareschal, J.-C. (1995). Ground temperature history in central Europe from borehole temperature data. *Geophysical Journal International*, **121**(3), 805–817. DOI: 10.1111/j.1365-246X.1995.tb06440.x.

Collins, M., Booth, B. B. B., Bhaskaran, B., Harris, G. R., Murphy, J. M., Sexton, D. M. H., and Webb, M. J. (2011a). Climate model errors, feedbacks and forcings: a comparison of perturbed physics and multi-model ensembles. *Climate Dynamics*, **36**(9), 1737–1766. DOI: 10.1007/s00382-010-0808-0.

Collins, W. J., Bellouin, N., Doutriaux-Boucher, M., Gedney, N., Halloran, P., Hinton, T., Hughes, J., Jones, C. D., Joshi, M., Liddicoat, S., Martin, G., O'Connor, F., Rae, J., Senior, C., Sitch, S., Totterdell, I., Wiltshire, A., and Woodward, S. (2011b). Development and evaluation of an Earth-System model – HadGEM2. *Geoscientific Model Development*, **4**(4), 1051–1075. DOI: 10.5194/gmd-4-1051-2011.

Cook, B. I., Ault, T. R., and Smerdon, J. E. (2015a). Unprecedented 21st century drought risk in the American Southwest and Central Plains. *Science Advances*, **1**(1). DOI: 10.1126/sciadv.1400082.

Cox, P. M., Betts, R. A., Jones, C. D., Spall, S. A., and Totterdell, I. J. (2000). Acceleration of global warming due to carbon-cycle feedbacks in a coupled climate model. *Nature*, **408**, 184 EP –.

Cuesta-Valero, F. J., García-García, A., Beltrami, H., Zorita, E., and Jaume-Santero, F. (2019). Long-term Surface Temperature (LoST) database as a complement for GCM preindustrial simulations. *Climate of the Past*, **15**(3), 1099–1111. DOI: 10.5194/cp-15-1099-2019.

Cuesta-Valero, F. J., García-García, A., Beltrami, H., González-Rouco, J. F., and García-Bustamante, E. (2020). Long-Term Global Ground Heat Flux and Continental Heat Storage from Geothermal Data. *Climate of the Past Discussions*, **2020**, 1–27. DOI: 10.5194/cp-2020-65.

Cuesta-Valero, F. J., García-García, A., Beltrami, H., and Smerdon, J. E. (2016). First assessment of continental energy storage in CMIP5 simulations. *Geophysical Research Letters*. n/a–n/a. DOI: 10.1002/2016GL068496.

Davis, M. G., Harris, R. N., and Chapman, D. S. (2010). Repeat temperature measurements in boreholes from northwestern Utah link ground and air temperature changes at the decadal time scale. *Journal of Geophysical Research: Solid Earth*, **115**(B5). DOI: 10.1029/2009JB006875.

Deitrick, R., Barnes, R., Quinn, T. R., Armstrong, J., Charnay, B., and Wilhelm, C. (2018a). Exo-Milankovitch Cycles. I. Orbits and Rotation States. *The Astronomical Journal*, **155**(2), 60. DOI: 10.3847/1538-3881/aaa301.

Deitrick, R., Barnes, R., Bitz, C., Fleming, D., Charnay, B., Meadows, V., Wilhelm, C., Armstrong, J., and Quinn, T. R. (2018b). Exo-Milankovitch Cycles. II. Climates of G-dwarf Planets in Dynamically Hot Systems. *The Astronomical Journal*, **155**(6), 266. DOI: 10.3847/1538-3881/aac214.

Demezhko, D. Y. and Gornostaeva, A. A. (2015a). Late Pleistocene–Holocene ground surface heat flux changes reconstructed from borehole temperature data (the Urals, Russia). *Climate of the Past*, **11**(4), 647–652. DOI: 10.5194/cp-11-647-2015.

Demezhko, D. Y. and Gornostaeva, A. A. (2015b). Reconstructions of ground surface heat flux variations in the urals from geothermal and meteorological

data. *Izvestiya, Atmospheric and Oceanic Physics*, **51**(7), 723–736. DOI: 10.1134/S0001433815070026.

Dommenget, D. (2016). A simple model perturbed physics study of the simulated climate sensitivity uncertainty and its relation to control climate biases. *Climate Dynamics*, **46**(1), 427–447. DOI: 10.1007/s00382-015-2591-4.

Dommenget, D. and Rezny, M. (2017). A Caveat Note on Tuning in the Development of Coupled Climate Models. *Journal of Advances in Modeling Earth Systems*, n/a–n/a. DOI: 10.1002/2017MS000947.

Donahue, A. S. and Caldwell, P. M. (2018). Impact of Physics Parameterization Ordering in a Global Atmosphere Model. *Journal of Advances in Modeling Earth Systems*, n/a–n/a. DOI: 10.1002/2017MS001067.

Donner, L. J., Wyman, B. L., Hemler, R. S., Horowitz, L. W., Ming, Y., Zhao, M., Golaz, J.-C., Ginoux, P., Lin, S. J., Schwarzkopf, M. D., Austin, J., Alaka, G., Cooke, W. F., Delworth, T. L., Freidenreich, S. M., Gordon, C. T., Griffies, S. M., Held, I. M., Hurlin, W. J., Klein, S. A., Knutson, T. R., Langenhorst, A. R., Lee, H.-C., Lin, Y., Magi, B. I., Malyshev, S. L., Milly, P. C. D., Naik, V., Nath, M. J., Pincus, R., Ploshay, J. J., Ramaswamy, V., Seman, C. J., Shevliakova, E., Sirutis, J. J., Stern, W. F., Stouffer, R. J., Wilson, R. J., Winton, M., Wittenberg, A. T., and Zeng, F. (2011). The Dynamical Core, Physical Parameterizations, and Basic Simulation Characteristics of the Atmospheric Component AM3 of the GFDL Global Coupled Model CM3. *Journal of Climate*, **24**(13), 3484–3519. DOI: 10.1175/2011JCLI3955.1.

Dressing, C. D., Spiegel, D. S., Scharf, C. A., Menou, K., and Raymond, S. N. (2010). Habitable Climates: The Influence Of Eccentricity. *The Astrophysical Journal*, **721**(2), 1295–1307. DOI: 10.1088/0004-637x/721/2/1295.

Dufresne, J.-L., Foujols, M.-A., Denvil, S., Caubel, A., Marti, O., Aumont, O., Balkanski, Y., Bekki, S., Bellenger, H., Benshila, R., Bony, S., Bopp, L., Braconnot, P., Brockmann, P., Cadule, P., Cheruy, F., Codron, F., Cozic, A., Cugnet, D., de Noblet, N., Duvel, J.-P., Ethé, C., Fairhead, L., Fichefet, T., Flavoni, S., Friedlingstein, P., Grandpeix, J.-Y., Guez, L., Guilyardi, E., Hauglustaine, D., Hourdin, F., Idelkadi, A., Ghattas, J., Joussaume, S., Kageyama, M., Krinner,

G., Labetoulle, S., Lahellec, A., Lefebvre, M.-P., Lefevre, F., Levy, C., Li, Z., Lloyd, J., Lott, F., Madec, G., Mancip, M., Marchand, M., Masson, S., Meurdesoif, Y., Mignot, J., Musat, I., Parouty, S., Polcher, J., Rio, C., Schulz, M., Swingedouw, D., Szopa, S., Talandier, C., Terray, P., Viovy, N., and Vuichard, N. (2013). Climate change projections using the IPSL-CM5 Earth System Model: from CMIP3 to CMIP5. English. *Climate Dynamics*, **40**(9-10), 2123–2165. DOI: 10.1007/s00382-012-1636-1.

Dundas, C. M., Bramson, A. M., Ojha, L., Wray, J. J., Mellon, M. T., Byrne, S., McEwen, A. S., Putzig, N. E., Viola, D., Sutton, S., Clark, E., and Holt, J. W. (2018). Exposed subsurface ice sheets in the Martian mid-latitudes. *Science*, **359**(6372), 199–201. DOI: 10.1126/science.aao1619.

Dunne, J. P., John, J. G., Adcroft, A. J., Griffies, S. M., Hallberg, R. W., Shevliakova, E., Stouffer, R. J., Cooke, W., Dunne, K. A., Harrison, M. J., Krasting, J. P., Malyshev, S. L., Milly, P. C. D., Phillipps, P. J., Sentman, L. T., Samuels, B. L., Spelman, M. J., Winton, M., Wittenberg, A. T., and Zadeh, N. (2012). GFDL's ESM2 Global Coupled Climate–Carbon Earth System Models. Part I: Physical Formulation and Baseline Simulation Characteristics. *Journal of Climate*, **25**(19), 6646–6665. DOI: 10.1175/JCLI-D-11-00560.1.

Dutton, A., Carlson, A. E., Long, A. J., Milne, G. A., Clark, P. U., DeConto, R., Horton, B. P., Rahmstorf, S., and Raymo, M. E. (2015). Sea-level rise due to polar ice-sheet mass loss during past warm periods. *Science*, **349**(6244). DOI: 10.1126/science.aaa4019.

Dutton, J. A. (2002). *The Ceaseless Wind: An Introduction to the Theory of Atmospheric Motion*. Mineola, New York: Dover Publications.

Eyring, V., Bony, S., Meehl, G. A., Senior, C. A., Stevens, B., Stouffer, R. J., and Taylor, K. E. (2016a). Overview of the Coupled Model Intercomparison Project Phase 6 (CMIP6) experimental design and organization. *Geoscientific Model Development*, **9**(5), 1937–1958. DOI: 10.5194/gmd-9-1937-2016.

Fernández-Donado, L., González-Rouco, J. F., Raible, C. C., Ammann, C. M., Barriopedro, D., García-Bustamante, E., Jungclaus, J. H., Lorenz, S. J., Luterbacher, J., Phipps, S. J., Servonnat, J., Swingedouw, D., Tett, S. F. B., Wag-

ner, S., Yiou, P., and Zorita, E. (2013). Large-scale temperature response to external forcing in simulations and reconstructions of the last millennium. *Climate of the Past*, **9**(1), 393–421. DOI: 10.5194/cp-9-393-2013.

Ferrari, R., Jansen, M. F., Adkins, J. F., Burke, A., Stewart, A. L., and Thompson, A. F. (2014). Antarctic sea ice control on ocean circulation in present and glacial climates. *Proceedings of the National Academy of Sciences*, **111**(24), 8753–8758. DOI: 10.1073/pnas.1323922111.

Flato, G., Marotzke, J., Abiodun, B., Braconnot, P., Chou, S., Collins, W., Cox, P., Driouech, F., Emori, S., Eyring, V., Forest, C., Gleckler, P., Guilyardi, E., Jakob, C., Kattsov, V., Reason, C., and Rummukainen, M. (2013). "Evaluation of Climate Models". In: *Climate Change 2013: The Physical Science Basis. Contribution of Working Group I to the Fifth Assessment Report of the Intergovernmental Panel on Climate Change*. Ed. by T. Stocker, D. Qin, G.-K. Plattner, M. Tignor, S. Allen, J. Boschung, A. Nauels, Y. Xia, V. Bex, and P. Midgley. Cambridge, United Kingdom and New York, NY, USA: Cambridge University Press. Chap. 9, pp. 741–866. DOI: 10.1017/CBO9781107415324.020.

Forster, P. M., Andrews, T., Good, P., Gregory, J. M., Jackson, L. S., and Zelinka, M. (2013). Evaluating adjusted forcing and model spread for historical and future scenarios in the CMIP5 generation of climate models. *Journal of Geophysical Research: Atmospheres*, **118**(3), 1139–1150. DOI: 10.1002/jgrd.50174.

Franck, S, Block, A, von Bloh, W, Bounama, C, Schellnhuber, H.-J, and Svirezhev, Y (2000). Habitable zone for Earth-like planets in the solar system. *Planetary and Space Science*, **48**(11). 1099 –1105. DOI: https://doi.org/10.1016/S0032-0633(00)00084-2.

Friedlingstein, P., Cox, P., Betts, R., Bopp, L., von Bloh, W., Brovkin, V., Cadule, P., Doney, S., Eby, M., Fung, I., Bala, G., John, J., Jones, C., Joos, F., Kato, T., Kawamiya, M., Knorr, W., Lindsay, K., Matthews, H. D., Raddatz, T., Rayner, P., Reick, C., Roeckner, E., Schnitzler, K. G., Schnur, R., Strassmann, K., Weaver, A. J., Yoshikawa, C., and Zeng, N. (2006). Climate–Carbon Cycle Feedback Analysis: Results from the C4MIP Model Intercomparison. *Journal of Climate*, **19**(14), 3337–3353. DOI: 10.1175/JCLI3800.1.

García-García, A, Cuesta-Valero, F. J., Beltrami, H, and Smerdon, J. E. (2016). Simulation of air and ground temperatures in PMIP3/CMIP5 last millennium simulations: implications for climate reconstructions from borehole temperature profiles. *Environmental Research Letters*, **11**(4), 044022.

García-García, A., Cuesta-Valero, F. J., Beltrami, H., and Smerdon, J. E. (2019). Characterization of Air and Ground Temperature Relationships within the CMIP5 Historical and Future Climate Simulations. *Journal of Geophysical Research: Atmospheres*, **124**(7), 3903–3929. DOI: 10.1029/2018JD030117.

Gent, P. R., Danabasoglu, G., Donner, L. J., Holland, M. M., Hunke, E. C., Jayne, S. R., Lawrence, D. M., Neale, R. B., Rasch, P. J., Vertenstein, M., Worley, P. H., Yang, Z.-L., and Zhang, M. (2011). The Community Climate System Model Version 4. *Journal of Climate*, **24**(19), 4973–4991. DOI: 10.1175/2011JCLI4083.1.

Gentine, P., García-García, A., Meier, R., Cuesta-Valero, F., Beltrami, H., Davin, E., and Seneviratne, S. (2019). "Large recent continental heat storage". Submitted to Nature.

Giorgetta, M. A., Jungclaus, J., Reick, C. H., Legutke, S., Bader, J., Böttinger, M., Brovkin, V., Crueger, T., Esch, M., Fieg, K., Glushak, K., Gayler, V., Haak, H., Hollweg, H.-D., Ilyina, T., Kinne, S., Kornblueh, L., Matei, D., Mauritsen, T., Mikolajewicz, U., Mueller, W., Notz, D., Pithan, F., Raddatz, T., Rast, S., Redler, R., Roeckner, E., Schmidt, H., Schnur, R., Segschneider, J., Six, K. D., Stockhause, M., Timmreck, C., Wegner, J., Widmann, H., Wieners, K.-H., Claussen, M., Marotzke, J., and Stevens, B. (2013). Climate and carbon cycle changes from 1850 to 2100 in MPI-ESM simulations for the Coupled Model Intercomparison Project phase 5. *Journal of Advances in Modeling Earth Systems*, **5**(3), 572–597. DOI: 10.1002/jame.20038.

Gleckler, P. J., Durack, P. J., Stouffer, R. J., Johnson, G. C., and Forest, C. E. (2016). Industrial-era global ocean heat uptake doubles in recent decades. *Nature Clim. Change*, **6**(4), 394–398.

Gómez-Navarro, J. J., Zorita, E., Raible, C. C., and Neukom, R. (2017). Pseudo-proxy tests of the analogue method to reconstruct spatially resolved global

temperature during the Common Era. *Climate of the Past*, **13**(6), 629–648. DOI: 10.5194/cp-13-629-2017.

González-Rouco, F., von Storch, H., and Zorita, E. (2003). Deep soil temperature as proxy for surface air-temperature in a coupled model simulation of the last thousand years. *Geophysical Research Letters*, **30**(21). n/a–n/a. DOI: 10.1029/2003GL018264.

González-Rouco, J. F., Beltrami, H., Zorita, E., and von Storch, H. (2006). Simulation and inversion of borehole temperature profiles in surrogate climates: Spatial distribution and surface coupling. *Geophysical Research Letters*, **33**(1). n/a–n/a. DOI: 10.1029/2005GL024693.

González-Rouco, J. F., Beltrami, H., Zorita, E., and Stevens, M. B. (2009). Borehole climatology: a discussion based on contributions from climate modeling. *Climate of the Past*, **5**(1), 97–127. DOI: 10.5194/cp-5-97-2009.

Goodwin, P. (2018). On the Time Evolution of Climate Sensitivity and Future Warming. *Earth's Future*, **6**(9), 1336–1348. DOI: 10.1029/2018EF000889.

Gregory, J. M., Stouffer, R. J., Raper, S. C. B., Stott, P. A., and Rayner, N. A. (2002). An Observationally Based Estimate of the Climate Sensitivity. *Journal of Climate*, **15**(22), 3117–3121. DOI: 10.1175/1520-0442(2002)015<3117:AOBEOT>2.0.CO;2.

Griffies, S. M. (2004). *Fundamentals of Ocean Climate Models*. Princeton, New Jersey: Princeton University Press.

Hakim, G. J., Emile-Geay, J., Steig, E. J., Noone, D., Anderson, D. M., Tardif, R., Steiger, N., and Perkins, W. A. (2016). The last millennium climate reanalysis project: Framework and first results. *Journal of Geophysical Research: Atmospheres*, **121**(12). 6745–6764. DOI: 10.1002/2016JD024751.

Hanna, E., Navarro, F. J., Pattyn, F., Domingues, C. M., Fettweis, X., Ivins, E. R., Nicholls, R. J., Ritz, C., Smith, B., Tulaczyk, S., Whitehouse, P. L., and Zwally, H. J. (2013). Ice-sheet mass balance and climate change. *Nature*, **498**, 51 EP –.

Hansen, J., Nazarenko, L., Ruedy, R., Sato, M., Willis, J., Del Genio, A., Koch, D., Lacis, A., Lo, K., Menon, S., et al. (2005). Earth's energy imbalance: Confirmation and implications. *Science*, **308**(5727), 1431–1435.

Hansen, J., Sato, M., Kharecha, P., and Schuckmann, K. v. (2011). Earth's energy imbalance and implications. *Atmospheric Chemistry and Physics*, **11**(24), 13421–13449.

Harris, I., Jones, P., Osborn, T., and Lister, D. (2014). Updated high-resolution grids of monthly climatic observations – the CRU TS3.10 Dataset. *International Journal of Climatology*, **34**(3), 623–642. DOI: 10.1002/joc.3711.

Harris, R. N. and Chapman, D. S. (2001). Mid-latitude (30 °–60 ° N) climatic warming inferred by combining borehole temperatures with surface air temperatures. *Geophysical Research Letters*, **28**(5), 747–750. DOI: 10.1029/2000GL012348.

Harrison, S. P., Bartlein, P. J., Izumi, K., Li, G., Annan, J., Hargreaves, J., Braconnot, P., and Kageyama, M. (2015). Evaluation of CMIP5 palaeo-simulations to improve climate projections. *Nature Clim. Change*, **5**(8), 735–743.

Hartmann, A and Rath, V (2005). Uncertainties and shortcomings of ground surface temperature histories derived from inversion of temperature logs. *Journal of Geophysics and Engineering*, **2**(4), 299–311. DOI: 10.1088/1742-2132/2/4/S02.

Hartmann, D., Klein Tank, A., Rusticucci, M., Alexander, L., Brönnimann, S., Charabi, Y., Dentener, F., Dlugokencky, E., Easterling, D., Kaplan, A., Soden, B., Thorne, P., Wild, M., and Zhai, P. (2013). "Observations: Atmosphere and Surface". In: *Climate Change 2013: The Physical Science Basis. Contribution of Working Group I to the Fifth Assessment Report of the Intergovernmental Panel on Climate Change*. Ed. by T. Stocker, D. Qin, G.-K. Plattner, M. Tignor, S. Allen, J. Boschung, A. Nauels, Y. Xia, V. Bex, and P. Midgley. Cambridge, United Kingdom and New York, NY, USA: Cambridge University Press. Chap. 2, pp. 159–254. DOI: 10.1017/CBO9781107415324.008.

Hawkins, E., Ortega, P., Suckling, E., Schurer, A., Hegerl, G., Jones, P., Joshi, M., Osborn, T. J., Masson-Delmotte, V., Mignot, J., Thorne, P., and van Oldenborgh, G. J. (2017). Estimating Changes in Global Temperature since the

Preindustrial Period. *Bulletin of the American Meteorological Society*, **98**(9), 1841–1856. DOI: 10.1175/BAMS-D-16-0007.1.

Hegerl, G. C., von Storch, H., Hasselmann, K., Santer, B. D., Cubasch, U., and Jones, P. D. (1996). Detecting Greenhouse-Gas-Induced Climate Change with an Optimal Fingerprint Method. *Journal of Climate*, **9**(10), 2281–2306. DOI: 10.1175/1520-0442(1996)009<2281:DGGICC>2.0.CO;2.

Hegerl, G. C., Black, E., Allan, R. P., Ingram, W. J., Polson, D., Trenberth, K. E., Chadwick, R. S., Arkin, P. A., Sarojini, B. B., Becker, A., Dai, A., Durack, P. J., Easterling, D., Fowler, H. J., Kendon, E. J., Huffman, G. J., Liu, C., Marsh, R., New, M., Osborn, T. J., Skliris, N., Stott, P. A., Vidale, P.-L., Wijffels, S. E., Wilcox, L. J., Willett, K. M., and Zhang, X. (2015). Challenges in Quantifying Changes in the Global Water Cycle. *Bulletin of the American Meteorological Society*, **96**(7), 1097–1115. DOI: 10.1175/BAMS-D-13-00212.1.

Hermoso de Mendoza, I., Beltrami, H., MacDougall, A. H., and Mareschal, J.-C. (2020). Lower boundary conditions in land surface models – effects on the permafrost and the carbon pools: a case study with CLM4.5. *Geoscientific Model Development*, **13**(3), 1663–1683. DOI: 10.5194/gmd-13-1663-2020.

Hicks Pries, C. E., Castanha, C., Porras, R. C., and Torn, M. S. (2017). The whole-soil carbon flux in response to warming. *Science*, **355**(6332), 1420–1423. DOI: 10.1126/science.aal1319.

Hobbs, W., Palmer, M. D., and Monselesan, D. (2016). An Energy Conservation Analysis of Ocean Drift in the CMIP5 Global Coupled Models. *Journal of Climate*, **29**(5), 1639–1653. DOI: 10.1175/JCLI-D-15-0477.1.

Hopcroft, P. O., Gallagher, K., and Pain, C. C. (2007). Inference of past climate from borehole temperature data using Bayesian Reversible Jump Markov chain Monte Carlo. *Geophysical Journal International*, **171**(3), 1430–1439. DOI: 10.1111/j.1365-246X.2007.03596.x.

Hourdin, F., Mauritsen, T., Gettelman, A., Golaz, J.-C., Balaji, V., Duan, Q., Folini, D., Ji, D., Klocke, D., Qian, Y., Rauser, F., Rio, C., Tomassini, L., Watanabe, M., and Williamson, D. (2017). The Art and Science of Climate Model

Tuning. *Bulletin of the American Meteorological Society*, **98**(3), 589–602. DOI: 10.1175/BAMS-D-15-00135.1.

Hu, A., Meehl, G. A., Han, W., Yin, J., Wu, B., and Kimoto, M. (2013). Influence of Continental Ice Retreat on Future Global Climate. *Journal of Climate*, **26**(10), 3087–3111. DOI: 10.1175/JCLI-D-12-00102.1.

Hu, X., Taylor, P. C., Cai, M., Yang, S., Deng, Y., and Sejas, S. (2017). Inter-Model Warming Projection Spread: Inherited Traits from Control Climate Diversity. *Scientific Reports*, **7**(1), 4300. DOI: 10.1038/s41598-017-04623-7.

Huang, S., Pollack, H. N., and Shen, P.-Y. (2000). Temperature trends over the past five centuries reconstructed from borehole temperatures. *Nature*, **403**(6771), 756–758.

Hurrell, J. W., Holland, M. M., Gent, P. R., Ghan, S., Kay, J. E., Kushner, P. J., Lamarque, J.-F., Large, W. G., Lawrence, D., Lindsay, K., Lipscomb, W. H., Long, M. C., Mahowald, N., Marsh, D. R., Neale, R. B., Rasch, P., Vavrus, S., Vertenstein, M., Bader, D., Collins, W. D., Hack, J. J., Kiehl, J., and Marshall, S. (2013). The Community Earth System Model: A Framework for Collaborative Research. *Bulletin of the American Meteorological Society*, **94**(9), 1339–1360. DOI: 10.1175/BAMS-D-12-00121.1.

Hurtt, G., Chini, L., Frolking, S., Betts, R., Feddema, J., Fischer, G., Fisk, J., Hibbard, K., Houghton, R., Janetos, A., Jones, C., Kindermann, G., Kinoshita, T., Klein Goldewijk, K., Riahi, K., Shevliakova, E., Smith, S., Stehfest, E., Thomson, A., Thornton, P., van Vuuren, D., and Wang, Y. (2011). Harmonization of land-use scenarios for the period 1500–2100: 600 years of global gridded annual land-use transitions, wood harvest, and resulting secondary lands. English. *Climatic Change*, **109**(1-2), 117–161. DOI: 10.1007/s10584-011-0153-2.

IPCC (2007). *Climate Change 2007: The Physical Science Basis. Contribution of Working Group I to the Fourth Assessment Report of the Intergovernmental Panel on Climate Change*. Ed. by S. Solomon, D. Qin, M. Manning, Z. Chen, M. Marquis, K. Averyt, M. Tignor, and H. Miller. Cambridge, United Kingdom and New York, NY, USA: Cambridge University Press, p. 996.

IPCC (2013g). *Climate Change 2013: The Physical Science Basis. Contribution of Working Group I to the Fifth Assessment Report of the Intergovernmental Panel on Climate Change*. Cambridge, United Kingdom and New York, NY, USA: Cambridge University Press, p. 1535. DOI: 10.1017/CBO9781107415324.

Irving, D. B., Wijffels, S., and Church, J. A. (2019). Anthropogenic Aerosols, Greenhouse Gases, and the Uptake, Transport, and Storage of Excess Heat in the Climate System. *Geophysical Research Letters*, **46**(9), 4894–4903. DOI: 10.1029/2019GL082015.

Iversen, T., Bentsen, M., Bethke, I., Debernard, J. B., Kirkevåg, A., Seland, Ø., Drange, H., Kristjansson, J. E., Medhaug, I., Sand, M., and Seierstad, I. A. (2013). The Norwegian Earth System Model, NorESM1-M – Part 2: Climate response and scenario projections. *Geoscientific Model Development*, **6**(2), 389–415. DOI: 10.5194/gmd-6-389-2013.

Jacob, T., Wahr, J., Pfeffer, W. T., and Swenson, S. (2012). Recent contributions of glaciers and ice caps to sea level rise. *Nature*, **482**(7386), 514–518.

Jahn, A. and Holland, M. M. (2013). Implications of Arctic sea ice changes for North Atlantic deep convection and the meridional overturning circulation in CCSM4-CMIP5 simulations. *Geophysical Research Letters*, **40**(6), 1206–1211. DOI: 10.1002/grl.50183.

Jaume-Santero, F., Pickler, C., Beltrami, H., and Mareschal, J.-C. (2016). North American regional climate reconstruction from ground surface temperature histories. *Climate of the Past*, **12**(12), 2181–2194. DOI: 10.5194/cp-12-2181-2016.

Johnson, G. C., Lyman, J. M., and Loeb, N. G. (2016). Improving estimates of Earth's energy imbalance. *Nature Climate Change*, **6**, 639 EP –.

Jungclaus, J. H., Fischer, N., Haak, H., Lohmann, K., Marotzke, J., Matei, D., Mikolajewicz, U., Notz, D., and von Storch, J. S. (2013). Characteristics of the ocean simulations in the Max Planck Institute Ocean Model (MPIOM) the ocean component of the MPI-Earth system model. *Journal of Advances in Modeling Earth Systems*, **5**(2), 422–446. DOI: 10.1002/jame.20023.

Jungclaus, J. H., Lohmann, K., and Zanchettin, D. (2014). Enhanced 20th-century heat transfer to the Arctic simulated in the context of climate variations over the last millennium. *Climate of the Past*, **10**(6), 2201–2213. DOI: 10.5194/cp-10-2201-2014.

Knutti, R., Furrer, R., Tebaldi, C., Cermak, J., and Meehl, G. A. (2010). Challenges in Combining Projections from Multiple Climate Models. *Journal of Climate*, **23**(10), 2739–2758. DOI: 10.1175/2009JCLI3361.1.

Knutti, R. and Sedláček, J. (2012). Robustness and uncertainties in the new CMIP5 climate model projections. *Nature Climate Change*, **3**, 369 EP –. DOI: 10.1038/nclimate1716.

Knutti, R., Sedláček, J., Sanderson, B. M., Lorenz, R., Fischer, E. M., and Eyring, V. (2017a). A climate model projection weighting scheme accounting for performance and interdependence. *Geophysical Research Letters*, **44**(4), 1909–1918. DOI: 10.1002/2016GL072012.

Knutti, R., Rugenstein, M. A. A., and Hegerl, G. C. (2017b). Beyond equilibrium climate sensitivity. *Nature Geoscience*, **10**, 727–736. DOI: 10.1038/ngeo3017.

Kohl, T. (1999). Transient thermal effects below complex topographies. *Tectonophysics*, **306**(3), 311 –324. DOI: https://doi.org/10.1016/S0040-1951(99)00063-3.

Koven, C. D., Ringeval, B., Friedlingstein, P., Ciais, P., Cadule, P., Khvorostyanov, D., Krinner, G., and Tarnocai, C. (2011). Permafrost carbon-climate feedbacks accelerate global warming. *Proceedings of the National Academy of Sciences*, **108**(36), 14769–14774. DOI: 10.1073/pnas.1103910108.

Koven, C. D., Riley, W. J., and Stern, A. (2013). Analysis of Permafrost Thermal Dynamics and Response to Climate Change in the CMIP5 Earth System Models. *Journal of Climate*, **26**(6), 1877–1900. DOI: 10.1175/JCLI-D-12-00228.1.

Krakauer, N. Y., Puma, M. J., and Cook, B. I. (2013). Impacts of soil–aquifer heat and water fluxes on simulated global climate. *Hydrology and Earth System Sciences*, **17**(5), 1963–1974. DOI: 10.5194/hess-17-1963-2013.

Kuhlbrodt, T. and Gregory, J. M. (2012). Ocean heat uptake and its consequences for the magnitude of sea level rise and climate change. *Geophysical Research Letters*, **39**(18). DOI: 10.1029/2012GL052952.

Kundzewicz, Z. W., Kanae, S., Seneviratne, S. I., Handmer, J., Nicholls, N., Peduzzi, P., Mechler, R., Bouwer, L. M., Arnell, N., Mach, K., Muir-Wood, R., Brakenridge, G. R., Kron, W., Benito, G., Honda, Y., Takahashi, K., and Sherstyukov, B. (2014). Flood risk and climate change: global and regional perspectives. *Hydrological Sciences Journal*, **59**(1), 1–28. DOI: 10.1080/02626667.2013.857411.

Kurokawa, H., Sato, M., Ushioda, M., Matsuyama, T., Moriwaki, R., Dohm, J., and Usui, T. (2014). Evolution of water reservoirs on Mars: Constraints from hydrogen isotopes in martian meteorites. *Earth and Planetary Science Letters*, **394**, 179 –185. DOI: https://doi.org/10.1016/j.epsl.2014.03.027.

Lachenbruch, A. H. and Marshall, B. V. (1986). Changing Climate: Geothermal Evidence from Permafrost in the Alaskan Arctic. *Science*, **234**(4777), 689–696. DOI: 10.1126/science.234.4777.689.

Lanczos, C. (1961). *Linear differential operators*. New York: Van Nostrand, p. 564.

Landrum, L., Otto-Bliesner, B. L., Wahl, E. R., Conley, A., Lawrence, P. J., Rosenbloom, N., and Teng, H. (2013). Last Millennium Climate and Its Variability in CCSM4. *Journal of Climate*, **26**(4), 1085–1111. DOI: 10.1175/JCLI-D-11-00326.1.

Lane, A. C. (1923). Geotherms of Lake Superior Copper Country. *GSA Bulletin*, **34**(4), 703–720. DOI: 10.1130/GSAB-34-703.

Lembo, V., Folini, D., Wild, M., and Lionello, P. (2019). Inter-hemispheric differences in energy budgets and cross-equatorial transport anomalies during the 20th century. *Climate Dynamics*, **53**(1), 115–135. DOI: 10.1007/s00382-018-4572-x.

Lesperance, M., Smerdon, J. E., and Beltrami, H. (2010). Propagation of linear surface air temperature trends into the terrestrial subsurface. *Journal of Geophysical Research: Atmospheres*, **115**(D21). n/a–n/a. DOI: 10.1029/2010JD014377.

Levitus, S., Antonov, J., and Boyer, T. (2005). Warming of the world ocean, 1955–2003. *Geophysical Research Letters*, **32**(2). n/a–n/a. DOI: 10.1029/2004GL021592.

Levitus, S., Antonov, J. I., Boyer, T. P., Baranova, O. K., Garcia, H. E., Locarnini, R. A., Mishonov, A. V., Reagan, J. R., Seidov, D., Yarosh, E. S., and Zweng, M. M. (2012). World ocean heat content and thermosteric sea level change (0–2000 m), 1955–2010. *Geophysical Research Letters*, **39**(10). n/a–n/a. DOI: 10.1029/2012GL051106.

Levy, K., Woster, A. P., Goldstein, R. S., and Carlton, E. J. (2016). Untangling the Impacts of Climate Change on Waterborne Diseases: a Systematic Review of Relationships between Diarrheal Diseases and Temperature, Rainfall, Flooding, and Drought. *Environmental Science & Technology*, **50**(10). 4905–4922. DOI: 10.1021/acs.est.5b06186.

Li, J. and Heap, A. D. (2011). A review of comparative studies of spatial interpolation methods in environmental sciences: Performance and impact factors. *Ecological Informatics*, **6**(3), 228 –241. DOI: http://dx.doi.org/10.1016/j.ecoinf.2010.12.003.

Liepert, B. G. and Lo, F. (2013). CMIP5 update of 'Inter-model variability and biases of the global water cycle in CMIP3 coupled climate models'. *Environmental Research Letters*, **8**(2), 029401.

Lin, I. I., Goni, G. J., Knaff, J. A., Forbes, C., and Ali, M. M. (2013). Ocean heat content for tropical cyclone intensity forecasting and its impact on storm surge. *Natural Hazards*, **66**(3), 1481–1500. DOI: 10.1007/s11069-012-0214-5.

LLNL (2010). *CMIP5 Data Description*. https://pcmdi.llnl.gov/mips/cmip5/docs/standard_output.pdf?id=14 [Last acessed May 2020].

Lloyd, S. J., Kovats, R. S., and Chalabi, Z. (2011). Climate Change, Crop Yields, and Undernutrition: Development of a Model to Quantify the Impact of Climate Scenarios on Child Undernutrition. *Environmental Health Perspectives*, **119**(12), 1817–1823. DOI: 10.1289/ehp.1003311.

Loeb, N. G., Wielicki, B. A., Doelling, D. R., Smith, G. L., Keyes, D. F., Kato, S., Manalo-Smith, N., and Wong, T. (2009). Toward Optimal Closure of the Earth's Top-of-Atmosphere Radiation Budget. *Journal of Climate*, **22**(3), 748–766. DOI: 10.1175/2008JCLI2637.1.

Loeb, N. G., Lyman, J. M., Johnson, G. C., Allan, R. P., Doelling, D. R., Wong, T., Soden, B. J., and Stephens, G. L. (2012). Observed changes in top-of-the-atmosphere radiation and upper-ocean heating consistent within uncertainty. *Nature Geosci*, **5**(2), 110–113.

Loeb, N. G., Wang, H., Cheng, A., Kato, S., Fasullo, J. T., Xu, K.-M., and Allan, R. P. (2016). Observational constraints on atmospheric and oceanic cross-equatorial heat transports: revisiting the precipitation asymmetry problem in climate models. *Climate Dynamics*, **46**(9), 3239–3257. DOI: 10.1007/s00382-015-2766-z.

Long, M. C., Lindsay, K., Peacock, S., Moore, J. K., and Doney, S. C. (2013). Twentieth-Century Oceanic Carbon Uptake and Storage in CESM1(BGC)*. *Journal of Climate*, **26**(18), 6775–6800. DOI: 10.1175/JCLI-D-12-00184.1.

MacDougall, A. H., González-Rouco, J. F., Stevens, M. B., and Beltrami, H. (2008). Quantification of subsurface heat storage in a GCM simulation. *Geophysical Research Letters*, **35**(13), n/a–n/a. DOI: 10.1029/2008GL034639.

MacDougall, A. H., Beltrami, H., González-Rouco, J. F., Stevens, M. B., and Bourlon, E. (2010). Comparison of observed and general circulation model derived continental subsurface heat flux in the Northern Hemisphere. *Journal of Geophysical Research: Atmospheres (1984–2012)*, **115**(D12).

MacDougall, A. H., Avis, C. A., and Weaver, A. J. (2012). Significant contribution to climate warming from the permafrost carbon feedback. *Nature Geosci*, **5**(10), 719–721. DOI: 10.1038/ngeo1573.

MacDougall, A. H. and Beltrami, H. (2017). Impact of deforestation on subsurface temperature profiles: implications for the borehole paleoclimate record. *Environmental Research Letters*, **12**(7), 074014.

Mainelli, M., DeMaria, M., Shay, L. K., and Goni, G. (2008). Application of Oceanic Heat Content Estimation to Operational Forecasting of Recent At-

lantic Category 5 Hurricanes. *Weather and Forecasting*, **23**(1), 3–16. DOI: 10.1175/2007WAF2006111.1.

Manabe, S. and Wetherald, R. T. (1967). Thermal Equilibrium of the Atmosphere with a Given Distribution of Relative Humidity. *Journal of the Atmospheric Sciences*, **24**(3), 241–259. DOI: 10.1175/1520-0469(1967)024<0241:TEOTAW>2.0.CO;2.

Manabe, S., Bryan, K., and Spelman, M. J. (1975). A Global Ocean-Atmosphere Climate Model. Part I. The Atmospheric Circulation. *Journal of Physical Oceanography*, **5**(1), 3–29. DOI: 10.1175/1520-0485(1975)005<0003:AGOACM>2.0.CO;2.

Mardikis, M. G., Kalivas, D. P., and Kollias, V. J. (2005). Comparison of Interpolation Methods for the Prediction of Reference Evapotranspiration—An Application in Greece. *Water Resources Management*, **19**(3), 251–278. DOI: 10.1007/s11269-005-3179-2.

Mareschal, J.-C. and Beltrami, H. (1992). Evidence for recent warming from perturbed geothermal gradients: examples from eastern Canada. *Climate Dynamics*, **6**(3), 135–143. DOI: 10.1007/BF00193525.

Marsh, D. R., Mills, M. J., Kinnison, D. E., Lamarque, J.-F., Calvo, N., and Polvani, L. M. (2013). Climate Change from 1850 to 2005 Simulated in CESM1(WACCM). *Journal of Climate*, **26**(19), 7372–7391. DOI: 10.1175/JCLI-D-12-00558.1.

Masson-Delmotte, V., Schulz, M., Abe-Ouchi, A., Beer, J., Ganopolski, A., González Rouco, J., Jansen, E., Lambeck, K., Luterbacher, J., Naish, T., Osborn, T., Otto-Bliesner, B., Quinn, T., Ramesh, R., Rojas, M., Shao, X., and Timmermann, A. (2013). "Information from Paleoclimate Archives". In: *Climate Change 2013: The Physical Science Basis. Contribution of Working Group I to the Fifth Assessment Report of the Intergovernmental Panel on Climate Change*. Ed. by T. Stocker, D. Qin, G.-K. Plattner, M. Tignor, S. Allen, J. Boschung, A. Nauels, Y. Xia, V. Bex, and P. Midgley. Cambridge, United Kingdom and New York, NY, USA: Cambridge University Press. Chap. 5, pp. 383–464. DOI: 10.1017/CBO9781107415324.013.

Matthews, T. K. R., Wilby, R. L., and Murphy, C. (2017). Communicating the deadly consequences of global warming for human heat stress. *Proceedings of the National Academy of Sciences*, **114**(15), 3861–3866. DOI: 10.1073/pnas.1617526114.

Mauritsen, T., Stevens, B., Roeckner, E., Crueger, T., Esch, M., Giorgetta, M., Haak, H., Jungclaus, J., Klocke, D., Matei, D., Mikolajewicz, U., Notz, D., Pincus, R., Schmidt, H., and Tomassini, L. (2012). Tuning the climate of a global model. *Journal of Advances in Modeling Earth Systems*, **4**(3). n/a–n/a. DOI: 10.1029/2012MS000154.

McCullough, I. M., Davis, F. W., Dingman, J. R., Flint, L. E., Flint, A. L., Serra-Diaz, J. M., Syphard, A. D., Moritz, M. A., Hannah, L., and Franklin, J. (2016). High and dry: high elevations disproportionately exposed to regional climate change in Mediterranean-climate landscapes. *Landscape Ecology*, **31**(5), 1063–1075. DOI: 10.1007/s10980-015-0318-x.

McDougall, T. J. (2003). Potential Enthalpy: A Conservative Oceanic Variable for Evaluating Heat Content and Heat Fluxes. *Journal of Physical Oceanography*, **33**(5), 945–963. DOI: 10.1175/1520-0485(2003)033<0945:PEACOV>2.0.CO;2.

McDougall, T. J., Jackett, D. R., Wright, D. G., and Feistel, R. (2003). Accurate and Computationally Efficient Algorithms for Potential Temperature and Density of Seawater. *Journal of Atmospheric and Oceanic Technology*, **20**(5), 730–741. DOI: 10.1175/1520-0426(2003)20<730:AACEAF>2.0.CO;2.

McFarlane, N. (2011). Parameterizations: representing key processes in climate models without resolving them. *Wiley Interdisciplinary Reviews: Climate Change*, **2**(4), 482–497. DOI: 10.1002/wcc.122.

McGranahan, G., Balk, D., and Anderson, B. (2007). The rising tide: assessing the risks of climate change and human settlements in low elevation coastal zones. *Environment and Urbanization*, **19**(1), 17–37. DOI: 10.1177/0956247807076960.

McMichael, A. J., Woodruff, R. E., and Hales, S. (2006). Climate change and human health: present and future risks. *The Lancet*, **367**(9513), 859 –869. DOI: https://doi.org/10.1016/S0140-6736(06)68079-3.

McPherson, M., García-García, A., Cuesta-Valero, F. J., Beltrami, H., Hansen-Ketchum, P., MacDougall, D., and Ogden, N. H. (2017). Expansion of the Lyme Disease Vector Ixodes Scapularis in Canada Inferred from CMIP5 Climate Projections. *Environmental Health Perspectives*, **125**(5), 057008. DOI: 10.1289/EHP57.

Meehl, G. A., Washington, W. M., Arblaster, J. M., Hu, A., Teng, H., Kay, J. E., Gettelman, A., Lawrence, D. M., Sanderson, B. M., and Strand, W. G. (2013). Climate Change Projections in CESM1(CAM5) Compared to CCSM4. *Journal of Climate*, **26**(17), 6287–6308. DOI: 10.1175/JCLI-D-12-00572.1.

Melo-Aguilar, C., González-Rouco, J. F., García-Bustamante, E., Steinert, N., Jungclaus, J. H., Navarro, J., and Roldan-Gómez, P. J. (2019). Methodological and physical biases in global to sub-continental borehole temperature reconstructions: an assessment from a pseudo-proxy perspective. *Climate of the Past Discussions*, **2019**, 1–31. DOI: 10.5194/cp-2019-120.

Meyers, S. R. and Malinverno, A. (2018). Proterozoic Milankovitch cycles and the history of the solar system. *Proceedings of the National Academy of Sciences*, **115**(25), 6363–6368. DOI: 10.1073/pnas.1717689115.

Mieville, A., Granier, C., Liousse, C., Guillaume, B., Mouillot, F., Lamarque, J.-F., Grégoire, J.-M., and Pétron, G. (2010). Emissions of gases and particles from biomass burning during the 20th century using satellite data and an historical reconstruction. *Atmospheric Environment*, **44**(11), 1469 –1477. DOI: http://dx.doi.org/10.1016/j.atmosenv.2010.01.011.

Milankovitch, M. (1920). *Théorie Mathématique des Phénomènes Thermiques Produits par la Radiation Solaire*. Paris Gauthier-Villars.

Miller, R. L., Schmidt, G. A., Nazarenko, L. S., Tausnev, N., Bauer, S. E., DelGenio, A. D., Kelley, M., Lo, K. K., Ruedy, R., Shindell, D. T., Aleinov, I., Bauer, M., Bleck, R., Canuto, V., Chen, Y., Cheng, Y., Clune, T. L., Faluvegi, G., Hansen, J. E., Healy, R. J., Kiang, N. Y., Koch, D., Lacis, A. A., LeGrande, A. N., Lerner,

J., Menon, S., Oinas, V., Pérez García-Pando, C., Perlwitz, J. P., Puma, M. J., Rind, D., Romanou, A., Russell, G. L., Sato, M., Sun, S., Tsigaridis, K., Unger, N., Voulgarakis, A., Yao, M.-S., and Zhang, J. (2014). CMIP5 historical simulations (1850–2012) with GISS ModelE2. *Journal of Advances in Modeling Earth Systems*, **6**(2), 441–477. DOI: 10.1002/2013MS000266.

Moberg, A., Sonechkin, D. M., Holmgren, K., Datsenko, N. M., and Karlén, W. (2005). Highly variable Northern Hemisphere temperatures reconstructed from low- and high-resolution proxy data. *Nature*, **433**, 613 EP –.

Mottaghy, D. and Rath, V. (2006). Latent heat effects in subsurface heat transport modelling and their impact on palaeotemperature reconstructions. *Geophysical Journal International*, **164**(1), 236–245. DOI: 10.1111/j.1365-246X.2005.02843.x.

Nalder, I. A. and Wein, R. W. (1998). Spatial interpolation of climatic Normals: test of a new method in the Canadian boreal forest. *Agricultural and Forest Meteorology*, **92**(4), 211 –225. DOI: http://dx.doi.org/10.1016/S0168-1923(98)00102-6.

National Geophysical Data Center (2006). *Two-minute Gridded Global Relief Data (ETOPO2) v2*. https://www.ngdc.noaa.gov/mgg/global/etopo2.html. DOI: doi:10.7289/V5J1012Q.

NOAA (2019). *Borehole Database at National Oceanic and Atmospheric Administration's Server*. https://www.ncdc.noaa.gov/data-access/paleoclimatology-data/datasets/borehole [Last acessed September 2019].

Nowicki, S. M. J., Payne, A., Larour, E., Seroussi, H., Goelzer, H., Lipscomb, W., Gregory, J., Abe-Ouchi, A., and Shepherd, A. (2016). Ice Sheet Model Intercomparison Project (ISMIP6) contribution to CMIP6. *Geoscientific Model Development*, **9**(12), 4521–4545. DOI: 10.5194/gmd-9-4521-2016.

Oleson, K. W., Lawrence, D. M., Bonan, G. B., Flanner, E. K., Lawrence, P. J., Levis, S, Swenson, S. C., Thornton, P. E., Dai, A, Decker, M, Dickinson, R, Feddema, J, Heald, C. L., Hoffman, F, Lamarque, J.-F., Mahowald, N, Niu, G.-Y., Qian, T, Randerson, J, Running, S, Sakaguchi, K, Slater, A, Stockli, R, Wang, A, Yang, Z.-L., Zeng, X., and Zeng, X. (2010). *Technical description*

of version 4.0 of the Community Land Model (CLM). Tech. rep. NCAR Technical Note NCAR/TN-478+STR. National Center for Atmospheric Research, Boulder, CO.

PAGES 2k-PMIP3 Group (2015). Continental-scale temperature variability in PMIP3 simulations and PAGES 2k regional temperature reconstructions over the past millennium. *Climate of the Past*, **11**(12), 1673–1699. DOI: 10.5194/cp-11-1673-2015.

PAGES Hydro2k Consortium (2017). Comparing proxy and model estimates of hydroclimate variability and change over the Common Era. *Climate of the Past*, **13**(12), 1851–1900. DOI: 10.5194/cp-13-1851-2017.

Palmer, M. D. and McNeall, D. J. (2014). Internal variability of Earth's energy budget simulated by CMIP5 climate models. *Environmental Research Letters*, **9**(3), 034016.

Palmer, M. D., McNeall, D. J., and Dunstone, N. J. (2011). Importance of the deep ocean for estimating decadal changes in Earth's radiation balance. *Geophysical Research Letters*, **38**(13). n/a–n/a. DOI: 10.1029/2011GL047835.

Pan, Y., Li, L., Jiang, X., Li, G., Zhang, W., Wang, X., and Ingersoll, A. P. (2017). Earth's changing global atmospheric energy cycle in response to climate change. *Nature Communications*, **8**, 14367 EP –.

Patz, J. A., Gibbs, H. K., Foley, J. A., Rogers, J. V., and Smith, K. R. (2007). Climate Change and Global Health: Quantifying a Growing Ethical Crisis. *EcoHealth*, **4**(4), 397–405. DOI: 10.1007/s10393-007-0141-1.

Peacock, S. and Maltrud, M. (2006). Transit-Time Distributions in a Global Ocean Model. *Journal of Physical Oceanography*, **36**(3), 474–495. DOI: 10.1175/JPO2860.1.

Pendergrass, A. G. and Hartmann, D. L. (2014a). Changes in the Distribution of Rain Frequency and Intensity in Response to Global Warming. *Journal of Climate*, **27**(22), 8372–8383. DOI: 10.1175/JCLI-D-14-00183.1.

Pendergrass, A. G. and Hartmann, D. L. (2014b). The Atmospheric Energy Constraint on Global-Mean Precipitation Change. *Journal of Climate*, **27**(2), 757–768. DOI: 10.1175/JCLI-D-13-00163.1.

Phalkey, R. K., Aranda-Jan, C., Marx, S., Höfle, B., and Sauerborn, R. (2015). Systematic review of current efforts to quantify the impacts of climate change on undernutrition. *Proceedings of the National Academy of Sciences*, **112**(33), E4522–E4529. DOI: 10.1073/pnas.1409769112.

Phillips, N. A. (1956). The general circulation of the atmosphere: A numerical experiment. *Quarterly Journal of the Royal Meteorological Society*, **82**(352), 123–164. DOI: 10.1002/qj.49708235202.

Pickler, C., Beltrami, H., and Mareschal, J.-C. (2016). Laurentide Ice Sheet basal temperatures during the last glacial cycle as inferred from borehole data. *Climate of the Past*, **12**(1), 115–127. DOI: 10.5194/cp-12-115-2016.

Pickler, C., Gurza Fausto, E., Beltrami, H., Mareschal, J.-C., Suárez, F., Chacon-Oecklers, A., Blin, N., Cortés Calderón, M. T., Montenegro, A., Harris, R., and Tassara, A. (2018). Recent climate variations in Chile: constraints from borehole temperature profiles. *Climate of the Past*, **14**(4), 559–575. DOI: 10.5194/cp-14-559-2018.

Pierrehumbert, R. T. (2010). *Principles of planetary climate*. Cambridge University Press.

Pollack, H. N., Huang, S., and Shen, P.-Y. (1998). Climate Change Record in Subsurface Temperatures: A Global Perspective. *Science*, **282**(5387), 279–281. DOI: 10.1126/science.282.5387.279.

Pollack, H. N. and Smerdon, J. E. (2004). Borehole climate reconstructions: Spatial structure and hemispheric averages. *Journal of Geophysical Research: Atmospheres*, **109**(D11). n/a–n/a. DOI: 10.1029/2003JD004163.

Previdi, M., Smith, K. L., and Polvani, L. M. (2015). How Well Do the CMIP5 Models Simulate the Antarctic Atmospheric Energy Budget? *Journal of Climate*, **28**(20), 7933–7942. DOI: 10.1175/JCLI-D-15-0027.1.

Price, D. T., McKenney, D. W., Nalder, I. A., Hutchinson, M. F., and Kesteven, J. L. (2000). A comparison of two statistical methods for spatial interpolation of Canadian monthly mean climate data. *Agricultural and Forest Meteorology*, **101**(2), 81 –94. DOI: http://dx.doi.org/10.1016/S0168-1923(99)00169-0.

Rahmstorf, S. (1995). Climate drift in an ocean model coupled to a simple, perfectly matched atmosphere. *Climate Dynamics*, **11**(8), 447–458. DOI: 10.1007/BF00207194.

Rath, V., González Rouco, J. F., and Goosse, H. (2012). Impact of postglacial warming on borehole reconstructions of last millennium temperatures. *Climate of the Past*, **8**(3), 1059–1066. DOI: 10.5194/cp-8-1059-2012.

Reiter, M. (2005). Possible Ambiguities in Subsurface Temperature Logs: Consideration of Ground-water Flow and Ground Surface Temperature Change. *pure and applied geophysics*, **162**(2), 343–355. DOI: 10.1007/s00024-004-2604-4.

Rhein, M., Rintoul, S., Aoki, S., Campos, E., Chambers, D., Feely, R., Gulev, S., Johnson, G., Josey, S., Kostianoy, A., Mauritzen, C., Roemmich, D., Talley, L., and Wang, F. (2013). "Observations: Ocean". In: *Climate Change 2013: The Physical Science Basis. Contribution of Working Group I to the Fifth Assessment Report of the Intergovernmental Panel on Climate Change*. Ed. by T. Stocker, D. Qin, G.-K. Plattner, M. Tignor, S. Allen, J. Boschung, A. Nauels, Y. Xia, V. Bex, and P. Midgley. Cambridge, United Kingdom and New York, NY, USA: Cambridge University Press. Chap. 3, pp. 255–316. DOI: 10.1017/CBO9781107415324.010.

Riser, S. C., Freeland, H. J., Roemmich, D., Wijffels, S., Troisi, A., Belbéoch, M., Gilbert, D., Xu, J., Pouliquen, S., Thresher, A., Le Traon, P.-Y., Maze, G., Klein, B., Ravichandran, M., Grant, F., Poulain, P.-M., Suga, T., Lim, B., Sterl, A., Sutton, P., Mork, K.-A., Vélez-Belchí, P. J., Ansorge, I., King, B., Turton, J., Baringer, M., and Jayne, S. R. (2016). Fifteen years of ocean observations with the global Argo array. *Nature Climate Change*, **6**, 145–153. DOI: 10.1038/nclimate2872.

Rosenzweig, C., Elliott, J., Deryng, D., Ruane, A. C., Müller, C., Arneth, A., Boote, K. J., Folberth, C., Glotter, M., Khabarov, N., Neumann, K., Piontek, F., Pugh, T. A. M., Schmid, E., Stehfest, E., Yang, H., and Jones, J. W. (2014). Assessing agricultural risks of climate change in the 21st century in a global gridded crop model intercomparison. *Proceedings of the National Academy of Sciences*, **111**(9), 3268–3273. DOI: 10.1073/pnas.1222463110.

Roy, S., Harris, R. N., Rao, R. U. M., and Chapman, D. S. (2002). Climate change in India inferred from geothermal observations. *Journal of Geophysical Research: Solid Earth*, **107**(B7), ETG 5–1–ETG 5–16. DOI: 10.1029/2001JB000536.

Royer, D. L. (2006). CO2-forced climate thresholds during the Phanerozoic. *Geochimica et Cosmochimica Acta*, **70**(23). 5665 –5675. DOI: https://doi.org/10.1016/j.gca.2005.11.031.

Santer, B. D., Taylor, K. E., Wigley, T. M. L., Johns, T. C., Jones, P. D., Karoly, D. J., Mitchell, J. F. B., Oort, A. H., Penner, J. E., Ramaswamy, V., Schwarzkopf, M. D., Stouffer, R. J., and Tett, S. (1996). A search for human influences on the thermal structure of the atmosphere. *Nature*, **382**, 39 EP –. DOI: 10.1038/382039a0.

Santer, B. D., Bonfils, C. J. W., Fu, Q., Fyfe, J. C., Hegerl, G. C., Mears, C., Painter, J. F., Po-Chedley, S., Wentz, F. J., Zelinka, M. D., and Zou, C.-Z. (2019). Celebrating the anniversary of three key events in climate change science. *Nature Climate Change*, **9**(3), 180–182. DOI: 10.1038/s41558-019-0424-x.

Schädel, C., Schuur, E. A. G., Bracho, R., Elberling, B., Knoblauch, C., Lee, H., Luo, Y., Shaver, G. R., and Turetsky, M. R. (2014). Circumpolar assessment of permafrost C quality and its vulnerability over time using long-term incubation data. *Global Change Biology*, **20**(2), 641–652. DOI: 10.1111/gcb.12417.

Schmidt, G. A., Jungclaus, J. H., Ammann, C. M., Bard, E., Braconnot, P., Crowley, T. J., Delaygue, G., Joos, F., Krivova, N. A., Muscheler, R., Otto-Bliesner, B. L., Pongratz, J., Shindell, D. T., Solanki, S. K., Steinhilber, F., and Vieira, L. E. A. (2011). Climate forcing reconstructions for use in PMIP simulations

of the last millennium (v1.0). *Geoscientific Model Development*, **4**(1), 33–45. DOI: 10.5194/gmd-4-33-2011.

Schmidt, G. A., Annan, J. D., Bartlein, P. J., Cook, B. I., Guilyardi, E., Hargreaves, J. C., Harrison, S. P., Kageyama, M., LeGrande, A. N., Konecky, B., Lovejoy, S., Mann, M. E., Masson-Delmotte, V., Risi, C., Thompson, D., Timmermann, A., Tremblay, L.-B., and Yiou, P. (2014a). Using palaeo-climate comparisons to constrain future projections in CMIP5. *Climate of the Past*, **10**(1), 221–250. DOI: 10.5194/cp-10-221-2014.

Schmidt, G. A., Bader, D., Donner, L. J., Elsaesser, G. S., Golaz, J.-C., Hannay, C., Molod, A., Neale, R. B., and Saha, S. (2017). Practice and philosophy of climate model tuning across six US modeling centers. *Geoscientific Model Development*, **10**(9), 3207–3223. DOI: 10.5194/gmd-10-3207-2017.

Schmidt, G. A., Kelley, M., Nazarenko, L., Ruedy, R., Russell, G. L., Aleinov, I., Bauer, M., Bauer, S. E., Bhat, M. K., Bleck, R., Canuto, V., Chen, Y.-H., Cheng, Y., Clune, T. L., Del Genio, A., de Fainchtein, R., Faluvegi, G., Hansen, J. E., Healy, R. J., Kiang, N. Y., Koch, D., Lacis, A. A., LeGrande, A. N., Lerner, J., Lo, K. K., Matthews, E. E., Menon, S., Miller, R. L., Oinas, V., Oloso, A. O., Perlwitz, J. P., Puma, M. J., Putman, W. M., Rind, D., Romanou, A., Sato, M., Shindell, D. T., Sun, S., Syed, R. A., Tausnev, N., Tsigaridis, K., Unger, N., Voulgarakis, A., Yao, M.-S., and Zhang, J. (2014b). Configuration and assessment of the GISS ModelE2 contributions to the CMIP5 archive. *Journal of Advances in Modeling Earth Systems*, **6**(1), 141–184. DOI: 10.1002/2013MS000265.

Schurer, A. P., Mann, M. E., Hawkins, E., Tett, S. F. B., and Hegerl, G. C. (2017). Importance of the pre-industrial baseline for likelihood of exceeding Paris goals. *Nature Climate Change*, **7**(8), 563–567. DOI: 10.1038/nclimate3345.

Schuur, E. A. G., McGuire, A. D., Schadel, C., Grosse, G., Harden, J. W., Hayes, D. J., Hugelius, G., Koven, C. D., Kuhry, P., Lawrence, D. M., Natali, S. M., Olefeldt, D., Romanovsky, V. E., Schaefer, K., Turetsky, M. R., Treat, C. C., and Vonk, J. E. (2015). Climate change and the permafrost carbon feedback. *Nature*, **520**(7546), 171–179. DOI: 10.1038/nature14338.

Scoccimarro, E., Gualdi, S., Bellucci, A., Sanna, A., Giuseppe Fogli, P., Manzini, E., Vichi, M., Oddo, P., and Navarra, A. (2011). Effects of Tropical Cyclones on Ocean Heat Transport in a High-Resolution Coupled General Circulation Model. *Journal of Climate*, **24**(16), 4368–4384. DOI: 10.1175/2011JCLI4104.1.

Screen, J. A., Deser, C., Smith, D. M., Zhang, X., Blackport, R., Kushner, P. J., Oudar, T., McCusker, K. E., and Sun, L. (2018). Consistency and discrepancy in the atmospheric response to Arctic sea-ice loss across climate models. *Nature Geoscience*, **11**(3), 155–163. DOI: 10.1038/s41561-018-0059-y.

Seager, S. (2013). Exoplanet Habitability. *Science*, **340**(6132), 577–581. DOI: 10.1126/science.1232226.

Séférian, R., Gehlen, M., Bopp, L., Resplandy, L., Orr, J. C., Marti, O., Dunne, J. P., Christian, J. R., Doney, S. C., Ilyina, T., Lindsay, K., Halloran, P. R., Heinze, C., Segschneider, J., Tjiputra, J., Aumont, O., and Romanou, A. (2016). Inconsistent strategies to spin up models in CMIP5: implications for ocean biogeochemical model performance assessment. *Geoscientific Model Development*, **9**(5), 1827–1851. DOI: 10.5194/gmd-9-1827-2016.

Sellers, W. D. (1969). A Global Climatic Model Based on the Energy Balance of the Earth-Atmosphere System. *Journal of Applied Meteorology*, **8**(3), 392–400. DOI: 10.1175/1520-0450(1969)008<0392:AGCMBO>2.0.CO;2.

Sen Gupta, A., Muir, L. C., Brown, J. N., Phipps, S. J., Durack, P. J., Monselesan, D., and Wijffels, S. E. (2012). Climate Drift in the CMIP3 Models. *Journal of Climate*, **25**(13), 4621–4640. DOI: 10.1175/JCLI-D-11-00312.1.

Sen Gupta, A., Jourdain, N. C., Brown, J. N., and Monselesan, D. (2013). Climate Drift in the CMIP5 Models. *Journal of Climate*, **26**(21), 8597–8615. DOI: 10.1175/JCLI-D-12-00521.1.

Shen, P., Wang, K., Beltrami, H., and Mareschal, J.-C. (1992). A comparative study of inverse methods for estimating climatic history from borehole temperature data. *Global and Planetary Change*, **6**(2). 113 –127. DOI: https://doi.org/10.1016/0921-8181(92)90030-E.

Sherwood, S. C. and Huber, M. (2010). An adaptability limit to climate change due to heat stress. *Proceedings of the National Academy of Sciences*, **107**(21), 9552–9555. DOI: 10.1073/pnas.0913352107.

Sherwood, S. C., Bony, S., and Dufresne, J.-L. (2014). Spread in model climate sensitivity traced to atmospheric convective mixing. *Nature*, **505**(7481), 37–42. DOI: 10.1038/nature12829.

Slater, A. G. and Lawrence, D. M. (2013). Diagnosing Present and Future Permafrost from Climate Models. *Journal of Climate*, **26**(15), 5608–5623. DOI: 10.1175/JCLI-D-12-00341.1.

Smerdon, J. E. (2012). Climate models as a test bed for climate reconstruction methods: pseudoproxy experiments. *Wiley Interdisciplinary Reviews: Climate Change*, **3**(1), 63–77. DOI: 10.1002/wcc.149.

Smerdon, J. E., Pollack, H. N., Enz, J. W., and Lewis, M. J. (2003). Conduction-dominated heat transport of the annual temperature signal in soil. *Journal of Geophysical Research: Solid Earth*, **108**(B9). n/a–n/a. DOI: 10.1029/2002JB002351.

Smith, D. M., Allan, R. P., Coward, A. C., Eade, R., Hyder, P., Liu, C., Loeb, N. G., Palmer, M. D., Roberts, C. D., and Scaife, A. A. (2015). Earth's energy imbalance since 1960 in observations and CMIP5 models. *Geophysical Research Letters*, **42**(4), 1205–1213. DOI: 10.1002/2014GL062669.

Smith, R, Jones, P, Briegleb, B, Bryan, F, Danabasoglu, G, Dennis, J, Dukowicz, J, Eden, C, Fox-Kemper, B, Gent, P, Hecht, M, Jayne, S, Jochum, M, Large, W, Lindsay, K, Maltrud, M, Norton, N, Peacock, S, Vertenstein, M, and Yeager, S (2010). *The Parallel Ocean Program (POP) Reference Manual. Ocean Component of the Community Climate System Model (CCSM) and Community Earth System Model (CESM)*. Tech. rep. LAUR-01853. National Center for Atmospheric Research, Boulder, CO, p. 141.

Soden, B. J., Collins, W. D., and Feldman, D. R. (2018). Reducing uncertainties in climate models. *Science*, **361**(6400), 326–327. DOI: 10.1126/science.aau1864.

Soong, J. L., Phillips, C. L., Ledna, C., Koven, C. D., and Torn, M. S. (2020). CMIP5 Models Predict Rapid and Deep Soil Warming Over the 21st Century. *Journal of Geophysical Research: Biogeosciences*, **125**(2). e2019JG005266. DOI: 10.1029/2019JG005266.

Spiegel, D. S., Menou, K., and Scharf, C. A. (2008). Habitable Climates. *The Astrophysical Journal*, **681**(2), 1609–1623. DOI: 10.1086/588089.

Spiegel, D. S., Raymond, S. N., Dressing, C. D., Scharf, C. A., and Mitchell, J. L. (2010). Generalized Milankovitch Cycles Aand Long-Term Climatic Habitability. *The Astrophysical Journal*, **721**(2), 1308–1318. DOI: 10.1088/0004-637x/721/2/1308.

Stainforth, D. A., Downing, T. E., Washington, R., Lopez, A., and New, M. (2007). Issues in the interpretation of climate model ensembles to inform decisions. *Philosophical Transactions of the Royal Society of London A: Mathematical, Physical and Engineering Sciences*, **365**(1857), 2163–2177. DOI: 10.1098/rsta.2007.2073.

Stephens, G. L., Li, J., Wild, M., Clayson, C. A., Loeb, N., Kato, S., L'Ecuyer, T., Stackhouse, P. W., Lebsock, M., and Andrews, T. (2012). An update on Earth's energy balance in light of the latest global observations. *Nature Geoscience*, **5**(10), 691–696. DOI: 10.1038/ngeo1580.

Stevens, M. B., Smerdon, J. E., González-Rouco, J. F., Stieglitz, M., and Beltrami, H. (2007). Effects of bottom boundary placement on subsurface heat storage: Implications for climate model simulations. *Geophysical Research Letters*, **34**(2). n/a–n/a. DOI: 10.1029/2006GL028546.

Stevens, M. B., González-Rouco, J. F., and Beltrami, H. (2008). North American climate of the last millennium: Underground temperatures and model comparison. *Journal of Geophysical Research: Earth Surface*, **113**(F1). n/a–n/a. DOI: 10.1029/2006JF000705.

Stieglitz, M. and Smerdon, J. E. (2007). Characterizing Land–Atmosphere Coupling and the Implications for Subsurface Thermodynamics. *Journal of Climate*, **20**(1), 21–37. DOI: 10.1175/JCLI3982.1.

Stouffer, R. J., Manabe, S., and Bryan, K. (1989). Interhemispheric asymmetry in climate response to a gradual increase of atmospheric CO2. *Nature*, **342**, 660 –662. DOI: 10.1038/342660a0.

Suman, A., Dyer, F., and White, D. (2017). Late Holocene temperature variability in Tasmania inferred from borehole temperature data. *Climate of the Past*, **13**(6), 559–572. DOI: 10.5194/cp-13-559-2017.

Sun, Y., Joachimski, M. M., Wignall, P. B., Yan, C., Chen, Y., Jiang, H., Wang, L., and Lai, X. (2012). Lethally Hot Temperatures During the Early Triassic Greenhouse. *Science*, **338**(6105), 366–370. DOI: 10.1126/science.1224126.

Tang, Y., Li, L., Dong, W., and Wang, B. (2016). Reducing the climate shift in a new coupled model. *Science Bulletin*, **61**(6), 488–494. DOI: 10.1007/s11434-016-1033-y.

Taylor, K. E., Stouffer, R. J., and Meehl, G. A. (2011). An Overview of CMIP5 and the Experiment Design. *Bulletin of the American Meteorological Society*, **93**(4), 485–498. DOI: 10.1175/BAMS-D-11-00094.1.

Tjiputra, J. F., Roelandt, C., Bentsen, M., Lawrence, D. M., Lorentzen, T., Schwinger, J., Seland, Ø., and Heinze, C. (2013). Evaluation of the carbon cycle components in the Norwegian Earth System Model (NorESM). *Geoscientific Model Development*, **6**(2), 301–325. DOI: 10.5194/gmd-6-301-2013.

Tomas, R. A., Deser, C., and Sun, L. (2016). The Role of Ocean Heat Transport in the Global Climate Response to Projected Arctic Sea Ice Loss. *Journal of Climate*, **29**(19), 6841–6859. DOI: 10.1175/JCLI-D-15-0651.1.

Trenberth, K. E. (1997b). Using Atmospheric Budgets as a Constraint on Surface Fluxes. *Journal of Climate*, **10**(11), 2796–2809. DOI: 10.1175/1520-0442(1997)010<2796:UABAAC>2.0.CO;2.

Trenberth, K. E., Fasullo, J. T., and Balmaseda, M. A. (2014). Earth's Energy Imbalance. *Journal of Climate*, **27**(9), 3129–3144. DOI: 10.1175/JCLI-D-13-00294.1.

Trenberth, K. E., Fasullo, J. T., von Schuckmann, K., and Cheng, L. (2016). Insights into Earth's Energy Imbalance from Multiple Sources. *Journal of Climate*, **29**(20), 7495–7505. DOI: 10.1175/JCLI-D-16-0339.1.

Trenberth, K. E., Cheng, L., Jacobs, P., Zhang, Y., and Fasullo, J. (2018). Hurricane Harvey Links to Ocean Heat Content and Climate Change Adaptation. *Earth's Future*, **6**(5), 730–744. DOI: 10.1029/2018EF000825.

Trenberth, K. E., Zhang, Y., Fasullo, J. T., and Cheng, L. (2019). Observation-Based Estimates of Global and Basin Ocean Meridional Heat Transport Time Series. *Journal of Climate*, **32**(14), 4567–4583. DOI: 10.1175/JCLI-D-18-0872.1.

Turcotte, D. L. and Schubert, G. (2002). *Geodynamics*. 2nd Edition. Cambridge University Press.

Van Der Meer, D. G., Zeebe, R. E., van Hinsbergen, D. J. J., Sluijs, A., Spakman, W., and Torsvik, T. H. (2014). Plate tectonic controls on atmospheric CO2 levels since the Triassic. *Proceedings of the National Academy of Sciences*, **111**(12), 4380–4385. DOI: 10.1073/pnas.1315657111.

Van Wijk, W. R., Borghrst, A. J. W., Businger, J. A., Derksen, W. J., Schmidt, F. H., Scholte Ubing, D. W., and De Vries, D. A. (1963). *Physics of Plant Environment*. North-Holland Publishing Company - Amsterdam.

Vasseur, G., Bernard, P., de Meulebrouck, J. V., Kast, Y., and Jolivet, J. (1983). Holocene paleotemperatures deduced from geothermal measurements. *Palaeogeography, Palaeoclimatology, Palaeoecology*, **43**(3), 237 –259. DOI: https://doi.org/10.1016/0031-0182(83)90013-5.

Vaughan, D., Comiso, J., Allison, I., Carrasco, J., Kaser, G., Kwok, R., Mote, P., Murray, T., Paul, F., Ren, J., Rignot, E., Solomina, O., Steffen, K., and Zhang, T. (2013). "Observations: Cryosphere". In: *Climate Change 2013: The Physical Science Basis. Contribution of Working Group I to the Fifth Assessment Report of the Intergovernmental Panel on Climate Change*. Ed. by T. Stocker, D. Qin, G.-K. Plattner, M. Tignor, S. Allen, J. Boschung, A. Nauels, Y. Xia, V. Bex, and P. Midgley. Cambridge, United Kingdom and New York, NY, USA: Cambridge

University Press. Chap. 4, pp. 317–382. DOI: 10.1017/CBO9781107415324.012.

Vincenty, T. (1975). Direct and Inverse Solutions of Geodesics on the Ellipsoid with Application of Nested Equations. *Survey Review*, **23**(176), 88–93. DOI: 10.1179/sre.1975.23.176.88.

Volodin, E., Dianskii, N., and Gusev, A. (2010). Simulating present-day climate with the INMCM4.0 coupled model of the atmospheric and oceanic general circulations. English. *Izvestiya, Atmospheric and Oceanic Physics*, **46**(4), 414–431. DOI: 10.1134/S000143381004002X.

Von Schuckmann, K., Palmer, M. D., Trenberth, K. E., Cazenave, A., Chambers, D., Champollion, N., Hansen, J., Josey, S. A., Loeb, N., Mathieu, P. P., Meyssignac, B., and Wild, M. (2016). An imperative to monitor Earth's energy imbalance. *Nature Climate Change*, **6**, 138 EP –.

Von Schuckmann, K., Cheng, L., Palmer, M. D., Hansen, J., Tassone, C., Aich, V., Adusumilli, S., Beltrami, H., Boyer, T., Cuesta-Valero, F. J., Desbruyères, D., Domingues, C., García-García, A., Gentine, P., Gilson, J., Gorfer, M., Haimberger, L., Ishii, M., Johnson, G. C., Killick, R., King, B. A., Kirchengast, G., Kolodziejczyk, N., Lyman, J., Marzeion, B., Mayer, M., Monier, M., Monselesan, D. P., Purkey, S., Roemmich, D., Schweiger, A., Seneviratne, S. I., Shepherd, A., Slater, D. A., Steiner, A. K., Straneo, F., Timmermans, M.-L., and Wijffels, S. E. (2020). Heat stored in the Earth system: where does the energy go? *Earth System Science Data*, **12**(3), 2013–2041. DOI: 10.5194/essd-12-2013-2020.

Voosen, P. (2016). Climate scientists open up their black boxes to scrutiny. *Science*, **354**(6311), 401–402. DOI: 10.1126/science.354.6311.401.

Wada, A. and Chan, J. C. L. (2008). Relationship between typhoon activity and upper ocean heat content. *Geophysical Research Letters*, **35**(17). DOI: 10.1029/2008GL035129.

Wang, J and Bras, R. (1999). Ground heat flux estimated from surface soil temperature. *Journal of Hydrology*, **216**(3), 214 –226. DOI: https://doi.org/10.1016/S0022-1694(99)00008-6.

Washington, W. M. and Meehl, G. A. (1989). Climate sensitivity due to increased CO2: experiments with a coupled atmosphere and ocean general circulation model. *Climate Dynamics*, **4**(1), 1–38. DOI: 10.1007/BF00207397.

Watanabe, M., Suzuki, T., O'ishi, R., Komuro, Y., Watanabe, S., Emori, S., Takemura, T., Chikira, M., Ogura, T., Sekiguchi, M., Takata, K., Yamazaki, D., Yokohata, T., Nozawa, T., Hasumi, H., Tatebe, H., and Kimoto, M. (2010). Improved Climate Simulation by MIROC5: Mean States, Variability, and Climate Sensitivity. *Journal of Climate*, **23**(23), 6312–6335. DOI: 10.1175/2010JCLI3679.1.

Watanabe, S., Hajima, T., Sudo, K., Nagashima, T., Takemura, T., Okajima, H., Nozawa, T., Kawase, H., Abe, M., Yokohata, T., Ise, T., Sato, H., Kato, E., Takata, K., Emori, S., and Kawamiya, M. (2011). MIROC-ESM 2010: model description and basic results of CMIP5-20c3m experiments. *Geoscientific Model Development*, **4**(4), 845–872. DOI: 10.5194/gmd-4-845-2011.

Watts, N., Amann, M., Arnell, N., Ayeb-Karlsson, S., Belesova, K., Boykoff, M., Byass, P., Cai, W., Campbell-Lendrum, D., Capstick, S., Chambers, J., Dalin, C., Daly, M., Dasandi, N., Davies, M., Drummond, P., Dubrow, R., Ebi, K. L., Eckelman, M., Ekins, P., Escobar, L. E., Fernandez Montoya, L., Georgeson, L., Graham, H., Haggar, P., Hamilton, I., Hartinger, S., Hess, J., Kelman, I., Kiesewetter, G., Kjellstrom, T., Kniveton, D., Lemke, B., Liu, Y., Lott, M., Lowe, R., Sewe, M. O., Martinez-Urtaza, J., Maslin, M., McAllister, L., McGushin, A., Jankin Mikhaylov, S., Milner, J., Moradi-Lakeh, M., Morrissey, K., Murray, K., Munzert, S., Nilsson, M., Neville, T., Oreszczyn, T., Owfi, F., Pearman, O., Pencheon, D., Phung, D., Pye, S., Quinn, R., Rabbaniha, M., Robinson, E., Rocklöv, J., Semenza, J. C., Sherman, J., Shumake-Guillemot, J., Tabatabaei, M., Taylor, J., Trinanes, J., Wilkinson, P., Costello, A., Gong, P., and Montgomery, H. (2019). The 2019 report of The Lancet Countdown on health and climate change: ensuring that the health of a child born today is not defined by a changing climate. *The Lancet*, **394**(10211), 1836–1878. DOI: 10.1016/S0140-6736(19)32596-6.

Wu, T., Li, W., Ji, J., Xin, X., Li, L., Wang, Z., Zhang, Y., Li, J., Zhang, F., Wei, M., Shi, X., Wu, F., Zhang, L., Chu, M., Jie, W., Liu, Y., Wang, F., Liu, X., Li, Q.,

Dong, M., Liang, X., Gao, Y., and Zhang, J. (2013). Global carbon budgets simulated by the Beijing Climate Center Climate System Model for the last century. *Journal of Geophysical Research: Atmospheres*, **118**(10), 4326–4347. DOI: 10.1002/jgrd.50320.

Wu, T., Song, L., Li, W., Wang, Z., Zhang, H., Xin, X., Zhang, Y., Zhang, L., Li, J., Wu, F., Liu, Y., Zhang, F., Shi, X., Chu, M., Zhang, J., Fang, Y., Wang, F., Lu, Y., Liu, X., Wei, M., Liu, Q., Zhou, W., Dong, M., Zhao, Q., Ji, J., Li, L., and Zhou, M. (2014). An overview of BCC climate system model development and application for climate change studies. English. *Journal of Meteorological Research*, **28**(1), 34–56. DOI: 10.1007/s13351-014-3041-7.

Wu, X., Lu, Y., Zhou, S., Chen, L., and Xu, B. (2016). Impact of climate change on human infectious diseases: Empirical evidence and human adaptation. *Environment International*, **86**, 14 –23. DOI: https://doi.org/10.1016/j.envint.2015.09.007.

Wunsch, C. and Heimbach, P. (2008). How long to oceanic tracer and proxy equilibrium? *Quaternary Science Reviews*, **27**(7–8), 637 –651. DOI: http://dx.doi.org/10.1016/j.quascirev.2008.01.006.

Xiao-Ge, X., Tong-Wen, W., and Jie, Z. (2013). Introduction of {CMIP5} Experiments Carried out with the Climate System Models of Beijing Climate Center. *Advances in Climate Change Research*, **4**(1), 41 –49. DOI: http://dx.doi.org/10.3724/SP.J.1248.2013.041.

Yukimoto, S., Adachi, Y., Hosaka, M., Sakami, T., Yoshimura, H., Hirabara, M., Tanaka, T. Y., Shindo, E., Tsujino, H., Deushi, M., Mizuta, R., Yabu, S., Obata, A., Nakano, H., Koshiro, T., Ose, T., and Kitoh, A. (2012). A New Global Climate Model of the Meteorological Research Institute: MRI-CGCM; -Model Description and Basic Performance-. *Journal of the Meteorological Society of Japan. Ser. II*, **90A**, 23–64. DOI: 10.2151/jmsj.2012-A02.